


<b>Title</b>	Digital signal processing for fiber-optic communication systems
<b>Author(s)</b>	Ouyang, Xing
<b>Publication date</b>	2017
<b>Original citation</b>	Ouyang, X. 2017. Digital signal processing for fiber-optic communication systems. PhD Thesis, University College Cork.
<b>Type of publication</b>	Doctoral thesis
<b>Rights</b>	<p>© 2017, Xing Ouyang.</p> <p><a href="http://creativecommons.org/licenses/by-nc-nd/3.0/">http://creativecommons.org/licenses/by-nc-nd/3.0/</a></p> 
<b>Embargo information</b>	No embargo required
<b>Item downloaded from</b>	<a href="http://hdl.handle.net/10468/4700">http://hdl.handle.net/10468/4700</a>

Downloaded on 2018-08-23T20:02:20Z

# DIGITAL SIGNAL PROCESSING FOR FIBER-OPTIC COMMUNICATION SYSTEMS

BY

XING OUYANG



PHOTONICS SYSTEM GROUP, TYNDALL NATIONAL INSTITUTE  
DEPARTMENT OF ELECTRICAL AND ELECTRONIC ENGINEERING  
UNIVERSITY COLLEGE CORK, IRELAND

A THESIS SUBMITTED TO  
THE NATIONAL UNIVERSITY OF IRELAND, CORK  
FOR THE DEGREE OF  
DOCTOR OF PHILOSOPHY (PH.D.)

SUPERVISORS: DR. JIAN ZHAO  
PROF. PAUL TOWNSEND  
DR. ROBERT MANNING

MENTOR: DR. FATIMA GUNNING

HEAD OF SCHOOL OF ENGINEERING: PROF. WILLIAM MARNANE



# Contents

<b>Contents</b>	<b>iii</b>
<b>Declaration</b>	<b>ix</b>
<b>List of Tables</b>	<b>xiii</b>
<b>List of Figures</b>	<b>xv</b>
<b>List of Notations, Operators and Abbreviations</b>	<b>xxiii</b>
<b>Abstract</b>	<b>xxvii</b>
<b>Chapter 1 Introduction</b>	<b>1</b>
§1.1 A Brief History of Fiber-Optic Systems .....	5
§1.1.1 The Birth of Optical Source — Laser.....	10
§1.1.2 The Birth of Optical Channel — Optical Fiber .....	12
§1.1.3 The Evolution of Fiber-Optic Systems.....	13
§1.2 Digital Signal Processing in the Advanced Fiber-Optic Systems .....	17
§1.2.1 Orthogonal Frequency-Division Multiplexing.....	20
§1.2.2 Fast-OFDM — A Variant of OFDM.....	23
§1.2.3 Discrete Fresnel Transform .....	26
§1.2.4 Orthogonal Chirp-Division Multiplexing.....	28
§1.3 Outline of the Dissertation .....	30

§1.4	Contributions of the Dissertation .....	32
<b>Chapter 2 Mathematical Models of Digital Communication Systems</b>		<b>37</b>
§2.1	Overview of a Communication System .....	40
§2.2	Transmitter .....	43
§2.2.1	Digital Modulation Formats .....	44
§2.2.2	Baseband Waveform Modulation.....	48
§2.2.3	Passband Carrier Modulation.....	53
§2.3	Communication Channel.....	55
§2.3.1	Additive White Gaussian Channel .....	56
§2.3.2	Linear Time-Invariant Filtering Channel.....	57
§2.4	Receiver.....	59
§2.4.1	Coherent Detection .....	60
§2.4.2	Sampling and Discrete-Time Model .....	61
§2.4.3	Channel Equalization and Decision .....	62
<b>Chapter 3 Fiber-Optic Communication Systems</b>		<b>65</b>
§3.1	Optical Transmitter.....	67
§3.1.1	Directly Modulated Lasers.....	67
§3.1.2	External Electro-optic Modulators .....	69
§3.2	Optical Fibers.....	75
§3.2.1	Multimode Fiber.....	76
§3.2.2	Single-Mode Fiber .....	77
§3.3	Optical Receiver .....	85
§3.3.1	Optical Direct Detection.....	85
§3.3.2	Optical Coherent Detection.....	86

<b>Part I</b>	<b>91</b>
<b>Chapter 4 Double-Sideband Modulated Fast-OFDM</b>	<b>93</b>
§4.1 Background .....	95
§4.2 System Model of the DSB Fast-OFDM .....	98
§4.2.1 Digital Implementation of the DSB Fast-OFDM .....	99
§4.2.2 Inability of Channel Equalization .....	101
§4.3 Proposed DSB Fast-OFDM System .....	104
§4.4 Numerical Simulation.....	107
§4.4.1 Results under Wireless Channel .....	107
§4.4.2 Results under Optical Multimode Fiber Channel .....	108
§4.5 Experimental Implementation .....	111
§4.5.1 Experimental Setup .....	111
§4.5.2 Experimental Results.....	113
§4.6 Summary .....	117
<b>Chapter 5 Single-Sideband Modulated Fast-OFDM</b>	<b>119</b>
§5.1 Background .....	121
§5.2 Mathematical Model of SSB Fast-OFDM.....	123
§5.2.1 Digital Implementation of the SSB Fast-OFDM.....	124
§5.2.2 Inter-Carrier Interference in SSB Fast-OFDM.....	126
§5.3 Proposed SSB Fast-OFDM System.....	130
§5.4 Numerical Simulation.....	134
§5.4.1 ICI versus Number of Subcarriers.....	135
§5.4.2 BER Performance versus OSNR.....	137
§5.5 Experimental Validation.....	139
§5.5.1 Experimental Setup .....	139

§5.5.2	Experimental Results.....	141
§5.6	Summary .....	143
<b>Part II</b>		<b>145</b>
<b>Chapter 6</b>	<b>Orthogonal Chirp-Division Multiplexing</b>	<b>147</b>
§6.1	Overview .....	150
§6.2	Fresnel Integral Transformation .....	153
§6.2.1	Fresnel Integral.....	153
§6.2.2	Derivation of Discrete Fresnel Transform.....	155
§6.2.3	Properties of the Discrete Fresnel Transform .....	159
§6.2.4	The Convolution Theorem of Discrete Fresnel Transform.....	161
§6.3	Principle of Orthogonal Chirp-Division Multiplexing .....	162
§6.3.1	Chirp Spread Spectrum .....	163
§6.3.2	Principle of Orthogonal Chirp-Division Multiplexing .....	163
§6.3.3	System Model of OCDM under LTI Channel .....	168
§6.4	Discussions.....	172
§6.4.1	Spectra of the Analog and Digital OCDM Signals .....	173
§6.4.2	Relation between the Fourier Transform and the Fresnel Transform.....	174
§6.4.3	Compatibility to the OFDM Systems.....	175
§6.4.4	Implementation Complexity of OCDM System .....	178
§6.4.5	Peak-to-Average Power Ratio of OCDM Signals.....	180
§6.5	Numerical Simulation.....	181
§6.5.1	Wireless Communication Systems.....	181
§6.5.2	Fiber-Optic Communication Systems .....	192
§6.6	Experimental Implementation .....	200
§6.6.1	Experimental Setup .....	200

## CONTENTS

---

§6.6.2 Experimental Results.....	202
§6.7 Conclusion.....	203
<b>Chapter 7 Conclusions and Future Work</b>	<b>205</b>
<b>List of Publications</b>	<b>209</b>
<b>Reference</b>	<b>211</b>



# Declaration

I, Xing Ouyang hereby certify that I am the sole author of this thesis. Except where indicated, all the work presented in this thesis is solely attributed to the author. The author participated in the design and implementation of all experiments except where explicitly stated. Precise details of collaborators may be ascertained from the list of co-authors in the List of Publications.

I declare that this thesis is the candidate's own work and has not been submitted for another degree, either at University College Cork or elsewhere.

Author's Name: Xing Ouyang

Date: 28 February 2017

Signature:

A handwritten signature in black ink, reading "Xing Ouyang", enclosed within a rectangular box.



# Acknowledgements

Here, I would like to express my grateful appreciation to my Supervisor Jian Zhao, who brings the opportunity for my PhD with the funding to support my research, my Co-supervisors Bob Manning and Paul Townsend and my mentor Fatima Gunning who help me a lot with their kindness and encouragement.

It is a great time for me to meet the colleagues in Photonics Systems Group, Tyndall National Institute, and the friends in the quite town Cork to spend my four years PhD here. That's a warm and lifelong memory for myself.

Also, I would like to acknowledge the Science Foundation Ireland Grant 11/SIRG/I2124, which support my PhD study, and also the Science Foundation Ireland (13/TIDA/I2718) and the MODE-GAP, EU 7th Framework Program 258033, which I was able to take part in.



# List of Tables

Table 2-1 Example of Codebooks for 4-QAM and 16-QAM .....	47
Table 6-1 Additional Arithmetic Complexity of the OCDM System Compared to the OFDM System.....	179
Table 6-2 Power Delay Profile of the EVA Model .....	184



# List of Figures

Figure 1–1. Capacity of a communication system with additive white Gaussian noise. ....	9
Figure 1–2. Illustration of the spectra of FDM system of different conditions. ....	21
Figure 1–3. Illustration of (a) Fresnel diffraction, and (b) the diffraction pattern on the plane. ....	26
Figure 1–4. Illustration of Talbot effect. ....	27
Figure 1–5. Illustrations of (a) a linear chirp with a normalized chirp rate 128 and a duration 1 second, and (b) its power spectrum density.....	28
Figure 1–6. Illustration of a family of 16 orthogonal waveforms in OFDM and OCDM. The in-phase (solid) and the quadrature (dots) components of the linear (a) waveforms in OFDM, and (b) chirped waveforms in OCDM. ....	29
Figure 2–1. Block diagram of a general communication system under a linear channel with additive noise.....	38
Figure 2–2. Block diagram of a transmitter comprising an information encoder, which outputs the binary bits, and a modulator, which maps the bits onto the constellation diagram.....	43
Figure 2–3. Illustration of the constellation diagrams of (a) PAM-2, (b) PAM-4, (c) PAM-8, and (d) QPSK, (e) 8-PSK, (f) 16-PSK, (g) 4-QAM, (h) 16-QAM, and (i) 64-QAM. ....	45

Figure 2–4. Illustrations of the constellation diagram based on Gray code for (a) 4-QAM and (b) 16-QAM.....	48
Figure 2–5. Examples of Nyquist waveforms and their spectra: Rectangular waveform in (a) and (b), Sinc waveform in (c) and (d), and raised cosine waveforms with various roll-off factors $\beta = 0, 0.5$ , and 1 in (e) and (f). .....	52
Figure 2–6. Illustration of the inphase (above) and quadrature (below) components of a carrier modulated in QPSK with rectangular wave. ....	54
Figure 2–7. Illustration of the spectra of a baseband signal and its passband copy. ....	55
Figure 3–1. Block diagram of fiber-optic communication system. ....	66
Figure 3–2. Illustrations of (a) a directly modulated laser and (b) its characteristics of relation between input current and output power.....	67
Figure 3–3. Structures of (a) phase modulator, (b) Mach-Zehnder modulator, and (c) IQ modulator.....	70
Figure 3–5. Transfer function of optical Mach-Zehnder modulator.....	72
Figure 3–6. Basic structures of (a) multimode fibers and (b) single-mode fibers and illustrations of light propagation in them.....	76
Figure 3–7. Dispersion-induced broadening of a Gaussian pulse in a fiber at different distances (0, 25, 100 and 300 km) and pulse width (25 ps and 100 ps). .....	84
Figure 3–8. Optical direct detection using a single photodiode.....	85
Figure 3–9. Optical coherent receiver composed of optical 90° hybrid and a pair of balanced photodiodes for single-polarization optical receiver....	87
Figure 4–1. Illustration of the spectra of the subcarriers of (a) conventional OFDM signal and (b) Fast OFDM signal.....	94
Figure 4–2. System diagrams of the conventional DCT Fast-OFDM system. ....	100
Figure 4–3. Example of a channel with symmetric CIR around 0.....	101

Figure 4–4. Example of practical channels with non-symmetric CIR. ...	102
Figure 4–5. Example of the diagonal and off diagonal entries of CFR matrix $\Lambda$ of (a) conventional OFDM and (b) DCT-F-OFDM under LTI channel with non-symmetrical CIR. ....	103
Figure 4–6. System diagram of the proposed DCT based fast OFDM with single-tap equalizer. ....	104
Figure 4–7. BER performance of the FDE-based Fast OFDM using ZF (diamond) and MMSE (square), and that of the proposed scheme (dot) for (a) 2-ASK and (b) 4-ASK under the ITU channel model B. ....	108
Figure 4–8. BER performance of the FDE-based fast OFDM using ZF (diamond) and MMSE (square), and the proposed scheme (dot) for (a) 2-ASK and (b) 4-ASK under the optical MMF channel. ....	109
Figure 4–9. Experiment setup of the proposed optical IM/DD fast OFDM under 1.55 $\mu\text{m}$ standard SMF and 2 $\mu\text{m}$ HC-PBGF systems; the component surrounded by a dashed line is exclusive to the 2 $\mu\text{m}$ system. The insets (a)-(c) illustrate the measured electrical spectra of the signal, and the insets (d)-(h) are the measured optical spectra in the 2 $\mu\text{m}$ system at the positions indicated in the experiment setup, respectively. ....	110
Figure 4–10. The CIRs of the 1.55- $\mu\text{m}$ system in (a) B2B and (b) 80 km SSMF cases, and (c) the corresponding CFRs; The CIR of the 2- $\mu\text{m}$ system in (d) B2B and (e) 1.15 km PBGF cases, and the corresponding CFRs. ....	114
Figure 4–11. BER versus OSNR of the proposed and FDE based fast OFDM in the 1.55- $\mu\text{m}$ standard SMF system. ....	115
Figure 4–12. BER versus OSNR of the proposed and FDE based fast OFDM in the 2- $\mu\text{m}$ HC-PBGF system. ....	116
Figure 5–1. Illustration of the spectra of (a) DSB modulated Fast-OFDM signal, (b) sideband filter, and (c) SSB modulated Fast-OFDM signal. ...	120
Figure 5–2. Illustration of (a) the waveform of OFDM signal and (b) its spectrum, and (c) the corresponding Fast-OFDM signal by truncating the signal by half, and (d) its spectrum. ....	122
Figure 5–3. System diagram of conventional SSB modulated Fast-OFDM based on DFT. ....	125

Figure 5–4. The analytically relationship between $\lambda_{\text{SNR}}$ and $\lambda_{\text{SINR}}$ with respect to $N$ , defined in Eq. (5.15). .....	128
Figure 5–5. Theoretical BER performance of the conventional SSB modulated Fast-OFDM system and the proposed SSB modulated Fast-OFDM system (●) with (a) 4-ASK, (b) 8-ASK, and (c) 16-ASK.....	130
Figure 5–6. Block diagram of the proposed SSB modulated Fast-OFDM based on DFT.....	131
Figure 5–7. Experiment setup for the proposed SSB Fast OFDM.....	134
Figure 5–8. Theoretical and simulated received SNR, $\lambda$ , versus different number of subcarriers in the conventional Fast-OFDM scheme and the proposed Fast-OFDM. ....	135
Figure 5–9. The received constellation diagrams of received 4-ASK signal of conventional Fast-OFDM with $N =$ (i) 64, (ii) 256, and (iii) 1024, and that of the proposed scheme with $N =$ (iv) 64, (v) 256, and (vi) 1024, at OSNR = 25 dB. ....	136
Figure 5–10. BER performances of the conventional Fast-OFDM ( $\circ/\square/\diamond$ ) and the proposed Fast-OFDM system ( $\bullet/\blacksquare/\blacklozenge$ ). ( $\circ/\bullet$ for $N = 64$ , $\square/\blacksquare$ for $N = 256$ , and $\diamond/\blacklozenge$ for $N = 1024$ .).....	137
Figure 5–11. BER performances versus OSNR of the conventional Fast-OFDM ( $\circ/\square$ ), the one with interference mitigation ( $\blacktriangleright/\blacktriangleleft$ ) and the proposed Fast-OFDM system ( $\bullet/\blacksquare$ ). ( $\blacktriangleright/\blacktriangleleft$ denotes 8/32 ICI estimation subcarriers, respectively.).....	138
Figure 5–12. Experiment System setup for the proposed coherent optical SSB Modulated Fast-OFDM system. ....	140
Figure 5–13. One-shot observations of the measured channel frequency responses for (a) 4-ASK and (b) 8-ASK. ....	141
Figure 5–14. (a) BER performance versus OSNR of the proposed Fast-OFDM in B2B transmission; (b) the measured constellation diagram of (b) 4-ASK at OSNR = 23 dB and (c) 8-ASK at OSNR = 26 dB. ....	142
Figure 6–1. Illustration of chirps: (a) Near-field Kirchhoff-Fresnel diffraction of a circular aperture, and (b) its diffraction pattern on the	

second plate; (c) linear chirp waveform which is ‘up-chirp’ from 0 to 1 second and is ‘down-chirp’ from 1 to 2 second, and (d) its spectrogram. 151

Figure 6–2. Illustration of (a) the multi-code chirp waveform and (b) the orthogonal chirp-division multiplexing in the temporal-frequency-chirp dimension. .... 152

Figure 6–3. Illustration of (a) the multi-code chirp waveform and (b) the orthogonal chirp-division multiplexing in the temporal-frequency-chirp dimension. .... 154

Figure 6–4. Example of the optical field of Talbot image at the fractional Talbot distance; the fields at the crosses (×) are zero due to destructive interference and at the circles (○) are nonzero. .... 156

Figure 6–5. Illustration of the families of 16 orthogonal waveforms in OFDM and OCDM. (a) The inphase and (b) the quadrature components of the orthogonal linear exponential waveforms in OFDM, and (c) the inphase and (d) the quadrature components of the orthogonal chirp waveforms in OCDM. .... 165

Figure 6–6. Schematic diagram of the OCDM transceiver (a) multiplexing and (b) demultiplexing a bank of  $N$  modulated orthogonal chirp waveforms. .... 166

Figure 6–7. Schematic diagram of the proposed digital implementation of OCDM. .... 168

Figure 6–8. Proposed single-tap FDE for the OCDM system. .... 170

Figure 6–9. Illustrations of the spectra of (a) analog and (b) digital implementations for OCDM. The lines denote the instantaneous frequency of each chirp. .... 173

Figure 6–10. Schematic diagram of OFDM system (excluding the dash components) and the diagram of OCDM system based on the OFDM system (including the dash components). .... 177

Figure 6–11. The PAPR characteristics of the OFDM, DFT-P-OFDM, and OCDM signals with 256 and 1024 subcarriers/chirps modulated in 16-QAM. .... 180

Figure 6–12. BER performances of the OCDM systems with both ZF and MMSE equalizers and the OFDM system under the 10-ray multipath Rayleigh fading channel. ....	183
Figure 6–13. BER performances of the OCDM systems and the DFT precoded OFDM system under the 10-ray multipath Rayleigh fading channel. ....	184
Figure 6–14. BER performance of the OCDM systems with both ZF and MMSE equalizers and the OFDM system under the LTE extended vehicle A channel model with receiver diversity; (a) 4-QAM, (b) 16-QAM, and (c) 64-QAM. ....	185
Figure 6–15. BER performance of the OFDM, DFT-precoded OFDM, and OCDM systems under the LTE extended vehicle A channel model with various guard interval length. (a) 4-QAM, (b) 16-QAM, and (c) 64-QAM. ....	187
Figure 6–16. The BER performance of SC-FDE and OCDM systems with iterative block decision feedback equalization with (a) 0.8- $\mu$ s and (b) 3.2- $\mu$ s GI. ....	188
Figure 6–17. The BER performance of the OFDM, SC-FDE and OCDM using forward error coding with 3.2- $\mu$ s GI and code rates of (a) 2 / 3 and (b) 3 / 4. ....	190
Figure 6–18. Schematic diagram of the CO-OCDM system. Excluding the components in the dashed boxes, the transmitter and receiver #2 form the diagram of a conventional CO-OFDM system. Insets: illustrations of the (i) transmitted OCDM signal and the (ii) received OCDM signal distorted by dispersion and noise; (a) time-domain and (b) frequency-domain equalizers in the receiver #1. ....	191
Figure 6–19. Pulse broadening $\Delta T$ along with the transmission distance of SMF with different dispersion parameters. ....	193
Figure 6–20. Average Q factor versus transmission distance of the CO-OCDM and CO-OCDM systems with different guard interval (GI) length. ....	194
Figure 6–21. Average Q factors versus input powers of CO-OFDM and CO-OCDM systems at various SMF transmission with 6.4-ns GI. ....	195

Figure 6–22. OSNR penalties of (a) CO-OFDM and (b) CO-OCDM systems of 16-QAM to achieve a $\text{BER} = 10^{-4}$ at different transmission distance. ....	196
Figure 6–23. BER versus OSNR performance of the CO-OFDM/OCM systems with (a) 1.6-ns and (b) 3.2-ns GI. ....	197
Figure 6–24. Q factor of each (a) subcarrier in the CO-OFDM or each (b) chirp in the CO-OCM with 3.2-ns GI at a received OSNR = 15 dB. ....	198
Figure 6–25. (a) Q factor and (b) BER versus Input pPower of the CO-OCM system over 80-km standard SMF transmission. ....	201
Figure 6–26. Experiments results of the BER versus OSNR of the CO-OFDM and CO-OCM systems. ....	201
Figure 6–27. The measured (a) power spectral densities (PSDs) and (b) Q-factors of each subchannel/chirp in the CO-OFDM and CO-OCM systems. ....	202



# List of Notations, Operators and Abbreviations

## MATHEMATICAL NOTATIONS:

Variables are denoted in italic letters. Vectors are denoted in bold italic lowercase, and matrices in bold normal uppercase letters. The  $n$ -th entry of a vector  $\mathbf{x}$  is  $x(n)$ , and the  $(m, n)$ -th entry of a matrix  $\mathbf{H}$  is  $H(m, n)$ .

## MATHEMATICAL OPERATORS

$(\cdot)^*$	Complex conjugate of a complex variable, vector or matrix
$(\cdot)^T$	Transpose of a vector or matrix
$(\cdot)^H$	Hermitian of a vector or matrix
$\Re\{\cdot\}$	Real part of a complex variable, vector or matrix
$\Im\{\cdot\}$	Image part of a complex variable, vector or matrix
$*$	Linear convolution
$\circledast$	Circular convolution
$\mathcal{F}\{\cdot\}$	Fourier transform
$\mathcal{N}(\mu, \sigma^2)$	Normal distribution with mean $\mu$ and variance $\sigma^2$

## ACRONYM AND ABBREVIATIONS

ADC	Analog-to-Digital Converter
-----	-----------------------------

ASK	Amplitude Shift Keying
ASE	Amplified Spontaneous Emission
AWG	Arbitrary Waveform Generator
B2B	Back-to-Back
BPSK	Binary Phase-Shift Keying
BPF	Band-Pass Filter
CFR	Channel Frequency Response
CIR	Channel Impulse Response
CSI	Channel State Information
DAC	Digital-to-Analog Converter
DCT	Discrete Cosine Transform
DFT	Discrete Fourier Transform
DFnT	Discrete Fresnel Transform
DMT	Discrete Multi-Tone
DPO	Digital Phosphor Oscilloscope
DSB	Double-Sideband
DSL	Digital Subscriber Line
DSP	Digital Signal Processing
DST	Discrete Sine Transform
EDFA	Erbium-Doped Fiber Amplifier
EVM	Error Vector Magnitude
ESA	Electronic Spectrum Analyzer
FDM	Frequency Division Multiplexing
GI	Guard Interval
LEAF	Large Effective Area Fiber
LPF	Low-Pass Filter
MMF	Multi-Mode Fiber
MMSE	Minimum Mean Square Error
MZM	Mach-Zehnder Modulator
OBPF	Optical Band-Pass Filter
OCDM	Orthogonal Chirp-Division Multiplexing

CO-OCDM	Coherent-Optical OCDM
OFDM	Orthogonal Frequency-Division Multiplexing
CO-OFDM	Coherent-Optical OFDM
OSA	Optical Signal Analyzer
PAM	Pulse Amplitude Modulation
PSD	Power Spectral Density
PSK	Phase-Shift Keying
PDM	Polarization Division Multiplexing
QAM	Quadrature Amplitude Modulation
QPSK	Quadrature Phase-Shift Keying
SMF	Single-Mode Fiber
S-SMF	Standard Single-Mode Fiber
SSB	Single-Sideband
TDFA	Thulium-Doped Fiber Amplifier
WDM	Wavelength Division Multiplexing
ZF	Zero-Forcing



# Abstract

As the available bandwidth of optical fibers has been almost fully exploited, Digital Signal Processing (DSP) comes to rescue and is a critical technology underpinning the next generation advanced fiber-optic systems. Literally, it contributes two principal enforcements with respect to information communication. One is the implementation of spectrally-efficient modulation schemes, and the other is the guarantee of the recovery of information from the spectrally-efficient optical signals after channel transmission.

The dissertation is dedicated to DSP techniques for the advanced fiber-optic systems. It consists of two main research topics. The first topic is about Fast-orthogonal frequency-division multiplexing (OFDM) — a variant OFDM scheme whose subcarrier spacing is half of that of conventional OFDM. The second one is about Fresnel transform with the derivation of an interesting discrete Fresnel transform (DFnT), and the proposal of orthogonal chirp-division multiplexing (OCDM), which is fundamentally underlain by the Fresnel transform.

In the first part, equalization and signal recovery problems result from the halved subcarrier spacing in both double-sideband (DSB) and single-sideband (SSB) modulated Fast-OFDM systems are studied, respectively. By exploiting the relation between the multiplexing kernels of Fast-OFDM systems and Fourier transform, equalization algorithms are proposed for respective Fast-OFDM systems for information recovery. Detailed analysis is also provided. With the proposed algorithms, the DSB Fast-OFDM was experimentally implemented by intensity-modulation and direct detection in the conventional 1.55- $\mu\text{m}$  and the emerging 2- $\mu\text{m}$  fiber-optic systems,

and the SSB Fast-OFDM was first implemented in coherent fiber-optic system with a spectral efficiency of 6 bit/s/Hz at 36 Gbps, for the first time.

In the second part, Fresnel transform from optical Fresnel diffraction is studied. The discrete Fresnel transform (DFnT) is derived, as an interesting transformation that would be potentially useful for DSP. Its properties are proved. One of the attractive properties, the convolution-preservation property states that the DFnT of a circular convolution of two sequences is equal to the DFnT of either one convolving with the other.

One application of DFnT is practically utilized in the proposal of OCDM. In the OCDM system, a large number of orthogonal chirped waveforms are multiplexed for high-speed communication, achieving the maximum spectral efficiency of chirp spread spectrum systems, in the same way as OFDM attains the maximum spectral efficiency of frequency-division multiplexing. Owing to the unique time-frequency properties of chirped waveforms, OCDM outperforms OFDM and single-carrier systems, and is more resilient against the noise effect, especially, when time-domain and frequency-domain distortions are severe. Experiments were carried out to validate the feasibility and advantages of the proposed OCDM systems.

# Chapter 1

## Introduction

It is impossible to argue that the tremendous achievement of the human society is built on any single technology. Information and communication technology does contribute to the advent of the *Information Age*, the most prosperous and glorious era in the human history following the *Industrial Age*. Communication systems are technically the apparatus that exchanges information among information nodes, like human and artificially intelligent devices with logic, which are able to record, process, and understand the information and even able to regulate their states and actions in response to the information depending on their ‘knowledge’. Communication systems enable instantaneous information exchange over a vast distance, nearly at the speed of light, breaking through the temporal and spatial limitations on communicating information.

Literally, optical communication systems are the system that conveys information in the form of light; fiber-optic communication systems are the optical communication system in which the information-bearing lightwave propagates in optical fibers. Since the 1960s, the fiber-optic communication systems, both theoretically and practically, become the only communication systems that are capable of supporting information communications at the data rate of trillions bits per second over distance up to thousands of kilometers across the Earth.

From the perspective of information theory, the total achievable capacity of a communication system is the product of available *bandwidth (spectrum)* and

achievable *spectral efficiency*. In contrast to other wired and wireless communication systems, where the available bandwidth is limited or sometimes even a scarce resource due to the nature of the channel media, the bandwidth of a piece of optical fiber is however beyond one's imagination.

Since the birth of fiber-optic communications in the 1960s, it took decades to explore the usable bandwidth of the optical fiber for information communication. Before the 2000, two practically useful techniques, optical amplifier and wavelength-division multiplexing exploited the potential bandwidth of the optical fibers. Following the exploration of the bandwidth of optical fibers, as of the beginning of the 2000, the exploration towards spectral efficiency began for fiber-optic communication systems.

Spectral efficiency is the measure of how much information can be modulated per unit bandwidth per second. The available bandwidth of a system much depends on the nature of the system itself, while the spectral efficiency of a system largely relies on the system design and engineering. Digital signal processing (DSP) is the technology that deals with the spectral efficiency issue, tying up the spectral efficiency of a communication system approaching its theoretical ceiling<sup>1</sup> and meanwhile guaranteeing the reliability of the system against failures and corruptions.

The outcome of the pursuit of spectral efficiency for fiber-optic systems is obvious. As the available bandwidth of the optical fiber had been 'almost' fully utilized and thus is 'almost' fixed, the capacity of the fiber-optic communication systems had been multiplied more than tenfold as the consequence of the multiplied spectral efficiency in the first decade since 2000, from 0.8 bit/s/Hz to 10 bit/s/Hz and beyond.

Digital signal processing essentially supports such advances in the exploration of spectral efficiency in the fiber-optic communication systems. DSP technology, on the one hand, enables advanced modulation formats, which realize spectrally efficient modulation of lightwave, and on the other hand it enables

---

<sup>1</sup> More specifically, based on Shannon's theory, coding theory is the technique achieving the capacity limit of a communication system. Digital signal processing is a more general concept when signal and information processing is involved in a communication system.

sophisticated dispersion compensation techniques, which promise information recovery from the highly spectrally-efficient modulated lightwave after transmission. With these ‘advances’, the fiber-optic systems of such kind are thus referred to as the advanced fiber-optic communication systems.

Moreover, the widespread deployment of DSP technology leads the fiber-optic communication systems into the digital age of their own in the history of the fiber-optic communications.

## A BRIEF OVERVIEW OF THIS DISSERTATION

The dissertation falls into the area of DSP technology. However, DSP is a rather broad field in both academia and industry wherever digital information and the process of the information occur in sight. Hence, the dissertation further concentrates on the DSP technology for the advanced fiber-optic systems. Still, the DSP technology for the advanced fiber-optic systems involves numerous advanced techniques that enable the advances of fiber-optic systems. Thus, the dissertation is boiled down to two topics related to the DSP technology in fiber-optic systems. One is orthogonal frequency-division multiplexing (OFDM) and a variant of OFDM scheme — Fast-OFDM, and the other is discrete Fresnel transform (DFnT) and its application to the proposal of the so-called orthogonal chirp-division multiplexing (OCDM) system.

Specifically, the first topic is dedicated to a variant of OFDM system, Fast-OFDM, targeting on the modulation and equalization problems unresolved in the literature and engineering implementation. Depending on the modulation scheme of Fast-OFDM signals, it is further divided into two parts, the double sideband (DSB) modulated Fast-OFDM and the single sideband (SSB) modulated Fast-OFDM. The modulation and equalization problems in each scheme are studied separately, as their mechanisms are somewhat different. Solutions are proposed for each of them. In addition, these solutions are both analytically and experimentally validated in the dissertation.

In the dissertation, the second topic includes the derivation of discrete Fresnel transform, an interesting transformation for digital signal processing, and

the proposal of orthogonal chirp-division multiplexing, an orthogonal multiplexing concept for high-speed data communication systems. In regard to the OCDM, the study are divided into two parts. The first is about the fundamental theory underlying the OCDM, which is about the Fresnel transform originating from the Fresnel diffraction in classic optics, and its discrete counterpart, discrete Fresnel transform (DFnT). The dissertation proposes the Fresnel transform for orthogonal chirp-division multiplexing and show how the orthogonality of the chirped waveforms is ensured based on the theory of Fresnel transform. Moreover, the DFnT is derived in the dissertation from the classic optic phenomenon, the Talbot effect. The DFnT forms the basis of digital implementation of the concept of OCDM. Moreover, except for its application in OCDM, the DFnT could be a more general and powerful mathematical tool for digital signal processing for its useful properties, just as the Fourier transform and discrete Fourier transform (DFT) in the area of digital signal processing. One important and attractive property of DFnT, the convolution-preservation property is also derived in this dissertation.

Based on the theory of Fresnel transform and DFnT, the second part is about the concept of OCDM. The OCDM system is proposed for high-speed communication, and system models are developed for different communication systems along with detailed analyses. Intensive numerical simulations are provided and experimental implementation were carried out to validate the feasibility of the OCDM system. The results confirm the advantages of the proposed OCDM system over other multiplexing techniques including the single-carrier system and multicarrier system, namely OFDM.

This chapter is for an introduction of the dissertation. Section §1.1 is a brief view on the history of fiber-optic communications, and Section §1.2 discusses the role of DSP technology in fiber-optic communication systems, and how it participates in its evolution to the advanced fiber-optic communication system. Subsections §1.2.1, §1.2.2, §1.2.3, and §1.2.4 are served as the briefs for the research topics in the dissertation, which are OFDM, Fast-OFDM, discrete Fresnel transform, and OCDM, respectively. Section §1.3 outlines the organization of the dissertation and Section §1.4 details its contributions.

## §1.1 A Brief History of Fiber-Optic Systems

The history of fiber-optic communication is the story that tells how light transmits through fibers over years. In the fiber-optic systems, optical source and optical channel are two of the most essential components. The first emits light beams which is the carrier bearing information; the second serves as the physic medium conveying the information-bearing light over vast distance.

In the history of half century-old fiber-optic communication, the invention of the laser and optical fiber announces the birth of fiber-optic communications, and they are the protagonists on the stage casting the story of fiber-optic communication. Revolving around the lasers and optical fibers, other crucial roles of inventions and technologies, such as, optical amplifiers, wavelength-division multiplexing, digital signal processing, and even the most recent mode-division multiplexing emerge and boost the fiber-optic communication to ever higher phases.

### A BRIEF BIOGRAPHY OF FIBER-OPTIC COMMUNICATION

In the 1950s, fiber-optic communication was fertilized in a seed of light, waiting for a drop of water to sprout. Without the intention for fiber-optic communications, the laser<sup>2</sup>, as the optical source, and the optical fiber<sup>3</sup>, as the optical channel, were independently invented in two distinct fields. Though it was expected that the invention of the laser would launch optical communication into a completely new era, no one then had expected that it, together with the optical fiber, would bring about a revolution sweeping over the *Industrial Age* and even the entire society of human beings. Though the revolution was not in sight then, the birth of fiber-optic communication nonetheless had already been happening there, waiting someone to unveil its future.

---

<sup>2</sup> Laser was theoretically predicted by Arthur L. Schawlow and Charles H. Townes in their paper in 1958, based on Townes's work in Maser, the microwave oscillator. The first experimental demonstration was actually in the very beginning of 1960s, by Theodore Maiman, at Hughes Research Laboratories in Malibu on May 16, 1960.

<sup>3</sup> The concept of optical fiber takes a long time before its current form, the clad optical fiber. Around the beginning of the 1950s, the practical invention of the clad optical fiber which was pioneered by Møller Hansen, Abraham van Heel and Brian O'Brien *et al.*

In the 1960s, fiber-optic communication was given birth in its infancy, lying in the cradle of laboratory. Optical communication was revived with the invention of laser since the very beginning of the 1960s. However, it took the decade to find a suitable medium, transparent and robust enough to support the propagation of the lasing light. With the very drop of water, a bold prediction that the loss of the glass fiber can be lower than 20 dB/km in 1966, fiber-optic communication was given birth. People gradually started to believe that optical fiber is the channel medium they dreamt of for decades.

In the 1970s, fiber-optic communication was in its toddlerhood, growing up rapidly, and ready for its stretch-out out of laboratories. During the decade, the laser became more and more stable and the optical fiber got clearer and clearer. Following a series of experiments in the laboratories in United States, United Kingdom and Japan, the fiber-optic systems soon went out for field trials with success in the second half of 1970s. Telephone companies reverted their focus to the fiber-optic communication systems, which were on its way to build the backbone of inter-continental networks.

In the 1980s, fiber-optic communication was in its childhood, revealing its brilliant aptitudes. After the first commercial step of providing telephone services in the late of the 1970s, the deployment of fiber-optic systems was rolling all around the earth. Researchers in the laboratories were becoming more and more familiar with the lasers and the behavior of light in the optical fibers, and they were capable of fabricating lasers emitting light beams of longer wavelength, from 0.8  $\mu\text{m}$  to 1.3  $\mu\text{m}$ , and finally to around 1.55  $\mu\text{m}$  for transmitting light in the glass fibers at the ultimately lowest loss, and drawing fibers with narrower diameters, from 100  $\mu\text{m}$  to 50  $\mu\text{m}$  and finally to less than 10  $\mu\text{m}$  for supporting light propagation in a single path (mode) with negligible dispersion. The upgraded fiber-optic systems were soon commercially followed, and their deployment were accelerating all around the world.

In the 1990s, fiber-optic communication was in its adolescent, supporting the revolution of the digital flood. By the spur of the Internet and the emergence of the World Wide Web, which provides much more interesting and at-

tractive services rather than the monotonous voice and text, fiber-optic communication systems inevitably became the only choice left to people to be capable of supporting the “Nets” and the “Webs” due to its inherently invincible superiority. Remarkably, two of the most elegant inventions in the 1990s, optical amplifiers<sup>4</sup> and wavelength-division multiplexing<sup>5</sup> set off the potential of fiber-optic systems and fundamentally extend the reach and capacity of fiber-optic systems. With the tremendous capacity practically unveiled to people, a “Gold Rush” surged with unimaginable amount of money plunging into the building of the networks of fibers. Fueled by the “greedy” money, the capacity of fiber-optic networks exploded and for the first time it exceeded people’s demands for capacity. The explosive growth of the fiber-optic communication systems continued. At the end of the twentieth century, the fiber-optic industry seemed to be a booming market. However, booming bubbles were emerging beneath the booming market.

In the 2000s, fiber-optic communication was in its adulthood, continuing its strides into a new digital phase in his life after his first Waterloo, the bust of the so-called ‘Telecom Bubbles’. The first decade of the 21st century was an eventful decade in the history of Information Age, so was it in the fiber-optic society. With the greedy pursuit of money, people could not stop themselves from laying new fiber cables around the world. The glut of fiber all of a sudden came into sight at the turn of the Millennium. On March 10, 2000, Friday, as the NASDAQ hit \$5132.52, the burst of the “Telecom Bubbles” began, just like the chain reaction in an atomic bomb. The burst lasted over exact two and half years plus one month, as the NASDAQ finally braked at \$1108.49 on October 10, 2002, the day before another Friday, with almost four-fifth of the money evaporated.

---

<sup>4</sup> Optical amplifier, more specifically doped fiber amplifier was invented during the 1960s, and the optical amplifier practically for fiber-optic communication was erbium-doped fiber amplifier (EDFA) which was demonstrated in Southampton University.

<sup>5</sup> Strictly speaking, wavelength-division multiplexing is not an invention but an antiquity idea in the area of communications. In the fiber-optic communication systems, it was not practical until the invention of the optical amplifier, which is able to boost the weakening optical signal without extracting the digital information back to the electrical domain. Without optical amplifiers, at each relay node, each wavelength should be split out, converted into the electrical domain, and then modulated back into the corresponding wavelength and combined together for transmission, resulting a costly and bulky relay node.

It seems that the fiber-optic industry and society should be in a depression in response to the slump in the stock market. It was however not the case. The busting bubbles in the beginning of 21st century just washed out the greedy money. Technically, the fiber-optic industry and the fiber-optic society continued their progress.

## DIGITAL ERA OF FIBER-OPTIC COMMUNICATION

The prominent progress of fiber-optic communication in the first decade of the twenty-first century is that it literally and also practically evolved into digital communication, benefitted from the revival of optical coherent detection and the advances of the high-speed CMOS technology. Fiber-optic communication therefore entered its own *Digital Era*.

Optical coherent detection and high-speed CMOS technologies are the two backups supporting the full digitalization of fiber-optic communication. In the view of mathematics, coherent detection hits the ultimate receive sensitivity that a communication system could be because it is able to retrieve all the information modulated onto the lightwave. Hence, digital signal processing can be applied to manipulate the holographic information in the optical domain. On the other hand, high-speed CMOS technology makes the implementation of the sophisticated digital signal processing techniques practically possible to process the high-speed optical information by the electronic devices. With the two technologies, the DSP technology is enabled for fiber-optic communication to fully process the information of light, just like solving math on a piece of paper.

The most obvious advance is that the advanced modulation formats and digital signal processing algorithms, which are before exclusive to electronic communication, are migrated to the fiber-optic systems. The most obvious benefit is that the potential of the fiber-optic systems is released, pushing towards the limit of Shannon's Theory<sup>6</sup> [1, 2], which is

---

<sup>6</sup> The Shannon's Theory formulated here is the most fundamental equation with the assumption of additive white Gaussian noise. In fiber-optic communications, except to the noise, nonlinear degradation exists in optical fiber, and the capacity of an optical fiber should be

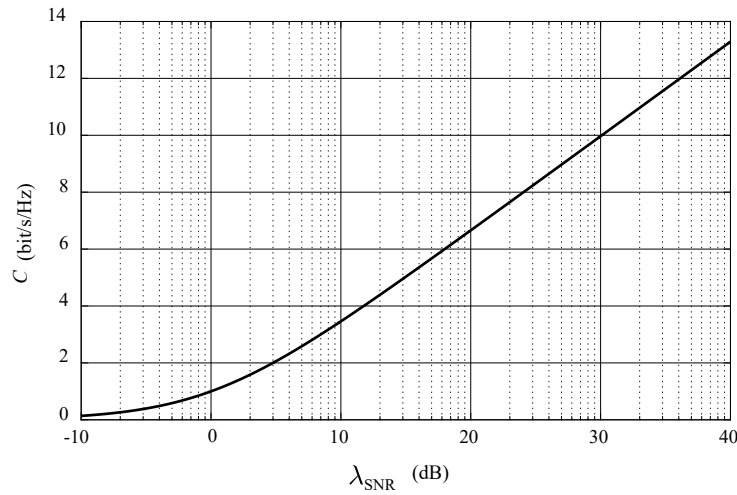


Figure 1–1. Capacity of a communication system with additive white Gaussian noise.

$$\begin{aligned}
 C &= W \log_2 (1 + \lambda_{\text{SNR}}) \\
 &= W \log_2 \left( 1 + \frac{E_s}{N_0} \right).
 \end{aligned} \tag{1.1}$$

The equation tells us that the capacity of a communication system in terms of bit rate,  $C$  (bit/s), is the product of bandwidth and the logarithmic function of signal-to-noise ratio (SNR), the ratio of the energy per symbol  $E_s$  (Joule) to the power spectral density of the noise  $N_0$  (Watt  $\times$  second).

With appropriate manipulation on Eq. (1.1), i.e., normalizing the capacity  $C$  with respect to the bandwidth  $W$ , as depicted in Figure 1–1, it also tells us that, if some SNR is guaranteed in a communication system, we can find some way, most probably by techniques falling into the scope of digital signal processing, to guarantee the capacity of the system with respect to the given SNR.

As a convinced result of the equation, the achievable capacity of fiber-optic systems is boosted more than tenfold in corresponding to the increase of the spectral efficiency of a single-mode light beam in the optical fiber, multiplying from less than 1 bit/s/Hz to more than 10 bit/s/Hz during the 2000s.

In half century since the birth of fiber-optic communication, the fiber-optic

---

more carefully examined considering the nonlinear effect in the fiber, referring to the Non-linear Shannon Capacity.

systems finally evolved to digital communication system. Digital signal processing technology is a powerful tool for a communication system, as long as the mathematics works for the possibility. For example, two astonishingly remarkable techniques are mode-division multiplexing and more dedicated orbital-angular-momentum-division multiplexing, which elegantly utilize the electromagnetic properties of photons to boost the capacity of optical communication systems. In the advanced fiber-optic communication systems, digital signal processing techniques are indispensable to make the information recoverable in the systems by de-multiplexing the signal in a sophisticated manner.

### §1.1.1 The Birth of Optical Source — Laser

The invention of the laser, *Light Amplification by Stimulated Emission of Radiation*, announced a new era in optics, and even the whole human society. On May 16, 1960, Theodore Maiman won the laser race and made the first working laser at Hughes Research Laboratories in Malibu, firing reddish pulses from a ruby cylinder [3]. The laser demonstration is the first embodiment of the elegant theoretical prediction [4] by Charles H. Townes, who invented the precursor of the laser in the microwave spectrum, the maser, and his brother-in-law Arthur L. Schawlow. For the contribution to the maser-laser, Townes was awarded the Nobel Prize in Physics 1964 “*for fundamental work in the field of quantum electronics, which has led to the construction of oscillators and amplifiers based on the maser-laser principle*”<sup>7</sup>, and for the contribution to the laser spectroscopy, Schawlow was co-awarded the Nobel Prize in Physics 1981 “*for their contribution to the development of laser spectroscopy*”<sup>8</sup>.

---

<sup>7</sup> The Nobel Prize in Physics 1964 was divided, one half awarded to Charles Hard Townes, the other half jointly to Nicolay Gennadiyevich Basov and Aleksandr Mikhailovich Prokhorov “for fundamental work in the field of quantum electronics, which has led to the construction of oscillators and amplifiers based on the maser-laser principle”.

— “The Nobel Prize in Physics 1964”. Nobelprize.org. Nobel Media AB 2014. Web. 26 Aug 2016. [http://www.nobelprize.org/nobel\\_prizes/physics/laureates/1964/index.html](http://www.nobelprize.org/nobel_prizes/physics/laureates/1964/index.html)

<sup>8</sup> The Nobel Prize in Physics 1981 was divided, one half jointly to Nicolaas Bloembergen and Arthur Leonard Schawlow “for their contribution to the development of laser spectroscopy” and the other half to Kai M. Siegbahn “for his contribution to the development of high-resolution electron spectroscopy”.

— “The Nobel Prize in Physics 1981”. Nobelprize.org. Nobel Media AB 2014. Web. 27 Aug 2016. [http://www.nobelprize.org/nobel\\_prizes/physics/laureates/1981/index.html](http://www.nobelprize.org/nobel_prizes/physics/laureates/1981/index.html)

The invention of the laser in the very beginning of the 1960s greatly stimulated the whole optical society. In the field of optical communications, people for a long time had been expecting a coherent optical source. In the same year following Theodore's demonstration, Bell Labs showed the potential of using laser for communications by shooting laser pulses through the atmosphere over 25 miles [5].

In the early years, the lasers were not practically suitable for the purpose of communications. They were bulky and relatively unstable. Later in December 1960, the Helium-Neon laser, which is capable of continuously emitting light beam for the first time, was demonstrated successfully [6]. The gas lasers were adequate for experiments in laboratories, but still too bulky and thus not suitable for a practical communication system. In 1962, the much more compact semiconductor laser was first demonstrated [7]. However, the homojunction laser diode then was extremely unstable, and it worked only in liquid nitrogen. Until 1970, the first laser diode able to work in room temperature using the heterojunction structure were successfully fabricated [8, 9]. It was the milestone in the way of applying lasers in our daily life. With the tiny laser diodes, communications with lightwave became practical. Zhores Alferov and Herbert Kroemer were the two of the pioneers who were co-awarded the Nobel Prize in Physics 2000 “*for developing semiconductor hetero-structures used in high-speed and optoelectronics*”<sup>9</sup>.

Before the laser diodes stepped into commercialized optical communication systems, people first needed stable lasers in mass production, which were able to continuously work for decades [10-12]. Until 1977, it was reported by Bell Labs that the double-heterojunction laser diodes were capable of continuously working with average life time over a century if it is at room temperature [13].

---

<sup>9</sup> The Nobel Prize in Physics 2000 was awarded “for basic work on information and communication technology” with one half jointly to Zhores I. Alferov and Herbert Kroemer “for developing semiconductor hetero-structures used in high-speed and optoelectronics” and the other half to Jack S. Kilby “for his part in the invention of the integrated circuit”. — “The Nobel Prize in Physics 2000”. *Nobelprize.org*. Nobel Media AB 2014. Web. 21 Sep 2016. [http://www.nobelprize.org/nobel\\_prizes/physics/laureates/2000/index.html](http://www.nobelprize.org/nobel_prizes/physics/laureates/2000/index.html)

### §1.1.2 The Birth of Optical Channel — Optical Fiber

During the same interim of the birth of the laser, another competition in finding an ideal medium to support the transmission of lasing light from the lasers. In contrast to the laser that demonstrates the capability for optical communication since its birth, it took a long time to convince people that the glass fiber is the ideal medium for optical communications.

The first substantial breakthrough in fiber optics is the practical realization of total internal refraction in the glass fiber, drawing the fibers with cladding whose refractive index is lower than that of the core [14, 15]. The cladded fiber is one remarkable step in fiber optics, though people only came up with one of the naivest communication scheme, the endoscopy, which, so to say, delivers light into human's body and then retrieves the image from the light back [16].

The second breakthrough in fiber optics is the imagination of applying the optical fiber for communications. Though optical fibers were used for tricks, delivering luminosity and medical imaging for a long time, communicating information over a piece of optical fiber was first 'practically' envisioned by Charles K. Kao in the 1960s [17]. He believed that the loss of glass fiber can be lower than 20 dB/km, though a loss of more than 1000 dB/km was observed at that time and most people were skeptical about his idea. 43 years later, he was awarded the 2009 Nobel Prize in Physics for "*groundbreaking achievements concerning the transmission of light in fibers for optical communication*"<sup>10</sup>.

Attenuation was the first barrier in the application of optical fiber for communications. Though Kao along with George Hockman had concluded in 1966 that the loss of the glass fiber can be lower than 20 dB/km [17], Kao's envision had not been widely accepted until he measured a bulk-fused glass with a loss of 4 dB/km two years later. Since then, several groups began the competition

---

<sup>10</sup> The Nobel Prize in Physics 2009 was divided, one half awarded to Charles Kuen Kao "for groundbreaking achievements concerning the transmission of light in fibers for optical communication", the other half jointly to Willard S. Boyle and George E. Smith "for the invention of an imaging semiconductor circuit - the CCD sensor".

— "The Nobel Prize in Physics 2009". Nobelprize.org. Nobel Media AB 2014. Web. 27 Aug 2016. [http://www.nobelprize.org/nobel\\_prizes/physics/laureates/2009/index.html](http://www.nobelprize.org/nobel_prizes/physics/laureates/2009/index.html)

of fabricating optical fiber of low loss. The Corning Glass Works won the first breakthrough. In 1970 a piece of Titanium-doped fiber was successfully fabricated at Corning with a loss of 16 dB/km, or maybe as low as 15 dB/km at 633 nm [18], and in 1972, the Germanium-doped fiber with a loss of 4 dB/km in the wavelength region from 800 nm to 850 nm [19]. In Japan, 0.47 dB/km loss was reported in 1976 [20], and a loss of 0.2 dB/km at 1.55  $\mu\text{m}$  that almost hits the theoretical limit was reported in 1978 [21]. Nowadays, a loss of 0.2 dB/km is still the standard value in the datasheet of the commercial silica fiber.

### §1.1.3 The Evolution of Fiber-Optic Systems

Towards higher capacity and longer distances, as well as lower cost, the fiber-optic communication systems evolve over several distinct generations, each of which is marked by representative techniques and progresses that contribute to the evolution.

In the early days of fiber-optic communications, as the attenuation of optical fibers became practical for communication over long distance, researchers and telephone companies were driven by the attractive potentials of optical fibers to plunge, without any slight hesitation, into the development and deployment of fiber-optic systems. In 1975, when a short fiber-optic link was “accidentally” put in service in England for the first time to replace the electronic communication system of Dorset police that was failed by lightening shock, optical fibers started the career of telecommunication. Meanwhile, a silent competition started in getting the commercial fiber-optic products workable.

As fiber-optic systems were still in experimental phase in the peaceful continent of Europe, the competition was much more intense in North America. In 1977, as field trials of fiber-optic communication systems were taking place in Chicago by AT&T, General Telephone and Electronics suddenly announced their demonstration of telephone services to the public over optical fiber at a speed of 6 Mbit/s in Long Beach, California. After reading the news, AT&T in Chicago soon set off their own telephone traffics, consisting of 672 voice channels at a speed of 45 Mbit/s over 2.4 km. In 1980, AT&T introduced their first commercial fiber-optic system, FT-3 that connected Richmond and New York

City at a data rate of 45 Mbit/s in 1983 and it was extended to Boston in the following year [22].

In the 1970s, the glass fibers easily conquered all the other opponents, such as, microwave, coaxial cables, millimeter waveguides and hollow-core optical tubes, for its unrivalled advantages, which are extremely low loss, high capacity, low cost and flexibility. For example, in the end of 1970s, Bell Labs decided to give up coaxial cables for submarine systems, and AT&T, British Post Office, and Standard Telephones and Cables announced using optical fiber for transatlantic communication system. The result was the transatlantic telephone system, TAT-8, which was completed in 1988.

The systems in the beginning of the 1980s were the first-generation system, which employs multimode fibers together with the GaAs semiconductor lasers that operates at the wavelength of 0.8  $\mu\text{m}$ . The distance of the first-generation systems was limited by the relatively large attenuation, which is about 4 dB/km at the 0.8- $\mu\text{m}$  window. In the systems, repeaters were spaced apart at about 10 km for information delivery at 45 Mbit/s. Still, the 10-km repeater spacing was indeed a remarkable reach compared with other systems equipped with millimeter waveguides and coaxial cables.

To extend the reach of the fiber link, the operation wavelength was diverted from 0.8  $\mu\text{m}$  to 1.3  $\mu\text{m}$  by employing the InGaAsP laser diodes, which launches the light beams with a loss of 0.4 dB/km in the fiber. This kind of systems in the early 1980s was the second-generation fiber-optic system coined by the 1.3- $\mu\text{m}$  window. In this generation, the data rate of the systems was limited considerably because of the multimode propagation of light beams in the multimode fibers, which results in severe inter-symbol interference. To overcome the multimode-dispersion problem, single-mode fibers were put into service in the mid of the 1980s. Coincidentally, the 1.3- $\mu\text{m}$  window is the zero-dispersion region of silica fibers, which means the minimum impairments from chromatic dispersion for longer transmission distance. By operating at the 1.3- $\mu\text{m}$  window using single-mode fibers, the repeater spacing was extended to up to 50 km with data rate hitting 2 Gbit/s.

The theoretical minimum of attenuation of the glass fibers is in the vicinity

of 1.55  $\mu\text{m}$ , while the zero-dispersion region occurs at 1.3  $\mu\text{m}$ . Balancing between the attenuation and dispersion, the third fiber-optic system was evolved to 1.55  $\mu\text{m}$  because lower attenuation means larger repeater distance, and thus less installation and maintenance expense when deploying the systems. So the third-generation system was marked by the 1.55- $\mu\text{m}$  window and the corresponding lasers. On the other hand, to overcome the chromatic dispersion problem, dispersion management techniques were developed, such as dispersion-shifted fibers that shift the zero-dispersion region to 1.55  $\mu\text{m}$  and distributed feedback laser diodes that excite single longitudinal mode. With these technologies, the third-generation systems were able to work at above 2 Gbit/s with repeating distance up to 100 km.

The first three generations of fiber-optic systems were the exploration for the ultimately lowest attenuation promised by glass fibers, diverting the wavelength from 0.8  $\mu\text{m}$  to 1.3  $\mu\text{m}$ , and finally to 1.55  $\mu\text{m}$ . The fourth-generation fiber-optic system was the exploration for the ultimately widest bandwidth promised by the fibers, and it started evolving since the late 1980s. This fourth generation was supported by two fascinating yet practically useful techniques, the optical fiber amplifiers and the wavelength-division multiplexing. The optical amplifiers make the inline optical signal amplification possible. The optical information can be amplified and extended without using the electronic amplifiers that relay the information in an expensive optical-electrical-optical mode. Combining with the optical amplifiers, the idea of using WDM also becomes practical because optical signals can be amplified and extended without converting the optical signals back to electrical signals. Otherwise if the electronic amplifiers are adopted, each wavelength channel should be split out and amplified separately using an electronic amplifier, which is economically impossible in a system comprising hundreds of wavelength channels.

During the 1990s, along with the fourth-generation systems, advances happened everywhere in the optical technologies, including optical fibers, lasers, optical amplifiers, and so on. For instance, in the WDM systems, dispersion-compensation fibers were developed for dispersion management to replace the dispersion-shift fibers. By carefully introducing some amounts of dispersion,

the nonlinear distortion, namely four-wave mixing among the wavelength-division multiplexed channels can be mitigated. Other examples include dry fibers, wideband optical fiber amplifiers. As there were innumerable technology advances, we will not refer to each of them here. More interesting stories about them can be found in the literature, for example in Jeff's historical books, "*City of Light: The Story of Fiber Optics*" and "*Beam: The Race to Make the Laser*", and Agrawal's and Senior's technical books dedicated to fiber-optic communication systems [23-25] etc.

Reflection on the bandwidth explosion of optical fibers can be found in the post-deadline papers reported in the two leading conferences and exhibitions in the field of optical communications. One is Optical Fiber Communication (OFC) Conference and Exhibition in the United States and the other is European Conference on Optical Communication (ECOC) in Europe.

On March 3, 2000, three days before the bust of the "Telecom Bubbles" in NASDAQ, in the post-deadline session of Optical Fiber Conference, records on the highest and longest fiber-optic signal transmission stimulated people's confidence in fiber-optic communications. For example, in Bell Labs, 82 wavelength channels, each of them operating at 40 Gbit/s, hit a data rate of 3.28 Tbit/s over 300-km fiber transmission. Meanwhile, by combining 160 wavelength channels, each of which was operating at a speed of 20 Gbit/s with 0.4-nm (equivalently 50 GHz) channel spacing, the total 3.2-Tbit/s signals, spanning over 64 nm in wavelength, and were successfully transmitted over 1,500 km in the NEC Labs.

In the following year, by upgrading their 20-Gbit/s data rate per channel to 40 Gbit/s, and increasing the number of wavelength channels to 273, 10.92 Tbit/s signals, spanning 100 nm in wavelength, over 117 km was recorded and reported in the post-deadline session in the 2001 Optical Fiber Communication Conference [26]. In the same conference, the researchers in Alcatel employed polarization-division multiplexing recorded 10.2 Tbit/s signal transmitted over 100 km at a spectral efficiency of 1.28 bit/s/HZ. In their demonstration, there were 128 wavelength channels, each of which consists of two 42.7 Gbit/s (40

Gbit/s taking forward error correction overhead into account) polarization-division multiplexed signals.

Behind the astonishing records are the amazing optical fiber technologies, which are innumerable and a few of their names are, for example, high-performance lasers, high-speed modulators, low-loss fibers, dispersion compensation fibers, optical amplifiers, and wavelength-division multiplexing (WDM), and as well as the polarization-division multiplexing [27-32] etc.

Until the fourth generation, the spatial reach and available bandwidth of the optical fiber had been almost fully exploited. Although there are some specific limitation in the optical fibers, such as fiber nonlinearity, needed to be solved, spectral efficiency is the next primary quest in fiber-optic systems.

## §1.2 Digital Signal Processing in the Advanced Fiber-Optic Systems

In more than 30 years, from the end of the 1970s to the beginning of the 2000s, fiber-optic communication systems witness a surge in information revolution, and support the advent of Information Age. The first four generations of fiber-optic systems take advantages of the two merits offered by the inherent clarity of optical fibers; one is the extremely low loss and the other is the tremendous vast usable bandwidth, which can be reflected by a single chart, from 1260 nm to 1675 nm, which were divided into six bands, that from the **O**riginal (1260–1360 nm) and **E**xtended (1360–1460 nm) bands, to the **S**hort (1460–1530 nm), **C**onventional (1530–1565 nm), **L**ong (1565–1625 nm), and **U**ltra-long (1625–1675 nm) wavelength bands, spanning 58.95 Terahertz or 58,950,000,000,000 Hertz.

In the decade of the 1990s, the capacity, or we say data rate which is a more intuitive measure of capacity, doubled every 6 months, due to the expansion in bandwidth. Nonetheless, when we refer to capacity of a communication system from the view of information theory, the capacity is the product of two factors. One is the bandwidth, and the other is spectral efficiency.

For example, in the 2001 record, the 10.92 Tbit/s signals were spanning over 100 nm in wavelength (covering S-, C-, and L-bands), which is approximately in total 13.65 Terahertz in bandwidth. In terms of the spectral efficiency, one can inferred from the ratio

$$\frac{10.92 \text{ (Tbit/s)}}{13.65 \text{ (THz)}} \approx 0.8 \text{ (bit/(s} \cdot \text{Hz))}$$

merely. That we say “merely” is because in electronic communications systems, spectral efficiency over 10 bit/s/Hz was a reality in the commercial systems already, and the digital signal processing are of importance for the advance in spectral efficiency in the electronic systems. Although another record of 10.2 Tbit/s signal transmission, by employing polarization-division multiplexing, reached the spectral efficiency of 1.28 bit/s/Hz for a single wavelength channel, the spectral efficiency is still 0.64 bit/s/Hz for each polarization multiplexed channel.

Prior to the application of advanced digital signal processing for fiber-optic communication systems, simple modulation formats, such as on-off keying and duo-binary modulation, are preferred. However, they offer low spectral efficiency, which is lower than 1 bit/Hz/s per polarization. Hence, in fiber-optic communication, in the direction of greedy pursuit of higher capacity, the pursuit of spectral efficiency inevitably becomes the only choice as the available bandwidth of the optical fibers has been fully exploited. The historic trend with regards to the evolution of capacity is also true in other communication systems, especially the wireless mobile system.

The benefits of applying DSP technology in the fiber-optic communication systems, in principle, can be categorized into two main functions. The first one is the application of spectrally efficient modulation techniques, and the second is the enhancement in signal recovery that guarantees the successful recovery of the spectrally efficient signals, which experiences severe impairments after transmission.

In wired and wireless communication systems, the spectral efficiency had already hit up to 10 bit/s/Hz within a relatively narrow bandwidth of several

mega Hertz two decades ago [33, 34]. Before 2000, DSP technology was almost exclusive to the electrical communication systems. Recently, in the fiber-optic communication systems, with the maturity of coherent optical detection and progress of high-speed electronics, DSP achieves tremendous progress for the fiber-optic communication. For example, combining with polarization division multiplexing, in the recently experiments a 2048 QAM signal transmitted information with spectral efficiency of 15.3 bit/s/Hz at a speed over 66 Gbit/s using a single optical wavelength [35-37]; combining with the mode division multiplexing, a spectral efficiency of 43.63 bit/s/Hz is achieved by using 30 spatial modes within a single multimode fiber using a single wavelength [38]. In these demonstrations, the DSP technology is one of the indispensable foundations underlying the astonishing achievements.

Another remarkable advantage promised by DSP technology is that the detrimental effect in the optical fiber can be compensated at the receiver. In optical fiber, dispersion, which include chromatic dispersion, polarization mode dispersion etc., is one of the major factors limiting the data rate of a fiber-optic system. It introduces linear distortion on the signal. The effect of dispersions is proportional to the length of fiber transmission and the bandwidth of the signal. Previously in fiber-optic systems, the bulky in-line compensation modules using dispersion compensation fiber (DCF) are inserted into fiber link to compensate the chromatic dispersion. However, it increases the labor on system design and deployment, and is not suitable for fiber-optic systems aiming for flexible network routing. Other approaches to mitigate the effect of dispersion effect include robust modulation formats using, such as, duobinary, and the spectral shaping techniques at the transmitter using “pre-chirping” etc. [39]. However, these technologies should be carefully designed for various fiber-optic systems. For example, the “pre-chirping” is suitable for a fixed distance of optical link, and if the distance of link changes, the pre-chirped signal will be mismatched with the link and introduce residual chromatic dispersion.

With the introduction of DSP for fiber-optic system, not only the chromatic dispersion but the polarization mode dispersion and even the fiber nonlinear effect can be compensated. Compared to its optical counterpart, electronic

compensation via DSP is more flexible since the structure of optical links (networks) are transparent. The detrimental effects can be compensated at the receiver end without considering the physical structure of the optical link.

There are numerous advanced techniques enabled by DSP technology, and in this dissertation, we will focus on the multicarrier transmission systems, including orthogonal frequency-division multiplexing and a variant of OFDM system — Fast-OFDM, and also propose an orthogonal chirp-division multiplexing scheme based on the discrete Fresnel transform in this dissertation.

### §1.2.1 Orthogonal Frequency-Division Multiplexing

Multicarrier systems, in contrast to single-carrier systems, are communication systems that transmit information via multiple spectrally separated carriers. It can also be called frequency-division multiplexing when we refer to the information multiplexing scheme because information is simultaneously transmitted over the frequency-domain sub-channels that share the same channel medium. That is different to the single-carrier systems or equivalently time-division multiplexing scheme in which information is transmitted in order upon a single carrier along with the time axis. Strictly speaking, the concept of single-carrier and multicarrier is different to the concept of time-division multiplexing and frequency-division multiplexing because the former is about how the information is conveyed over the logical channels while the latter is about how the physical channel medium is shared for information conveying. Nonetheless, they are exchangeable most of the time.

As shown in Figure 1–2 (a), by dividing the entire bandwidth into the spectrally disjoint sub-bands, frequency-division multiplexing or multicarrier system conveys information over the sub-bands, each of which is corresponding to a single-carrier channel and is parallel to the other channels in the frequency domain. We call the sub-bands as sub-channels or subcarriers hereafter. Guard bands are inserted between the subcarriers to avoid interference between them. The guard bands should be chosen to be sufficiently large to separate the subcarriers, or otherwise inter-subcarrier interference occurs between the subcarriers, as shown in Figure 1–2 (b). Although the guard bands can be compressed

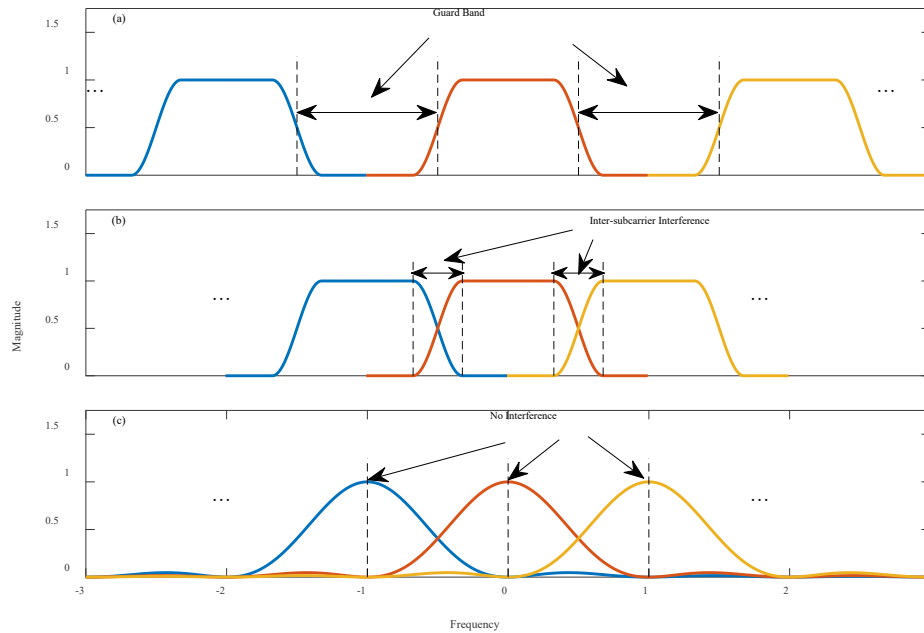


Figure 1–2. Illustration of the spectra of FDM system of different conditions. (a) Conventional FDM system with sufficient guard bands, (b) a FDM system with inter-carrier interference due to spectral overlapping induced by insufficient guard bands, and (c) the orthogonal FDM condition with spectral overlapping but no interference presenting at the frequency sampling points at each subcarriers.

to a certain limit by compacting the spacing of the subcarriers, spectral efficiency is limited less than half of the theoretical Nyquist rate.

Orthogonal frequency-division multiplexing, as illustrated in Figure 1–2 (c), is such a frequency-division multiplexing scheme that the spectral efficiency achieves the critical point exactly at the Nyquist rate by overlapping the subcarriers in the spectrum and meanwhile information on the subcarriers can be extracted without any interference in favor of the “orthogonality”. High-speed communication is realized by synthesizing a large number of orthogonal narrowband subcarriers, which are essentially harmonics. The narrowband subcarriers have fairly long symbol period and thus is robust against inter-symbol interference due to dispersion, and simple single-tap equalizers can be easily applied to compensate each subcarriers. In contrast, in wideband single-carrier systems, as symbol period is extremely small, the symbols are sensitive to the

inter-symbol interference during channel transmission, and multi-tap equalizers, which involve considerably intensive computation complexity as the dispersion is severe, should be employed for dispersion compensation.

The concept of OFDM was initially proposed by Chang in the Bell Labs in the 1960s. Mathematically speaking, given a symbol period  $T$ , if the frequency spacing of the subcarriers,  $\Delta f$ , are at multiple of the reciprocal of symbol period  $T$ , that

$$\Delta f = \frac{1}{T_s}, \quad (1.2)$$

the synthesized signal of the bunch of subcarriers,  $s(t)$ , is

$$s(t) = \sum_k x(k) e^{j2\pi k \Delta f \cdot t} \quad (1.3)$$

where  $0 < t \leq T$  and  $k$  is the index of the  $k$ -th subcarrier. Each of the orthogonal subcarriers can be demodulated without any interference from the other subcarriers even if its spectrum overlaps with the other subcarriers (see Figure 1–2 (c)), by its matched-filter, as

$$\begin{aligned} \hat{x}(m) &= \int s(t) e^{-j2\pi m \Delta f \cdot t} dt \\ &= x(m), \end{aligned} \quad (1.4)$$

where  $\hat{x}(m)$  is the demodulated symbol on the  $m$ -th subcarrier.

However it did not get much attention then because digital electronics was still in its infancy. In the 1970s, efforts were made to realize the orthogonality for the OFDM systems in analog approach by using filters, and the hardware complexity to achieve the orthogonality in the OFDM was a still challenge.

Until the 1980s, two ideas fueled the OFDM for electronic communication systems. One is the proposal of digital implementation of the OFDM system by using the computationally efficient fast Fourier transform (FFT), and the other is the proposal of a cyclic prefix for OFDM signal to make the OFDM signals meet the convolution-multiplication property of the DFT. Since then, OFDM revived for information communication, and the ADSL system was the

first success of OFDM for commercial system in the 1990s. In wireless communications, OFDM becomes the core candidate in physical layer in 3GPP, and it later evolved from the beyond 3G standard LTE to the 4G LTE-Advance and even the future 5G system.

In optical communications, OFDM intervened around 2006 along with the advance of the high-speed electronic technology, which is the physical support of the DSP technology. With the abundant experience of the OFDM system in electronic communication, OFDM has been one of the hottest topics from both scientific and industrial points in the optical society.

In fiber-optic communication, depending on the application scenarios, there mainly two research targets, to which OFDM is dedicated. The first one is the intensity-modulation and direct-detection (IM/DD) fiber-optic systems for the low-cost short-reach systems, such as access networks, front-haul facilities and data centers. The second is the coherent fiber-optic systems for high-capacity and/or long-haul systems, such as the intercontinental networks. Depending on the applications requirements, various OFDM schemes are proposed. In this dissertation, we will focus on a variant of OFDM system, namely Fast-OFDM.

### §1.2.2 Fast-OFDM — A Variant of OFDM

Generally speaking, OFDM is actually a terminology for the FDM or multicarrier systems whose subcarriers are mutually orthogonal, achieving the maximal spectral efficiency at the Nyquist rate. OFDM can be adapted into a communication system depending on the specific requirements and applications.

Fast-OFDM is a variant of OFDM system, by further reducing the subcarrier spacing by half compared to the OFDM system. In the mathematical words, the subcarrier spacing in Eq. (1.2) is rewritten as

$$\Delta f = \frac{1}{2T_s}. \quad (1.5)$$

One may be wondering if the halved subcarrier spacing increases the spectral efficiency by twice. However, it is not true. In the Fast-OFDM system, the phase of the subcarriers should be well-aligned to remain the “orthogonality”.

It means that the subcarriers in Fast-OFDM offers only a single dimension for modulation to encode the information while the subcarriers in the conventional OFDM have two independent dimensions for information modulation.

Different schemes can be adopted to implement the Fast-OFDM systems for various applications. For example, the double-sideband modulated Fast-OFDM system, which can be realized by the real-valued cosine transforms, is suitable for baseband transmission and intensity or envelope modulation systems. More details about the double-sideband modulated Fast-OFDM can be found in Chapter 4 in this dissertation. For spectrally efficient systems, single-sideband modulated Fast-OFDM system can be implemented by using the complex-valued Fourier transform by truncating the time-domain signal by half. The single-sideband modulated Fast-OFDM will be studied in Chapter 5.

The concept of Fast-OFDM was presented in 2002, and then introduced for fiber-optic communications around 2009. For its unique property, Fast-OFDM is an interesting candidate of OFDM systems, and has its applications for different purpose. For example, the double-sideband (DSB) modulated Fast-OFDM scheme is suitable for the baseband systems, such as the DSL systems, and IM/DD fiber-optic systems. In contrast, the discrete multi-tone (DMT) system is an OFDM variant, by mapping complex-conjugated subcarriers around the DC, for these applications. For coherent detection systems, the SSB modulated Fast-OFDM scheme could be a choice by transmitting the spectrally efficient single-sideband modulated signals.

In spite of the interesting features of Fast-OFDM systems due to the halved subcarrier spacing, there are limitations and drawbacks due to the halved subcarrier-spacing, which greatly restrict the application of Fast-OFDM systems. For example, the multiplexing kernels in the Fast-OFDM systems, neither the discrete cosine transform nor the truncated discrete Fourier transform, possess the convolution-multiplication property as the Fourier transform does. In the following, we have a brief discussion about how the drawbacks arise and to what extent they limit the application of Fast-OFDM system.

## ✚ EQUALIZATION PROBLEMS HANGING OVER THE FAST-OFDM

In the DSB modulated OFDM, DCT is employed for subcarrier multiplexing. There are four types of DCTs and all of them are orthogonal transforms, and in particular the second and the third DCTs are a transform pair that are mutual inverse, and are adopted to implement the DSB modulate Fast-OFDM system. If there is no channel transmission and timing synchronization is assumed to be perfect, the receiver is able to recover the information because DCT is orthogonal. However, if there is channel transmission, DCT should possess a convolution-multiplication property, similar to that of DFT, to guarantee that the information is recoverable in the frequency domain. Fortunately, the DCTs possess a symmetric convolution-multiplication property. According to the symmetric convolution-multiplication property of DCT, if the channel impulse response is a symmetric function, and the sampling timing is exact at the symmetric point and symmetric prefix and suffix are attached to the Fast-OFDM signal, the information can be recovered, and the symmetric channel becomes multiplicative coefficient on each subcarriers. Nonetheless, practical channel can hardly satisfy the symmetric requirement, and exact sampling timing is a strict operation for the OFDM based systems. The difficulties restrict the application of the DSB modulated Fast-OFDM system in a practical communication system.

The situation gets worse in the SSB modulated Fast-OFDM system. In SSB Fast-OFDM, a truncated DFT, which is not even orthogonal or unitary, is employed for subcarrier multiplexing. The loss of orthogonality of the multiplexing kernel leads to severe interference between the subcarriers even if there is no channel transmission. Moreover, if channel transmission presents, which is inevitable situation in any practical communication system, there is no convolution property, not even the symmetric convolution property as the DCT possesses. If the channel response is ideal, which is a Dirac impulse, with perfect timing synchronization, interference degrades the system performance due to loss of orthogonality. If the channel is not flat or there is residual timing offset, the system cannot even work correctly due to the absence of a convolution

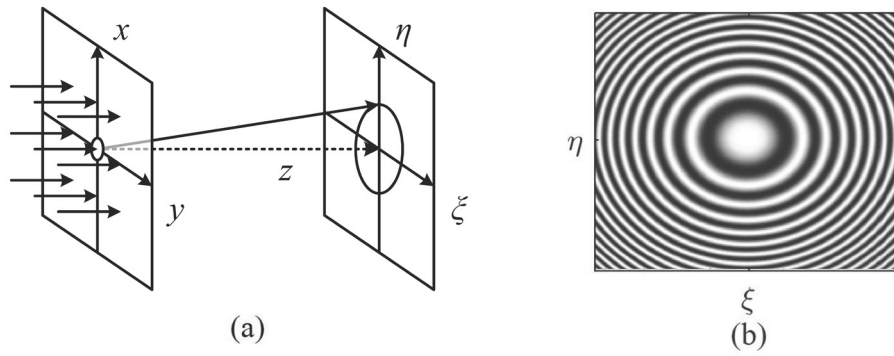


Figure 1–3. Illustration of (a) Fresnel diffraction, and (b) the diffraction pattern on the plane.

property.

For the DSB modulated Fast-OFDM systems, several methods had been proposed to resolve the channel equalization problem. For example, it is proposed to transmit a symmetric replica of the Fast-OFDM signal to emulate a symmetric channel. The data rate is reduced by halved as a tradeoff. Another proposal is the adoption of time-domain pre-filter at the receiver end to shape the overall impulse response of the system to be symmetric. However, the reason why we choose OFDM, as well as the Fast-OFDM, is to avoid the use of complex time-domain filter that has a polynomial complexity with respect to the dispersion.

In this dissertation, the channel equalization and signal recovery problems in the DSB and SSB modulated Fast-OFDM systems are addressed in Chapter 4 and Chapter 5, respectively.

### §1.2.3 Discrete Fresnel Transform

Fresnel transform is a trigonometric integral transform that constantly occurs in optics and physics to describe the diffraction pattern of grating, as shown in Figure 1–3. It is of the same transform family as the Fourier transform as the canonical transformation, but Fourier transform is more widespread and powerful in numerous scientific subjects for its elegant mathematic properties, and one of its famous properties is the convolution-multiplication property, namely the convolution theory. It states that the Fourier transform of a convolution is the point-wise multiplication of the Fourier transforms. The discrete version

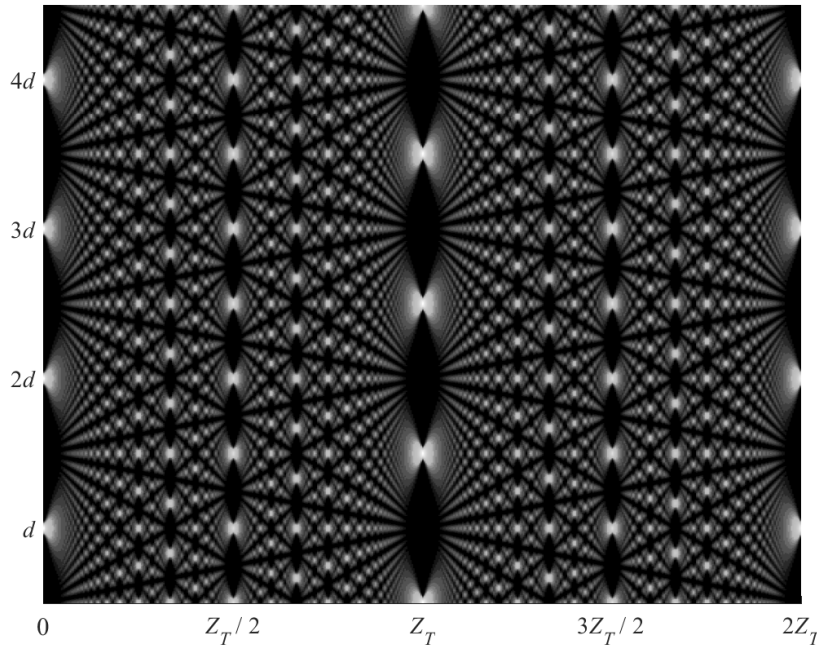


Figure 1–4. Illustration of Talbot effect.

of Fourier transform, discrete Fourier transform makes the Fourier transform practically useful in the field of digital signal processing and other areas.

In contrast, the Fresnel transform is always interpreted by the Fourier transform and rarely used for digital signal processing. One reason is that the Fresnel transform does not hold the easy properties as the Fourier transform does. Another one is that, although there are some derivations of the discrete Fresnel transform, there is no discrete Fresnel transform in the literature inheriting the corresponding properties of the Fresnel transform in the continuous domain. For example, some of the DFNTs are not even orthogonal, and no convolution property has been observed from the derivations. The awkward situation may be partly because of the powerful Fourier transform and partly because physicists usually employ the DFNT to describe the coefficients of diffraction fields in the so-called Talbot image, as illustrated in Figure 1–4, rather than regarding it as a general mathematic tool.

In this dissertation, a discrete Fresnel transform is derived, and the derived DFNT possesses the corresponding properties to that of the continuous Fresnel

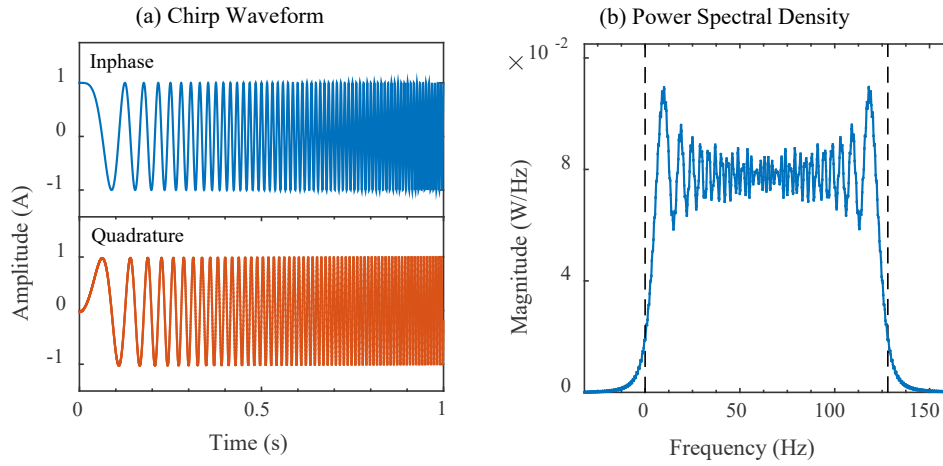


Figure 1–5. Illustrations of (a) a linear chirp with a normalized chirp rate 128 and a duration 1 second, and (b) its power spectrum density.

transform. One important properties with regards to the convolution process is also proved. The convolution property of the DF<sub>n</sub>T is, somewhat, different to that of the DFT. It is shown that the DF<sub>n</sub>T preserves the convolution, and the convolution-preservation property of DF<sub>n</sub>T states that the DF<sub>n</sub>T of a circular convolution of two functions is the convolution between one of the functions and the DF<sub>n</sub>T of the other. These properties could possibly make the Fresnel transform more attractive than before as a general mathematical tool, for applications such as digital signal processing.

#### §1.2.4 Orthogonal Chirp-Division Multiplexing

The proposal of the concept of orthogonal chirp-division multiplexing is the first concrete application of discrete Fresnel transform in this dissertation in favor of the chirped phase in the Fresnel transforms.

Chirped waveforms, as illustrated in Figure 1–5, have a long history in radar and communication systems for its unique and attractive properties, including its constant amplitude and the capabilities of spreading spectrum and pulse compression, etc. In communication systems, the chirped waveforms are resilient to the detrimental effects, such as interference and noise, in the communication channels, and secure the information by hiding the signal even below the noise floor. However, nothing comes free and the spectral efficiency of the

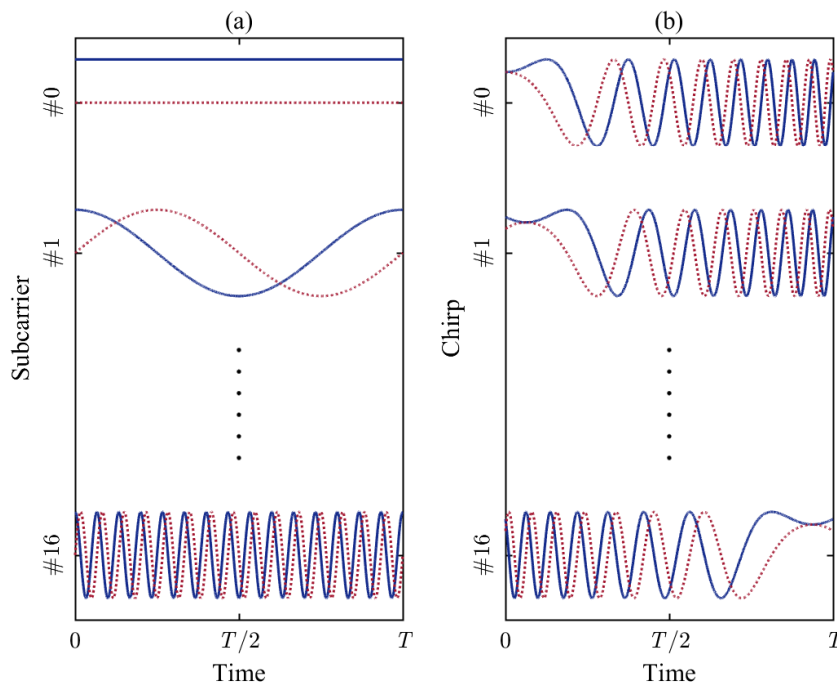


Figure 1–6. Illustration of a family of 16 orthogonal waveforms in OFDM and OCDM. The in-phase (solid) and the quadrature (dots) components of the linear (a) waveforms in OFDM, and (b) chirped waveforms in OCDM.

chirp spread spectrum system is sacrificed for these advantages, because only one chirped waveform, which occupies a wideband, can be modulated for transmission each time to avoid interference.

Orthogonal chirp-division multiplexing is in essence the principle of multiplexing a large number of orthogonal chirped-waveforms that sharing the same bandwidth simultaneously for high-speed communication, as illustrated in Figure 1–6. It achieves the maximum spectral efficiency for the CSS systems theoretically, and meanwhile it inherits the advantages of the CSS. The very fundamental theory behind the OCDM is the Fresnel transform and discrete Fresnel transform. The orthogonality of the Fresnel transforms ensures the interference-free multiplexing of the chirps, and their convolution-property mathematically formulates the transmission of OCDM signals over communication channels. More dedicated system designs and algorithms are also proposed in this dissertation by utilizing the properties of discrete Fresnel transform. One example is the proposal of an algorithm to implement the single-tap equalizers

to simplify the complexity of the OCDM, and its complexity is similar to the OFDM systems. Moreover, for the intrinsic relation between the Fresnel transform and Fourier transform, it is shown that the OCDM system can be easily integrated into the widespread OFDM systems, and it potentially provides better performance than the OFDM systems.

In Chapter 6, analysis is also provided to show the advantages of the proposed OCDM system, and numerical simulations are carried out to study the performance of OCDM system from different aspects, such as the resilience to different system impairments and the performances of nonlinear equalizers and forward error coding. Experiments were also successfully implemented to validate the feasibility and advantages of the proposed OCDM system in coherent optic systems at a data rate of 36 Gbit/s. The results further confirm that the OCDM systems outperforms the OFDM and single-carrier frequency-domain equalization systems, especially, in severe channel conditions.

### §1.3 Outline of the Dissertation

This dissertation is organized as follows.

In Chapter 2, we briefly introduce the basis of a digital communication system and the essential mathematical models formulating a digital communication system, which mainly include information modulation and demodulation, and the channel models based on the linear time-invariant theory in continuous time and discrete time models, and the discrete-time model in the matrix form.

In Chapter 3, the building blocks of a fiber-optic communication system are presented based on Chapter 2, and the basic components and devices employed in the advanced fiber-optic systems are introduced. Based on the mathematical model in Chapter 2, the mathematical models of optical modulator, optical fiber channel, and optical receiver are studied.

In Chapter 4, the DSB modulated Fast-OFDM system based on DCT is studied. With the formulation of the model of the DSB modulated Fast-OFDM signal over general LTI channel, the inability of applying single-tap equalization

in the DSB Fast-OFDM system, resulting in significant performance degradation, is analytically revealed as the result of the symmetric-convolution property of the DCT.

The algorithm to efficiently implement the single-tap equalization for the DSB modulated Fast-OFDM system is proposed. Numerical simulations are provided in both multimode fiber and wireless radio channels to validate the advantages of the proposed scheme. Experiments are carried out to implement the proposed scheme into IM/DD system in both the conventional 1.55  $\mu\text{m}$  system using standard SMF and the new 2  $\mu\text{m}$  system using HC-PBGF.

In Chapter 5, the SSB modulated Fast-OFDM system based on the truncated DFT is studied. It is shown that in the SSB modulated Fast-OFDM, the transform kernel does not hold a convolution property and is even not orthogonal. Except for the inability of applying single-tap equalizers, there is severe inter-carrier interference existed the system. As a result, the performance is limited even there is not channel transmission, and the degradation is more pronounced as the number of subcarriers is small. The closed-form bit-error ratio performance of the convention SSB modulated Fast-OFDM signal is derived in this Chapter to give a more clear view on how the interference affects the system.

The transceiver design of the SSB modulated Fast-OFDM is proposed with efficient single-tap equalization and signal recovery algorithm that completely eliminates the nasty inter-carrier interference. As a consequence, the proposed SSB Fast-OFDM gets better performance than the convention schemes, and the channel impairments can be easily compensated. Numerical simulation and experimental implementation under conventional 1.55- $\mu\text{m}$  system are performed to show the advantage of the proposed scheme. Moreover, in the experiment, the SSB modulated Fast-OFDM signal is transmitted at 36 Gbit/s with a spectral efficiency of 6 bit/s/Hz, for the first time.

Chapter 6 is logically divided in two parts; one is the discrete Fresnel transform and the other is orthogonal chirp-division multiplexing, which is the application of the DF<sub>n</sub>T in communication system. In particular, the continuous Fresnel transform and DF<sub>n</sub>T mathematically formulate the principle of OCDM in continuous-time and discrete-time models, respectively.

Firstly, the discrete Fresnel transform is derived from the Talbot effect, and the unique properties possessed by the DF<sub>n</sub>T in this dissertation are presented. Of the properties, the convolution-preservation property is the highlight of the DF<sub>n</sub>T, which states that the DF<sub>n</sub>T of a circular convolution of two is equal to the DF<sub>n</sub>T of either one circularly convolving with the other. Its relation with other chirp sequences and polynomial phase sequence is also discussed.

Secondly, according to the Fresnel transform and the DF<sub>n</sub>T proposed in this dissertation, the principle of orthogonal chirp-division multiplexing (OCDM) is proposed to multiplex a bunch of orthogonal linearly chirped-waveforms for high-speed communication. Based on the convolution-preservation property of DF<sub>n</sub>T, the transmission of OCDM signals under linear time-invariant filtering channel, which is able to model the most majority of communication channels, is analytically studied. The detailed system design of OCDM is also discussed. It is shown that the OCDM is able to easily be integrated to the widespread OFDM systems with minor revisions.

Simulation under both the wireless and fiber-optic channels are provided to validate the feasibility of the OCDM system and to show its advantages over the OFDM system. The proposed OCDM system is also experimentally implemented with a data rate of 36 Gbit/s using coherent optical detection.

## §1.4 Contributions of the Dissertation

The contribution of the thesis mainly has two parts. The first part is dedicated to the DSB and the SSB modulated Fast-OFDM systems, to resolve the channel equalization and signal recovery problems therein. The second part is the derivations of the DF<sub>n</sub>T, as well as the derivation of its unique properties, and the proposal the OCDM system, which gets superior performance than the conventional OFDM and SC-FDE systems.

### DOUBLE-SIDEBAND AND SINGLE-SIDEBAND MODULATED FAST-OFDM SYSTEMS

In the first part, we target on the equalization and signal recovery problems in the SSB and DSB Fast OFDM systems, which have bothered the implementation of the Fast-OFDM systems for a long time. The basic principle to resolve the problems is to utilize the halved subcarrier spacing of Fast-OFDM signals compared to that of conventional OFDM signals. Using dedicated algorithms, both the DSB and the SSB modulated Fast-OFDM signal can be demodulated without interferences, and single-tap equalizers can be applied for channel dispersion compensation.

By doing so, the system complexity of both systems can be greatly relieved for the application of simple single-tap equalization and the exact timing synchronizations in the systems are no longer compulsory.

Detailed performance analyses for both systems are also provided. For example, in the SSB modulated Fast-OFDM system, the closed-form BER performance is derived as a function of received signal-to-noise ratio and the number of subcarriers, which is useful when implementing the systems in practical systems.

For the DSB modulated Fast-OFDM system, simulation under multimode fiber and wireless radio channels, in which severe inter-mode dispersion and multipath propagation dispersion exist, are carried out to validate the proposed DSB Fast-OFDM system. Advantages are reflected in these results and discussions over the conventional DSB Fast-OFDM system. Moreover, experiments in both the conventional 1.55- $\mu\text{m}$  silica single-mode fiber system and the new 2- $\mu\text{m}$  system using hollow-core photonic bandgap fiber were successfully implemented to validate the advantages.

For the SSB modulated Fast-OFDM system, simulations under single-mode fiber using coherent optical detection are provided, and the comparison with conventional SSB modulate Fast-OFDM are investigated in detail. As a result of the settlement of the equalization problem and inter-carrier interference, the proposed SSB modulated Fast-OFDM signal was successfully demonstrated at a speed of 36 Gbit/s, with a spectral efficiency of 6 bit/s/Hz.



## DISCRETE FRESNEL TRANSFORM AND ORTHOGONAL CHIRP-DIVISION MULTIPLEXING

In the second part in Chapter 6, the main contributions are the discrete Fresnel transform and the so-called OCDM system.

In the literature, Fresnel integral transform is always regarded as a mathematical description of the Fresnel diffraction. Some studies focused on the discrete Fresnel transform is to numerically analyze the Talbot effect, and there is no decent representation of a discrete Fresnel transform as a general mathematical tool. One reason may be that the Fourier transform is a more powerful for its attractive mathematic properties, and another may be that the discrete Fresnel transforms derived before loss some important properties because physicians almost just need the numerical values in the discrete Fresnel transform.

In this dissertation, by the careful assumption of the Talbot effect which is formulated by infinite periodic extended gratings, the discrete Fresnel transform is derived. Compared to other discrete Fresnel transform, the discrete Fresnel transform here possesses useful mathematical properties, such as completeness, unitary etc. One important property in terms of convolution is also proved here, namely the convolution-preservation property that says the DF<sub>n</sub>T of a circular convolution is equal to the DF<sub>n</sub>T of either one circularly convolving with the other. It is an important property in lots of area, just like the convolution-multiplication property of the Fourier transform, which says the Fourier transform of a convolution two functions is equal to the multiplication of their Fourier transforms.

A new concept of orthogonal multiplexing scheme for high-speed communication, named as orthogonal chirp-division multiplexing is proposed. In the proposed OCDM system, under certain conditions, the linearly chirped-waveforms are mutually orthogonal. It means that though the chirped-waveforms occupy the same temporal period and frequency band, the information can be modulated onto and demodulated from these waveforms without any interference.

Chirped waveforms have a long history for the purpose of secure and robust

communication, technically named frequency modulation or chirp spread spectrum. However, in the CSS system, spectral efficiency is sacrificed because there are severe interference in the system if two chirps are transmitted simultaneously. The proposal of OCDM successfully solves this problem in a sense of orthogonality, and it achieves the maximum spectral efficiency for the CSS systems in the view of Nyquist and Shannon. The relation between OCDM and CSS is somewhat similar to the OFDM and frequency-division multiplexing. In the conventional FDM systems, guard bands are inserted between the frequency sub-bands, while OFDM, under certain conditions, achieves the maximum spectral efficiency by spacing the spectrally overlapped sub-bands in the same period.

It will be shown that the Fresnel transform and discrete Fresnel transform mathematically underlies the OCDM system since the kernels of Fresnel transforms are linear chirped phase. The orthogonal chirps can be exactly described by the Fresnel transform, and moreover their unique properties can be applied for the OCDM system. In more detail, the continuous Fresnel transform formulates the continuous-time OCDM system model and the discrete Fresnel transform formulates the discrete-time OCDM system model and the digital implementation of the OCDM system. Based on the Fresnel transforms, the performance of the OCDM system over linear time-invariant filtering channel are analyzed in detail.

Simulations are also provided to investigate the proposed OCDM system in both wireless radio and single-mode fiber channels. It is shown that in favor of the chirped-waveforms the OCDM outperforms both the single-carrier and the OFDM systems, especially in severe conditions. For example, for the nature of spectrum spreading, OCDM gets considerable improvement in wireless multipath channel by utilizing the multipath diversity compared to the OFDM system. For the temporal spreading, the performance of OCDM system is much better than the single-carrier systems in the case of insufficient guard interval. In the wireless radio channel, the performance are investigated using antenna diversity, nonlinear equalizers and forward error coding. In addition, the compatibility to the OFDM system is discussed to show that the OCDM system can be easily integrated to the existed OFDM systems.

Furthermore, experiments over coherent optical system were carried out to study the proposed CO-OCDM system at a data rate of 36 Gbit/s. The experiment results are in consistent with the analysis and numerical simulation. It is confirmed that the CO-OCDM system is more resilient to the noise effect than the CO-OFDM system if there is no signal pre-emphasis. Since the signal pre-emphasis requires a close loop in the system, the OCDM system seems to be more practical to implement high-speed communication systems.

## Chapter 2

# Mathematical Models of Digital Communication Systems

The formulation of mathematical models of the building blocks in a communication system is of the most crucial importance for the analysis and design of the system. The essential elements of a digital communication system, as illustrated in Figure 2–1, consist of a *transmitter*, which processes the information from the source and modulates the information onto physical carrier desirable for transmission, a *channel*, which serves as the physical medium between the transmitter and the receiver, taking care of the transmission of the information-bearing carrier, and a *receiver*, which demodulates the information from the carrier and delivers the recovered information to the destination.

Roughly speaking, the transmitter consists of an information encoder and a modulator and the receiver consists of a demodulator and an information decoder. The *mathematical model of the information encoder* describes how the information from the source is encoded, typically, in the form of bits, and the *mathematical model of the modulator* describes how the information bits are manipulated and modulated onto the physical properties of a carrier, which is suitable for transmission, such as the electrical field in copper wire, the electromagnetic wave in wireless radio, and even the electromagnetic wave in the

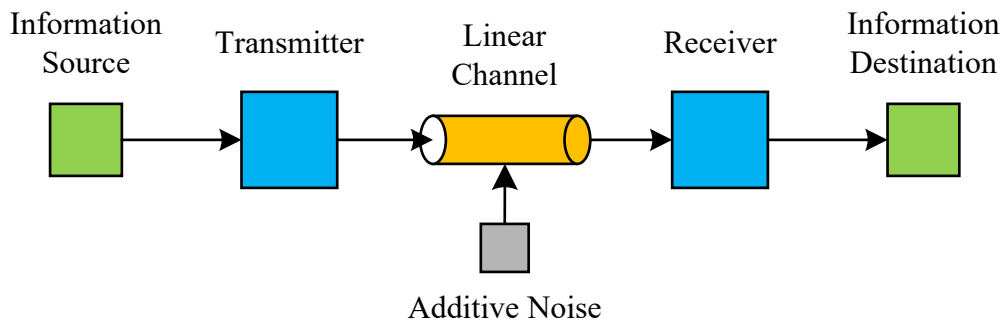


Figure 2–1. Block diagram of a general communication system under a linear channel with additive noise.

form of light. The *mathematical model of demodulator* describes how the information are extracted from the properties of the carrier quantitatively. Generally, additionally operations, such as synchronization and distortion compensation, are required to guarantee information recovery as there are various distortions and corruptions imposed on the carrier during the transmission in the channel. The *mathematical model of information decoder* describes how the information bits are recovered from the digital numbers with fidelity high enough.

The characteristics of the physical channel affect or even determine the design of a communication system. If there is no distortion and corruption at all from the channel, the information can be perfectly recovered by the receiver, and there would be no challenge for the design of communication systems. In fact, there are various detrimental effects in communication channels, which make the design of a communication system fascinatedly challenging. The first, as well as the most critical, step towards the challenges is mathematically modelling the channel of interest, to abstracting the most important physical features of the channel, as exact as possible.

This chapter is dedicated to the mathematical models of the elementary functional blocks in a digital communication system, as shown in Figure 2–1. Specifically, we will be presenting the models of information encoder and modulator at the transmitter and that of demodulator and decoder at the receiver. We pay much attention to the most fundamental channel model, i.e.,

the linear time-invariant (LTI) filtering channel with the additive white Gaussian noise (AWGN), which can be applied to most communication channels, such as the wireless radio channel, copper wire, and coaxial cable, as well as the optical fiber channel, the leading role of this thesis.

Based on the mathematical models discussed in this chapter, we can easily apply these mathematical models into the analysis and design of the fiber-optic communication systems in Chapter 3. Fiber-optic communication system is a very specific, as well as, one of the most successful implementations of digital communications. As a digital communication system, fiber-optic communication system is comprised of *transmitter*, which encodes and modulates abstract information to binary bits to electrical waveform and eventually in the form of lightwave for fiber transmission, *optical fibers*, the most practically ideal channel media available in the earth capable of conveying the information of optical form from several meters to hundreds and thousands of kilometers, and *receiver* which, inversely to the transmitter, recovers the information from the received optical signal.

This Chapter is organized as follows.

In Section §2.1, we briefly present the basic elements required for a digital communication system and describe their functions from the perspective of information.

Section §2.2 presents mathematical models of the functional blocks at the transmitter, including digital modulation formats, baseband waveform modulation, and passband carrier modulation. In §2.2.1, *Digital Modulation Formats* describe how the information bits are mapped into symbols that abstract the quantitative properties of a waveform for baseband modulation. In §2.2.2, *Baseband Waveform Modulation* discusses the properties of certain baseband waveforms, including their temporal and spectral shapes and how the waveforms are modulated by the symbols. In §2.2.3, *Passband Carrier Modulation* is the process of modulating the baseband waveforms onto a sinusoid carrier for the purpose of transmitting the information within desired passband of the physical channel, which could be the radio frequency of an electromagnetic wave, or be the optical spectrum of lightwave.

In Section §2.3, according to the linear time-invariant (LTI) system theory and stochastic process, the mathematical model of LTI filtering channel with AWGN is investigated.

Section §2.4 presents models of the functional blocks at the receiver, which perform reverse operations to those at the transmitter to recover the transmitted information. In §2.4.1, *Coherent Detection*, inverse to the *Passband Carrier Modulation*, converts the signal from passband to baseband for baseband signal processing. In §2.4.2, *Sampling* is the process of extracting the discrete-time information from the received continuous-time baseband signal. According to the Nyquist-Shannon sampling theory, which is the premier of digital communications, information can be recovered without any loss, and the system can be mathematically expressed in discrete-time model, and further in the more concise matrix form. In §2.4.3, *Channel Equalization* is the method, based on the estimated channel state information, compensating the distortions on the signal during channel transmission, and *Decision* is the process of recovering the transmitted information bits with the highest fidelity even in the presence of noise and interference.

## §2.1 Overview of a Communication System

Figure 2–1 illustrates the basic block diagram of a communication system that connects the information source and the information destination. The very mission of essentially all the communication systems is to deliver the information from the source(s) to the destination(s) in a unidirectional or bidirectional way via some physical channel(s). Transmitter is the interface that feeds the information from the source into the channel, and receiver is the interface that extracts the information from the channel to the destination. In Figure 2–1, it is a unidirectional communication system with one information source and destination, and it can be easily generalized into various situations as mentioned or not.

The information source, in a general sense, contains or generates the information of interest, called message. The message could be colors and hues of a

landscape, characters in novels, and noisy grumbles in the whispering oceans. No matter what the content is in the message, the message can be represented by a stream of binary bits via operations, such as sampling, quantization, and source coding. The binary bits contain all the information of the message or majority of its information with negligible loss.

In some applications where security is in priority, cryptographic coding is often utilized to secure the information. To guarantee the information recovery after travelling through unreliable communication channels many digital communication systems employ channel coding or forward error correction.

At the transmitter, modulator serves as the interface of conveying the binary bits onto physical signals that bear the information of the bits. Typically, modulation involves two processes. In the first step, the modulator, according to a certain codebook, maps the binary bits into symbols, which quantitatively represent the properties of the physical waveforms under modulation, such as the amplitude and phase of an electromagnetic wave. In the second step, the modulator generates the physical waveforms based on the symbols, and conveys the waveforms into a signal suitable for transmission. For example, in wireless communications, the waveforms are modulated onto a radio frequency of electromagnetic signal; in the coaxial cable, the waveforms are conveyed in electrical field; in the fiber-optic communication, the waveforms are in the form of optical lightwave.

The transmitter feeds the signal into a physical channel, which delivers the signal to a receiver. During transmission, the information-bearing signal will experience various detrimental effects from the channel. For example, if only the linear effects are considered, the detriments can be categorized as a) attenuation, b) dispersion, and c) additive noise.

Attenuation is the phenomenon in which the power of signal loses during transmission. It is a multiplicative effect which represents the ratio of the received power to the transmitted power.

Dispersion, in a broad sense, is the effect that the phase velocity and usually the attenuation vary for different frequency components of the signals. In fiber-optics, dispersion, or specifically chromatic dispersion is a term usually

used to specify the frequency depended phase velocity. Dispersion can be applied in various wave propagation scenarios. For example, in the wireless radio channel, multipath propagation introduces different delayed paths for the electromagnetic waves arriving at the receiver. It is also a dispersive effect since the paths with different propagation lengths result in different effective velocities for different frequency components. Dispersion can be modeled, according to the LTI system theory as the convolution of the original signal with the channel impulse response (CIR). In addition, the attenuation effect can also be considered as part of the dispersive effect since attenuation is a multiplicative coefficient.

Additive noise is a noise model to emulate the additive corruptions on the signal. It can generalize, for example, the thermal noise in the electronic components, the amplified spontaneous emission in the optical amplifier, and the shot noise in the photodiodes, etc. The additive noise is usually modeled statistically as the Gaussian process, and such noise model is termed as additive Gaussian noise. In addition, if the noise has a ‘relatively’ flat power spectral density, we term it as additive white Gaussian noise (AWGN).

As the signal arrives at the receiver, the receiver perceives the signal and extracts the physical properties of the signal into mathematical quantities. The demodulator performs the inverse operations to the modulator. It extracts the information from the signal into the most likely symbols that may be transmitted by the transmitter. The following decoder interprets the information into the message that is most likely transmitted.

The received signal is usually blurred during the transmission. To recover the information with the minimal errors, the receiver should always compensate the distortions. As mention before, as long as the channel is linear or almost linear, there are mainly two detrimental effects, dispersion and additive noise. The dispersion can be usually estimated via some method termed channel estimation. According to the estimated channel state information, it can be compensated via the methods termed as channel equalization or channel compensation. On the other hand, the noise is usually unknown. Fortunately, based on the Shannon’s theory, which announces the birth of information theory, the

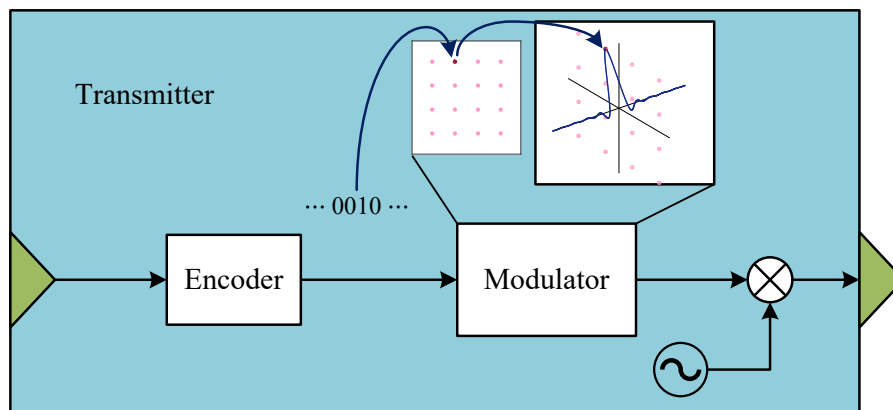


Figure 2–2. Block diagram of a transmitter comprising an information encoder, which outputs the binary bits, and a modulator, which maps the bits onto the constellation diagram.

information can be transmitted almost without loss at a given speed for a given noise power.

## §2.2 Transmitter

In the digital communication systems, a transceiver comprises of two inversely functional pairs, the information encoder and decoder, and the modulator and demodulator. The information encoder and decoder serve as the interfaces between the abstract information and the binary bits that is the quantitative information comprehensible by the “transceiver”. The modulator and demodulator are the interfaces between the bits and the quantitative properties of a physical waveform that are perceivable by the “transceiver”. Specifically, the modulator at the transmitter encodes the bits onto the properties of the waveforms, such as its amplitude, phase, frequency, and even the polarization and spatial distribution, according to some rules. The demodulator at the receiver extracts the information from the modulated waveforms onto the most likely bits according to the rule inverse to the rule adopted by the modulator.

In this section, we will present the principle of modulating the quantitative properties of the waveforms, and the principle of choosing the basic shape of

the waveforms. Accordingly, we can easily apply the general models of digital communication systems to the advanced fiber-optic communication systems.

The terminology for the first principle is *Modulation Formats*, such as amplitude shift-keying (ASK) or pulse amplitude modulation (PAM) which modulates the amplitude of the waveforms, and phase shift-keying (PSK) which modulates the phase of the waveforms, and quadrature amplitude modulation (QAM) which modulates both the amplitude and phase of the waveforms. The modulation formats largely determine the spectral efficiency of a system. For example, if we choose a higher level modulation format, more information can be stuffed into a single waveform, and on the contrary a lower level modulation contains less information in a single waveform. Nonetheless, higher modulation formats are more sensitive to the noise and fading effects from the channel.

The second principle involves the terminology, pulse shaping. The shape of the pulse (waveform) determines the physical properties of the pulse, and it thus affects the spectral efficiency and also the resilience of the system against the detrimental effects from the channel. In the design of waveforms, one expects a waveform with well-constraint spectral shape. It means that the designed waveform occupies less bandwidth. On the other hand, one also expects that the waveform has desired temporal shape so that a train of modulated waveforms will not interfere with each other. It will be shown that the design criterion for a desired waveform should comply with the Nyquist interference-symbol interference criterion.

### §2.2.1 Digital Modulation Formats

Modulation formats are the rule regulating how the binary bits are modulated onto the properties of a waveform. The simplest and most efficient approach is to modulate the amplitude of a waveform, such as in PAM. If one wants to modulate, for example, 1, 2, or 3 bits at a time, the amplitude of a waveform should have  $2^1 = 2$ ,  $2^2 = 3$  or  $2^3 = 8$  distinctive levels, as shown in Figure 2–3 (a), (b), and (c), respectively. If only the phase of a waveform is modulated i.e., PSK, with 2, 3, and 4 bits at a time, respectively, one can employ the constellation diagrams in Figure 2–3 (d) QPSK, (e) 8-PSK, and (f) 16-PSK. In

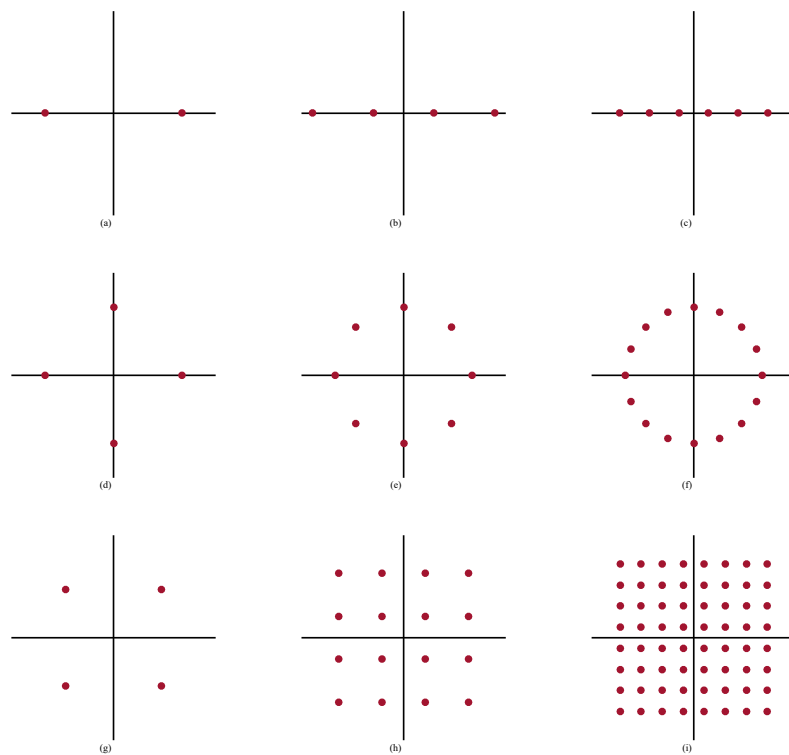


Figure 2–3. Illustration of the constellation diagrams of (a) PAM-2, (b) PAM-4, (c) PAM-8, and (d) QPSK, (e) 8-PSK, (f) 16-PSK, (g) 4-QAM, (h) 16-QAM, and (i) 64-QAM.

QAM, the complex envelope, including the amplitude and phase, of a waveform is utilized for modulation, and more distinct modulation levels can be obtained. For example, in the same complex plane, the (g) 4-QAM, (h) 16-QAM, and (i) 64-QAM are able to modulate 2, 4, and 6 bits at a time, respectively, as shown in Figure 2–3.

Depending on the application scenarios, different modulation formats can be adopted appropriately. For example, if the system is baseband transmission or intensity modulation, ASK can be adopted. If the channel fluctuates and the receiver is sensitive to amplitude change, PSK can be adopted because the PSK signal has constant amplitude. If higher spectral efficiency is in demand, QAM can be adopted because it efficiently maps the constellations in the complex plane. In addition, it can be observed in Figure 2–3 that QPSK and 4-QAM are basically the same except for a phase rotation.

Intuitively, the higher the modulation level is, the higher spectral efficiency one can achieve. For example, if the Baud rate, which is the transmission rate of the modulated waveforms per second, is fixed, 64-QAM has a spectral efficiency of 6 bit/s/Hz, while that of the 16-QAM and the 4-QAM are 4 bit/s/Hz and 2 bit/s/Hz, respectively. On the other hand, if one wants to stuff more bits into a single symbol for higher spectral efficiency, higher energy is needed to achieve the same performance if the noise level is fixed.



## CODEBOOK OF MODULATION FORMATS

The process of relating the information bits to the symbols, according to some rule, is called mapping. The symbols, on one hand, represent the bits and on the other hand dictate the property of the waveforms. For example, if only the complex envelope of the waveforms are employed, in PAM, PSK, or QAM, for modulation, the symbols are complex numbers indicating the positions of the constellations, as shown in Figure 2–3. In addition to the complex envelope, the polarization state, the spatial state (mode in multimode fiber) and even the angular momentum of photons can be utilized for modulation, and these futuristic modulation techniques are extremely attractive in the future fiber-optic communication systems. In this thesis, we only focus on the complex envelope of a single optical beam in the fiber.

During the mapping process, bits are grouped block by block, and based on the combination of the bits in a block, a symbol is chosen from a set of symbols with size  $M$ ,  $\mathcal{S} = \{s_m \mid m = 0, 1, \dots, M-1\}$ , namely the codebook. In principle, the size  $M$  should be no less than the number of possible combinations of the bits. If there are  $b$  bits in a block, we need a codebook including  $M \geq 2^b$  distinct symbols, so that the modulator can encode all the  $2^b$  possible combinations of the bits. For example, if there are 2 bits grouped every block, one can choose a codebook,

$$\mathcal{S} = \{s_m \mid m = 0, 1, 2, 3\} \quad (2.1)$$

to encode all the possible bits

$$\mathcal{B} = \{b_1 b_0 \mid 00, 01, 10, 11\}. \quad (2.2)$$

TABLE 2-1  
EXAMPLE OF CODEBOOKS FOR 4-QAM AND 16-QAM

(a) 4-QAM			(b) 16-QAM		
$\mathcal{B}$	$\mathcal{S}$		$\mathcal{B}$	$\mathcal{S}$	
$b_1b_0$	$\Re\{s_m\}$	$\Im\{s_m\}$	$b_3b_2b_1b_0$	$\Re\{s_m\}$	$\Im\{s_m\}$
0 0	+1	+1	0 0 0 0	+1	+1
0 1	+1	-1	0 0 0 1	+1	+3
1 0	-1	+1	0 0 1 0	+3	+1
1 1	-1	-1	0 0 1 1	+3	+3
			0 1 0 0	+1	-1
			0 1 0 1	+1	-3
			0 1 1 0	+3	-1
			0 1 1 1	+3	-3
			1 0 0 0	-1	+1
			1 0 0 1	-1	+3
			1 0 1 0	-3	+1
			1 0 1 1	-3	+3
			1 1 0 0	-1	-1
			1 1 0 1	-1	-3
			1 1 1 0	-3	-1
			1 1 1 1	-3	-3

In practice, we use a codebook which has a set of exact  $M = 2^b$  symbols.

During transmission, the waveforms (symbols) will be distorted by interferences and corrupted by noise. Symbol error occurs if the noise is so large that a received symbol deviates from the transmitted symbol and is indistinguishable from another symbol. One expects a mapping scheme in which, if a symbol error occurs, the number of misinterpreted bits (bit errors) caused by the symbol error can be minimized. Gray code is the mapping scheme that satisfies the requirement, and it is widely used in digital communication systems.

In Table 2-1, the codebooks of (a) 4-QAM and (b) 16-QAM are provided according to the long-time evolution standard by 3GPP. In Figure 2-4, the

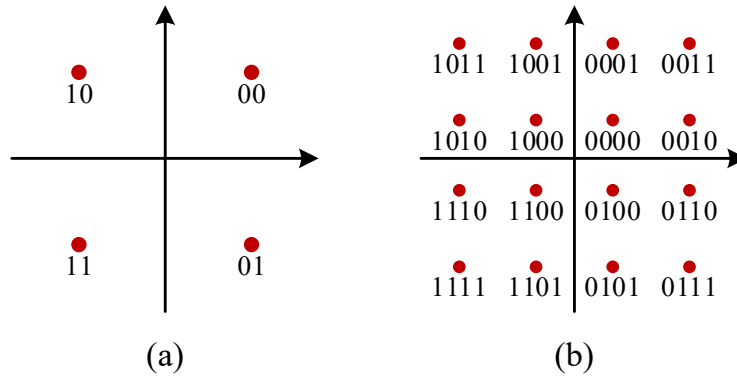


Figure 2-4. Illustrations of the constellation diagram based on Gray code for (a) 4-QAM and (b) 16-QAM.

corresponding constellation diagrams of the codebooks are illustrated. It is obvious that for any pair of neighboring constellations there is only one-bit difference. If a symbol is corrupted by noise, and most probably fall into one of the adjacent constellation areas, the possible number of bit errors due to the blurred symbol is most probably no greater than 1.

Here, one can mathematically express a sequence of symbols as

$$\mathcal{S}_{\text{III}} := \{s(n) \mid s(n) \in \mathcal{S}, \quad n = \cdots 0, 1, 2, \cdots\}. \quad (2.3)$$

Sometimes, we would like to express the symbol sequence along with time. Employing the Dirac delta function  $\delta(t)$ , we have

$$s_{\text{III}}(t) = \sum_n s(n) \cdot \delta(t - nT_s). \quad (2.4)$$

where  $T_s$  is the symbol period.

### §2.2.2 Baseband Waveform Modulation

The symbols which represent the information bits describe the complex envelope of the basic waveforms for modulation, and the shape of the waveforms determines the physical properties of the modulated signal, which is the group of the modulated waveforms arranged in time or frequency.

Assuming that the baseband waveform is given by a function  $g(t)$ . The symbols are in essence the coefficients modulating the waveforms. Recalling the

symbol train in Eq. (2.4), the modulated baseband time-domain signal is generated by convolution, as

$$\begin{aligned}
 s(t) &= g(t) * s(t)_{\text{III}} \\
 &= g(t) * \left( \sum_n s(n) \cdot \delta(t - nT_s) \right) \\
 &= \sum_n s(n) \cdot g(t - nT_s).
 \end{aligned} \tag{2.5}$$

In the above equation, the modulated signal  $s(t)$  is a train of waveforms modulated by  $s(n)$ , ordered in time. For the design of the baseband waveforms, we would like to see the waveforms being transmitted as quickly as possible without interference between each other. On the other hand, the desired spectra of the waveforms should be well confined or shaped in a bandlimited manner to reject unwanted interference out of the system bandwidth, minimizing the corruption. In some communication systems, for example, in the wireless communications, where the spectral resource is scarce and the requirements on the spectra of the signal are strictly regulated by law, the shape of the waveform should be carefully designed.

The answer to the first desired property of a waveform is the Nyquist intersymbol interference (ISI) criterion, which tells what the shapes of the waveforms should be and how fast the waveforms can be transmitted without ISI. The waveforms satisfying the criterion are called the Nyquist waveforms. Inspecting Eq. (2.5), for example, if we have a waveform  $g(t)$ , which is modulated and transmitted periodically at a period of  $T_s$ , the exact preferable property we want is that, at the exact sampling point  $t = 0$ , we have the desired symbol  $s(0)$ , and at the other sampling points at multiples of  $T_s$ ,  $t = nT_s$ ,  $n \neq 0$ , the waveform hits zero. Mathematically, the condition is

$$g(t) \Big|_{t=nT_s} = \frac{1}{\sqrt{T_s}} \begin{cases} 1 & n = 0 \\ 0 & n \neq 0 \end{cases} \tag{2.6}$$

for  $n \in \mathbb{Z}$ . In such condition, we can perfectly get the desired symbols, namely the complex envelope of the desired waveform, without the interference from other symbols (ISI).

The condition in Eq. (2.6) expresses the Nyquist ISI free criterion in the

time domain. Before applying the Fourier transform, multiplying a Dirac delta comb on both sides of Eq. (2.6), we have

$$\sqrt{T_s} \sum \delta(t - nT_s) \cdot g(t) = \delta(t). \quad (2.7)$$

Applying Fourier transform on both sides, the Nyquist ISI criterion in the frequency domain is

$$\sum_{k=-\infty}^{+\infty} G\left(f - \frac{k}{T_s}\right) = 1, \quad (2.8)$$

at all frequency  $f$ , where  $G(f)$  is the Fourier transform of  $g(t)$ .

The Nyquist ISI criterion in Eq. (2.6) and Eq. (2.8) is astonishingly simple yet ultimately elegant. Nonetheless, it is a rather general criterion, and almost no requirement imposes on the shape of the waveform and on its spectrum. To answer the second requirement for designing a well-shaped and well-bandlimited waveform for modulation, more meticulous considerations should be taking into account. Follows are examples of some well-designed Nyquist waveforms.

## EXAMPLES OF NYQUIST WAVEFORMS

The most naïve, simplest yet effective waveform may be in rectangular shape, and we call it rectangular pulse or function, as

$$g_{rect}(t) = \frac{1}{\sqrt{T_s}} \Pi\left(\frac{t}{T_s}\right) = \frac{1}{\sqrt{T_s}} \begin{cases} 1 & |t| < \frac{T_s}{2} \\ 0 & |t| > \frac{T_s}{2} \end{cases}, \quad (2.9)$$

where  $\Pi(t)$  is the normalized rectangular function. Sometimes, the definition of  $\Pi(t)$  at  $t = \pm 0.5T_s$  is undefined, and sometimes, it can be defined equal to 0, 1, or 0.5. In Figure 2–5 (a), the rectangular function is illustrated, and its spectrum is in Figure 2–5 (b), which is

$$\begin{aligned}
G_{rect}(f) &= \mathcal{F} \left\{ \frac{1}{\sqrt{T_s}} \Pi \left( \frac{t}{T_s} \right) \right\} \\
&= \frac{1}{\sqrt{T_s}} \text{sinc} \left( \frac{f}{T_s} \right) = \frac{1}{\sqrt{T_s}} \frac{\sin \pi \frac{f}{T_s}}{\pi \frac{f}{T_s}},
\end{aligned} \tag{2.10}$$

where  $\text{sinc}(f)$  denotes the normalized sinc function. If the rectangular pulses are transmitted repeatedly at a period of  $T_s$ , there will be no interference if we examine the waveform in Eq. (2.9) with the criterion in Eq. (2.6) or its spectrum in Eq. (2.10) with the criterion in Eq. (2.8). It can also be observed that the first null points of the spectrum are at  $\pm 1/T_s$ , and the tails extend infinitely with its amplitude scaled by  $1/T_s$  over frequency.

In some application where the spectrum of the signal should be strictly confined within a bandwidth of  $B$ , taking the time-frequency duality of the Fourier transform into account, one can easily deduce that if the sinc function is used as the shape of the time-domain waveform, the resulting spectrum can be well fitted into a bandwidth of  $B$ . The time-domain waveform thus is given by

$$g_{\text{sinc}}(t) = \frac{1}{\sqrt{T_s}} \text{sinc} \left( \frac{t}{T_s} \right) = \frac{1}{\sqrt{T_s}} \frac{\sin \pi \frac{t}{T_s}}{\pi \frac{t}{T_s}}, \tag{2.11}$$

where  $T_s = 1/B$ , and its spectrum is

$$\begin{aligned}
G_{\text{sinc}}(f) &= \mathcal{F} \left\{ \frac{1}{\sqrt{T_s}} \text{sinc} \left( \frac{t}{T_s} \right) \right\} \\
&= \frac{1}{\sqrt{T_s}} \Pi \left( \frac{f}{T_s} \right) = \begin{cases} 1 & |f| < \frac{B}{2} \\ 0 & |f| > \frac{B}{2} \end{cases}.
\end{aligned} \tag{2.12}$$

The corresponding waveform and its spectrum are respectively illustrated in Figure 2–5 (c) and (d).

The rectangular and sinc functions are two of the most basic shapes for a waveform could be. The ISI free transmission with bandlimited requirement

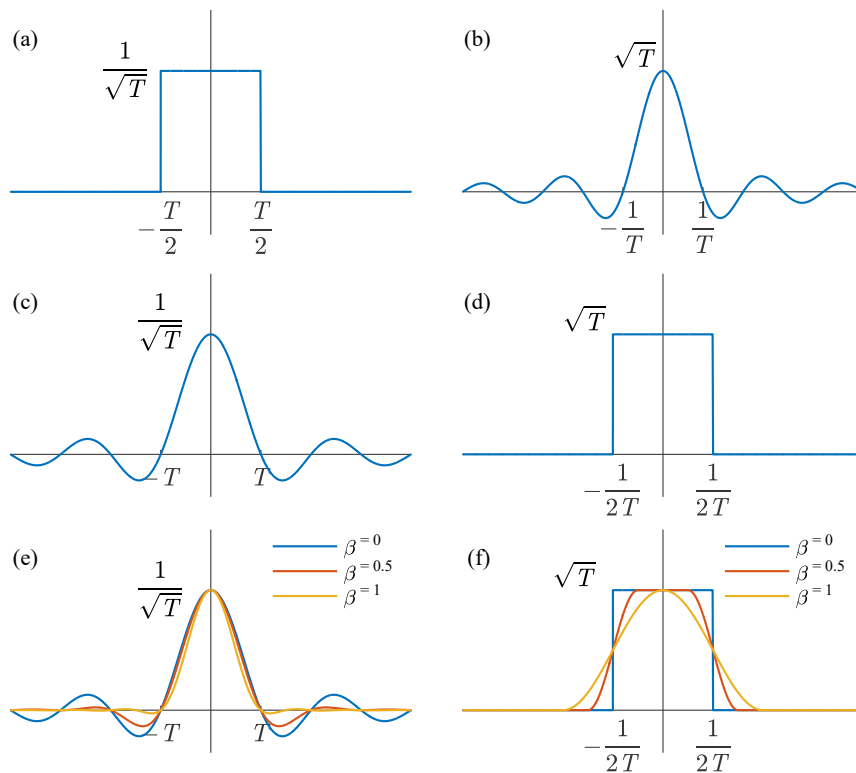


Figure 2–5. Examples of Nyquist waveforms and their spectra: Rectangular waveform in (a) and (b), Sinc waveform in (c) and (d), and raised cosine waveforms with various roll-off factors  $\beta = 0, 0.5$ , and  $1$  in (e) and (f).

can be achieved by them between the time domain and the frequency domain. Nonetheless, one may have a question about if there is a waveform whose shape and spectrum are strictly confined in both time and frequency domains. Unfortunately, there is no such a waveform, and the bitter reality is governed by the time-frequency uncertainty principle,

$$\Delta t \times \Delta f \geq \frac{1}{4\pi} \quad (2.13)$$

where  $\Delta t$  and  $\Delta f$  are standard ‘deviations’ of the time and frequency of a signal, from the view of probability density.

Though none waveform can be ideally confined both temporally and spectrally, there are waveforms balancing the requirements on time and frequency. The raised-cosine waveform is one of the best choices, which is defined as

$$g_{rc}(t) = \frac{1}{\sqrt{T}} \operatorname{sinc}\left(\frac{t}{T}\right) \frac{\cos\left(\frac{\pi\beta t}{T}\right)}{1 - \left(\frac{2\beta t}{T}\right)^2}, \quad (2.14)$$

with its spectrum as

$$G_{rc}(f) = \begin{cases} \sqrt{T} & |f| \leq \frac{1-\beta}{2T} \\ \frac{\sqrt{T}}{2} \left\{ 1 + \cos\left(\frac{\pi T}{\beta} \left(|f| - \frac{1-\beta}{2T}\right)\right) \right\} & \frac{1-\beta}{2T} < |f| \leq \frac{1+\beta}{2T} \\ 0 & |f| > \frac{1+\beta}{2T} \end{cases} \quad (2.15)$$

where  $\beta$  is called the roll-off factor, and  $T$  is the Nyquist period. Raised-cosine waveforms are also a Nyquist waveform, and its time-domain waveform and spectrum are shown in Figure 2–5 (e) and (f), respectively. The amplitude of the raised-cosine waveform decreases along with the time proportional to  $1/(t - t^3\beta^2)$ , while  $1/t$  in sinc waveform. The higher the  $\beta$  is, the lower the lagging tail becomes. If the roll-off factor  $\beta = 0$ , the raised-cosine waveform reduces to the sinc waveform. The cut-off bandwidth is also defined by the roll-off factor  $\beta$ , as

$$B = (1 + \beta) \frac{1}{T} \quad (2.16)$$

Thus, with a properly designed raised-cosine waveform, the bandwidth requirement can be met with a well-defined time-domain pulse.

### §2.2.3 Passband Carrier Modulation

The baseband signal can be directly fed into a physical channel for transmission or modulated into a frequency band, depending on the physical properties of the channel medium and on the spectrum allocations. In most cases of communication systems, the channel, or more exactly the transfer function of the channel is not ideally flat over the entire spectra. In other words, the channel does not allow a signal to be transmitted at any frequency. In a communication

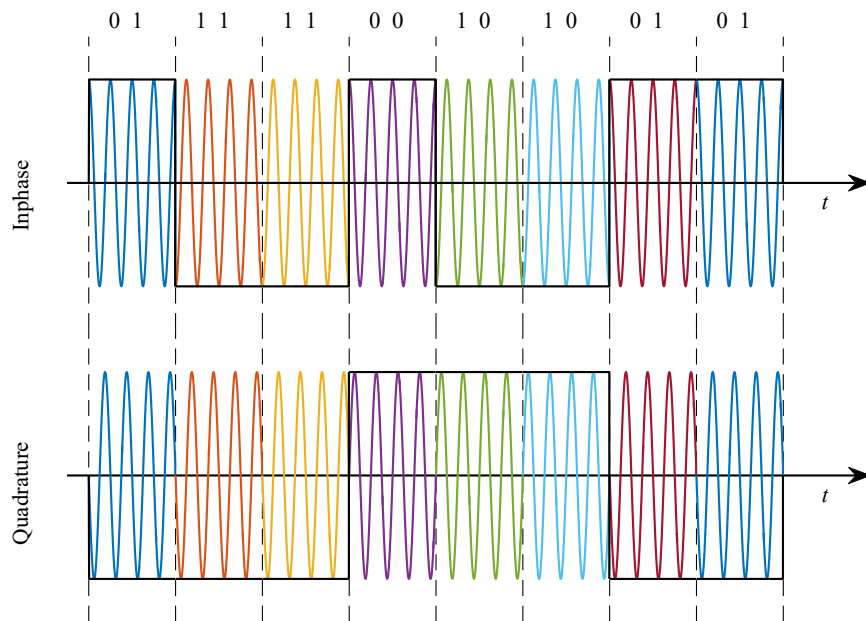


Figure 2–6. Illustration of the inphase (above) and quadrature (below) components of a carrier modulated in QPSK with rectangular wave.

channel, some frequency bands attenuate the signal dramatically, while some allow the signal to be transmitted clearly enough. The frequency band suitable for signal transmission is called the passband of the channel, and different channel has different passband. For example, a piece of coaxial cable is able to support a baseband transmission of bandwidth up to 1 GHz; a well-designed transmission line can support transmission at up to 100 GHz; the optical silica single-mode fibers have transparent windows for lightwave of wavelength from 800 nm to 1700 nm with an astonishing bandwidth of more than a hundred trillion Hertz. In some communication systems, the channel is shared by various spectral links between the information sources and destinations. The most straightforward sharing strategy is to allocate different frequency bands for different links.

The purpose of carrier modulation is to modulate or move the baseband signal to the passband of a channel for transmission. It is mathematically the multiplication of the baseband signal and a sinusoidal waveform, the carrier. In Figure 2–6, for example, baseband signals of rectangular waveforms in QPSK

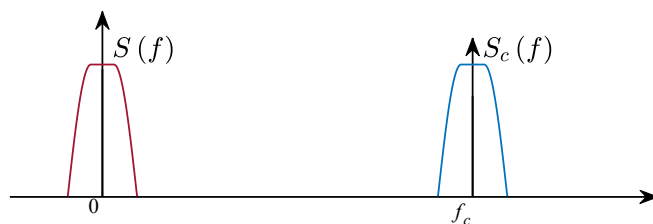


Figure 2–7. Illustration of the spectra of a baseband signal and its pass-band copy.

are modulated by sine waves with normalized frequency of 4. The passband modulated signal is in essence the multiplication of the baseband signal and a sinusoid carrier of a frequency  $f_c$ , and the math is rather simple, as

$$\begin{aligned} s_c(t) &= e^{j2\pi f_c t} \times s(t) \\ &= e^{j2\pi f_c t} \times \sum_n s(n) \cdot g(t - nT_s). \end{aligned} \quad (2.17)$$

According to the Fourier transform, the spectrum of the carrier-modulated signal is

$$\begin{aligned} S_c(f) &= \mathcal{F}\{S_c(f)\} \\ &= \mathcal{F}\{e^{j2\pi f_c t} \times s(t)\} \\ &= S(f - f_c), \end{aligned} \quad (2.18)$$

with the frequency shift by  $f_c$  to right, as illustrated in Figure 2–7.

## §2.3 Communication Channel

In a communication system, channel takes care of the transmission of the information-bearing signal, and it is the most fundamental element that should be carefully considered, analyzed, and even exploited. During transmission, the signal will also be corrupted and distorted by the impairments in the channel, and to some extent the capacity of the system is determined by the channel. Therefore, a systematical channel modeling is the critical process, guaranteeing the theoretical viability and practical feasibility of the communication system.

Basically, a channel is the medium that bridges the information source and its destination. The medium includes the physical channel, in which the modulated electromagnetic wave is transmitted, such as the coaxial cable, power line, optical fiber, and even the air and empty free space. It can also include any components in the transceiver, such as the front amplifiers which boost the power of the electrical or optical signals, the pulse-shaping filters which generate the baseband waveform, and the band-pass filters which remove the out-of-band noise, etc. Essentially, any devices and media that convey and modify the information-bearing signal can be regarded as a part of the channel.

In a communication system, the signal may be subject to different impairments from the channel, including linear and nonlinear distortions, frequency offset, phase jitter, and noises of different types, etc. All the impairments can be regarded as parts of the channel. However, it is almost impossible to characterize all the impairments into a single channel model. If one tries to do this, the channel model could be hardly tractable. A practical approach of channel modelling is to abstract the most important characteristics of the channel.

In the section, we take the perspective of information theory on the channel that the channel is a theoretical system with certain mathematical impairments that introduce corruption and distortions on the signal of interest. We will take two of the most elementary and powerful channel models, the additive white Gaussian noise (AWGN) channel and the linear time-invariant (LTI) filtering channel into account, which are two of the simplest models that are capable of characterizing the major linear effects of a communication channel. The first one effectively is a stochastic process from a view of probability and the second is effectively a system from the view of the linear time-invariant system theory.

### §2.3.1 Additive White Gaussian Channel

AWGN is a basic noise model that statistically describes the signal corruptions during transmission in nature. *Additive* means that the noise is independent of the signal and overlaps with the signal; *White* means that the power spectral density of the noise is flat over the entire bandwidth of interest and thus the

noise is also uncorrelated; *Gaussian* means that the noise is a stochastic process of independent<sup>11</sup> Gaussian distribution with zero mean. The AWGN channel can be modeled in either a continuous-time or a discrete-time process. Depending on whether it is continuous or discrete, the definition is slightly different.

In the continuous-time model, for example, the received signal is the transmitted signal  $s(t)$  corrupted by AWGN, as

$$r(t) = s(t) + v(t). \quad (2.19)$$

The AWGN  $v(t)$  is a continuous-time stochastic process, defined as

$$\{v(t) | t \in \mathcal{T}\} \quad (2.20)$$

where  $\mathcal{T}$  is a totally ordered set, *time*, and  $v(t)$  are independent Gaussian distributions with zero mean. The variance of the continuous AWGN is defined by its power spectral density as

$$|\mathcal{F}\{v(t)\}|^2 = \sigma_n^2 \quad (2.21)$$

The discrete case can be easily inferred from the continuous one by setting  $\mathcal{T} = \mathbb{N}$ , and  $n \in \mathbb{N}$ , as

$$\{v(n) | n \in \mathcal{T}\} \quad (2.22)$$

and

$$v(n) \stackrel{i.i.d}{\sim} \mathcal{N}(0, \sigma_n^2) \quad (2.23)$$

The AWGN model is capable of modelling many types of noises, such as, the thermal noise in electronics and the amplified spontaneous emission noise in optics. With slight modification, the AWGN can be well adapted into various noise models, such as the band-limited AWGN.

### §2.3.2 Linear Time-Invariant Filtering Channel

Linear time-invariant filter is the most fundamental channel model according

---

<sup>11</sup> The condition of “independent” is a condition more rigorous than “uncorrelated”.

to the theory of linear time-invariant systems, which describes the responses of a LTI system to arbitrary input signals. *Linear* means that the input signals and the output signals are a linear map; *Time-Invariant* means that the relations between the input signals and the output signals are independent of time but only on the time delay.

Though theoretically *everything changes and nothing stands still*, most of the communication media can be modeled as an LTI filtering channel, and in practice, with some suitable constraints on the time, the linear channel effects can be well approximated by an LTI system. In the wireless mobile channel, the channel is always changing because of the mobility of users, and the main impairments are due to the changes. Nonetheless, considering that the wireless channels change in the order of seconds or tens milliseconds and that signals typically change in less than a microsecond, the wireless mobile channel can be approximated as an LTI channel within a period of milliseconds. The fiber-optic channel comprising optical fibers is more stable than the wireless mobile channel, and it remains unchanged in several hours or even days.

The LTI filtering channel can also be modeled in either continuous-time or discrete-time. In the continuous-time model, for example, the impulse response of an LTI channel is given by the output, denoted as  $h(t)$ , if the input is a Dirac impulse  $\delta(t)$ . The frequency response of the channel can be represented by the Fourier transform of the impulse response, as

$$H(f) = \mathcal{F}\{h(t)\} \quad (2.24)$$

The discrete-time model can also be easily derived from the continuous-time case by sampling the continuous-time system at discrete time.

Here, recalling the transmitted signal in Eq. (2.5), the signal distorted by the LTI channel and corrupted by the AWGN is given as

$$r(t) = h(t) * s(t) + v(t). \quad (2.25)$$

If we look at the signal in the frequency domain, we have

$$\begin{aligned} R(f) &= \mathcal{F}\{r(t)\} = \mathcal{F}\{h(t) * s(t) + v(t)\} \\ &= H(f) \cdot S(f) + v_{\Omega}(f), \end{aligned} \quad (2.26)$$

where  $v_{\Omega}(f)$  is the frequency-domain noise.

The LTI filtering channel model has some elegant properties, which makes the analysis easier. For example, consider a communication system consisting of a front-end amplifier whose impulse response is  $h_1(t)$ , a driver  $h_2(t)$ , some part of the channel  $h_3(t)$ , etc. The impulse response of the entire system (channel) is

$$h(t) = h_1(t) * h_2(t) * h_3(t) * \dots \quad (2.27)$$

It means that we can divide the system under study into subsystems, and then study each subsystem and get the knowledge of the entire system by convolving all the subsystems. The analysis on the system can be simplified by looking the system in the frequency domain, as

$$H(f) = H_1(f) \times H_2(f) \times H_3(f) \times \dots \quad (2.28)$$

where  $H_1(f)$ ,  $H_2(f)$ , and  $H_3(f)$  are the Fourier transforms of  $h_1(t)$ ,  $h_2(t)$ , and  $h_3(t)$ , etc. Eq. (2.28) tells us that the frequency response of the entire system is the product of the frequency responses of all the subsystems.

## §2.4 Receiver

At the receiver end, if the transmitted signal is fortunate enough that the signal is perceivable and intelligible by the receiver, the receiver retrieves the signal from the channel and tries to recover the information from the received signal. Intuitively, the receiver performs the operations reverse to the transmitter to extract the information and delivers it to the destination. The basic processes involve a signal detection module, which converts the signal at a passband down to the baseband for signal processing, a bunch of signal processing modules, which try to recover the blurred signal after transmission, and a decision module, which recovers the transmitted message based on the recovered signal, and passes it to the information destination.

### §2.4.1 Coherent Detection

The receiver first needs to convert the signal at a passband to the baseband for baseband signal processing. Depending on different applications, there are different detection methods by considering the cost and implementation feasibility of a system. For example, in electrical communication systems, a direct-conversion receiver is able to demodulate the radio frequency to baseband. In optical communication, a direct detection receiver perceives the change of the intensity of the light and converts the changing intensity to electrical signal. More advanced optical coherent receiver is capable of demodulating the signal at the optical spectra to electrical signal at baseband, preserving all the information of the modulated optical carrier.

Technically, coherent detection is the detection method which converts the signal modulated at a passband down to baseband for signal processing. The practical implementation of a coherent detection can be different for different systems, and for some system it is still a challenging task. However, the mathematical model of a coherent detection receiver is quite simple. Revisiting Figure 2–7, the process of coherent detection is to demodulate the signal  $s(t)$  untouched from the passband signal  $s_c(t)$ , and mathematically the processing can be accomplished by multiplying another carrier with frequency  $-f_c$ , as

$$s(t) = e^{-j2\pi f_c t} \times s_c(t), \quad (2.29)$$

If we consider the channel effects in Eq. (2.25), we can substitute  $s(t)$  there by  $s_c(t)$  in Eq. (2.17) and performing the coherent detection, as

$$\begin{aligned} r(t) &= e^{-j2\pi f_c t} \times h(t) * s_c(t) + v(t) \\ &= h(t) * s(t) + v(t). \end{aligned} \quad (2.30)$$

In addition to the coherent detection, there are also other necessary operations that should be done to ensure the performance of the detected signal. For example, before coherent detection, the signal power should be boost to compensate the power loss during transmission. Here, it should be noted that the noise term  $v(t)$  is added after coherent detection. Considering  $s(t)$ , the baseband signal of interest is bandlimited, the out-of-band noise,  $v(t)$ , should be removed out from the received signal by a baseband filter. After a baseband filter, the

noise becomes bandlimited, and we will use the same notation without loss of generality.

### §2.4.2 Sampling and Discrete-Time Model

In digital communication systems, the continuous-time baseband signal should be converted into the discrete-time domain via sampling to allow the application of advanced digital signal processing technologies at the receiver. The theory underlying the process of sampling that bridges continuous-time signals and discrete-time signals is the Nyquist-Shannon sampling theorem. The theory tells us that given a continuous-time baseband signal, of which there is no frequency components exceeding a frequency  $B$ , the signal can be represented by a discrete-time signal sampled at a frequency no less than  $2B$  without any information loss (aliasing).

Revisiting the received baseband signal in Eq. (2.30), the received signal is the convolution of the transmitted signal  $s(t)$  and the channel impulse response  $h(t)$  adding the noise. If we employ the sinc function as pulse shaping function, see Figure 2–5 (c), the bandwidth of the signal is  $B = 0.5 / T_s$ , and we can get the discrete-time signal by sampling at a frequency of  $T_s$ , and we have

$$\begin{aligned} r(m) = r(t)_{|_{mT_s}} &= h(mT_s) * s(mT_s) + v(mT_s) \\ &= h(mT_s) * \sum_n s(nT_s) g(mT_s - nT_s) + v(mT_s), \end{aligned} \quad (2.31)$$

where  $g(t)$  is the pulse-shaping waveform. Considering that the waveforms are Nyquist, the received discrete-time signal can be further given by

$$r(m) = h(m) * s(m) + v(m), \quad (2.32)$$

where  $h(m)$  and  $v(m)$  denote the discrete-time signals of  $h(mT_s)$  and  $v(mT_s)$ , respectively. Performing discrete Fourier transform on both sides of Eq. (2.32), the received frequency-domain signal is

$$R(m) = H(m)S(m) + v_\Omega(m), \quad (2.33)$$

where  $R(m)$ ,  $H(m)$ ,  $S(m)$ , and  $v_\Omega(m)$  are the discrete Fourier transforms of  $r(m)$ ,  $h(m)$ ,  $s(m)$  and  $v(m)$ , respectively.

It should be noted if other waveform rather than the sinc function is adopted, the spectrum of the received signal cannot be limited within the bandwidth  $B$ . If there is no dispersion, in which  $h(t) = \delta(t)$ , there is no distortion from the aliasing signal because Nyquist waveform is adopted though the bandwidth of the Nyquist waveform is greater than  $B$ . However, if the dispersion is not ideal, the channel impulse response  $h(t)$  alters the transmitted signal at the receiver, and the received signal does not meet the Nyquist criterion any more. As a result, aliasing introduces interference when one performs sampling at the Nyquist period  $T_s$ . To counteract the aliasing problem, oversampling is usually required in practice to compensate the channel before extracting the symbols from the received signal. Nonetheless, for analyzing purpose, sampling exactly at the Nyquist frequency  $1/T_s$  is convenient for handling the system.

### §2.4.3 Channel Equalization and Decision

The transmitted signal is almost ready there, as shown in Eq. (2.32) in the time domain or (2.33) in the frequency domain. Nonetheless, the information symbols are obscured by channel, and interference incurs. The process cancelling the channel distortion due to the term  $h(t)$  in the time domain or  $H(f)$  in the frequency domain (or  $h(l)$  and  $H(m)$  in the corresponding discrete-time domain) is called channel equalization.

Here, we take the discrete-time case in Eq. (2.30) for example. Similar result can be observed in Eq. (2.32). Expanding the convolution operation, one can get

$$\begin{aligned} r(m) &= h(m) * s(m) + v(m) \\ &= \sum_l h(l) s(m-l) + v(m). \end{aligned} \quad (2.34)$$

If  $h(l) \neq \delta(l)$ , for a received sample,  $r(m)$ , it is the desired transmitted symbol,  $s(m)$ , interfered by adjacent symbols,  $s(m-l)$ , scaled by  $h(l)$ . Such interference due to imperfect channel impulse response is termed as inter-symbol interference. Therefore, the process of equalization is to find a filter,  $w(m)$ , filtering out the channel distortion, i.e.,  $w(m) * h(m) = \delta(m)$ , so that

$$\begin{aligned}
\hat{s}(m) &= w(m) * r(m) \\
&= w(m) * h(m) * s(m) + w(m) * v(m) \\
&= s(m) + w(m) * v(m).
\end{aligned} \tag{2.35}$$

In the frequency domain, Eq. (2.35) is equivalent to the discrete Fourier transform on both sides, as

$$\begin{aligned}
\hat{S}(m) &= \mathcal{F}\{\hat{s}(m)\} \\
&= W(m)H(m)S(m) + W(m)v_{\Omega}(m) \\
&= S(m) + W(m)v_{\Omega}(m).
\end{aligned} \tag{2.36}$$

Therefore, the frequency response of the filter is desired as

$$W(m) = H^{-1}(m), \tag{2.37}$$

and its time-domain coefficients can be readily derived as

$$w(m) = \mathcal{F}^{-1}\{W(m)\} = \mathcal{F}^{-1}\{H^{-1}(m)\}. \tag{2.38}$$

The equalizer  $w(m)$  defined in Eq. (2.37) and (2.38) completely removes the channel distortion out, and the interference from other symbols is forced to be zeros. Such equalizers are termed as zero-forcing (ZF) equalizer. With the ZF equalizer, the received symbols are forced to be the transmitted symbol unbiasedly. However, the noise term, as shown in Eq. (2.36) is no longer white. If there is a deep notch in the frequency response, namely  $|H(m)|^2 \approx 0$ ,  $|W(m)|^2$  could be infinitely large. The desired signal after equalization, as a result, will be overwhelmed by the enlarged noise.

To overcome the noise enlargement in ZF equalizers, minimum mean square error (MMSE) equalizers can be considered. The MMSE equalizers equalizes the channel by minimizing the square errors between the input and output. The equalizer in the frequency domain is given by

$$W_{\text{MMSE}}(m) = \frac{H^*(m)}{|H(m)|^2 + \sigma^2}, \tag{2.39}$$

where  $\sigma^2$  is the noise-to-signal power ratio and its time-domain filter is

$$w_{\text{MMSE}}(m) = \mathcal{F}^{-1}\{W_{\text{MMSE}}(m)\} = \mathcal{F}^{-1}\left\{\frac{H^*(m)}{|H(m)|^2 + \sigma^2}\right\}. \tag{2.40}$$

The equalized signal can thus be obtained by substituting  $W_{\text{MMSE}}(m)$  into  $W(m)$  in Eq. (2.36) or  $w_{\text{MMSE}}(m)$  into  $w(m)$  Eq. (2.35).

## Chapter 3

# Fiber-Optic Communication Systems

Fiber-optic communication systems are the communication systems, in which information are conveyed in the form of lightwave propagating in optical fibers. Optical fiber, serving as physical channel medium for communications, promises advantages man ever craved, including extremely low attenuation supporting transmission of hundreds of kilometers and vast capacity available for data communication of hundreds of Terabits per second, the capacity that allows all the population in the world speaking telephone simultaneously over a single piece of fiber. The advantages directly dictate that fiber-optic communication systems are exclusive for long-haul and high-speed communications.

In a fiber-optic communication system, apart from the functional blocks in a general digital communication system as mentioned in Chapter 2, the fiber-optic transceiver consists of light source that provides optical carrier, electronic components that load the electrical information upon the optical carrier at the transmitter, and optic-electronic components that extract the information from the optical carrier back to the electrical form at the receiver end. Figure 3–1 illustrates the basic block diagram of a fiber-optic communication system with the emphasis on its differences to a conventional digital communication system. From the perspective of information, fiber-optic communication sys-

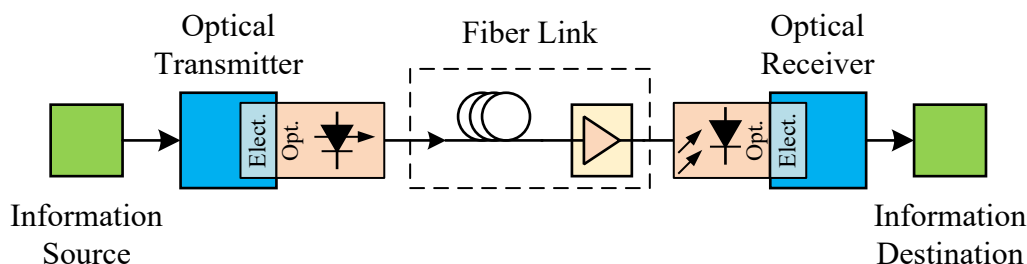


Figure 3–1. Block diagram of fiber-optic communication system.

tems contain all the functional blocks which a communication system possesses, and therefore the mathematical models introduced in Chapter 2 can be easily applied to the analysis and design of the fiber-optic communication systems.

This chapter is dedicated to the essential components used in the advanced fiber-optic communication system and to introduce their properties. Especially, we will focus on external modulators that are ideal for implementing advanced modulation formats and on coherent optical receiver that is able to extract all the information from the modulated optical carrier, enabling advanced digital signal processing at the receiver end.

Channel characterization and modeling are always the most important in the design of any communication systems. There is no exception for the fiber-optic communication systems. Thus, another focus in this chapter is the study of the effects of signal transmission over optical fibers, in which dispersions and optical noise, as well as nonlinear effects, are imposed on the optical signal.

This chapter is organized as follows. Section §3.1 is for optical transmitters, introducing optical modulation techniques, including directly modulated lasers, and external modulators. Section §3.2 discusses the mathematical characteristics of optical fiber channel in detail. Section §3.3 focuses on optical receivers, namely, optical direct detection and optical coherent receiver.

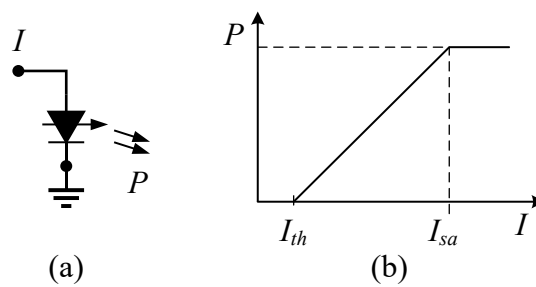


Figure 3–2. Illustrations of (a) a directly modulated laser and (b) its characteristics of relation between input current and output power.

## §3.1 Optical Transmitter

In fiber-optic communication systems, light sources, normally, laser diodes or occasionally light-emitting diodes (LEDs) provide optical carrier at the transmitter for modulation, and photodetectors, routinely photodiodes, convert intensity of the received lightwave back into electrical current for information recovery. In the advanced fiber-optic systems, coherent receiver, in which another laser is employed as a local oscillator for optical beating in photodiodes to reproduce information in the phase of the received lightwave, is preferable.

According to where lightwave is modulated, there are direct modulation and external modulation, and to which properties of the lightwave are modulated, there are intensity modulation, frequency modulation, optical field modulation, polarization modulation, and optical mode modulation etc. At the receiver, depending on the adopted modulation techniques, detection techniques should be applied accordingly. In this section, we will focused on the conventional optical modulation techniques used in the fiber-optical systems.

### §3.1.1 Directly Modulated Lasers

Directly modulated laser (DML) is the simplest optical modulation technique, as shown in Figure 3–2, by directly varying the laser drive current to modulate the intensity of light. In the DML systems, modulation is achieved by directly

applying electrical signal on laser drive current, and hence DML module is the most compact, as well the simplest, optical modulation device. For a directly modulated laser operating within its linear region, its output optical power can be approximately characterized as

$$P_{\text{out}}(t) \propto \alpha I_{\text{in}}(t) - I_{\text{th}}, \quad (3.1)$$

where  $P_{\text{out}}(t)$  is the output optical power,  $\alpha$  is a coefficient associating to laser efficiency,  $I_{\text{th}}$  is the laser threshold that is a DC bias, and  $I_{\text{in}}(t)$  is the driving current, which should be greater than the threshold current  $I_{\text{th}}$ .

In favor of its simplicity, low cost, and effectiveness of modulating the output power, DMLs are popularly available for commercial systems operating at 10 Gbps and even up to 20 Gbps and 40 Gbps [40], and achieve 100 Gbps transmission, boosted by the DSP technologies, in the laboratory [41]. Nonetheless, owing to the device specific chirp when directly modulating the drive current, DMLs suffer from inherent drawbacks in systems of long distance transmission. The device specific chirp broadens signal spectra, resulting in spectral leakage that is undesirable in highly compact wavelength-division multiplexing (WDM) systems, and also distorts the shape of modulated waveforms, resulting in inter-symbol interference (ISI) that severely blurs the transmitted signal. In particular, if the chirp is constructively added to the dispersion during transmission, the reach of the DML systems is largely limited due to the degraded dispersion effect.

Through specific designs, the chirp in DMLs can be deliberately exploited. For example, followed by a chirp manage component, like an optical filter that shapes the optical spectrum of the output from lasers, the DML becomes the so-called chirp-managed laser (CML). With careful engineering, the CML systems is dispersion-tolerant and are able to support transmission over long distance [42-44]. Another more flexible alternative is the application of DSP technologies. With the knowledge of the characteristics of DML and fiber link, the powerful DSP can be applied at the transmitter side for pre-compensating the chirp induced by laser, and even the dispersion in fiber [45].

### §3.1.2 External Electro-optic Modulators

In the advanced fiber-optic systems, external optical modulators are preferable because the laser works alone as an optical source providing continuous optical carrier. External modulators take the continuous wave as the input, apply the modulated electrical signal onto the optical carrier, and produce the modulated optical signal with better quality for transmission.

In contrast to EAMs which modulate light through absorption, another kind of modulators based on phase modulation is more preferable to implement advanced modulation formats because additional optical properties, and thus dimensions, are exploited for information modulation. In such modulators, phase modulation is achieved by the electro-optic effect that the refractive index of a waveguide is proportional to the applied electrical field. By varying the refractive index of the waveguide, the phase of light beam passing through the waveguide is consequently modulated.

Figure 3–4 illustrates the structures of three basic modulators of such kind, namely (a) optical phase modulator, (b) Mach-Zehnder modulator, and (c) optical IQ modulator or nested Mach-Zehnder modulator.

Phase modulator is the most elementary structure based on the electro-optic effect. In the phase modulator, the phase of light carrier can be modulated by modulating the electrical field. Using the simplest phase modulator, more complicated optical modulators can be fabricated. For instance, by constructing a Mach-Zehnder interferometer using two branches of phase modulators, the amplitude, as well as intensity, of optical carrier can be modulated by interfering two phase modulated optical carriers. Such modulator are thus named as Mach-Zehnder modulator (MZM). Moreover, IQ modulator can be built by combining two MZMs with a phase difference of  $90^\circ$ . Except to the three structures, other modulation formats, such as the frequency shift keying, can also be easily achieved with dedicated designs.

#### §3.1.2.1 Optical Phase Modulator

Phase modulator is the basic electro-optic modulator. In Figure 3–4 (a), a phase

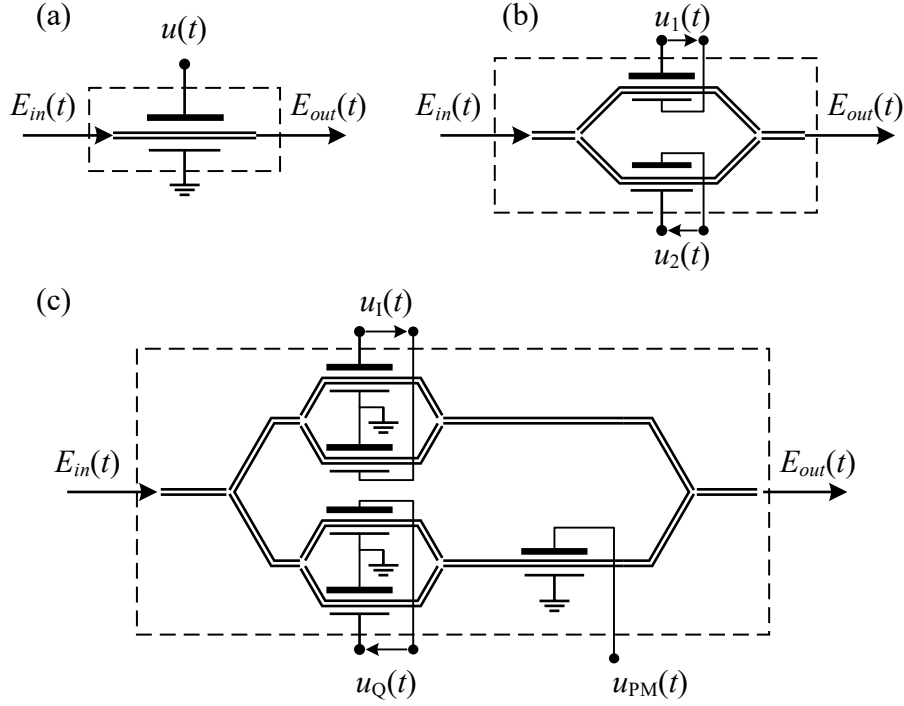


Figure 3–3. Structures of (a) phase modulator, (b) Mach-Zehnder modulator, and (c) IQ modulator.

modulator is composed of a waveguide and electrodes. The waveguide is made up of material exhibiting electro-optic effect, such as LiNbO<sub>3</sub>, GaAs and InP [46-49]. In the LiNbO<sub>3</sub> based phase modulator, the phase of output light is ideally proportional to the applied electrical field, and the intensity of the light is independent of the electrical field. LiNbO<sub>3</sub> also offers easier fiber-to-chip coupling. On the other hand, the III-V material InP allows the modulator to be easily integrated with laser diode into a more compact optical device.

As a beam of light passes through a waveguide, the phase difference between the input and the output depends on the length of the waveguide and its refractive index. As the length of waveguide does not change, the phase can be modulated by changing its refractive index with applied electrical field. Given the incoming optical field  $E_{in}(t)$  and applied voltage  $u(t)$ , and omitting a constant phase shift due to the length of waveguide, the transfer function of the phase modulator is

$$E_{out}(t) = E_{in}(t) \cdot e^{j\pi \frac{u(t)}{V_\pi}}. \quad (3.2)$$

where  $V_\pi$  is the voltage causing a phase shift of  $\pi$ . The parameter  $V_\pi$  is a critical parameter for the electro-optic modulators, depending on the material of the waveguide and the engineering of modulators. According to Eq. (3.3), one can easily implement phase modulation based on the PSK scheme.

### §3.1.2.2 Mach-Zehnder Modulator

According to the principle of Mach-Zehnder interferometer, the amplitude of optical field can be altered by combining two, or more, phase modulators, as shown in Figure 3–4 (b). In MZM, the input light beam is split into two tributaries, each of which is a phase modulator. The phase modulators can be modulated independently, and we call this case as dual-drive MZM. Given that the  $V_\pi$  of the two phase modulators are the same and that their driving voltage are  $u_1(t)$  and  $u_2(t)$ , the output optical field is

$$E_{\text{out}}(t) = \frac{1}{2} E_{\text{in}}(t) \cdot \left[ e^{j\pi \frac{u_1(t)}{V_\pi}} + e^{j\pi \frac{u_2(t)}{V_\pi}} \right]. \quad (3.3)$$

If one operates the dual-drive MZM in a push-push mode, in which  $u_1(t) = u_2(t) = u(t)/2$ , the dual-drive MZM reduces to the phase modulator, and Eq. (3.4) becomes

$$E_{\text{out}}(t) = E_{\text{in}}(t) \cdot e^{j\pi \frac{u(t)}{2V_\pi}}. \quad (3.4)$$

If the dual-drive MZM works in push-pull mode, in which  $u_1(t) = -u_2(t) = u(t)/2$ , the output optical field is

$$E_{\text{out}}(t) = E_{\text{in}}(t) \cdot \cos\left(\pi \frac{u(t)}{2V_\pi}\right). \quad (3.5)$$

According to the relation between the optical field and optical power, Eq. (3.6) can be further given in terms of the input and output optical intensities

$$\begin{aligned} P_{\text{out}}(t) &= |E_{\text{out}}(t)|^2 = \left| E_{\text{in}}(t) \cdot \cos\left(\pi \frac{u(t)}{2V_\pi}\right) \right|^2 \\ &= \frac{1}{2} P_{\text{in}}(t) \left[ 1 + \cos\left(\pi \frac{u(t)}{V_\pi}\right) \right]. \end{aligned} \quad (3.6)$$

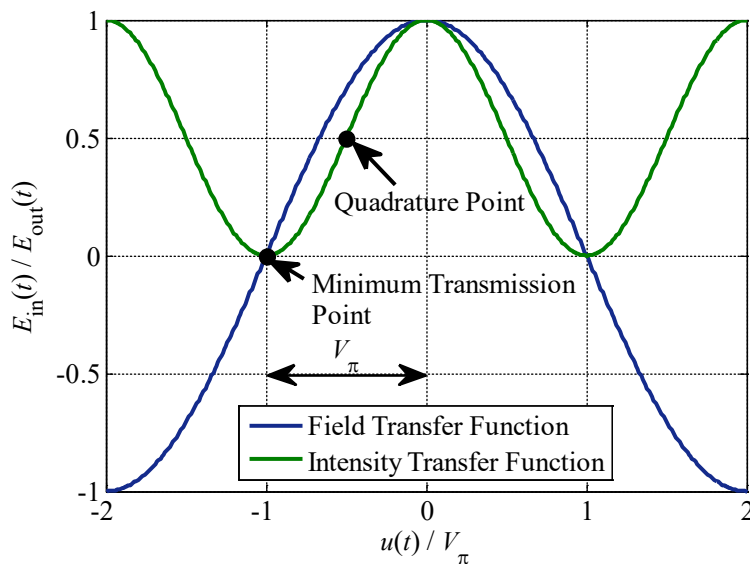


Figure 3-4. Transfer function of optical Mach-Zehnder modulator.

In Figure 3-5, the transfer functions of optical field and optical intensity of a MZM are provided. It can be observed that the voltage inducing a phase shift of  $\pi$  is defined with respect to the phase of the output optical intensity, and the voltage to achieve a phase shift of  $\pi$  for MZM is  $u(t) = 2V_{\pi}$ .

From Eq. (3.6) and (3.7), one can observe that the modulated optical field and intensity are not linearly proportional to the voltage applied but are sinusoidal functions of the voltage. Hence, there are differences between the shapes of the modulating electrical signal and the modulated optical signal. In a practical system design, the nonlinearity of the transfer function of MZMs should be carefully considered. For example, if the pulse shaping waveform is a rectangular function, the peak-to-peak driving voltage can be swung between the transmission maxima as quickly as possible to reduce the nonlinear effect. If one wants to get well-defined pulse shaping waveforms, the peak-to-peak voltage can be set fairly small, for example, less than a quarter of  $V_{\pi}$ , to avoid operating the modulator in the nonlinear region.

### IMPLEMENTATION OF OPTICAL INTENSITY MODULATION

To realize different modulation formats, MZM should be carefully tuned based

on Eq. (3.6) and (3.7) [50, 51]. For example, if optical on-off key (OOK) is required, optical intensity is used for modulation. Assuming that the electrical signal is modulated in 2-ASK as

$$s(t) = \sum x(k)g(t - kT), \quad (3.7)$$

where  $x(k)$  are, depending on the message, drawn from  $\{\pm 1\}$ , and  $g(t)$  is rectangular waveform given in Figure 2–5 (a). The MZM should be biased at the quadrature point with a DC bias equal to  $-0.5V_\pi$  with peak-to-peak voltage  $V_{p-p} = V_\pi$ , as

$$u(t) = \frac{V_\pi}{2}s(t) - \frac{1}{2}V_\pi, \quad (3.8)$$

Substituting Eq. (3.9) into Eq. (3.7), we have

$$\begin{aligned} P_{\text{out}}(t) &= \frac{1}{2}P_{\text{in}}(t) \cdot \left[ 1 + \cos\left(\pi \frac{V_\pi s(t)}{2V_\pi} - \frac{\pi}{2}\right) \right] \\ &= \frac{1}{2}P_{\text{in}}(t) \cdot \left[ 1 + \sin \frac{\pi}{2} s(t) \right]. \end{aligned} \quad (3.9)$$

Considering that the amplitude of the BPSK signal  $s(t)$  swings between  $-1$  and  $+1$  and that the transition time from 0 to 1, or 1 to 0, of the rectangular function arbitrarily approaches 0, we have the approximation that

$$\sin \frac{\pi}{2} s(t) \approx s(t), \quad (3.10)$$

Eq. (3.10) is further given by

$$P_{\text{out}}(t) \approx P_{\text{in}}(t)s'(t) = P_{\text{in}}(t) \sum x'(k)g(t - kT), \quad (3.11)$$

where  $x'(k)$  are drawn from  $\{0, 1\}$ . Hence, optical intensity is achieved by OOK.

## IMPLEMENTATION OF OPTICAL FIELD MODULATION

If one wants to modulate the amplitude of optical field, and 2-ASK, for example, is adopted. We can adjust the  $V_{p-p}$  to  $2V_\pi$  with a DC bias at  $-V_\pi$ . The electrical signal  $u(t)$  is thus given by

$$u(t) = V_\pi s(t) - V_\pi, \quad (3.12)$$

where  $s(t)$  is the baseband BPSK signal that is the same as Eq. (3.8). Substituting Eq. (3.13) into (3.6), we have

$$\begin{aligned} E_{out}(t) &= E_{in}(t) \cdot \cos \left[ \pi \frac{V_{\pi} s(t) - V_{\pi}}{2V_{\pi}} \right] \\ &= E_{in}(t) \cdot \sin \frac{\pi}{2} s(t). \end{aligned} \quad (3.13)$$

Using the same approximation in Eq. (3.11),

$$E_{out}(t) \approx E_{in}(t) \cdot s(t). \quad (3.14)$$

Therefore, if one wants to achieve amplitude shift keying (ASK), the MZM is biased at the minimum transmission point with a DC bias equal to  $-V_{\pi}$  and the peak-to-peak voltage is  $2V_{\pi}$ . High-level modulation formats can also be easily applied to implement optical field modulation based on the above principle.

### §3.1.2.3 Optical IQ Modulator

In the advanced modulation formats, both the inphase and the quadrature components of optical carrier are utilized for modulation to achieve higher spectral efficiency. Equivalently, symbols are mapped into the two-dimension constellation diagram. Based on different criteria, quadrature amplitude modulation (QAM) can be implemented, and Figure 2–3 (d)-(f) provides the simplest QAM mapping scheme based on a squared constellation diagram. In principle, such modulation formats can be implemented by combining two amplitude modulation with a controlled phase between them.

Optical IQ modulator is the very modulator that implements the advance IQ modulation formats in fiber-optic communication systems, as shown in Figure 3–4 (c). It consists of two MZMs with one of them followed by a phase modulator. In practice, the phase modulator is always bias at the voltage that induces  $90^{\circ}$  phase difference between the two MZMs. Both the MZMs have the same  $V_{\pi}$  and are operated in the push-pull mode. The transfer function of the optical IQ modulator is

$$E_{\text{out}}(t) = E_{\text{in}}(t) \cdot \left[ \cos\left(\frac{u_1(t)}{2V_\pi}\right) + j \cdot \cos\left(\frac{u_Q(t)}{2V_\pi}\right) \right]. \quad (3.15)$$

where  $u_1(t)$  and  $u_Q(t)$  are modulation signals applied on the in-phase and quadrature MZMs, respectively. Therefore, by loading the in-phase and quadrature baseband signal into the two MZM with  $90^\circ$  phase shift, QAM can be implemented to achieve highly spectral-efficiency modulation.

### IMPLEMENTATION OF OPTICAL QAM FORMATS

If a QAM modulation format, for example, a 4-QAM is adopted, the baseband signal is given by Eq. (2.3), and  $x(k)$  are drawn from Figure 2–4 (b). The electrical signals of in-phase and quadrature components are thus given by

$$u_1(t) = V_\pi \cdot \Re\{s(t)\} - V_\pi, \quad (3.16)$$

and

$$u_Q(t) = V_\pi \cdot \Im\{s(t)\} - V_\pi, \quad (3.17)$$

respectively. As 4-QAM is adopted, we use the same assumptions in Section §3.1.3.2. Substituting Eq. (3.17) and (3.18) into Eq. (3.16), we have

$$\begin{aligned} E_{\text{out}}(t) &= E_{\text{in}}(t) \cdot \left[ \cos\left(\pi \frac{V_\pi \cdot \Re\{s(t)\} - V_\pi}{2V_\pi}\right) + j \cdot \cos\left(\pi \frac{V_\pi \cdot \Im\{s(t)\} - V_\pi}{2V_\pi}\right) \right] \\ &= E_{\text{in}}(t) \cdot \left[ \sin \frac{\pi}{2} \Re\{s(t)\} + j \cdot \cos \frac{\pi}{2} \Im\{s(t)\} \right] \\ &\approx E_{\text{in}}(t) \cdot [\Re\{s(t)\} + j \cdot \Im\{s(t)\}] \\ &= E_{\text{in}}(t) \cdot s(t). \end{aligned} \quad (3.18)$$

## §3.2 Optical Fibers

Optical fibers serve as the physical medium that is transparent to information transmission in the form of light. Optical fibers consist of a core in which light

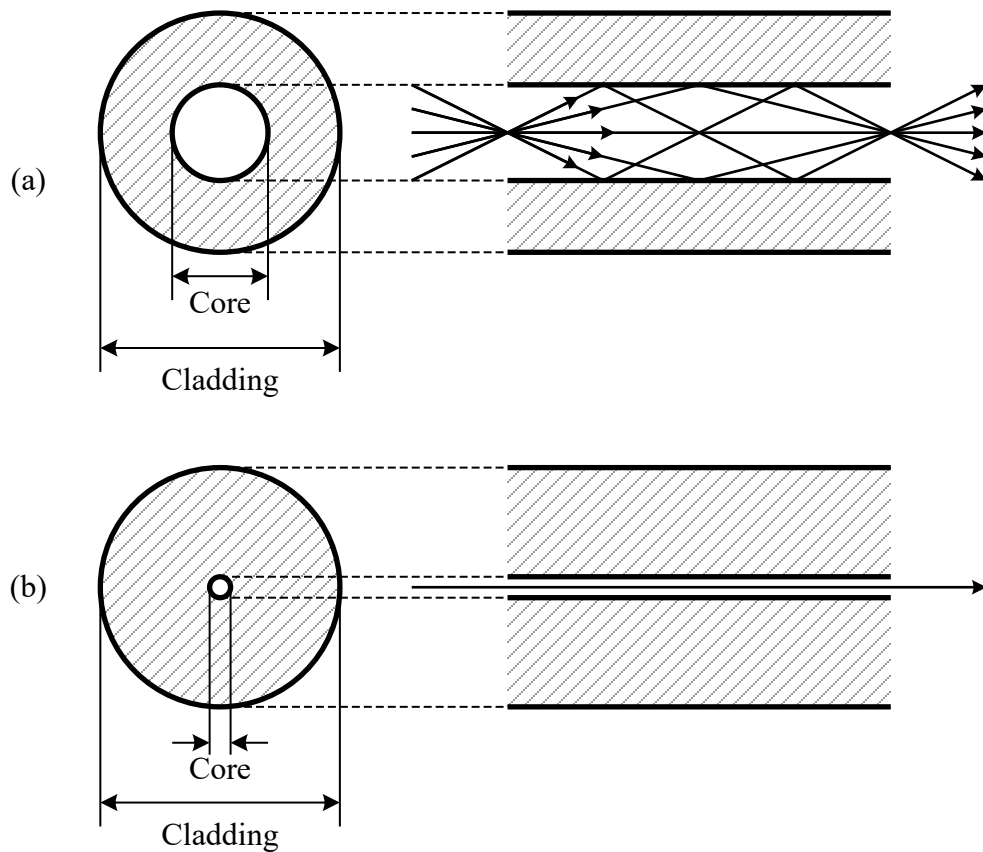


Figure 3–5. Basic structures of (a) multimode fibers and (b) single-mode fibers and illustrations of light propagation in them.

travels, surrounded by cladding which confines the light in the core, thanks to the phenomenon of total internal reflection that dielectric wave-guiding provided by refractive-index difference between core and cladding.

The subject revolving around the scientific research and engineering applications using optical fibers is fiber optics. There are different types of optical fibers depending on the purposes of how to use them. In fiber-optic communication systems, for example, depending on the diameter of the fiber, there are multimode fibers (MMFs), which support many propagation paths, and single-mode fibers (SMFs), which support only a single path for light propagation.

### §3.2.1 Multimode Fiber

Multimode fibers, whose core diameter is fairly larger than the wavelength of light, support more than one propagation paths, i.e. transverse modes, as shown

in Figure 3–6 (a). The standardized MMFs in optical Ethernet, for example, have core diameter about 50  $\mu\text{m}$ , surrounded by cladding of 125-micron diameter. For its large diameter, multimode fibers are easy for light coupling from lasers and to photodiodes, and for joining fibers to fibers, which is a favorable property for paving fiber links. Its capacity, however, is also limited by the distortion induced from light travelling through different paths due to its large diameter. Hence, MMFs are suitable for communication systems targeting relative low data rate ( $< 10$  Gbits) of short-reach ( $< 1$  km) applications.

Although the divergence of propagation paths (transverse modes) in multimode fiber induces intermodal interference that limits its capacity, the feature of multimodal propagation can be utilized in an ingenious approach by multiplexing distinct light links onto different distinguishable modes for communication, multiplying the capacity of a single piece of fiber. Such technique is named mode-division multiplexing (MDM). In MDM systems, data are split into difference streams and each stream is fed into a specific mode in the MMF for transmission. If the MMF is well-designed and engineered, the data is able to travel within the MMF at their own mode, with minimum intermodal interference to other modes. At the receiver, with the advanced digital signal processing techniques for data recovery and interference cancellation, similar to the multiple-input multiple-output technique in wireless communication systems, each data stream can be de-multiplexed.

### §3.2.2 Single-Mode Fiber

Single-mode fiber, in contrast to the multimode fiber, is a type of optical fiber whose core diameter is designed so small that only a single path (mode) exists for light propagation within the fiber, as illustrated in Figure 3–6 (a). Intermodal interference in single-mode fiber vanishes as a result of the single-mode transmission, and its capacity is improved significantly. The advantages make single-mode fibers suitable for high-speed ( $> 10$  Gbps) communication systems over long distance ( $> 1\text{km}$ ).

Although single-mode fibers are relatively ideal channel, compared to any

other channel media including the multimode fibers, there are physical limitations still, such as chromatic dispersion, polarization-mode dispersion, and nonlinearities, in single-mode fibers, especially in the demands for fiber-optic systems over 100 Gbps targeting transmission over 40 km. In this section, we focus on the characteristics of single-mode fibers and their impacts on optical pulses that are traveling therein.

In the single-mode fiber, as an optical pulse passes through the fiber, various physical effects are given rise to changes on the light, which in most cases are regarded as impairments. Different models can be developed for different applications. In the fiber-optic communications, the optical fiber can be almost exclusively described by the following propagation equation

$$\frac{\partial E(t, z)}{\partial z} + \frac{\alpha}{2} E(t, z) = j \cdot \sum_{m=1}^{\infty} \frac{j^m \cdot \beta_m}{m!} \frac{\partial^m E(t, z)}{\partial t^m} + j \cdot \gamma |E(t, z)|^2 E(t, z), \quad (3.19)$$

where  $E(t, z)$  is the optical field at distance  $z$  and time  $t$ ,  $\alpha$  is the attenuation coefficient,  $\beta_m$  is the  $m$ -th order dispersion parameter,  $\gamma$  is the nonlinear parameter. It should be noted that above equation is based on some assumptions for simplification. For instance, in Eq. (3.20) single polarization is considered and the Raman Effect is omitted; the term  $E(t, z)$  is the slowly varying envelope of the pulse which can be regarded as the optical field in baseband at the central frequency  $f_0 = \omega_0 / 2\pi$ , and  $\beta_m$  are defined as

$$\beta_m = \left. \frac{\partial^m \beta}{\partial \omega^m} \right|_{\omega=\omega_0}. \quad (3.20)$$

In Eq. (3.20), the first term describes the optical field  $E(t, z)$  propagating in the fiber. The second term in the left-hand side denotes attenuation, and the two terms in the right-hand side represent chromatic dispersion and the nonlinear Kerr effect, respectively. The equation can be trimmed to be more concise and simpler form depending on the specific applications. In the section, we take a deep look on the optical single-mode fibers and formulate the transmission model for communication signals.

Eq. (3.20) is a well-enough pulse propagation model for channel characterization in fiber-optic communication systems. In this Chapter, we will study the linear models of optical fiber channels and integrate the models into the general transmission model introduced in Section §2.3 Communication Channel based on the linear time-invariant theory for the topics studied in the following Chapters. It should be noted that the nonlinearity term in Eq. (3.20) will not be considered here. However, it is one of the most important subjects in current and as well future fiber-optic systems. Especially, the compensation of nonlinear impairments should be carefully considered because fiber nonlinearity interacts with the attenuation and dispersion effects in a complicated time-frequency manner. More sophisticated models and insightful understanding on fiber-optics can be found in these excellent literatures [24, 25, 52, 53].

### §3.2.2.1 Attenuation

In the pulse propagation equation of single-mode fiber in Eq. (3.20), the second term about  $\alpha$  tells the effect of attenuation. In the case of, for example, a beam of unmodulated continuous wave in the fiber, an extremely simple model dealing with only attenuation arises, by forcing the left-hand side to be zero, as

$$\frac{\partial E(t, z)}{\partial z} + \frac{\alpha}{2} E(t, z) = 0, \quad (3.21)$$

with the solution

$$E(t, z) = e^{-\frac{\alpha}{2}z} \cdot E(t, 0), \quad (3.22)$$

The power of the optical signal is

$$P(t, z) = |E(t, z)|^2 = e^{-\alpha z} \cdot P(t, 0), \quad (3.23)$$

with attenuation

$$\frac{P(t, z)}{P(t, 0)} = e^{-\alpha z}. \quad (3.24)$$

In commercially available single-mode fibers, the attenuation is typically from 0.16 dB/km to 0.5 dB/km in the optical window from 1300 to 1700 with the hydrogen absorption being carefully handled. The attenuation coefficient unit

in decibel is

$$\begin{aligned}\alpha_{dB} &= \frac{10 \log_{10} e^{-\alpha z}}{z} \\ &= \alpha \times 10 \log_{10} e \approx 4.343 \times \alpha.\end{aligned}\quad (3.25)$$

The model in Eq. (3.22) is suitable for continuous wave analysis or optical signal with fairly narrowband, which introduces negligible dispersion after fiber transmission. If the bandwidth of the optical signal is above gigahertz, chromatic dispersion should be carefully considered.

### §3.2.2.2 Chromatic Dispersion

Chromatic dispersion, formulated by the first term in the right-hand side in Eq. (3.20), describes the phenomenon that the phase velocity of the optical pulse varies for different frequency components. The reason why we use light pulse in the model when referring to chromatic dispersion is because pulse occupies a relatively broad spectrum, and chromatic dispersion happens if multiple frequency components exists in the fiber. Although chromatic dispersion induces only phase change on the spectrum of the signal, the shape of the optical signal in the time domain is consequently changed, resulting in pulse broadening that is inter-symbol interference (ISI) in signal transmission.

Omitting the nonlinear part in Eq. (3.20), one obtains

$$\frac{\partial E(t, z)}{\partial z} + \frac{\alpha}{2} E(t, z) = j \cdot \sum_{m=1}^{\infty} \frac{j^m \cdot \beta_m}{m!} \frac{\partial^m E(t, z)}{\partial t^m}, \quad (3.26)$$

and the frequency duality is

$$\frac{\partial E(\omega, z)}{\partial z} = \left( j \cdot \sum_{m=1}^{\infty} \frac{\beta_m}{m!} \Delta \omega^m - \frac{\alpha}{2} \right) E(\omega, z), \quad (3.27)$$

The solution to Eq. (3.28) in the frequency domain is simply

$$\begin{aligned}E(\omega, z) &= e^{\left( -\frac{\alpha}{2} + j \cdot \sum_{m=1}^{\infty} \frac{\beta_m}{m!} \Delta \omega^m \right) z} E(\omega, 0) \\ &= e^{-\frac{\alpha}{2} z} e^{j \beta(\omega) z} \cdot E(\omega, 0),\end{aligned}\quad (3.28)$$

where  $\alpha$  accounts for the attenuation and  $\beta(\omega)$  for the chromatic dispersion that

is the frequency depended phase due to the frequency depended refractive index of the fiber. The term

$$H(w, z) = e^{\frac{\alpha}{2}z} e^{j\beta(\omega)z}, \quad (3.29)$$

in Eq. (3.29) is the transfer function of the fiber channel.

From (3.29), one can easily deduce that the dispersion coefficients  $\beta_m$  we formulated in Eq. (3.20) are actually the Taylor coefficients of  $\beta(\omega)$  as

$$\beta(\omega) = \sum_{m=1}^{\infty} \frac{\beta_m}{m!} \Delta\omega^m = \sum_{m=1}^{\infty} \frac{\beta_m}{m!} (\omega - \omega_0)^m. \quad (3.30)$$

It should be noted that in Eq. (3.31) we actually omit an initial phase parameter  $\beta_0$ , a common phase which is independent of the optical pulse and fiber channel and thus does not affect the analysis.

The first derivative of  $\beta(\omega)$ , namely  $\beta_1$ , denotes the group velocity of a wave packet in the fiber. It is proportional to the angular phase velocity  $\omega$ , and thus  $\beta_1$  does not change the shape of optical pulses as they travel down through the fiber. However, in practical waveguide material for optical fibers, the material is dispersive, and it means that high order group velocity parameters,  $\beta_m$  for  $m > 2$ , are not equal to zero, and they contribute to the dispersion effect on the optical pulse.

In single-mode fibers, the second group velocity parameter,  $\beta_2$ , is the called the group velocity dispersion (GVD) parameter, and the third parameter,  $\beta_3$ , is the differential GVD parameter, etc. In practical fiber-optic systems, the second order group velocity parameter, namely GVD parameter dominates the dispersive effect in most cases.

The time-domain solution to Eq. (3.27) can be readily obtained by performing an inverse Fourier transform on  $E(\omega, z)$  in Eq (3.29) with respect to  $\omega$ , as

$$\begin{aligned} E(t, z) &= \mathcal{F}\{E(\omega, z)\} = \frac{1}{2\pi} \int E(\omega, z) e^{j\omega t} d\omega \\ &= \frac{1}{2\pi} \int e^{\left(\frac{\alpha}{2} + j \sum_{m=1}^{\infty} \frac{\beta_m \Delta\omega^m}{m!}\right)z} E(\omega, 0) e^{j\omega t} d\omega. \end{aligned} \quad (3.31)$$

According to convolution theorem, the term,

$$h(t, z) = \frac{1}{2\pi} \int e^{\left(-\frac{\alpha}{2} + j \sum_{m=1}^{\infty} \frac{\beta_m \Delta \omega^m}{m!}\right)z} e^{j\omega t} d\omega, \quad (3.32)$$

can be abstracted from Eq. (2.32). In Eq. (3.33),  $h(t, z)$  can be regarded as the signal-dependent impulse response of the fiber channel, which is determined by the spectrum of the optical pulse transmitted inside the fiber.

In the following, we will take some special situations derived from the fiber model in Eq. (3.27) for examples, to understand how pulses propagate through an optical fiber.

### OPTICAL FIBER WITH ATTENUATION

In an ideal optical fiber whose refractive coefficient does not change with respect to the frequency or in an optical fiber in which a beam of light with single wavelength is traveling, all the frequency components have the same velocity and thus the same delay. In other words, the group velocity is a constant, and the terms  $\beta_m = 0$  for  $m \geq 2$ . The frequency-domain description of the optical field after a fiber transmission at distance,  $z$ , is

$$E(\omega, z) = e^{-\frac{\alpha}{2}z} e^{j\beta_1 \Delta \omega \cdot z} \cdot E(\omega, 0), \quad (3.33)$$

and the time-domain description is

$$E(t, z) = e^{-\frac{\alpha}{2}z} e^{-j\beta_1 \omega_0 \cdot z} E(t - \beta_1 z, 0). \quad (3.34)$$

Therefore, the frequency transfer function and the channel impulse response of the idea optical fiber with attenuation and propagation delay are given by

$$H(\omega) = e^{-\frac{\alpha}{2}z} e^{j\beta_1 z(\omega - \omega_0)}, \quad (3.35)$$

and the time-domain description is

$$\begin{aligned} h(t) &= \mathcal{F}^{-1}\{H(\omega, z)\} \\ &= e^{-\frac{\alpha}{2}z} \delta(t - \beta_1 z), \end{aligned} \quad (3.36)$$

respectively.

### OPTICAL FIBER WITH GROUP VELOCITY DISPERSION

In practical fiber-optic communication systems, the bandwidth of the modulated optical signal is about tens billion Hertz, which is relatively small compared to the frequency of the optical carrier  $f_0 = 2\pi\omega_0$  that is typically at around hundreds of trillion Hertz. We can approximate the group velocity by using the group velocity dispersion (GVD) parameter  $\beta_2$  as

$$\beta(\omega) = \beta_1\Delta\omega + \frac{1}{2}\beta_2\Delta\omega^2. \quad (3.37)$$

According to Eq. (3.38), the frequency-domain description of the optical field after the fiber transmission is

$$E(\omega, z) = e^{-\frac{\alpha}{2}z} e^{j\left(\beta_1\Delta\omega + \frac{1}{2}\beta_2\Delta\omega^2\right)z} \cdot E(\omega, 0). \quad (3.38)$$

The time-domain description of the optical field usually does not have analytical solution with respect to  $E(\omega, 0)$ <sup>12</sup>. The transfer function of the optical fiber is given by

$$H(\omega, z) = e^{-\frac{\alpha}{2}z} e^{j\left(\beta_1\Delta\omega + \frac{1}{2}\beta_2\Delta\omega^2\right)z} \quad (3.39)$$

and the corresponding channel impulse response can be solved by calculating the inverse Fourier transform on Eq. (3.40), as

$$h(t, z) = \mathcal{F}^{-1}\{H(\omega, z)\}. \quad (3.40)$$

According to the convolution theorem, the time-domain description of the optical field is thus given by

$$E(t, z) = h(t, z) * E(t, 0). \quad (3.41)$$

Usually, we describe the group velocity dispersion by using a dispersion parameter, which is defined as

---

<sup>12</sup> In some cases, closed-form solution can be obtained. For example, for Gaussian pulses.

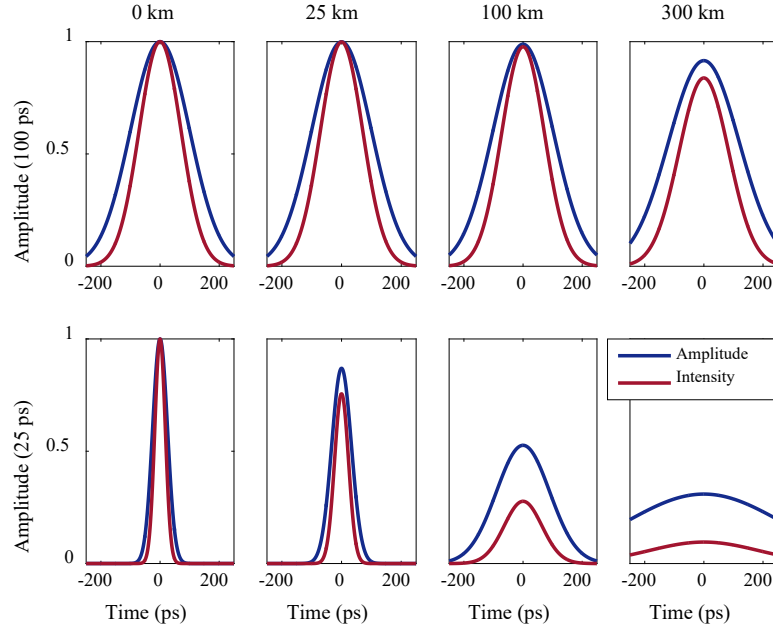


Figure 3–6. Dispersion-induced broadening of a Gaussian pulse in a fiber at different distances (0, 25, 100 and 300 km) and pulse width (25 ps and 100 ps).

$$\begin{aligned}
 D &= \frac{d}{d\lambda} \left( \frac{1}{v_g} \right) = \frac{d}{d\lambda} \left( \frac{d\beta}{d\omega} \right) \\
 &= \frac{d\omega}{d\lambda} \cdot \frac{d^2\beta}{d\omega^2} = -\frac{2\pi c}{\lambda^2} \beta_2,
 \end{aligned} \tag{3.42}$$

where  $v_g$  is the group velocity of the optical pulse.

To demonstrate the effect of chromatic dispersion, a Gaussian pulse is used as the input of an optical fiber with  $D = 19 \text{ ps}/(\text{km} \cdot \text{nm})$ . The pulse in the fiber at 0, 25, 100, and 300 km is illustrated in Figure 3–7. It can be seen that the extent of pulse broadening depends on the initial pulse width and transmission distance. Shorter pulses correspond to higher symbol rate and occupy broader bandwidth, and thus experience more serious dispersion-induced broadening effects than wider pulses which have narrower bandwidth and thus lower data rate. Consequently, the dispersive pulses will extend into neighboring pulses, resulting in serious ISI. In long-haul transmission systems where optical amplifiers are used to compensate the signal power loss, the accumulated dispersion in the optical pulse becomes the dominant limitation.

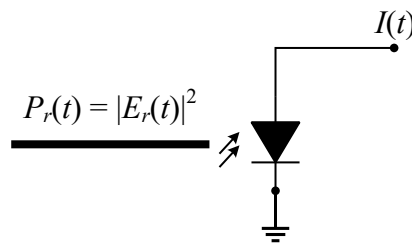


Figure 3–7. Optical direct detection using a single photodiode.

### §3.3 Optical Receiver

As the light travels down to the end of fiber link, arriving at receiver, the optical signal is perceived and converted back to electrical domain. According to the modulation formats, corresponding detection techniques should be applied.

There are two straightforward detection schemes, direct detection that converts the intensity of light beam to electrical current and coherent detection that retrieves the optical field information of light beam, including the phase and amplitude. Direct detection is the simplest and most efficient approach for intensity modulation schemes by a single photodiode, whose bandwidth can be up to 100 GHz. In direct detection system, the phase information is completely lost as the photodiode is a square-law detection. On the other hand, if advanced modulation formats, such as PSK and QAM, involving phase modulation are adopted, optical coherent detection should be employed to recover all the modulated information at the receiver end.

#### §3.3.1 Optical Direct Detection

In the fiber-optic systems employing direct detection, photodiode serves as the interface that converts the optical signal back to the electrical signal, as shown in Figure 3–8. The output current of the photodiode is proportional to the input optical power (intensity), as

$$I(t) = R \cdot |E_r(t)|^2 = R \cdot P_r(t), \quad (3.43)$$

where  $E_r(t)$  is the input optical field to the photodiode,  $R$  is the responsivity of the photodiode, and  $I(t)$  is the output electric current.

### §3.3.2 Optical Coherent Detection

In the advanced fiber-optic communication systems, information is modulated onto both amplitude and phase of an optical carrier. At the receiver, to preserve all the information in the optical field, coherent detection should be employed.

Optical coherent detection is the technique capable of extracting all the information with optimal receiver sensitivity [54]. The concept of optical coherent detection was demonstrated and attracted considerable attention during the 1980s. However, the advent of optical amplifiers and WDM technology, and the unstable phase tracking and immature high-speed digital circuits faded the interest in optical coherent detection. Although it had been theoretically shown that coherent detection can approach the capacity limit of optical-fiber channel, it is not practical in commercial optic-fiber systems until circa 2005.

Around the 2000, as the bandwidth of optical fiber was fully expanded and the Internet continued to boom, improving the spectral efficiency is one solution to cater for the capacity demand. Although differential modulation formats and self-homodyne receiver relieves the rigorous requirement of laser linewidth, receiver sensitivity is still far from the theoretical limit unless coherent detection is adopted [55]. Moreover, coherent detection, combining with digital signal processing (DSP), is capable of compensating the linear impairments completely and mitigating the nonlinear impairments in optical fiber channel [56].

The high-speed analog-to-digital convertor (ADC) and narrow linewidth local oscillator (LO), etc., enable coherent detection with DSP to compensate the linear impairment of optical fiber [57]. For example, Kikuchi *et al.* demonstrated a 40 Gbits/s quadrature phase shift keying (QPSK) transmission over 200 km with spectral efficiency 2.5 bit/s/Hz in 2006 [58]. In 2010, 69.1 TBits/s transmission over 240 km with spectral efficiency of 6.4 bit/s/Hz was demonstrated in 2010, in which there were 432 channels each of which conveys 171

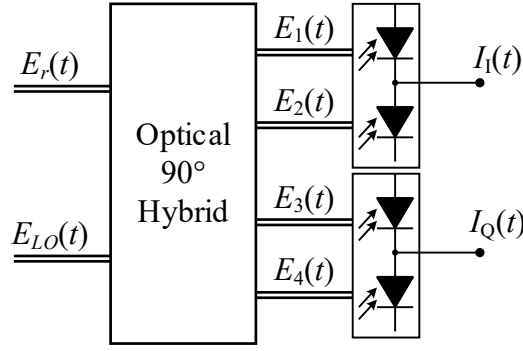


Figure 3–8. Optical coherent receiver composed of optical  $90^\circ$  hybrid and a pair of balanced photodiodes for single-polarization optical receiver.

Gbits/s 16-ary QAM (16-QAM) polarization division multiplexing (PDM) signals [59].

In the optical coherent detection, the essential element comprising the optical coherent receiver is the so-called optical  $90^\circ$  hybrid which is essentially a  $2 \times 4$  multimode interferometer, which has two input ports, one for signal and the other for local oscillator. The optical fields of the four output ports can be mathematically represented by

$$\mathbf{E}_{\text{out}} = \begin{pmatrix} E_1(t) \\ E_2(t) \\ E_3(t) \\ E_4(t) \end{pmatrix} = \mathbf{M} \mathbf{E}_{\text{in}} = \frac{1}{2} \begin{pmatrix} 1 & 1 \\ 1 & -1 \\ 1 & j \\ 1 & -j \end{pmatrix} \begin{pmatrix} E_r(t) \\ E_{LO}(t) \end{pmatrix}, \quad (3.44)$$

where  $\mathbf{M}$  is the transfer matrix of the optical  $90^\circ$  hybrid, and  $E_r(t)$  and  $E_{LO}(t)$  are the optical fields of incoming signal and local oscillator (LO), respectively. Following the optical hybrid, there are a pair of balanced photodiode. Providing that the responsivities of the photodiodes are the same i.e.,  $R$ , the output electrical currents of the balanced photodiodes are

$$I_I(t) = R \cdot |E_1(t)|^2 - R \cdot |E_2(t)|^2, \quad (3.45)$$

and

$$I_Q(t) = R \cdot |E_3(t)|^2 - R \cdot |E_4(t)|^2, \quad (3.46)$$

respectively. Substituting  $E_1(t)$  and  $E_2(t)$  into Eq. (3.46) one can get

$$\begin{aligned}
I_1(t) &= \frac{1}{4} R \cdot \left[ |E_r(t) + E_{LO}(t)|^2 - |E_r(t) - E_{LO}(t)|^2 \right] \\
&= R \cdot \Re\{E_r(t)E_{LO}^*(t)\},
\end{aligned} \tag{3.47}$$

and,  $E_3(t)$  and  $E_4(t)$  into Eq. (3.47),

$$\begin{aligned}
I_Q(t) &= \frac{1}{4} R \cdot \left[ |E_r(t) + j \cdot E_{LO}(t)|^2 - |E_r(t) - j \cdot E_{LO}(t)|^2 \right] \\
&= R \cdot \Im\{E_r(t)E_{LO}^*(t)\}.
\end{aligned} \tag{3.48}$$

Ideally, the local oscillator is a continuous wave with frequency exactly at the frequency of the optical carrier, i.e., homodyne detection. Practically, this condition, however, can be hardly achieved. In practice, the optical signal is down-converted to the baseband with some frequency offset, and the frequency offset will be eliminated via frequency offset compensation.

If the optical frequency of the local oscillator (LO) is  $f_{LO}$  with phase noise  $\theta_{LO}(t)$ , and we take Eq. (3.14) into account, the received complex signal is

$$\begin{aligned}
r(t) &= E_1(t) + j \cdot E_Q(t) \\
&= R \cdot [\Re\{E_{in}(t)E_{LO}^*(t)\} + j \cdot \Im\{E_{in}(t)E_{LO}^*(t)\}] \\
&= R\sqrt{P_R P_{LO}} \cdot s(t) e^{j2\pi(f_c - f_{LO})t} \cdot e^{j[\theta_T(t) + \theta_{LO}(t)]} + n(t),
\end{aligned} \tag{3.49}$$

where  $s(t)$  is the complex baseband signal modulated on the optical carrier,  $P_R$  and  $P_{LO}$  are the power of the incoming signal and the LO, and  $n(t)$  is the additive noise term which includes the accumulated amplified spontaneous emission (ASE) noise from optical amplifiers and the shot noise from the laser source at the transmitter and that of LO at the receiver.

Although the frequency and phase of both the transmitter laser and the LO will drift over time in practical system, homodyne detection, in which  $f_c = f_{LO}$ , is of more interest. In homodyne detection, the frequency offset between  $f_c$  and  $f_{LO}$  is negligible and the residual frequency offset can be easily compensated via DSP algorithms. Another alternative coherent detection is heterodyne detection, in which there exists obvious frequency offset between the local oscillator and the carrier frequency. The received signal is first converted to an intermediate frequency and then baseband. In practical coherent optical system, there exists a phase noise term,  $\theta(t) = \theta_T(t) + \theta_{LO}(t)$ , due to the random variation

---

of lasers, and the phase noise can also be compensated using DSP algorithms.



# Part I



## Chapter 4

# Double-Sideband Modulated Fast-OFDM

In orthogonal frequency-division multiplexing, the condition of orthogonality is that the subcarrier spacing is the multiple of the reciprocal of symbol period, and both the amplitudes and the phases of the subcarriers can be employed for modulation. Fast-OFDM is the principle that the subcarrier spacing is further reduced by half to that in the OFDM that destroys orthogonality between the subcarriers, as shown in Figure 4–1. Intuitively, interference occurs as a result of the loss of orthogonality. By controlling the phase of the subcarriers of halved spacing, it can be shown that the interference can be rejected without degrading the system performance. It means that, given the same bandwidth, Fast-OFDM is able to stuff more, approximately doubled, subcarriers than OFDM. However, in the Fast-OFDM, the phases of the subcarriers are devoted without modulating information, and only one of the two quadrature components of the complex amplitudes of the subcarriers can be employed for modulation. Therefore, both the OFDM and the Fast-OFDM achieve the same spectral efficiency still.

In virtue of its unique properties, Fast-OFDM becomes more attractive than the conventional OFDM in some applications. However, problems incur in the Fast-OFDM system as the consequence of loss of orthogonality. Depending on different implementations, Fast-OFDM systems exhibit different pros and cons,

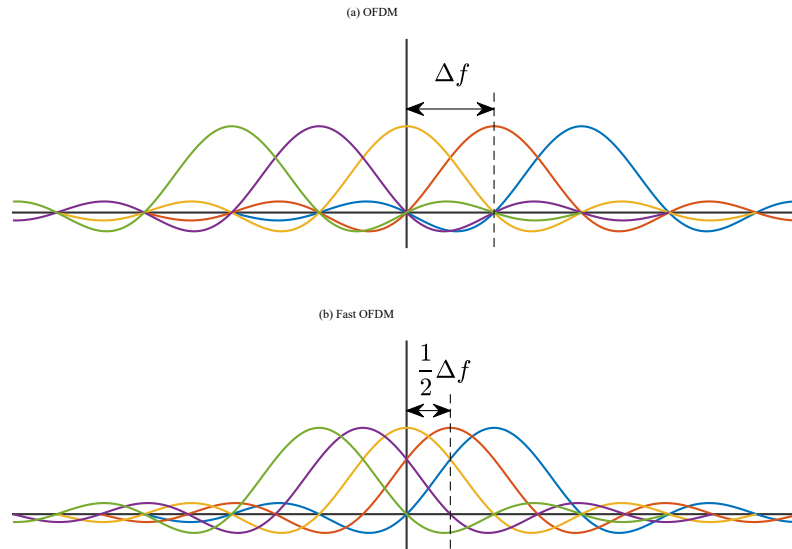


Figure 4–1. Illustration of the spectra of the subcarriers of (a) conventional OFDM signal and (b) Fast OFDM signal.

and the cons should be carefully considered and targeted accordingly.

In this thesis, we will consider both the double sideband (DSB) modulated Fast-OFDM signal in Chapter 4 and the single sideband modulated Fast-OFDM in Chapter 5 to deal with the problems arising from the loss of orthogonality.

This chapter, which is dedicated to the DSB modulated Fast-OFDM system, is organized as follows. Section §4.1 introduces the history and development of the DSB Fast-OFDM. In Section §4.2, the mathematical model of DSB Fast-OFDM system is formulated; the problems are analytically formulated to show that the channel distortion imposed on the DSB Fast-OFDM signal cannot be easily compensated, and interference occurs between the subcarrier as the convolution-multiplication property, possessed by the OFDM system, does not hold in the DSB Fast-OFDM system. Section §4.3 targets on the problems, and proposes a DSB Fast-OFDM system which is capable of equalizing the channel distortion with single-tap equalizers and of de-multiplexing the subcarriers of halved spacing without any interference. In Section §4.4, simulations are carried out in both wireless multipath fading channel and optical multi-mode fiber (MMF) channel to investigate the proposed Fast-OFDM system. In Section

§4.5, experimental results are provided to validate the feasibility of the proposed DSB Fast-OFDM system in both the conventional 1.55- $\mu\text{m}$  fiber-optic system using standard silica single-mode fiber (S-SMF) and the emerging 2- $\mu\text{m}$  system of hollow-core photonic bandgap fiber (HC-PBGF). Finally, Section §4.6 concludes this Chapter.

## §4.1 Background

With the widespread of OFDM, multicarrier systems become extremely attractive in the blueprint of the future communication systems since the late 1990s. Different multicarrier systems were proposed conceptually or even experimentally for different applications. Other than the discrete Fourier transform (DFT) in OFDM, researchers are especially interested in the multicarrier systems employing trigonometric transforms, e.g., discrete cosine transforms (DCT) and discrete sine transforms (DST), and discrete Hartley transform (DHT).

### THE BIRTH OF THE CONCEPT OF FAST-OFDM

In 2002, Rodrigues and Darwazeh proposed a concept of OFDM scheme for doubling the data rate of conventional OFDM by truncating the last half of the inverse DFT (IDFT) output in OFDM systems, and termed such scheme as Fast-OFDM [60]. In the scheme, it seems that the data rate is doubled because the same number of subcarriers can be delivered using halved time to the conventional OFDM. However, only single quadrature modulation schemes, such as pulse amplitude modulation (PAM) and amplitude shift keying (ASK), can be used in the Fast-OFDM, while quadrature amplitude modulation (QAM) can be used in the OFDM systems. The Fast-OFDM actually achieves the same data rate as the OFDM. In 2003, Xiong proposed to use the real-valued cosine waveforms to implement OFDM for subcarrier multiplexing and demultiplexing rather than the complex exponential waveforms in the conventional OFDM [61]. The subcarrier spacing of cosine waveforms is halved to that of the complex exponential waveforms since the cosine waveforms allow the condition

for orthogonality that

$$\frac{1}{T_s} \int_0^{T_s} \cos 2\pi m \frac{t}{2T_s} \cos 2\pi n \frac{t}{2T_s} dt = \begin{cases} 1 & m = n = 0 \\ \frac{1}{2} & m = n \neq 0 \\ 0 & m \neq n \end{cases} . \quad (4.1)$$

Moreover, the continuous-time Fast-OFDM signal can be generated digitally by using the DCT.

The spectra of these two Fast-OFDM schemes are equivalent to that illustrated in Figure 4–1 (b). The difference between them is that the first one generates SSB modulated Fast-OFDM signals while the second one generates DSB modulated Fast-OFDM signals. These two schemes become the prototypes of Fast-OFDM family. In this chapter, we will focus on the DSB Fast-OFDM, and the following chapter is dedicated to the SSB Fast-OFDM.

## LIMITATIONS OF FAST-OFDM FOR COMMUNICATIONS

Researchers began to investigate the possibility of applying the concept of Fast-OFDM for communications [62-67]. Soon, it was found that there exists a critical problem induced by Fast-OFDM waveforms. In the DSB Fast-OFDM, the cosine waveforms are orthogonal and the DCTs that implements the waveforms digitally, are also orthogonal. However, DCT does not possess the convolution-multiplication property as DFT. It means that if the DSB Fast-OFDM signal passes through a channel whose channel impulse response (CIR) is not an ideal Dirac impulse, the received subcarriers are no longer the products of channel frequency responses (CFR) and the transmitted subcarriers. Unwanted interference occurs between the subcarriers, resulting in significant degradation.

In fact, the cosine transform and DCT possess symmetric convolution-multiplication property, and the convolution theorem in terms of the DCT says that the DCT of the convolution of two symmetric sequences is equal to the multiplication of the DCT of the sequences [68]. The condition to meet symmetric

convolution-multiplication property requires the adoption of symmetric prefix and suffix for the transmitted Fast-OFDM signal and also requires the CIR to be a symmetric function. The second requirement is almost impossible for a practical communication system because there is no practical communication channel whose CIR function is symmetric. Moreover, the symmetric requirement imposes strict timing synchronization.

To deal with the symmetric requirement, compromises are made in [62, 63] to transmit a symmetric duplicate of the Fast-OFDM signal, sacrificing data rate by half. Additional operations are required at the receiver to make the equivalent CIR function to be symmetric. In [65], a receiver scheme is proposed to adopt a complicated time-domain equalizer to firstly filter the CIR to be symmetric before demodulating the Fast-OFDM signal. However, the advantage of using single-tap equalizers for multicarrier system for simplifying system complexity vanishes.

## FAST-OFDM IN OPTICAL COMMUNICATION SYSTEMS

Though the equalization problem makes the DSB Fast-OFDM scheme a poor competence to the conventional OFDM, the idea of DSB Fast-OFDM was introduced into optic-fiber communications in 2010 [69-73]. It is claimed that the DSB Fast-OFDM is suitable for the intensity modulated fiber-optic systems as the DCT directly generates the real-valued signal for transmission. On the other hand, if one wants to adapt the conventional OFDM for intensity modulation, an alternative OFDM scheme, discrete multi-tone (DMT) modulation should be adopted by mapping image subcarriers at the negative frequency, which are symmetric conjugations to the subcarrier at the positive frequency. In [74], it is also shown that the DSB Fast-OFDM system is suitable for full-field detection optical system with enhance receiver sensitivity.

In the fiber-optic communication systems, optical fiber is the almost ideal channel for signal transmission. Especially, for the Fast-OFDM, the chromatic dispersion in optical fiber is symmetric, and that, kind of, relieves the requirement of symmetric convolution for the DSB Fast-OFDM systems [75, 76]. However, strict timing synchronization is required during sampling for analog-

to-digital conversion, which greatly complicates the system [77]. In addition, chromatic dispersion is only an ideal mathematical model, and it is just one of many distortion effects in a fiber-optic system. As the data rate increases, the system becomes unstable since the shape of the CIR function of the entire system becomes far from symmetry.

## §4.2 System Model of the DSB Fast-OFDM

In the Fast-OFDM system, the DSB modulated Fast-OFDM signal is the synthesis of a bunch cosine waveforms, which are mutually orthogonal, as

$$s(t) = \sqrt{\frac{2}{T_s}} \sum_{k=0}^{N-1} \varepsilon(k) x(k) \cos 2\pi k \Delta f \times t, \quad 0 \leq t < T_s \quad (4.2)$$

where

$$\varepsilon(k) = \begin{cases} \sqrt{0.5} & k = 0 \\ 1 & k \neq 0 \end{cases}, \quad (4.3)$$

is a coefficient for normalization,  $T_s$  is the symbol period, and  $\Delta f = 1 / (2T_s)$  is the subcarrier spacing. According to Eq. (4.1), the subcarriers are orthogonal. If there is no channel dispersion but noise, the received signal is given as

$$r(t) = s(t) + v(t), \quad (4.4)$$

and each subcarrier can be demodulated by a corresponding matched filter as

$$\begin{aligned} \hat{x}(m) &= \sqrt{\frac{2}{T_s}} \varepsilon(m) \int_0^{T_s} r(t) \cos(2\pi m \Delta f \times t) dt \\ &= \frac{2}{T_s} \sum_{k=0}^{N-1} \varepsilon(k) x(k) \int_0^{T_s} r(t) \cos(2\pi m \Delta f \times t) \cos(2\pi k \Delta f \times t) dt \\ &\quad + v_{\Theta}(m) \\ &= x(m) + v_{\Theta}(m), \end{aligned} \quad (4.5)$$

where  $v_{\Theta}(m)$  is the noise after the matched filter.

In the above model, the channel dispersion is not considered, or equivalently it is considered ideally as a Dirac delta function, namely  $h(t) = \delta(t)$ . If there is

not the case that the channel is not ideal, the demodulation process in Eq. (4.5) does not hold. Nonetheless, if the CIR of channel is a symmetric function, one can easily, by using the property of Fourier transform, prove that the convolution-multiplication processing can be applied to the demodulation process.

### §4.2.1 Digital Implementation of the DSB Fast-OFDM

The Fast-OFDM system can be implemented in discrete-time domain by using DCT, and the system diagram is illustrated in Figure 4–2. In the DCT family, there are four types of DCT with slight differences [78]. The second and the third DCT types are transformation pair, which are orthogonal to each other.

The transmitter of the DCT based Fast-OFDM system is illustrated in Figure 4–2 (a). In contrast to the conventional OFDM, the time-domain signal block is generated using IDCT, i.e., the DCT of type III, which is given by

$$\begin{aligned} s(n) &= \mathcal{C}^{-1}\{x(k)\} \\ &= \sqrt{\frac{2}{N}} \sum_{k=0}^{N-1} \varepsilon(k) x(k) \cos\left[\frac{\pi}{N} k \left(n + \frac{1}{2}\right)\right], \quad n = 0, \dots, N-1, \end{aligned} \quad (4.6)$$

The received discrete-time signal without dispersion but only noise is

$$r(n) = s(n) + v(n), \quad (4.7)$$

and similar to Eq. (4.5), the symbols can be demodulated by performing the forward DCT, as

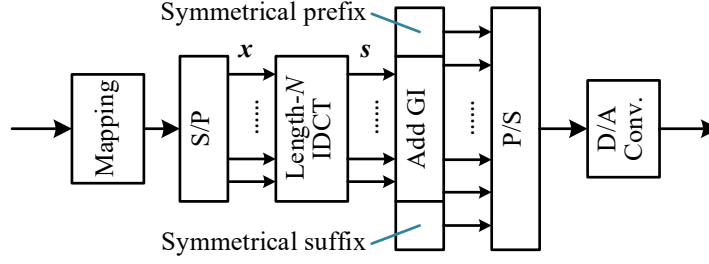
$$\begin{aligned} \hat{x}(m) &= \mathcal{C}\{r(n)\} \\ &= \sqrt{\frac{2}{N}} \varepsilon(m) \sum_{n=0}^{N-1} r(n) \cos\left[\frac{\pi}{N} m \left(n + \frac{1}{2}\right)\right] + \mathcal{C}\{v(n)\} \\ &= x(m) + v_{\odot}(m). \end{aligned} \quad (4.8)$$

The system model of the transmitted signal in Eq. (4.6), the received signal in Eq. (4.7), and the demodulated symbols in Eq. (4.8) can be given in the matrix form as,

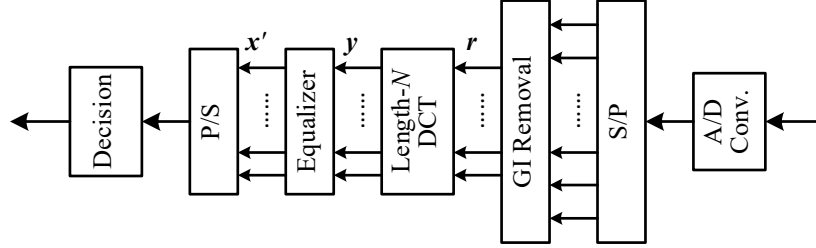
$$\mathbf{s} = \mathbf{C}^T \mathbf{x}, \quad (4.9)$$

for the transmitted signal,

(a) DCT based Fast-OFDM transmitter



(b) DCT based Fast-OFDM receiver I



(c) DCT based Fast-OFDM receiver II

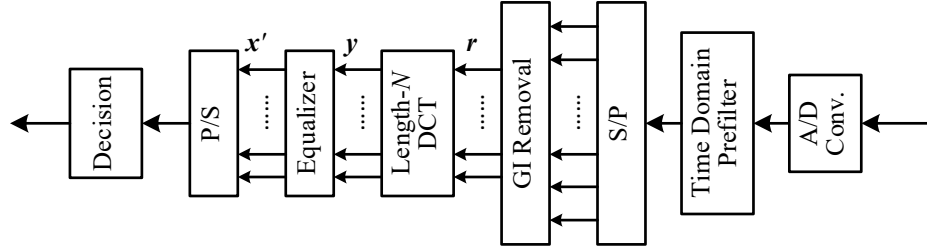


Figure 4–2. System diagrams of the conventional DCT Fast-OFDM system. (a) The transmitter, (b) the receiver for channel of symmetrical CIR, and (c) the receiver with a time-domain pre-filter for channel of non-symmetrical CIR.

$$\mathbf{r} = \mathbf{s} + \mathbf{v}, \quad (4.10)$$

for the received signal, and

$$\begin{aligned} \hat{\mathbf{x}} &= \mathbf{C}\mathbf{r} \\ &= \mathbf{x} + \mathbf{v}_{\Theta}, \end{aligned} \quad (4.11)$$

for the demodulated symbols, respectively, where  $\mathbf{C}$  denotes the DCT matrix.

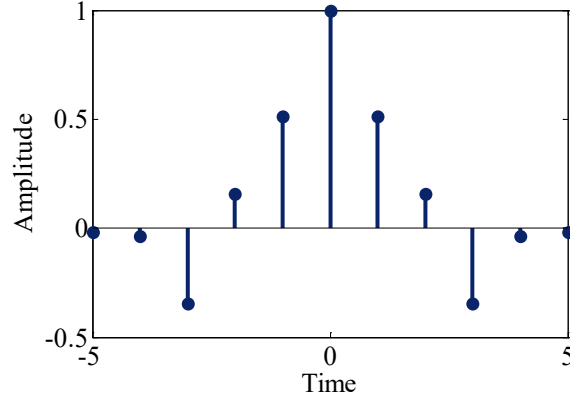


Figure 4–3. Example of a channel with symmetric CIR around 0.

### §4.2.2 Inability of Channel Equalization

In previous analysis, channel dispersion has not been considered. In this subsection, we will first assume that the CIR function is symmetric, and the received signal distorted by channel dispersion is

$$\mathbf{r} = \mathbf{H}\mathbf{s} + \mathbf{v}, \quad (4.12)$$

where  $\mathbf{H}$  is the CIR matrix. According to the symmetric convolution theorem in terms of the DCT [68, 79], it is shown that symmetrical prefix and suffix, as shown in Figure 4–2 (b), should be adopted. Moreover, if the CIR of the channel is symmetric, i.e., the CIR taps satisfy that  $h(l) = h(-l)$  for  $l = 1, \dots, L - 1$ , the equivalent CIR matrix  $\mathbf{H}$  is the sum of a symmetric circulant matrix and a Hankel matrix which is determined by the symmetric circulant matrix. In Figure 4–3, a channel with symmetric CIR is illustrated.

The received Fast-OFDM signal is transformed DCT as

$$\begin{aligned} \mathbf{y} &= \mathbf{C}\mathbf{r} = \mathbf{C}\mathbf{H}\mathbf{s} + \mathbf{C}\mathbf{v} \\ &= \mathbf{C}\mathbf{H}\mathbf{C}^T \mathbf{x} + \mathbf{v}_\Theta. \end{aligned} \quad (4.13)$$

According to the symmetric convolution of DCT, the channel term has an eigen-decomposition as  $\mathbf{\Lambda}_\Theta = \mathbf{C}\mathbf{H}\mathbf{C}^T$ , where  $\mathbf{\Lambda}_\Theta$  is a diagonal matrix, and Eq. (4.13) can be further given by

$$\mathbf{y} = \mathbf{\Lambda}_\Theta \mathbf{x} + \mathbf{v}_\Theta. \quad (4.14)$$

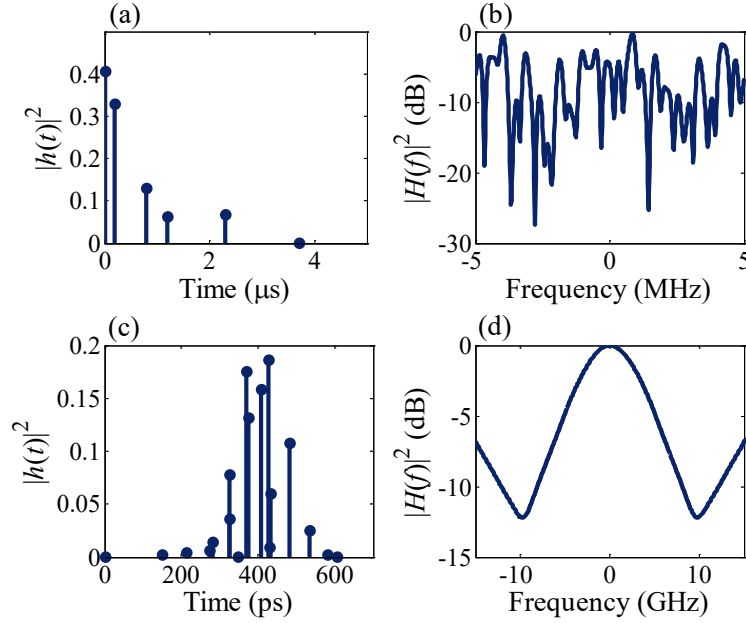


Figure 4–4. Example of practical channels with non-symmetric CIR. (a) The power delay profile and (b) power spectral density of the ITU channel model B of pedestrian environment; (c) the power coupling coefficients of modal group delay and (d) its power spectral density of a 300-m 62.5- $\mu\text{m}$  MMF with 20- $\mu\text{m}$  radial offset.

As  $\Lambda_\Theta$  is a diagonal matrix, whose  $m$ -th diagonal entries is the transfer function on the  $m$ -th subcarrier, the transmitted symbols thus can be recovered after the channel is compensated by single-tap equalizers.

In Eq. (4.14), it is assumed that the CIR of channel is symmetric. However, in practical channels, this condition can be hardly satisfied, and the CIR function of a practical communication systems hardly can be symmetric. Moreover, in some cases, the channel is even random over time, such as the fast fading channel in radio mobile systems.

In Figure 4–4, one-shot observations of typical channels' CIR functions and their power spectrum density (PSD) functions are provided. In Figure 4–4 (a) and (b) the ITU channel model B of pedestrian environment is considered, and in Figure 4–4 (c) and (d) a 300-m MMF is used with intensity modulation and direct detection [80]. In the MMF system, the operating wavelength is 1300 nm. The beam of directly modulated laser is Gaussian with full width at half

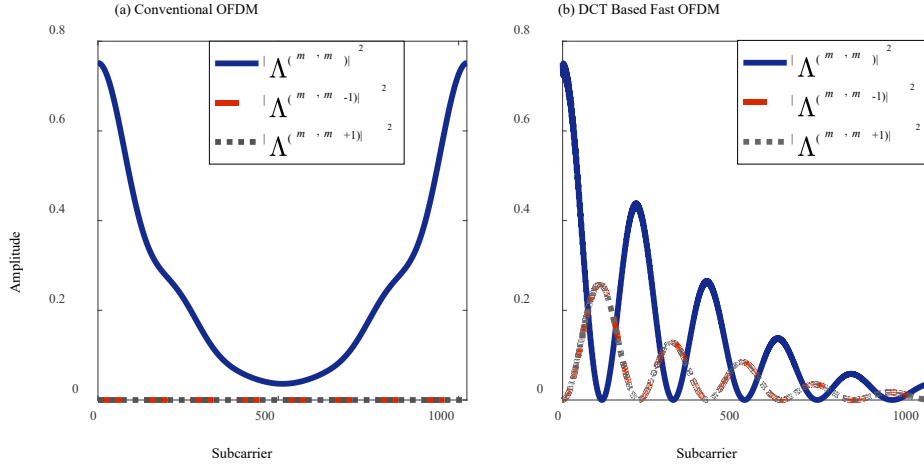


Figure 4–5. Example of the diagonal and off diagonal entries of CFR matrix  $\Lambda$  of (a) conventional OFDM and (b) DCT-F-OFDM under LTI channel with non-symmetrical CIR.

maximum of 7  $\mu\text{m}$  and a radial offset of 20  $\mu\text{m}$ . It can be observed that the CIR of both channels are not symmetric. In the wireless channel, the PSD is also non-symmetric and many deep notches can be observed in the frequency domain within the 10-MHz system bandwidth. In the MMF case, direct detection is used, resulting in CIR being real values. It should be noted that although the PSD in Figure 4–4 (d) is symmetrical, the channel transfer function is complex conjugate symmetric, rather than symmetric. In addition, no frequency notch occurs in MMF within the system bandwidth of practical interest (commonly  $< 5$  GHz).

The CFR matrices determine the features of the systems. To investigate the impact of the channel on DCT Fast-OFDM, we will analyze the CFR matrix  $\Lambda = \mathbf{F}\mathbf{H}\mathbf{F}^H$  in the conventional OFDM and the equivalent CFR matrix  $\Lambda_{\Theta} = \mathbf{C}\mathbf{H}\mathbf{C}^T$  in the DCT based Fast-OFDM. The MMF channel is adopted, whose CIR (the power coupling coefficients of modal group delay) is shown in Figure 4–4 (c).

In Figure 4–5, the diagonal  $\Lambda(m, m)$  entries and off diagonal  $\Lambda(m, m \pm 1)$  entries of  $\Lambda$  in both the conventional OFDM and the DCT-F-OFDM systems are plotted, respectively. The  $m$ -th diagonal entry is the channel gain of the  $m$ -th subcarrier and the off diagonal entries can be regarded as the interferences

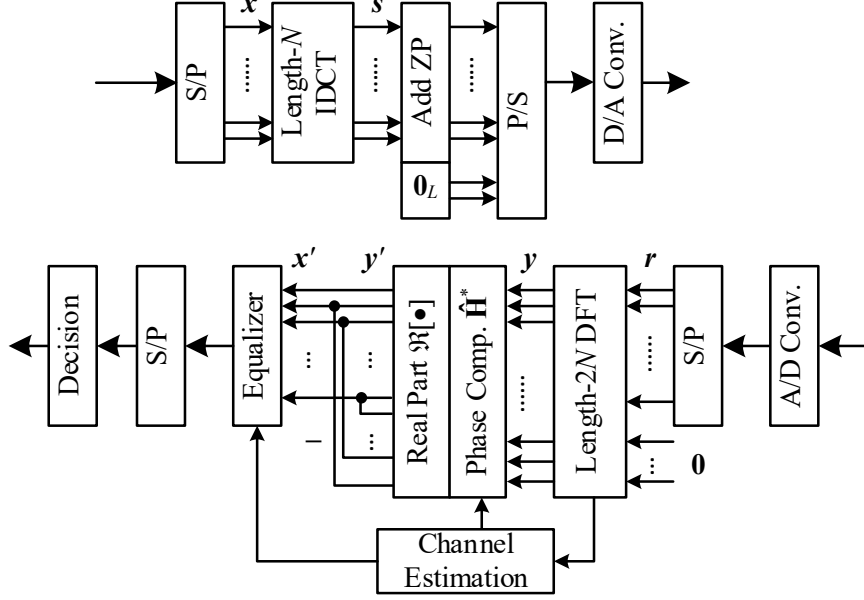


Figure 4–6. System diagram of the proposed DCT based fast OFDM with single-tap equalizer. S/P: serial-to-parallel; P/S: parallel-to-serial; D/A Conv.: digital-to-analog convertor; A/D Conv.: analog-to-digital convertor; ZP: zero-padding.

from adjacent subcarriers imposed on the  $m$ -th subcarrier. In the conventional OFDM, all of the off diagonal entries are zeros while in the Fast-OFDM the off diagonal entries are non-zero and interfered with the main diagonal entries. Therefore, it can be inferred that there exists inter-carrier interference (ICI) in the DCT Fast OFDM, as a result of the loss of the symmetric condition for the DCT.

### §4.3 Proposed DSB Fast-OFDM System

To resolve the channel equalization problem in the DCT based Fast-OFDM system under generalized LTI channels, in this section, a Fast-OFDM scheme with single-tap equalization algorithm is proposed, and its system diagram is provided in Figure 4–6. Compared with previous DCT Fast-OFDM schemes, in the proposed scheme, the guard interval is padded with zeros, as shown in Figure 4–6. At the receiver, taking the ZP based GI into account, the received

signal is a linear convolution of the CIR and transmitted signal corrupted by additive noise, given by

$$r_{zp}(n) = h(n) * s(n) + v(n), \quad n = 0, \dots, N + L - 1. \quad (4.15)$$

The received signal of length- $(N + L - 1)$  is zero padded to  $2N$  and take the DFT of length- $2N$  as

$$\begin{aligned} y(m) &= \mathcal{F}_{2N}[r_{zp}(n)] = \mathcal{F}_{2N}[h(n)] \cdot \mathcal{F}_{2N}[s(n)] + \mathcal{F}_{2N}[v(n)] \\ &= S(m) \cdot H(m) + v_{\Omega}(m). \end{aligned} \quad (4.16)$$

where  $m = 0, \dots, 2N - 1$ ,  $S(m)$  and  $H(m)$  are the DFT of zero-padded  $s(n)$  and  $h(n)$  of length- $2N$ , and  $v_{\Omega}(m)$  is the frequency-domain noise. With appropriate arithmetic operation, it can be further given by

$$\begin{aligned} y(m) &= e^{j\frac{\pi}{2N}m} H(m) \cdot e^{-j\frac{\pi}{2N}m} S(m) + v_{\Omega}(m) \\ &= \hat{H}(m) \cdot \hat{S}(m) + v_{\Omega}(m). \end{aligned} \quad (4.17)$$

Using Eq. (4.6), (4.16) and (4.17), we expand  $\hat{S}(m)$  as

$$\begin{aligned} \hat{S}(m) &= \sqrt{\frac{1}{2N}} \sum_{n=0}^{N-1} s(n) e^{-j\frac{2\pi}{2N}m\left(n+\frac{1}{2}\right)} \\ &= \sqrt{\frac{1}{2N}} \sum_{n=0}^{N-1} \sum_{k=0}^{N-1} \varepsilon(k) x(k) \cos \frac{2\pi}{2N} k \left(n + \frac{1}{2}\right) \cdot e^{-j\frac{2\pi}{2N}m\left(n+\frac{1}{2}\right)} \\ &= \frac{1}{N} \sum_{k=0}^{N-1} \varepsilon(k) x(k) \sum_{n=0}^{N-1} \cos \frac{2\pi}{2N} k \left(n + \frac{1}{2}\right) \cdot e^{-j\frac{2\pi}{2N}m\left(n+\frac{1}{2}\right)} \\ &= \sum_{k=0}^{N-1} x(k) G(k, m). \end{aligned} \quad (4.18)$$

The real part of  $G(k, m)$  is

$$\begin{aligned} G_R(k, m) &= \Re[G(k, m)] \\ &= \frac{\varepsilon(k)}{N} \sum_{n=0}^{N-1} \cos \frac{2\pi}{2N} k \left(n + \frac{1}{2}\right) \cos \frac{2\pi}{2N} m \left(n + \frac{1}{2}\right) \\ &= \begin{cases} 1 & m = 0 \\ 0.5\delta(m-k) & m = 1, \dots, N-1 \\ 0 & m = N \\ -0.5\delta(m-k) & m = N+1, \dots, 2N-1 \end{cases}. \end{aligned} \quad (4.19)$$

where  $\delta(m)$  is the Kronecker delta function, which equals one for  $m = 0$  and

equals 0 otherwise. In Eq. (4.19),  $G_R(k, m)$  is skew-symmetric around  $N$ , for  $m = 1, \dots, 2N - 1$ .

Assuming that the channel is perfectly estimated at the receiver, the phase of channel can be compensated first. Because the symbols are ASK modulated which is real-valued, we can extract the real part of the signal as

$$\begin{aligned} y'(m) &= \Re \left[ \hat{H}^*(m) y(m) \right] \\ &= \Re \left[ \left| \hat{H}(m) \right|^2 \sum_{k=0}^{N-1} x(k) G(m, k) + \hat{H}^*(m) v_\Omega(m) \right] \\ &= \left| \hat{H}(m) \right|^2 \sum_{k=0}^{N-1} x(k) G_R(m, k) + \hat{v}_R(m), \end{aligned} \quad (4.20)$$

where  $\hat{v}_R(m) = \Re \{ \hat{H}^*(m) v_\Omega(m) \}$ . Substitute Eq. (4.19) into (4.20)

$$y'(m) = \left| \hat{H}(m) \right|^2 \times \begin{cases} x(m) + \hat{v}_R(m) & m = 0 \\ 0.5x(m) + \hat{v}_R(m) & m = 1, \dots, N-1 \\ \hat{v}_R(m) & N \\ -0.5x(2N-m) + \hat{v}_R(m) & m = N+1, \dots, 2N-1 \end{cases}. \quad (4.21)$$

In Eq. (4.21), the estimation of  $x(m)$  can be obtained by multiplying  $y'(m)$  with  $|\hat{H}(m)|^{-2}$  in the positive frequency  $m = 1, \dots, N-1$ , or the negative frequency  $N+1, \dots, 2N-1$ . However, to maximally combine the received signal, we can combine the positive and negative symmetrically as

$$\begin{aligned} x'(m) &= y'(m) - y'(2N-m) \\ &= \frac{1}{2} \left( \left| \hat{H}(m) \right|^2 + \left| \hat{H}(2N-m) \right|^2 \right) x(m) + \hat{v}_c(m) \\ &= \hat{H}_c(m) x(m) + \hat{v}_c(m), \end{aligned} \quad (4.22)$$

where  $\hat{v}_c(m) = \hat{v}_R(m) - \hat{v}_R(2N-m)$ . As a result, the symbol on the  $m$ -th subcarrier can be easily compensated by a single-tap equalizer with coefficient  $\hat{H}_c(m)$ . The advantage of Eq. (4.22) is that it can combine the information symbols with maximal SNR if the positive and negative frequency response is not symmetrical, an example can be observed in Figure 4-4 (b), which is common in wireless communication systems.

## §4.4 Numerical Simulation

Simulations are performed to validate the feasibility and advantage of the proposed algorithm using MATLAB®. In the simulations, both wireless fading channel and fiber-optical MMF channel are considered to study the impacts of channels. It can be observed in Figure 4–4, the CIR of the channels are not symmetrical, and previous Fast OFDM schemes with single-tap equalizer cannot be used in such channels easily [63–67]. For comparison, frequency domain equalization (FDE) with block transmission is adopted [81–83] for the Fast OFDM based on DCT under these channels.

In the simulation, the wireless channel is modelled based on the ITU channel model B of pedestrian environment. In the MMF channel model, the operating wavelength is 1300 nm. The beam of direct modulated laser is Gaussian with full width at half maximum of 7  $\mu\text{m}$  and with a radial offset of 20  $\mu\text{m}$ . In the wireless channel, coherent receiver is always used and thus the PSD function is not symmetric while the PSD function in MMF channel is symmetric because direct detection is used, as illustrated in Figure 4–4.

### §4.4.1 Results under Wireless Channel

In the wireless simulation, the system bandwidth is 10 MHz and it is divided into 256 subcarriers. Both 2-ASK and 4-ASK are used. ZP-based GI is used in both schemes with the length 64. Zero-forcing (ZF) equalizer is applied in the proposed scheme, and in the FDE based Fast OFDM, both the minimum mean square error (MMSE) and ZF are adopted for comparison.

Figure 4–7 (a) and (b) show the BER versus  $E_b/N_0$  for both the FDE based Fast OFDM and the proposed scheme.  $E_b$  and  $N_0$  represent the signal power per bit and the noise spectral density, respectively. In the FDE based Fast-OFDM, the MMSE equalizer requires an  $E_b/N_0$  11 dB less than the ZF equalizer to achieve a bit error rate (BER) =  $10^{-5}$  for 2-ASK. The SNR advantage reduces to 4 dB for 4-ASK for its higher sensitivity to the noise enlargement. In the FDE based Fast OFDM using either criterion, noise at a spectral null is ampli-

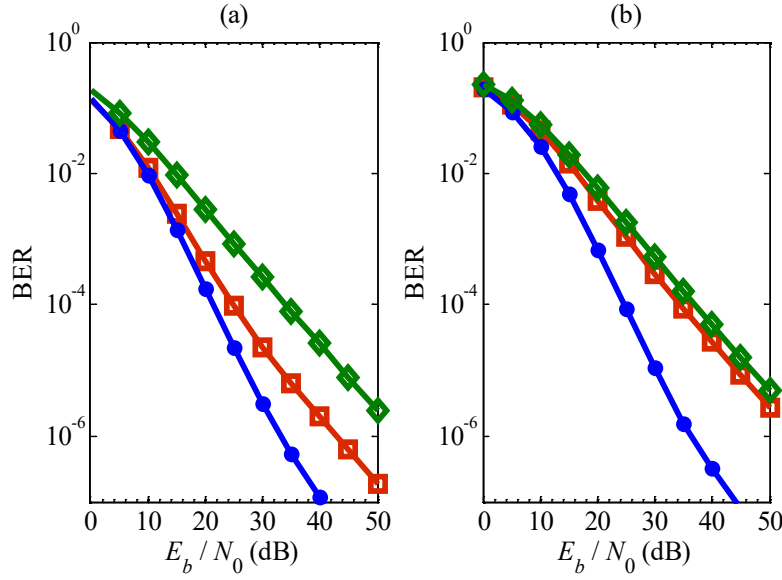


Figure 4–7. BER performance of the FDE-based Fast OFDM using ZF (diamond) and MMSE (square), and that of the proposed scheme (dot) for (a) 2-ASK and (b) 4-ASK under the ITU channel model B.

fied after equalization and degrades the performance of corresponding subcarriers. In addition, the amplified noise also spreads over other subcarriers when the signal is transformed from the frequency domain to the cosine domain using IFFT and DCT. In contrast, in the proposed scheme, the subcarrier at the positive and negative frequency with different frequency responses are maximally combined to mitigate the noise enlargement problem. In addition, decision can be directly made subcarrier by subcarrier after equalization so that the noise spreading effect does not exist. Therefore, the proposed scheme outperforms the FDE scheme based on MMSE by about 5 dB and 13 dB at  $\text{BER} = 10^{-5}$  for 2-ASK and 4-ASK, respectively.

#### §4.4.2 Results under Optical Multimode Fiber Channel

In the simulation under the optic MMF channel, we use intensity modulation and direct detection. The sampling rates of the digital-to-analog and analog-to-digital converters are 10 GS/s and the number of subcarriers is 256, of which 192 subcarriers are used for modulation. The electrical bandwidth is about 4

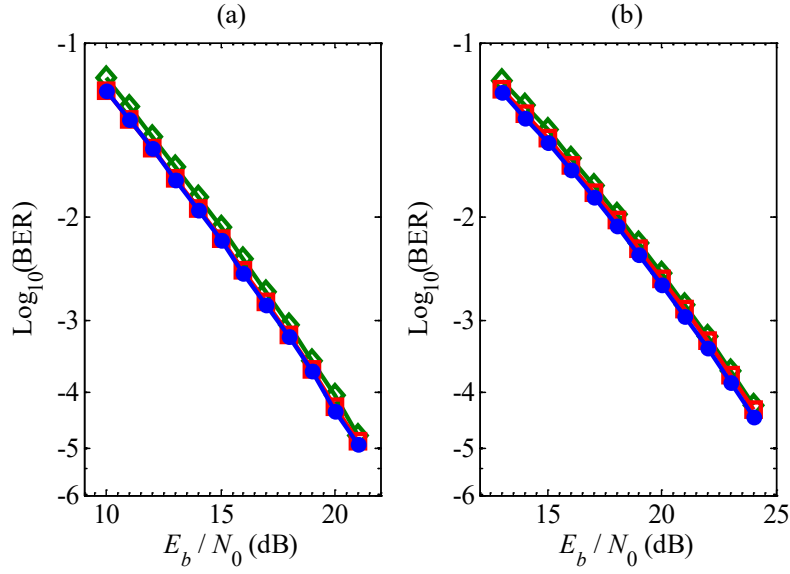


Figure 4–8. BER performance of the FDE-based fast OFDM using ZF (diamond) and MMSE (square), and the proposed scheme (dot) for (a) 2-ASK and (b) 4-ASK under the optical MMF channel.

GHz. In optical systems, reliability is required, and the system bandwidth commonly operates without spectral nulls. Within the system bandwidth ( $\sim 4$  GHz), we can see from Figure 4–4 (d) that the spectral power profile has no deep notches and is also symmetric. The level of the DC bias is optimized to balance the clipping noise and the DC-induced power penalty.

Figure 4–8 shows the BER versus the SNR. Because there is no notch in the spectrum, the MMSE-based FDE scheme shows only slightly better performance than the ZF based scheme. It is also shown that in contrast to the wireless channel, the proposed Fast OFDM scheme and the MMSE based FDE scheme have similar performance. It is because the PSD is symmetric such that the averaging effect in terms of the SNR in Eq. (4.22) is the same as that of the FDE-based scheme. In addition, the benefit of avoiding the noise spreading vanishes. Therefore, it can be inferred that the performance advantage of the proposed scheme over the FDE-based scheme occurs under channels with non-symmetric PSD.

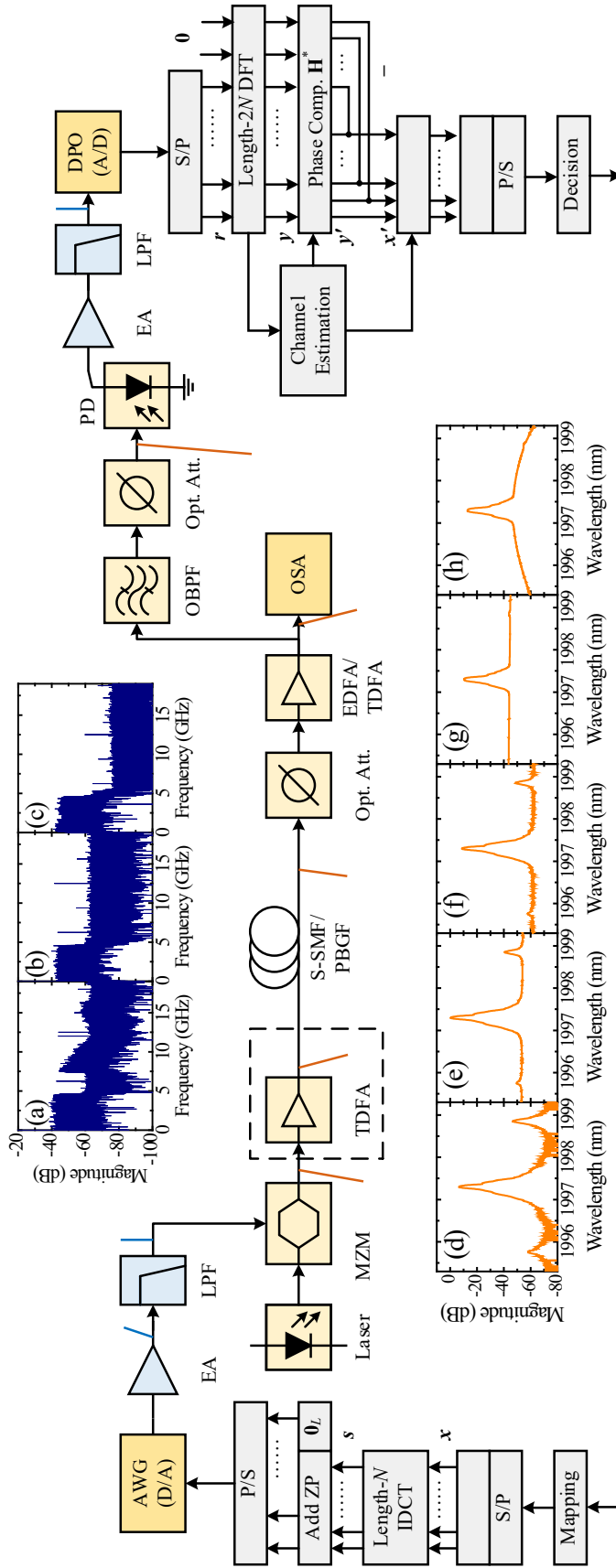


Figure 4–9. Experiment setup of the proposed optical IM/DD fast OFDM under 1.55  $\mu\text{m}$  standard SMF and 2  $\mu\text{m}$  HC-PBGF systems; the component surrounded by a dashed line is exclusive to the 2  $\mu\text{m}$  system. The insets (a)–(c) illustrate the measured electrical spectra of the signal, and the insets (d)–(h) are the measured optical spectra in the 2  $\mu\text{m}$  system at the positions indicated in the experiment setup, respectively.

## §4.5 Experimental Implementation

In this section, we implement the proposed algorithm into experiments in fiber-optic system using standard SMF (S-SMF) at 1.55  $\mu\text{m}$  and the new HC-PBGF at 2  $\mu\text{m}$ .

### §4.5.1 Experimental Setup

In Figure 4–9, the block diagram and experimental setup of the proposed optical IM/DD fast OFDM are shown. The bit stream was encoded into 4-ASK symbols and was grouped into block of length  $M = 288$  for serial-to-parallel (S/P) conversion. To reduce the peak to average power ratio of the fast OFDM signal, DCT precoding was used before multiplexing the symbols into subcarriers [84], i.e. the  $M$  ASK symbols were first operated by a length- $M$  DCT before subcarrier multiplexing. Then the time domain signal was generated by inverse DCT (IDCT) of length- $N$ , where  $N = 384$  was larger than  $M$  for oversampling to separate the aliasing signal. The first  $d = 6$  inputs of the IDCT were set to be zeros to avoid DC coupling. In the proposed scheme, the guard interval of length-16 was padded with zeros to avoid inter-symbol interference (ISI), and then the signal was parallel-to-serial (P/S) converted.

The time-domain signal was generated using MATLAB<sup>®</sup> and uploaded to the arbitrary waveform generator (AWG) with a DAC sampling rate of 12 GS/s. Thus, the bandwidth of the electrical signal was  $12 \times (6 + 288) / 384 / 2 \approx 4.6$  GHz, as shown in inset (a) of Figure 4–9. In the experiment, 4-ASK format was adopted, and thus the data rate excluding guard interval was  $12 \times 2 \times 288 / 384 = 18$  Gbit/s. To remove the aliasing signal, a low-pass filter (LPF) with 3-dB bandwidth of 5 GHz was used. The filtered electrical signal (see inset (b)) was fed into an electrical amplifier (EA) to drive the MZM for data modulation.

In the 1.55  $\mu\text{m}$  system, the  $V_\pi$  of the MZM was about 3.5 V and the MZM was biased at the optimal point for intensity modulation. The optical power into the fiber was  $-2$  dBm. The 80 km link consisted of two loops of 40 km corning SMF-28e+ standard SMF (SSMF) with attenuation coefficient  $\leq 0.2$

dB/km and dispersion coefficient  $\leq 18$  ps/(nm·km). At the receiver end, the received optical signal was amplified by an Erbium-doped fiber amplifier (EDFA). A 0.3 nm optical band-pass filter (OBPF) was used to remove the out-of-band amplified spontaneous emission (ASE) noise. The optical signal power to the photodiode (PD) was controlled by an optical power controller at a fixed power of 4 dBm.

On the other hand, the  $V_\pi$  of the 2  $\mu\text{m}$  MZM was about 9.5 V. The HC-PBGF had a 19-cell core structure with a length of 1.15 km. Its attenuation coefficient was about 2.8 dB/km at  $\lambda = 1990$  nm wavelength [30]. Both ends of the HC-PBGF were pigtailed for single mode operation [85]; the total insertion loss of the connectorized HC-PBGF span was 9.5 dB. The output power of the 2  $\mu\text{m}$  laser was 0 dBm, and decreased to  $-11$  dBm after the MZM. Due to the power limitation of the 2  $\mu\text{m}$  laser and the insertion loss of the HC-PBGF, the output of the MZM was followed by a home-made Thulium-doped fiber amplifier (TDFA) to boost the input power into the HC-PBGF. At the receiver, another TDFA was used, followed by a 1.6-nm OBPF to remove the out-of-band ASE noise. The input optical power into the 2  $\mu\text{m}$  photodiode was controlled at  $-3$  dBm. The optical spectra of the 2  $\mu\text{m}$  system are illustrated in insets (d)-(h).

In both systems, the received electrical signal was amplified and filtered by a LPF with a 3-dB bandwidth of 5 GHz, and sampled by a real-time oscilloscope, with a ADC sampling rate of 50 GS/s for offline processing. The signal was resampled to 12 GS/s and was processed by the receiver DSP algorithm based on Figure 4–9. Each signal frame consisted of a start-of-frame symbol, 8 frequency comb-type pilot symbols [86] and a payload consisting of 256 fast OFDM symbols. After symbol synchronization to identify the start of each fast OFDM symbol block, the fast OFDM signal was serial-to-parallel (S/P) converted. Channel estimation was realized using the pilot symbols.

In the proposed receive algorithm, fast OFDM symbols, including the guard interval, were zero-padded to length  $2N$  before a length- $2N$  DFT. Based on the linear convolution theory and the relationship of the DCT and the DFT, the signal after phase compensation,  $y'(m)$ , can be derived as

$$y'(m) = \begin{cases} |\hat{H}(m)|^2 x(m) + j \cdot C(m) & m = 0 \\ \frac{1}{2} |\hat{H}(m)|^2 x(m) + j \cdot C(m) & m = 1 \dots N-1 \\ 0 & m = N \\ -\frac{1}{2} |\hat{H}(m)|^2 x(2N-m) + j \cdot C(m) & m = N+1 \dots 2N-1 \end{cases} \quad (4.23)$$

where  $\hat{H}(m)$  and  $x(m)$  are the channel frequency response and the transmitted data at the  $m$ -th subcarrier, respectively, and  $C(m)$  represents the crosstalk on the  $m$ -th subcarrier from adjacent subcarriers. Note that  $x(m)$  is real-valued in fast OFDM and the crosstalk is projected to the imaginary axis, therefore the signal  $x'(m)$  can be obtained as

$$\begin{aligned} x'(m) &= \Re\{y'(m) - y'(2N-m)\} \\ &= \frac{1}{2} \left( |\hat{H}(m)|^2 + |\hat{H}(2N-m)|^2 \right) x(m). \end{aligned} \quad (4.24)$$

The response at the  $m$ -th subcarrier is the average of  $|\hat{H}(m)|^2$  and  $|\hat{H}(2N-m)|^2$ , which do not have to be the same. In addition, the averaging provides spectral diversity and can improve the system performance when the power spectral density of the channel is asymmetric. After equalization of the amplitude of  $x'(m)$ , the received information bits were detected for bit-error rate (BER) calculation.

For comparison, the frequency domain equalization (FDE) based on zero-forcing (ZF) was adopted in the experiment for compensating the non-symmetrical channel dispersion [87]. In the FDE based fast OFDM, the guard interval was also zero-padded to avoid any adjustment at the transmitter.

### §4.5.2 Experimental Results

Firstly, the temporal and frequency responses of the physical channels in the experiment were measured. In Figure 4–10 (a)-(c), the CIRs and channel frequency responses (CFRs) of the 1.55- $\mu\text{m}$  system are provided, respectively. The small tails, about 1 ns period, in the CIRs are mainly due to the anti-aliasing filter used in the experiment. In Figure 4–10 (d)-(f), the CIRs and CFRs of 2- $\mu\text{m}$  system are provided, respectively. Similar CIR profiles are observed, except that the tails of the CIRs in the 2- $\mu\text{m}$  system are slightly longer

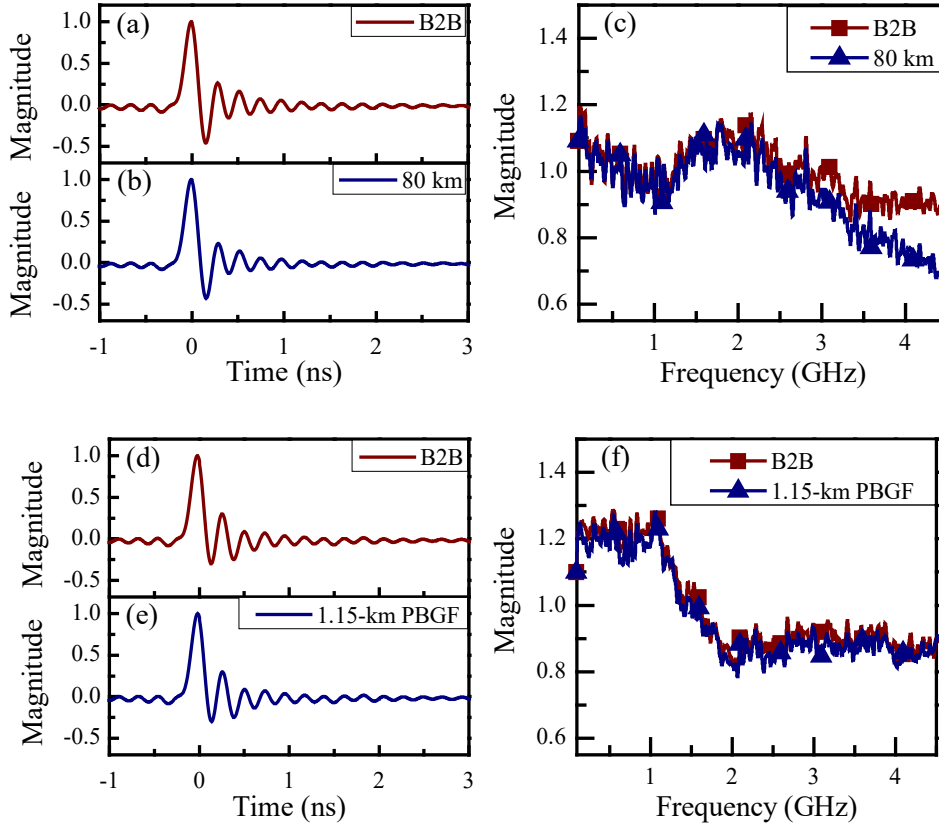


Figure 4–10. The CIRs of the 1.55- $\mu\text{m}$  system in (a) B2B and (b) 80 km SSMF cases, and (c) the corresponding CFRs; The CIR of the 2- $\mu\text{m}$  system in (d) B2B and (e) 1.15 km PBGF cases, and the corresponding CFRs.

than those at 1.55- $\mu\text{m}$ .

Due to the asymmetric CIR tail, as observed in Figure 4–10, the conventional fast OFDM cannot be applied to compensate the channel dispersion [30, 32, 61, 69, 72, 73], unless the equalization algorithms in [63, 65] are used. The FDE-based method is selected for comparison in this section because it shows as the most competitive solution to the proposed scheme in terms of the performance and complexity tradeoff.

#### §4.5.2.1 Results in the Standard SMF System at 1.55 $\mu\text{m}$

In Figure 4–11, the bit error rate (BER) performance was measured against the received (OSNR) with a resolution of 0.1 nm, which equals to 12.5 GHz bandwidth at 1.55  $\mu\text{m}$ . At a BER of  $10^{-4}$ , the required OSNR is 32.5 dB in the B2B

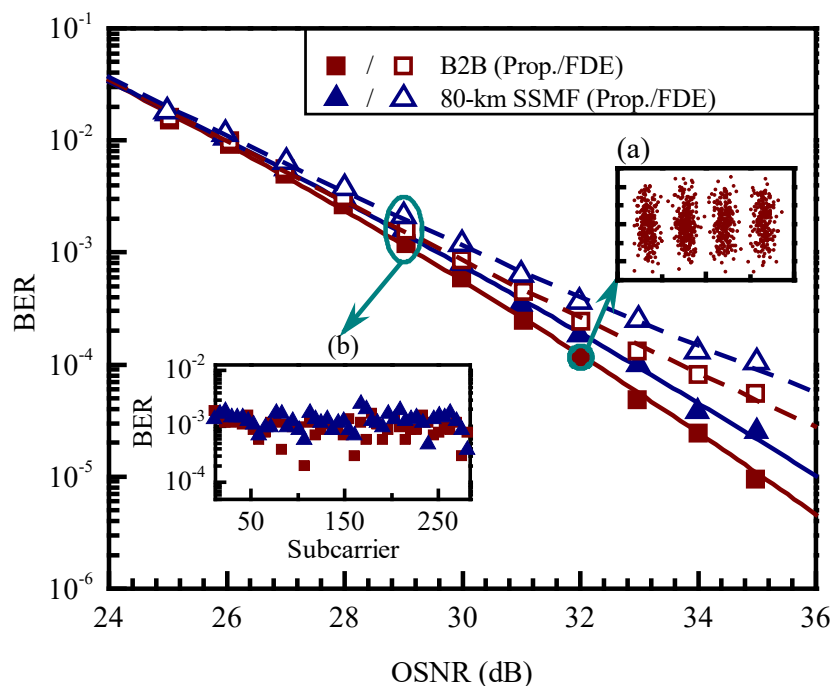


Figure 4–11. BER versus OSNR of the proposed and FDE based fast OFDM in the 1.55- $\mu$ m standard SMF system. Inset: (a) the received signal constellation of the proposed scheme in B2B case; (b) the BER of the subcarriers in both B2B (■) and 80 km SSMF (▲) cases.

case. The inset (a) in Figure 4–11 illustrates the received signal constellation in the 1.55  $\mu$ m system with back-to-back (B2B) at an OSNR of 32 dB. It can be observed that the interference is completely located in the imaginary axis. The inset (b) is the BER of each subcarrier in the proposed scheme in both B2B and 80 km SSMF cases. Only a slight OSNR penalty occurs after 80 km SSMF transmission compared to the B2B case, which is introduced by the fading effect due to direct detection. In Figure 4–11, the FDE based fast OFDM gets about 1-dB OSNR penalty with respect to the proposed scheme at  $\text{BER} = 10^{-4}$ . On the other hand, in the FDE based fast OFDM, one IFFT, one FFT and one DCT are required at the receiver end, resulting in higher implementation complexity. These confirm that the proposed single-tap equalization algorithm shows advantages in both performance and complexity over the FDE based scheme.

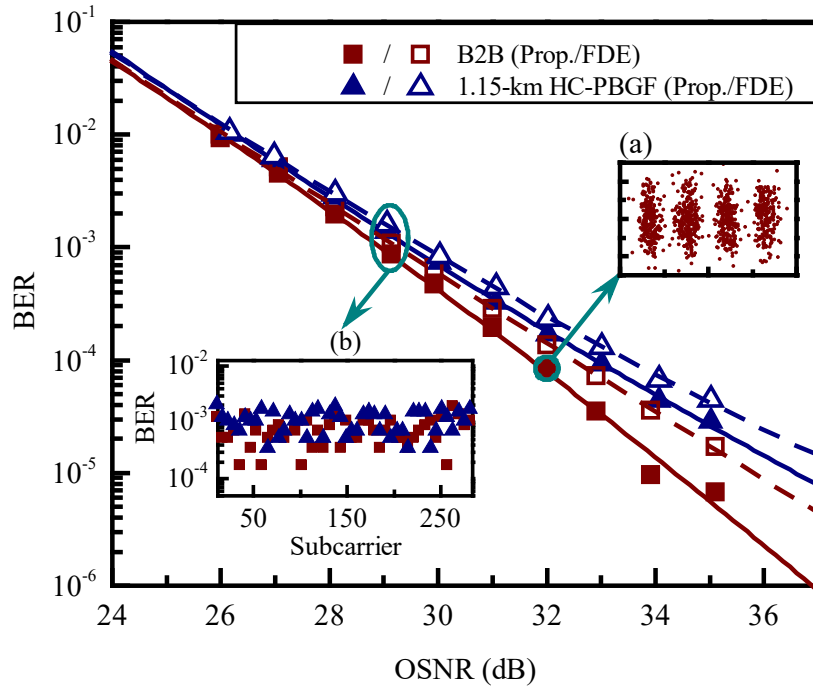


Figure 4–12. BER versus OSNR of the proposed and FDE based fast OFDM in the 2- $\mu$ m HC-PBGF system. Inset: (a) the received signal constellation of the proposed scheme in B2B case; (b) the BER of the subcarriers in both B2B (■) and 1.15 km HC-PBGF (▲) cases.

#### §4.5.2.2 Results in the HC-PBGF System at 2 $\mu$ m

In Figure 4–12, the BER versus OSNR performance was measured in the 2- $\mu$ m system. The OSNR resolution is 0.1 nm which equals to 7.5 GHz at 2  $\mu$ m. The received signal constellation of B2B case is provided in the inset (a) at an OSNR = 32 dB, and inset (b) shows the BER of each subcarrier in the proposed scheme in both B2B and 1.15 km HC-PBGF cases. At a BER of  $10^{-4}$ , the required OSNRs are 32 dB for B2B case and 33 dB after the HC-PBGF transmission. As the HC-PBGF is not ideally single mode, the effect of exciting higher order modes may be more pronounced at high OSNRs, producing a small penalty. On the other hand, the FDE based fast OFDM gets about 0.8 dB and 0.5 dB OSNR penalty compared to the proposed algorithm for the B2B and the 1.15 km HC-BPGF transmission, respectively.

It should be noted that the OSNR at 0.1 nm resolution in the 1.55 and 2  $\mu\text{m}$  systems corresponds to 12.5 GHz and 7.5 GHz, respectively. Therefore, at a fixed OSNR, there will be  $10 \times \log_{10}(12.5 / 7.5) = 2.2$  dB SNR (rather than OSNR) difference between the 1.55 and 2  $\mu\text{m}$  systems. It means that although the 1.55  $\mu\text{m}$  requires about 0.5 dB higher OSNR to achieve a  $\text{BER} = 10^{-4}$  in the B2B case, it still outperforms the 2  $\mu\text{m}$  systems by 1.7 dB.

## §4.6 Summary

In this section, we proposed a DCT-F-OFDM scheme to efficiently compensate generic LTI channels without the symmetric constraint on CIR with single-tap equalizers. In the proposed scheme, a conventional DCT-F-OFDM transmitter is adopted with DCT of length- $N$  and the guard interval is zero-padded. At the receiver, the DFT of length- $2N$  is used to compensate the channel dispersion with single-tap equalizers. After equalization, symbols are demultiplexed from each subcarrier without ICI and additional operations.

Simulations are performed to validate its feasibility under both the wireless multipath fading and optical MMF channels. Compared to previous methods, the proposed scheme is simpler and avoids the sacrifice of the net data rate. We have particularly compared this scheme with the FDE-based DCT-F-OFDM. It is shown that, except for lower complexity, the proposed scheme can achieve better performance than the FDE-based Fast OFDM under channels with non-symmetric PSD.



## Chapter 5

# Single-Sideband Modulated Fast-OFDM

In the DSB modulated Fast-OFDM system, information is modulated onto the cosine waveforms. According to the Fourier analysis, the cosine waveforms symmetrically distributes the information in two conjugate sidebands around the central frequency. In the baseband transmission, the central frequency is at zero, and the DSB Fast-OFDM signal achieves the Nyquist rate for information transmission. Thus, the DSB Fast-OFDM systems can be suitable for baseband related systems, such as the ADSL system and optical system of intensity modulation.

In a passband transmission system with coherent detection, one of the conjugate sidebands can be removed since they contain the same information and cutting either of them for transmission, as shown in Figure 5–1, doubles the spectral efficiency. The corresponding signal is SSB modulated Fast-OFDM signal. The SSB modulated signal can be generated in different ways. One can pass the DSB modulated signal to a filter, termed as Hilbert filter that removes one sideband out of the signal and preserves the other, as the one illustrated in Figure 5–1 (b). One can also generate a quadrature signal, which is the Hilbert pair of the DSB modulated Fast-OFDM signal, achieving SSB modulation.

In the SSB modulated Fast-OFDM systems, because of the halved subcarrier spacing, the same signal transmission problem exists as that in the DSB Fast-

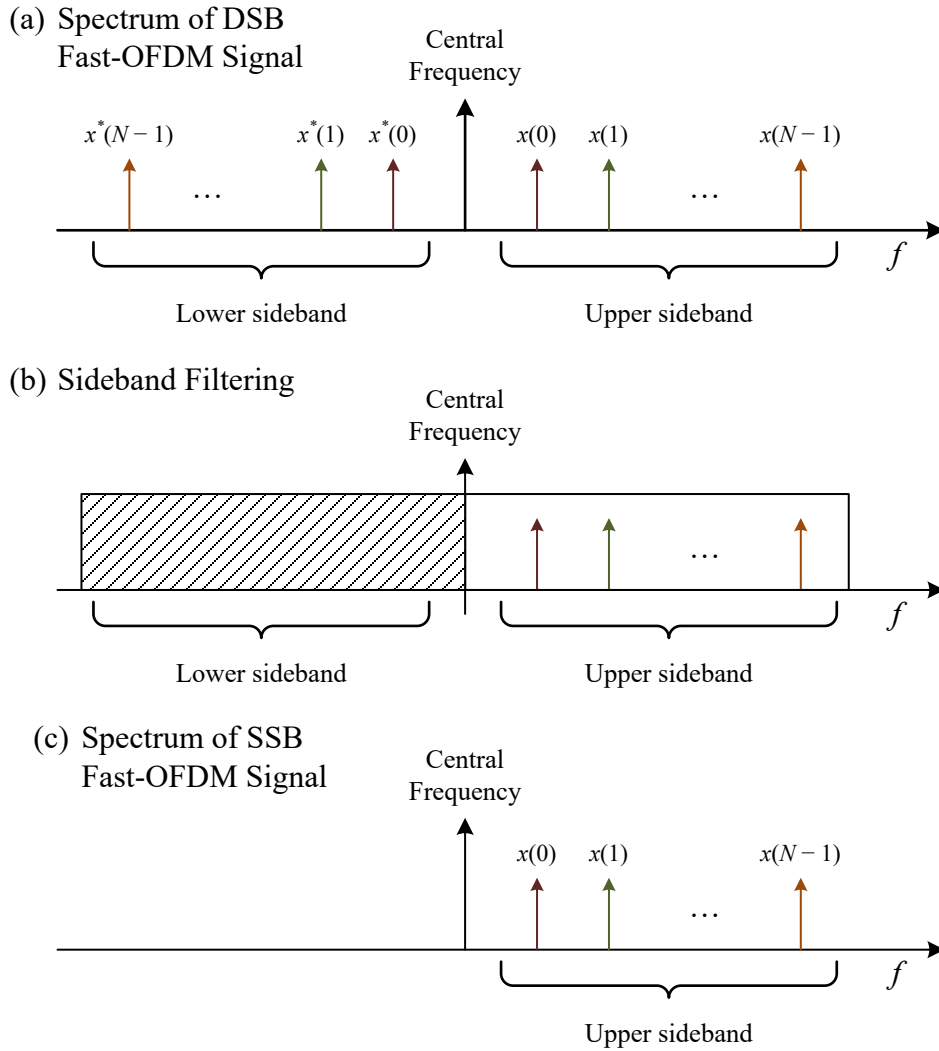


Figure 5–1. Illustration of the spectra of (a) DSB modulated Fast-OFDM signal, (b) sideband filter, and (c) SSB modulated Fast-OFDM signal.

OFDM, and the situation becomes somewhat bitter because the subcarriers in the SSB modulated Fast-OFDM signal is not even orthogonal and no convolution-multiplication property exists, nor even the symmetric one of DCT. In this Chapter, we will focus on the SSB modulated Fast-OFDM systems, dealing with the signal transmission problem induced by the halved subcarrier spacing.

The chapter is organized as follows. Section §5.1 briefly introduces the history of SSB modulated Fast-OFDM. In Section §5.2, the mathematical model of the SSB Fast-OFDM is formulated. It is shown that, except to the equalization problem due to the lack of a convolution-multiplication property, there is

severe inter-carrier interference (ICI) in the digital implementation of the SSB Fast-OFDM system. Moreover, the ICI is analytically investigated and the performance is derived in closed form for system evaluation. In Section §5.3, we propose a SSB Fast-OFDM system which is able to get rid of the ICI and the single-tap equalizers can be adopted for efficiently compensating channel distortion. In Section §5.4, simulation are performed to validate the feasibility and advantages of the proposed scheme, and Section §5.5 provides the experiment results in coherent optical system. Conclusion is finally provided in Section §5.6.

## §5.1 Background

The concept of Fast-OFDM first proposed by Rodrigues and Darwazeh in 2002 is the scheme that generates the SSB modulated Fast-OFDM signal [60]. In the system, the transmitter generates the conventional OFDM signal and then truncates the last half of the IDFT output. Based on the Fourier analysis, compressing a waveform in time by half is equivalent to extend its spectrum by a factor of 2 in frequency. The process of generating the SSB modulated Fast-OFDM signal by truncating the time-domain OFDM signal is shown in Figure 5–2. In the conventional OFDM system, the subcarrier spacing is equal to the first null point of the spectra of subcarriers. If one truncates the conventional OFDM signal by half, though the subcarrier spacing remains unchanged, the spectra of the subcarriers extend by a factor of 2. Equivalently, the normalized subcarrier spacing is halved to that in OFDM. In Figure 5–2 (d), at some frequency point,  $k\Delta f$ , the subcarrier will be interference by adjacent subcarriers. Nonetheless, it is shown in that [60], as long as the symbols are real-valued, the interference can be properly rejected from the signal wanted. However, in [60], when implementing the system digitally using discrete Fourier transform, the interference between the subcarrier has not been considered.

Until 2010, as the DSB modulated Fast-OFDM has been considered again in optical communications [62-67], the SSB modulated Fast-OFDM was also being studied [88-91]. In [88], the SSB modulated Fast-OFDM similar to [60]

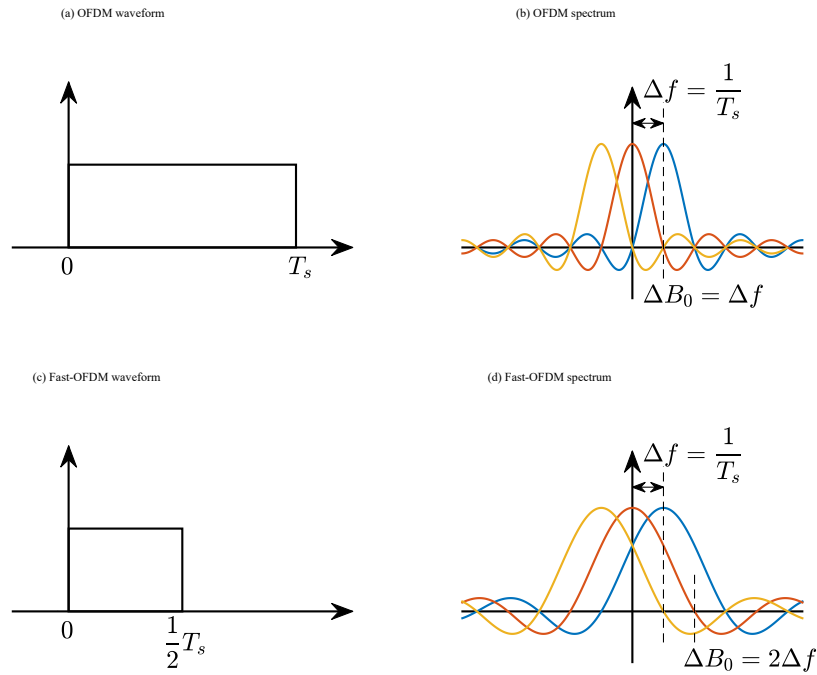


Figure 5–2. Illustration of (a) the waveform of OFDM signal and (b) its spectrum, and (c) the corresponding Fast-OFDM signal by truncating the signal by half, and (d) its spectrum.

is studied by assuming that the channel is perfectly compensated before sub-carrier demodulation. In [89], an interesting approach is demonstrated by interleaving two conventional OFDM signal with frequency offset equal to half of the subcarrier spacing. However, the scheme reduces the efficiency of the DAC by half and it is only demonstrated experimentally over DSB modulated optical carrier at a data rate of 10 Gbps. Still, the ICI due to non-orthogonal waveforms exists in these studies, and channel compensation cannot be done by single-tap equalizers in a straight manner. Several studies followed to deal with the ICI problem. For example, the authors in [90] considered the ICI problem, and proposed to use additional subcarriers to estimate the ICI, sacrificing the spectral efficiency of the system. In [91], it is shown that by using the fourth type DCT and DST at the receiver, the ICI can be completely eliminated, and symbols on the subcarriers of halved spacing can be perfectly demodulated without the loss of spectral efficiency. Nonetheless, the channel is assumed

perfect in [88-91], and therefore the SSB modulated Fast-OFDM system cannot be realized practically.

## §5.2 Mathematical Model of SSB Fast-OFDM

In this section, we will introduce the system model of the SSB modulated Fast-OFDM. Based on the model, the ICI problem due to the loss of orthogonality and the equalization problem due to the loss of convolution-multiplication property will be analytically studied.

In the SSB modulated Fast-OFDM system, assume that the symbol period is  $T_s$ , and there are  $2N$  subcarriers with subcarrier spacing  $\Delta f = 1 / 2T_s$ . Thus, the continuous-time domain Fast-OFDM signal is

$$s(t) = \sqrt{\frac{1}{T_s}} \sum_{k=0}^{2N-1} x(k) e^{j2\pi k \Delta f t}, \quad 0 \leq t < T_s. \quad (5.1)$$

Here, channel dispersion is not considered, and the received signal is

$$r(t) = s(t) + v(t). \quad (5.2)$$

where  $v(t)$  is the noise term. The symbol on the  $m$ -th subcarrier can be demodulated by its matched filter, as

$$\begin{aligned} \hat{x}(m) &= \sqrt{\frac{1}{T_s}} \int_0^{T_s} r(t) e^{-j2\pi m \Delta f t} dt \\ &= \frac{1}{T_s} \sum_{k=0}^{2N} x(k) \int_0^{T_s} e^{-j2\pi k \Delta f t} e^{j2\pi m \Delta f t} dt + \int_0^{T_s} v(t) e^{j2\pi m \Delta f t} dt \\ &= \frac{1}{T_s} \sum_{k=0}^{2N} x(k) \int_0^{T_s} e^{-j2\pi(k-m) \Delta f t} dt + v_{\Theta}(m) \\ &= \sum_{k=0}^{2N} e^{j\frac{\pi}{2}(m-k)} \frac{\sin \frac{\pi}{2}(m-k)}{\frac{\pi}{2}(m-k)} x(k) + v_{\Theta}(m), \end{aligned} \quad (5.3)$$

where  $v_{\Theta}(m)$  is the noise after matched filter. In Eq. (5.3), the coefficients in the last equation can be further expressed as

$$G(m-k) = e^{j\frac{\pi}{2}(m-k)} \frac{\sin \frac{\pi}{2}(m-k)}{\frac{\pi}{2}(m-k)}$$

$$= \begin{cases} 1 & \text{if } m = k \\ 0 & \text{if } m \neq k, \quad |m-k| \equiv 0 \pmod{2} \\ j^{m-k} \frac{\sin \frac{\pi}{2}(m-k)}{\frac{\pi}{2}(m-k)} & \text{if } m \neq k, \quad |m-k| \equiv 1 \pmod{2} \end{cases}, \quad (5.4)$$

which are real-valued in the the third condition that  $m \neq k$  and  $|m-k| \equiv 1 \pmod{2}$ . Considering the above equation, Eq. (5.3) can be further given as

$$\hat{x}(m) = x(m) + \underbrace{\sum_{k \neq m, |m-k| \equiv 1 \pmod{2}} G(m-k)x(k)}_{\text{Interference}} + v_{\Theta}(m), \quad (5.5)$$

in which the interference term is an imaginary number.

Therefore, if the transmitted symbols are modulated in real-valued, such as ASK, at the receiver, the transmitted symbols can be recovered by discarding the imaginary part after demodulation, as indicated in Eq. (5.5).

It should be noted here that it assumes the system is perfectly synchronized and that channel dispersion has not been considered in the above system model. If there is dispersion or there is any synchronization misalignment, it can be easily proved that the symbols are longer recoverable and the SSB modulated Fast-OFDM system will not be working correctly. Compared to the DSB Fast-OFDM system, there is no convolution-multiplication property existing. As a consequence, it becomes a challenge when one tries to implement the SSB Fast-OFDM system.

### §5.2.1 Digital Implementation of the SSB Fast-OFDM

In the continuous-time model of the SSB Fast-OFDM system, it is shown that if only real-valued modulated format is adopted, and the system is perfectly synchronized without any distortion, the SSB Fast-OFDM signal is recoverable

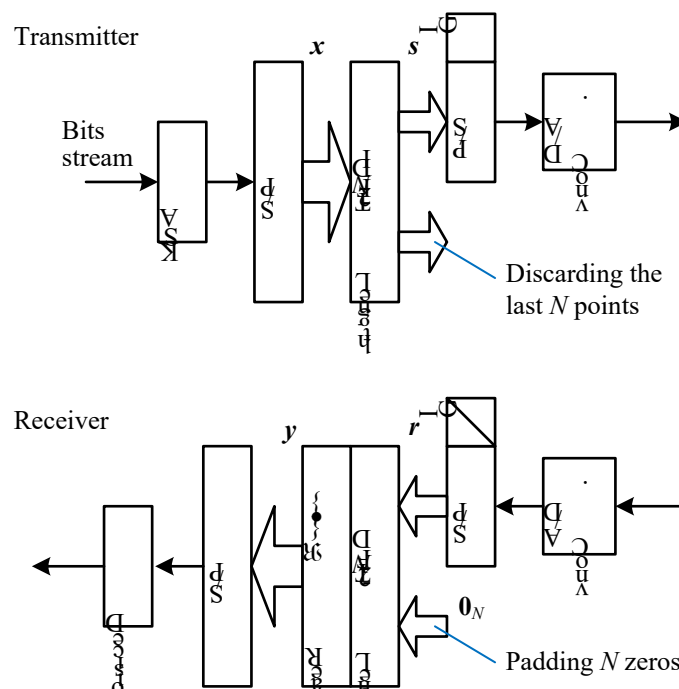


Figure 5–3. System diagram of conventional SSB modulated Fast-OFDM based on DFT.

by rejecting interference from adjacent subcarriers onto the imaginary plane. However, the system should be practically implemented using digital approach by using the advanced DSP technology. In this section, we will present the digital implementation of the SSB Fast-OFDM, and it is shown that, except to the inability to deal with channel dispersion, there exists severe inter-carrier interference in the digital system even there is no dispersion existed.

Figure 5–3 illustrates the system diagram of the conventional SSB modulated Fast-OFDM [60, 88-91]. At the transmitter, the ASK modulated symbols are grouped in block of length  $2N$ , and the time-domain signal is generated by using a length- $2N$  IDFT, truncating the last  $N$  output, as

$$s(n) = \sqrt{\frac{1}{N}} \sum_{k=0}^{2N-1} x(k) e^{j \frac{2\pi}{2N} nk}, \quad n = 0, \dots, N-1. \quad (5.6)$$

Here, the system is also perfectly synchronized and channel dispersion is not considered. At the receiver, the received length- $N$  signal is extended to length  $2N$  by padded zeros, and inverse operation is performed with a length- $2N$  DFT, as

$$\hat{x}(m) = \sqrt{\frac{1}{N}} \sum_{k=0}^{N-1} s(n) e^{-j\frac{2\pi}{2N}nk}, \quad n = 0, \dots, N-1. \quad (5.7)$$

Substitute Eq. (5.6) into (5.7), as

$$\hat{x}(m) = \sqrt{\frac{1}{N}} \sum_{k=0}^{2N-1} x(k) \sum_{n=0}^{N-1} e^{-j\frac{2\pi}{2N}n(m-k)}. \quad (5.8)$$

The inner summation in Eq. (5.8) is given by

$$\begin{aligned} G_D(m-k) &= \sum_{n=0}^{N-1} e^{-j\frac{2\pi}{2N}n(m-k)} \\ &= \delta(m-k) \\ &\quad + \delta((m-k-1)_2) \cdot \left[ 1 + j \cot \frac{\pi}{2N} (m-k) \right], \end{aligned} \quad (5.9)$$

where  $(\cdot)_2$  denotes modulo-2 operator. Discarding the imaginary part of  $G_D(m-k)$  and substituting it back into Eq. (5.8), the signal on the even and the odd subcarriers can be respectively given by

$$\begin{aligned} \hat{x}_{\Re}(2m) &= \Re\{y(2m)\} \\ &= x(2m) + \underbrace{\frac{1}{N} \sum_{k=0}^{N-1} x(2k+1)}_{\text{Interference}}, \end{aligned} \quad (5.10)$$

and

$$\begin{aligned} \hat{x}_{\Re}(2m+1) &= \Re\{y(2m+1)\} \\ &= x(2m+1) + \underbrace{\frac{1}{N} \sum_{k=0}^{N-1} x(2k)}_{\text{Interference}}. \end{aligned} \quad (5.11)$$

It can be observed from Eq. (5.10) and (5.11) that the interference terms come from neighboring subcarriers, and the interference on the even or the odd subcarriers is identical.

### §5.2.2 Inter-Carrier Interference in SSB Fast-OFDM

As shown in previous subsection, there is ICI between the subcarriers because the transform pair, indicated in Eq. (5.6) and (5.7), in the digital implementation are not orthogonal (unitary). Moreover, the transform pair do not possess

the convolution theory of any form. Therefore, if there exists dispersion in the channel, the performance of system will be significantly degraded.

In this section, by assuming perfect sampling time and synchronization, the bit-error rate (BER) performance is analytically derived in closed-form expression to show the mechanism of the degradation due to the ICI in conventional Fast-OFDM system [60, 88-91] under AWGN channel.

### IMPACT OF THE INTER-CARRIER INTERFERENCE

The interference terms are given in Eq. (5.10) for the even subcarriers and in Eq. (5.11) for the odd subcarriers. Rewriting the interference terms below, as

$$\varepsilon_{\mathfrak{R}}(2m) = \Re\{\varepsilon_{\text{ICI}}(2m)\} = \frac{1}{N} \sum_{k=0}^{N-1} x(2k+1), \quad (5.12)$$

and

$$\varepsilon_{\mathfrak{R}}(2m+1) = \Re\{\varepsilon_{\text{ICI}}(2m+1)\} = \frac{1}{N} \sum_{k=0}^{N-1} x(2k). \quad (5.13)$$

In the Fast-OFDM system, the  $M$ -ary ASK symbols  $x(k)$  are independent and identically distributed with mean  $\mu = 0$  and variance (signal power)  $\sigma^2 = \sigma_s^2$ . According to the central limit theorem, as  $N$  increases, the interferences

$$\varepsilon_{\mathfrak{R}}(m) \xrightarrow{d} \mathcal{N}\left(0, \frac{\sigma_s^2}{N}\right), \quad (5.14)$$

which has a mean  $\mu_e = 0$  and a variance  $\sigma_e^2 = \sigma_s^2 / N$ . Assuming that the signal-to-noise ratio (SNR) is  $\lambda_{\text{SNR}} = \sigma_s^2 / \sigma_n^2$ , where  $\sigma_n^2$  is the noise power, and that the ICI and the noise are mutually independent, the signal-to-interference-and-noise ratio (SINR) thus is given by

$$\begin{aligned} \lambda_{\text{SINR}} &= \frac{\sigma_s^2}{\sigma_e^2 + \sigma_n^2} = \frac{\sigma_s^2}{\frac{\sigma_s^2}{N} + \sigma_n^2} \\ &= \frac{\lambda_{\text{SNR}}}{1 + \frac{\lambda_{\text{SNR}}}{N}} \end{aligned} \quad (5.15)$$

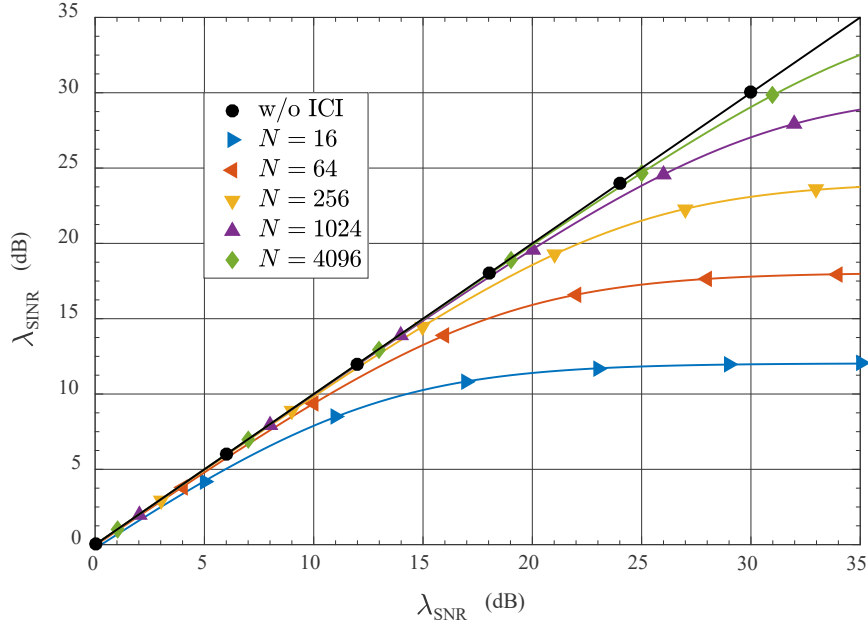


Figure 5–4. The analytically relationship between  $\lambda_{\text{SNR}}$  and  $\lambda_{\text{SINR}}$  with respect to  $N$ , defined in Eq. (5.15).

In Eq. (5.15), it can be observed that the SINR  $\lambda_{\text{SINR}}$  is determined by the SNR  $\lambda_{\text{SNR}}$  and the number of subcarriers  $N$ . If SNR is fixed, as  $N$  increases,  $\lambda_{\text{SINR}}$  approaches  $\lambda_{\text{SNR}}$ . It implies that the larger the number of subcarriers  $N$  is, the smaller the interference  $\lambda_{\text{SINR}}$  becomes. In Figure 5–4, the relations between  $\lambda_{\text{SNR}}$  and  $\lambda_{\text{SINR}}$  are plotted with various  $N$ , from 16 to 4096. It can be observed that the SINR decreases as the number of subcarriers  $N$  increases, and the achievable SINR is limited by the parameter  $N$ . If one gets  $\lambda_{\text{SNR}} \rightarrow +\infty$ , it can be obtained that

$$\lim_{\lambda_{\text{SNR}} \rightarrow +\infty} \lambda_{\text{SINR}} = \lim_{\lambda_{\text{SNR}} \rightarrow +\infty} \frac{\lambda_{\text{SNR}}}{1 + \frac{\lambda_{\text{SNR}}}{N}} = N. \quad (5.16)$$

It indicates that the upper bound of the achievable SINR  $\lambda_{\text{SINR}}$  is solely determined by the number of subcarriers  $N$ , as the SNR  $\lambda_{\text{SNR}}$  goes large enough. For example, in the cases of  $N = 16, 64, 256$ , the upper bounds are about 12.04, 18.06, and 24.08 dB, respectively. Even for  $N = 4096$ , the achievable SINR cannot go beyond 36.12 dB. It should be noted that  $N$  is chosen to be no greater

than 2048 or 4096 in practical applications to balance implementation complexity and performance.

### DERIVATION OF CLOSED-FORM BER PERFORMANCE

With the application of central limit theorem in Eq. (5.14), the SINR is derived in closed form in Eq. (5.15). It means that as the number of subcarriers is large enough, the interference term due to the ICI can be modeled as additive white Gaussian noise. Therefore, with the parameter  $\lambda_{\text{SINR}}$ , it is possible to derive the closed-form BER performance of the Fast-OFDM systems.

If  $M$ -ary ASK is adopted, for example, substituting  $\lambda_{\text{SINR}}$  into the BER function of ASK [92], the BER performance can be approximately given by

$$\begin{aligned} P_{e-\text{ASK}} &\approx \frac{2}{\log_2 M} \left(1 - \frac{1}{M}\right) Q \left( \sqrt{\frac{6}{M^2 - 1}} \lambda_{\text{SINR}} \right) \\ &= \frac{2}{\log_2 M} \left(1 - \frac{1}{M}\right) Q \left( \sqrt{\frac{6}{M^2 - 1}} \frac{N \lambda_{\text{SNR}}}{N + \lambda_{\text{SINR}}} \right) \end{aligned} \quad (5.17)$$

In Figure 5–5, the theoretical BER curves are plotted against  $\lambda_{\text{SNR}}$  according to Eq. (5.17). In the conventional Fast-OFDM, there is degradation, which gets worse as the number of subcarriers decreases. Because the ICI is proportional to the signal power, high-level modulation formats are more sensitive to the ICI. For example, in Figure 5–5 (c), the performance of 16-ASK becomes unacceptable for a practical system as the  $N$  is smaller than 512.

Inspecting the ICI terms in Eq. (5.12) and Eq. (5.13), one can observe that for any even subcarriers  $x(2m)$ , the ICI terms are identical, i.e.,  $\sum x(2k + 1)$ . For odd subcarriers, the ICI is  $\sum x(2k)$ . By utilizing this property, it is proposed to set some of the subcarriers to be zeros to estimate the ICI [90]. At the receiver, the ICI can be firstly estimated and then mitigated by subtracting the estimated ICI. Nonetheless, data rate is sacrificed for employing the null subcarriers.

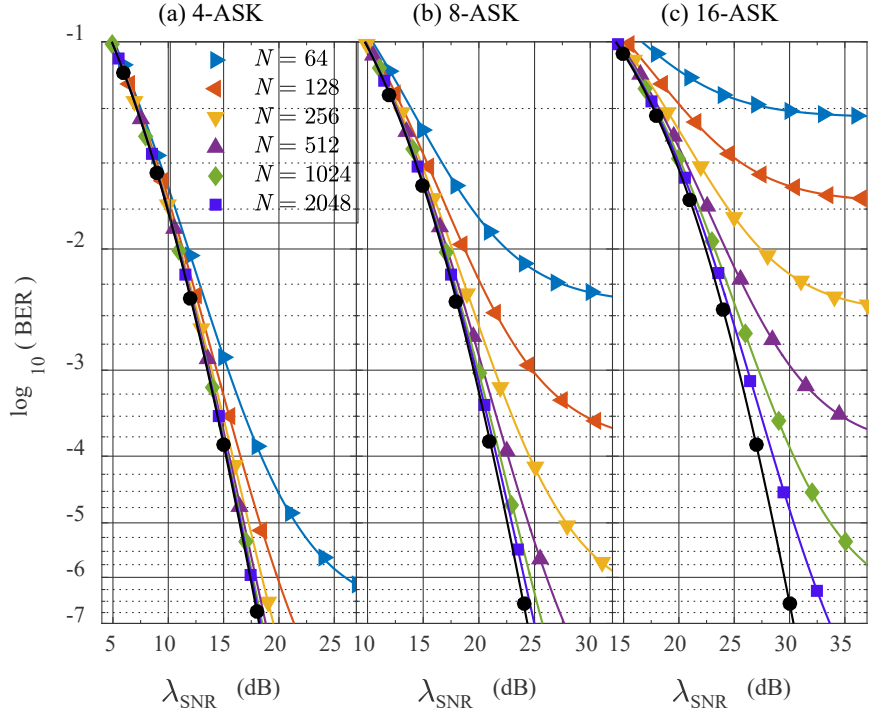


Figure 5–5. Theoretical BER performance of the conventional SSB modulated Fast-OFDM system and the proposed SSB modulated Fast-OFDM system (●) with (a) 4-ASK, (b) 8-ASK, and (c) 16-ASK.

### §5.3 Proposed SSB Fast-OFDM System

To eliminate the ICI term and to resolve the data rate loss problem in SSB modulated Fast-OFDM system as mentioned above, dedicated DSP algorithm is proposed to implement Fast-OFDM system. The channel equalization problem is also discussed and it is shown that the proposed scheme is able to compensate linear channel dispersion in the frequency domain using single-tap equalizers easily. Thus, the effect of linear channel will be discussed in terms of the proposed Fast-OFDM system. The mathematical model of the proposed algorithm is described in matrix form for brevity in this section.

Figure 5–6 provides the block diagram of the proposed Fast-OFDM system. At the transmitter, every  $2N$  ASK modulated symbols are weighted by linear phase, and then modulate  $2N$  subcarriers. The generated time-domain Fast-

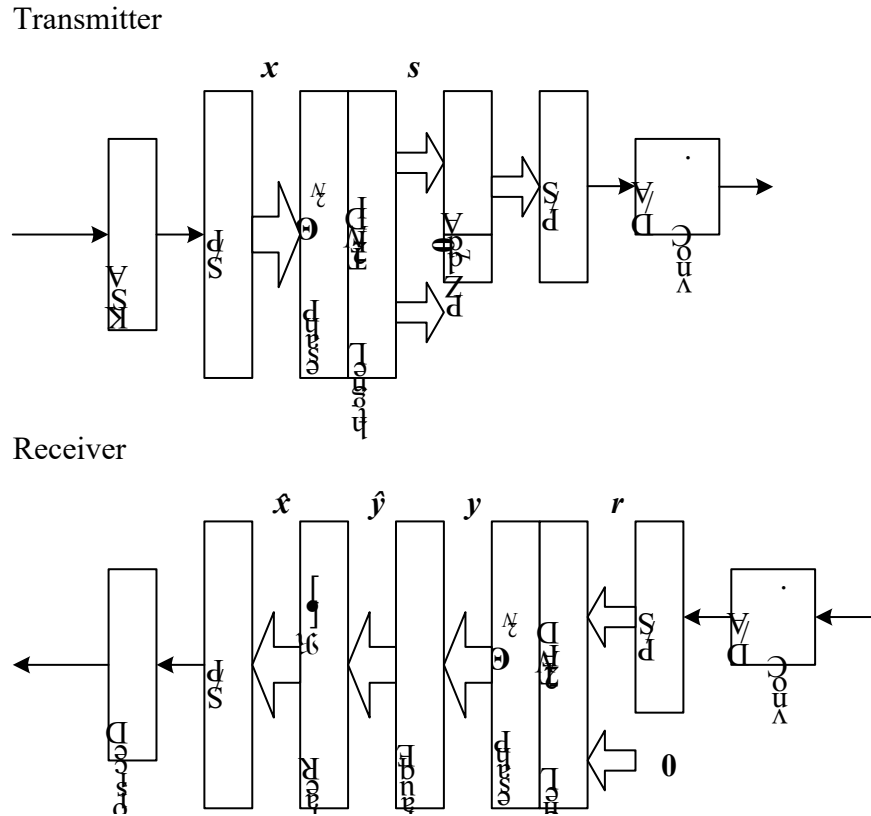


Figure 5–6. Block diagram of the proposed SSB modulated Fast-OFDM based on DFT.

OFDM signal is

$$\begin{aligned}
 s(n) &= \frac{1}{\sqrt{N}} \sum_{k=0}^{2N-1} x(k) e^{j \frac{2\pi}{2N} k \left( n + \frac{1}{2} \right)} \\
 &= \mathcal{F}_{2N}^{-1} \left\{ e^{j \frac{\pi}{2N} k} x(k) \right\} (n), \quad n = 0, 1, \dots, N-1,
 \end{aligned} \tag{5.18}$$

which can be implemented by a length- $2N$  IDFT, discarding the last  $N$  samples of its output. In the proposed scheme, GI is inserted between the Fast-OFDM blocks, and it is filled with zeros. The Fast-OFDM block with GI for transmission is

$$s_{\text{GI}}(n) = \begin{cases} s(n) & n = 0, 1, \dots, N-1 \\ 0 & n = N, \dots, N+L-1 \end{cases} \tag{5.19}$$

where  $L$  is the length of GI. In practice, the length of GI is larger than the maximum delay spread of channel.

The time-domain signal in Eq. (5.19) is parallel-to-serial (P/S) converted and fed into the digital-to-analog convertors (DACs). Electrical drivers following the DACs amplify the signals to drive an optical modulator. After the modulated optical signal travels through optical fiber, it experiences distortions, such as, chromatic dispersion (CD) and polarization mode dispersion (PMD) and is corrupted by additive noise, such as the amplified spontaneous noise (ASE), which is introduced by optical amplifiers after transmissions.

At the receiver, after the Fast-OFDM block is identified via frame synchronization, the received Fast-OFDM signal is given by

$$\begin{aligned} r(n) &= h(n) * s_{\text{GI}}(n) + z(n), \\ n &= 0, 1, \dots, N + L - 1, \end{aligned} \quad (5.20)$$

where  $h(n)$  is channel impulse response (CIR), and  $z(n)$  additive noise.

In the proposed Fast-OFDM system, as mentioned before, GI is filled with zeros. If the maximum delay spread of channel is no greater than the length of GI, there is no interference from adjacent Fast-OFDM blocks. Padding zeros to the end of  $r(n)$  to length  $2N$  and applying a  $2N$ -point DFT on Eq. (5.20), one obtains

$$\begin{aligned} y'(m) &= \mathfrak{F}_{2N} \{r(n)\}(m) + \mathfrak{F}_{2N} \{v(n)\}(m), \\ m &= 0, 1, \dots, 2N - 1. \end{aligned} \quad (5.21)$$

Applying the linear convolution theorem of the Fourier transform, Eq. (5.21) can be further given by

$$\begin{aligned} \mathfrak{F}_{2N} \{s_{\text{GI}}(n)\}(m) &= \frac{1}{\sqrt{N}} \sum_{n=0}^{N-1} s(n) e^{-j \frac{2\pi}{2N} mn} \\ &= \frac{1}{N} \sum_{k=0}^{2N-1} x(k) e^{-j \frac{\pi}{2N} k} \sum_{n=0}^{N-1} e^{-j \frac{2\pi}{2N} n(m-k)} \\ &= \frac{1}{N} \sum_{k=0}^{2N-1} x(k) \frac{e^{-j \frac{\pi}{2} (m-k)} \sin \frac{\pi}{2} (m-k)}{e^{-j \frac{\pi}{2N} m} \sin \frac{\pi}{2N} (m-k)}, \end{aligned} \quad (5.22)$$

and using the following identities, that are

$$e^{-j \frac{\pi}{2} (m-k)} = (-j)^{m-k} \quad (5.23)$$

and

$$\begin{aligned} & \frac{1}{N} \frac{\sin \frac{\pi}{2}(m-k)}{\sin \frac{\pi}{2N}(m-k)} \\ &= \begin{cases} 1 & m=k \\ 0 & m \neq k, \quad m-k \equiv 0(\text{mod } 2), \\ \varepsilon(m-k) & m-k \equiv 1(\text{mod } 2) \end{cases} \end{aligned} \quad (5.24)$$

Eq. (5.22) can be further simplified as

$$\begin{aligned} & \mathcal{F}_{2N} \{s_{\text{GI}}(n)\}(2m) \\ &= e^{j\frac{\pi}{N}m} \left[ x(2m) + j \underbrace{\sum_{k=0}^{N-1} (-1)^{m-k} \varepsilon(2m-2k-1)x(2k+1)}_{\varepsilon_{\text{ICI}}(2m)} \right] \end{aligned} \quad (5.25)$$

for even subcarriers, and

$$\begin{aligned} & \mathcal{F}_{2N} \{s_{\text{GI}}(n)\}(2m+1) \\ &= e^{j\frac{\pi}{N}\left(m+\frac{1}{2}\right)} \left[ x(2m+1) + j \underbrace{\sum_{k=0}^{N-1} (-1)^{m-k+1} \varepsilon(2m-2k+1)x(2k)}_{\varepsilon_{\text{ICI}}(2m+1)} \right] \end{aligned} \quad (5.26)$$

for odd subcarriers, respectively, where  $m = 0, 1, \dots, N-1$ . The terms  $\varepsilon_{\text{ICI}}(m)$  represent the interference, from which the even or odd subcarriers suffer.

According to Eqs. (5.25) and (5.26), the received symbols can be recovered by reverting the phase rotation as

$$\begin{aligned} y(m) &= e^{-j\frac{\pi}{2N}m} y'(m) \\ &= H(m)[x(m) + j \cdot \varepsilon_{\text{ICI}}(m)] + w(m), \end{aligned} \quad (5.27)$$

where  $H(m) = \mathcal{F}_{2N}\{h(n)\}$  is the channel frequency response (CFR), and  $\varepsilon_{\text{ICI}}(m)$  are the interference terms defined in Eqs. (5.25) and (5.26). If zero-forcing (ZF) equalizer is adopted, the signal is thus given by

$$\begin{aligned} \hat{y}(m) &= H^{-1}(m)y(m) \\ &= x(m) + j \cdot \varepsilon_{\text{ICI}}(m) + H^{-1}(m)w(m). \end{aligned} \quad (5.28)$$

In Eq. (5.28), the symbols  $x(m)$  are ASK modulated, and thus are real-valued.

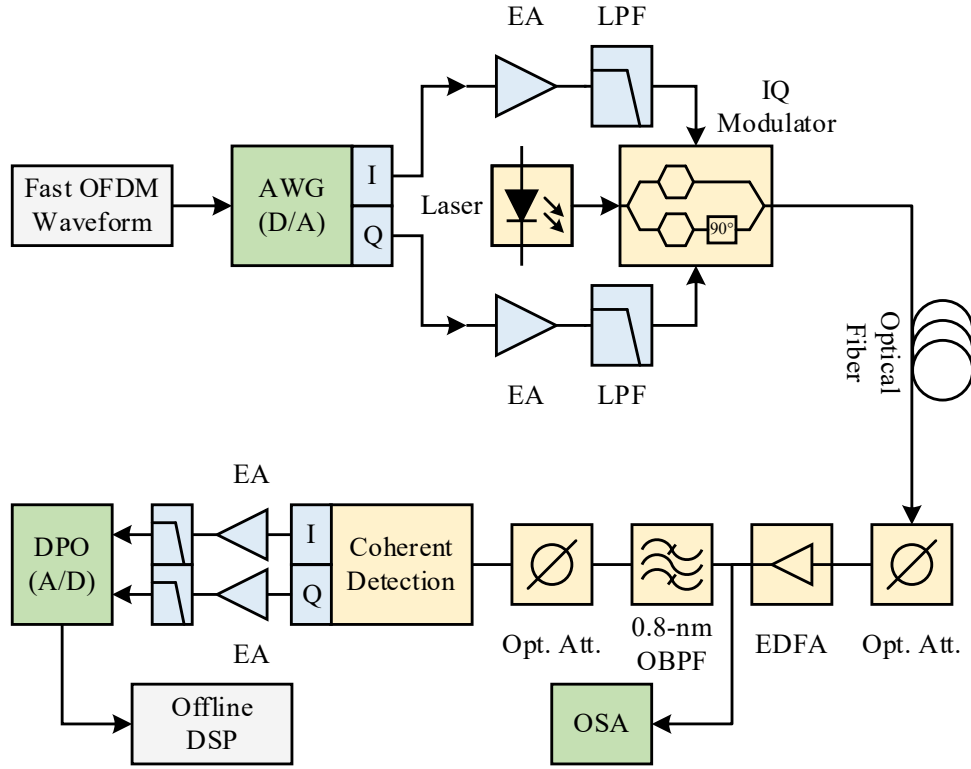


Figure 5–7. Experiment setup for the proposed SSB Fast OFDM.

Inspecting Eqs. (5.25) and (5.26), the interference term  $\varepsilon_{ICI}(m)$  is also real-valued and is projected onto the imaginary plane in Eq. (5.27). Thus, the real-valued symbols can be recovered at the receiver by discarding the imaginary part of  $\hat{y}(m)$ .

## §5.4 Numerical Simulation

In this section, simulations are performed to investigate the performance of the proposed Fast-OFDM system. Figure 5–7 illustrates the system setup. In the simulation, there are  $2N$  subcarriers;  $3/4$  of which are modulated with payload in ASK, and the oversampling ratio is thus  $4/3$ . The last  $N$  samples of the IDFT output are discarded. The time-domain Fast-OFDM block has a length of  $N$ . Between the blocks, ZP based GI is inserted; the GI is long enough to accommodate the dispersion after transmission. For comparison, the Fast-OFDM schemes in [89] and [90] are provided with the same parameters.

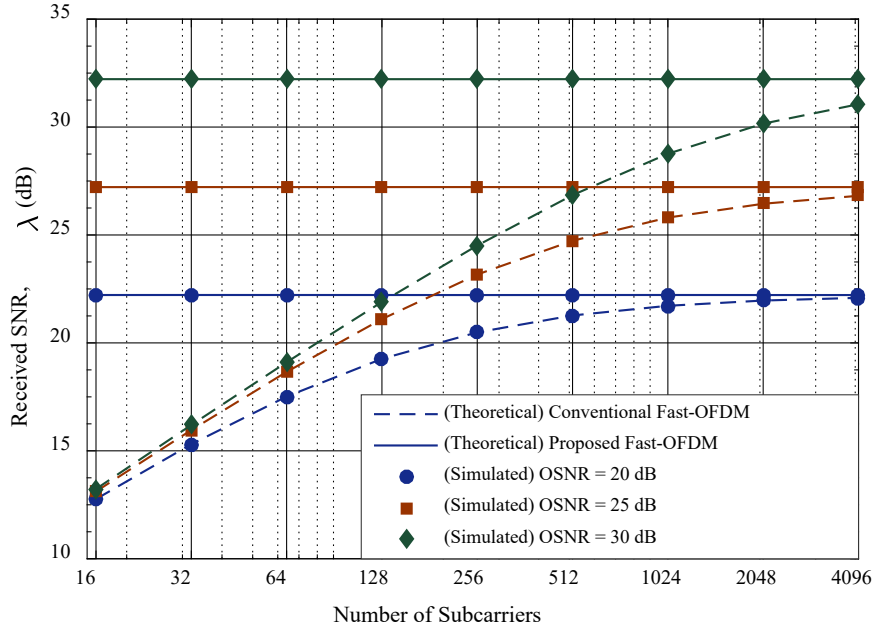


Figure 5–8. Theoretical and simulated received SNR,  $\lambda$ , versus different number of subcarriers in the conventional Fast-OFDM scheme and the proposed Fast-OFDM.

In the simulation, the sampling rate is set to be 20 GS/s. As a result, the bandwidth of the signal is about 15 GHz. The laser is operated at 1553 nm. It is assumed that the IQ modulator is operated within the linear region, and that the PDs have a responsivity of 1 A/W and follows the ideal 90° optical hybrids.

### §5.4.1 ICI versus Number of Subcarriers

In this subsection, we study the ICI term in the conventional Fast-OFDM. The performance is evaluated after back-to-back (B2B) transmission at fixed OSNRs of 20, 25, and 30 dB. In the simulation, the number of subcarriers  $2N$  increases from 32 to 8192, and only 4-ASK is adopted.

Figure 5–8 provides the received SNR,  $\lambda$  of different number of subcarriers  $N$ , where

$$\lambda = \frac{\sigma_s^2}{E[r(n) - s(n)]^2} \quad (5.29)$$

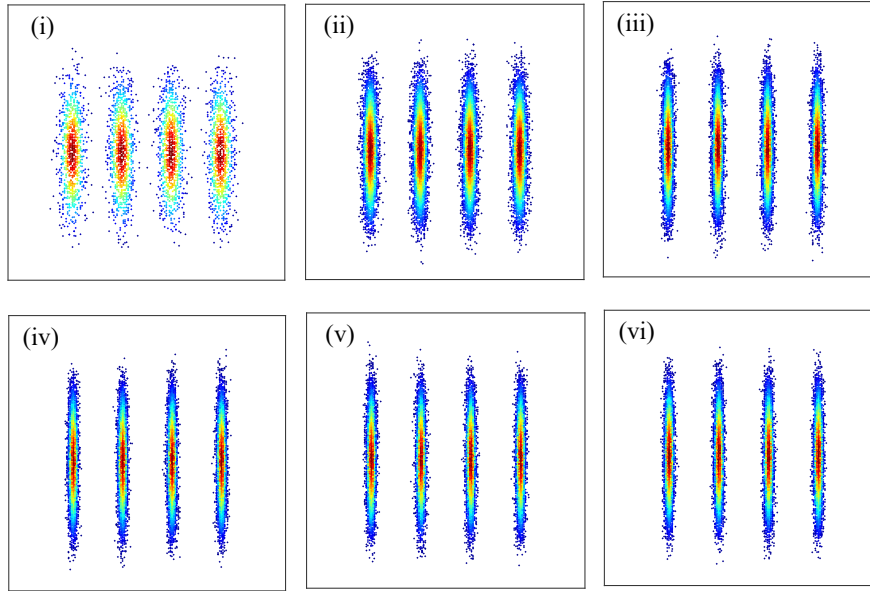


Figure 5–9. The received constellation diagrams of received 4-ASK signal of conventional Fast-OFDM with  $N =$  (i) 64, (ii) 256, and (iii) 1024, and that of the proposed scheme with  $N =$  (iv) 64, (v) 256, and (vi) 1024, at OSNR = 25 dB.

One can observe that the performance of the proposed scheme is independent of the number of subcarrier as there is no ICI. In contrast, in the conventional Fast-OFDM, the less the number of subcarriers, the worse the ICI. In the case of  $N = 16$  and OSNR = 30 dB, the penalty is about 20 dB compared to the proposed scheme. If  $N = 1024$ , the penalty reduces to 3 dB at the OSNR = 30 dB. In addition, the measured noise variances well fit the analytical performance as shown in Eq. (5.15).

Figure 5–9 illustrates the constellation diagrams of the received signal at a received OSNR = 25 dB. Referring to (5.25) and (5.26), the interferences are completely located in the imaginary plate. In the conventional Fast-OFDM, the constellation diagram becomes clearer as  $N$  increases from (i) 64, (ii) 256, to (iii) 1024, while the constellation diagrams of the proposed one with  $N =$  (iv) 64, (v) 256, and (vi) 1024 are the same.

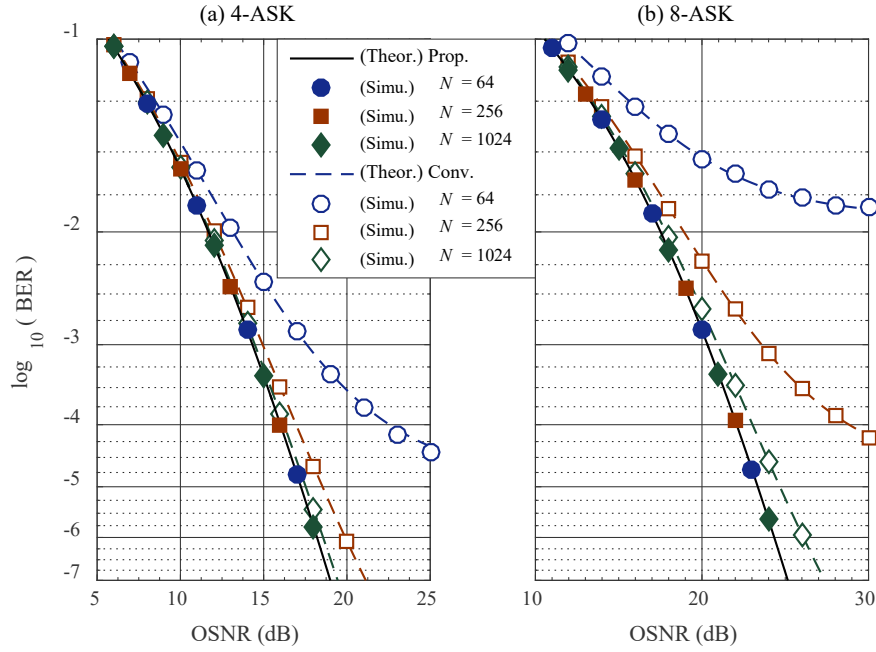


Figure 5–10. BER performances of the conventional Fast-OFDM ( $\circ/\square/\diamond$ ) and the proposed Fast-OFDM system ( $\bullet/\blacksquare/\blacklozenge$ ). ( $\circ/\bullet$  for  $N = 64$ ,  $\square/\blacksquare$  for  $N = 256$ , and  $\diamond/\blacklozenge$  for  $N = 1024$ .)

### §5.4.2 BER Performance versus OSNR

This subsection studies the bit-error rate (BER) performance of the proposed Fast-OFDM scheme. In the simulation, both (a) 4-ASK and (b) 8-ASK are adopted, and the number of subcarriers are  $2N = 128, 512$ , and  $2048$ . In addition, the performance of the ICI mitigation scheme in [90] is also provided for comparison. The performance is evaluated in terms of BER versus optical signal-to-noise ratio (OSNR), which is measured with the 0.1-nm resolution (12.5 GHz at 1553nm).

The BER performance of the conventional and the proposed schemes are shown in Figure 5–10 (a) for 4-ASK and (b) for 8-ASK. The proposed Fast-OFDM schemes of various  $N$  get the same BER performance. In the case of 4-ASK in Figure 5–10 (a), if  $N = 256$ , the proposed scheme gets about 1-dB OSNR improvement to that in [89], and if  $N = 1024$ , there is still slight improvement to the conventional scheme. If  $N = 64$ , there is a visible degradation

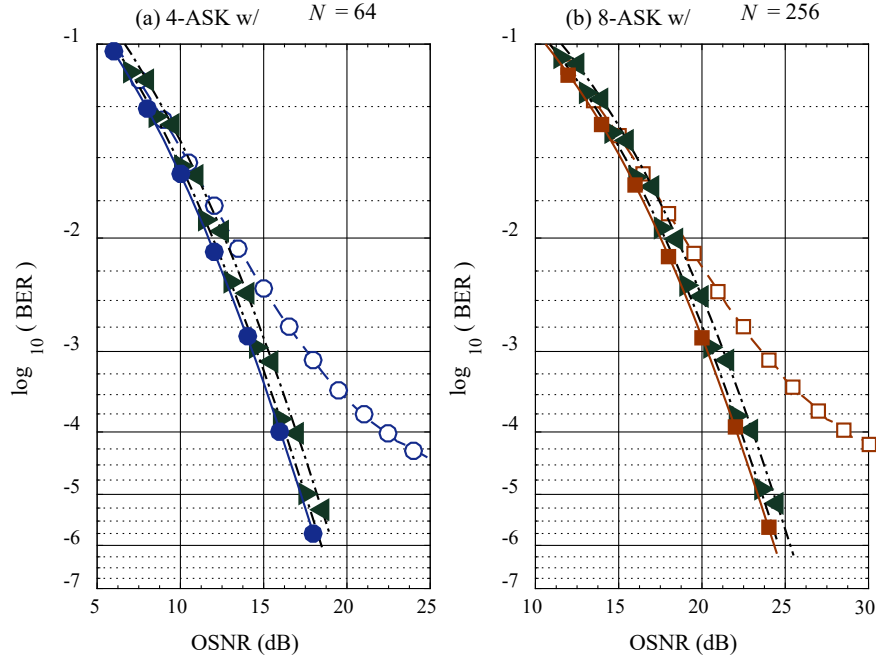


Figure 5–11. BER performances versus OSNR of the conventional Fast-OFDM ( $\circ/\square$ ), the one with interference mitigation ( $\blacktriangleright/\blacktriangleleft$ ) and the proposed Fast-OFDM system ( $\bullet/\blacksquare$ ). ( $\blacktriangleright/\blacktriangleleft$  denotes 8/32 ICI estimation subcarriers, respectively.)

in the conventional Fast-OFDM. For example, at a  $\text{BER} = 10^{-4}$ , the penalty is about 7 dB OSNR to the proposed scheme. In the case of 8-ASK, as high-level modulation scheme is more sensitive to the interference, the conventional Fast-OFDM has about 1-dB and 6-dB OSNR penalties to the proposed scheme for  $N = 1024$  and 256, respectively. If  $N = 64$ , there is even an error floor at a BER level of  $1 \times 10^{-2}$ . Therefore, in the conventional Fast-OFDM scheme, the ICI largely limits the performance for small number of subcarriers ( $< 512$ ) and for high level modulation scheme ( $> 4$ -ASK). In Figure 5–10, theoretical BER curves are also provided, and they well agree with the simulated results. In the simulation results, note that as only  $3/4$  subcarriers are loaded with data, the variance  $\sigma_e^2$  should be scaled by a factor of 0.75 before put it into Eq. (5.15).

The ICI estimation scheme is adopted for comparison and the system performances of (a) 4-ASK with 128 subcarriers and (b) 8-ASK with 512 subcarriers are provided in Figure 5–11. The ICI estimation scheme is able to efficiently mitigate the ICI effects. In Figure 5–11 (a) and (b), the ICI estimation

scheme gets about 4-dB OSNR improvement to the conventional scheme at a BER level of  $10^{-4}$ . If the number of subcarriers for ICI estimation is 8, there is about 1-dB gap to the proposed scheme. If the number of ICI estimation subcarriers increases to 32, the difference becomes negligible. The spectral efficiency loss due to the null subcarriers for ICI estimation, however, is about 33.3% for 128 subcarriers and 8.3% for 512 subcarriers.

## §5.5 Experimental Validation

In this section, we implemented experiment to validate the feasibility of the proposed SSB Fast OFDM scheme based on DFT. This section is organized as follows. The experiment setup is introduced in subsection §5.5.1, and the experiment results is presented in subsection §5.5.2.

### §5.5.1 Experimental Setup

In the subsection, experiments were carried out to implement the proposed coherent optical Fast-OFDM. The experimental setup is provided in Figure 5–12. In the experiment, we measured two setups. In the first setup, there are 1024 subcarriers out of which 768 are modulated by 4-ASK. In the second setup, there are 1024 subcarriers; 512 are modulated by 8-ASK. Consequently, if the sampling rate of DACs is fixed, these two setups achieve the same data rate, while the spectral efficiencies are 4 bit/s/Hz and 6 bit/s/Hz, respectively.

At the transmitter, the Fast OFDM signal is generated using MATLAB<sup>®</sup> and downloaded into an arbitrary waveform generator (AWG) operating at a sampling rate of 12 GS/s. The data rates of the two setups, excluding the 32-point GI, are 36 Gbps. The in-phase and quadrature signals at the output of AWG are fed into a dual-port amplifier to drive an optical IQ modulator, which is biased at the null point. The  $V_\pi$  of the modulator is about 5 V and the input peak-to-peak electrical signal is about 1.5 V to make sure that the optical IQ modulator is operated within the linear range. The laser is operated at 1553.4 nm.

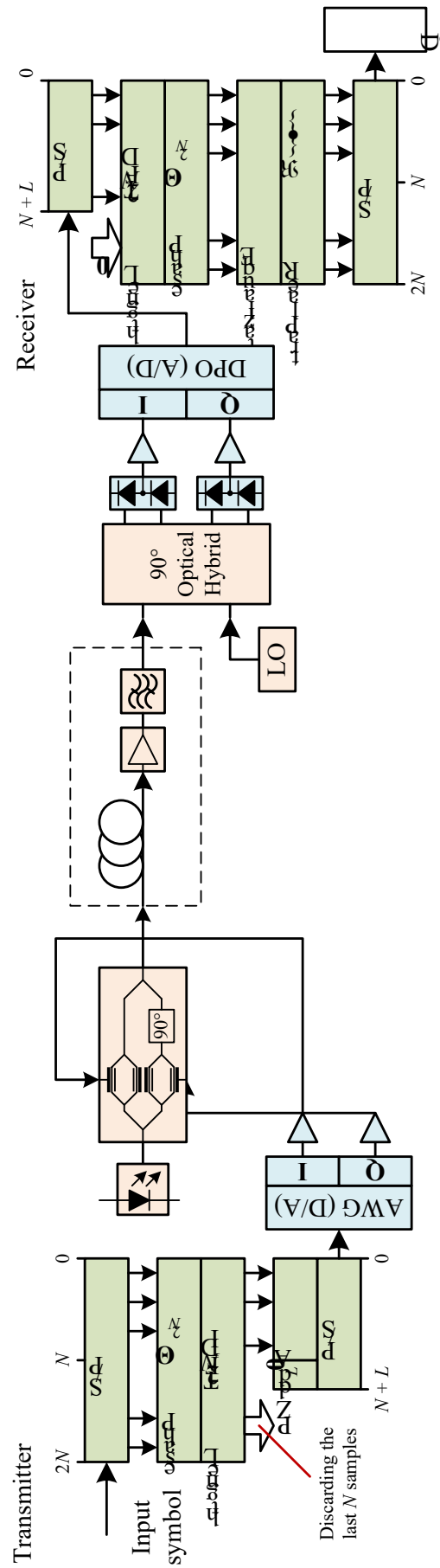


Figure 5–12. Experiment System setup for the proposed coherent optical SSB Modulated Fast-OFDM system.

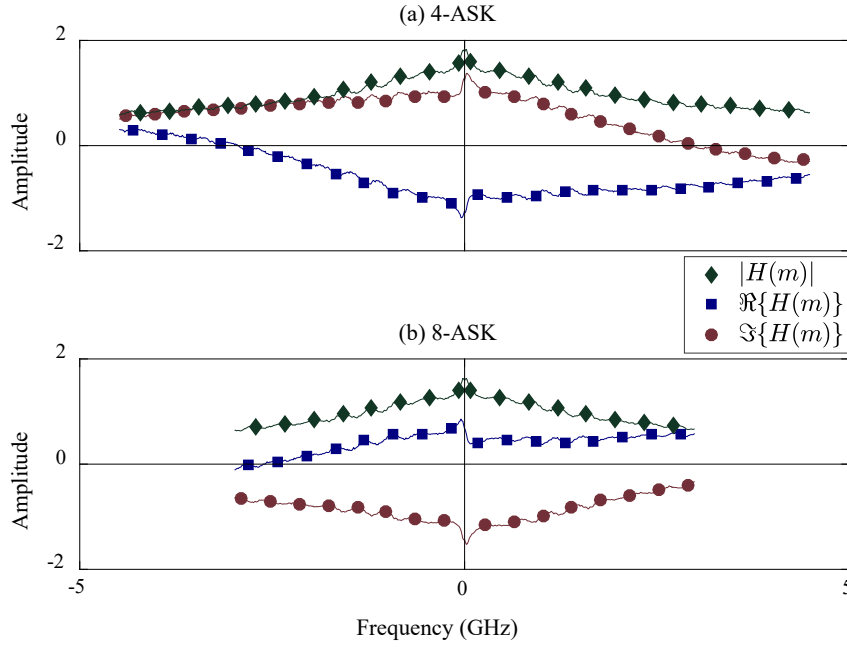


Figure 5–13. One-shot observations of the measured channel frequency responses for (a) 4-ASK and (b) 8-ASK.

At the receiver end, there is an optical attenuator to control the input power to the optical amplifier to adjust the received OSNR. The amplified optical signal at the output of the EDFA is split by a 10/90 optical splitter. The 10% output is connected into an optical spectrum analyzer (OSA) to measure the actual received OSNR at a resolution of 0.1 nm. The 90% output is followed by a 0.8-nm optical band-pass filter (OBPF) to reject out-of-band ASE noise. Following the OBPF, there is an optical power controller to fix the signal power into the coherent receiver, which converts the optical signal into electrical baseband signals. Another dual-port electrical amplifier boosts the electrical signals. The electrical signals are recorded by a real-time digital phosphor oscilloscope (DPO) with ADCs operating at 50 GS/s. Before performing signal recovery, the signal is firstly resampled down to 12 GS/s.

### §5.5.2 Experimental Results

Figure 5–13 provides the measured channel frequency responses of both setups, which are obtained by sending frequency-domain pilots. In the (a) 4-ASK case,

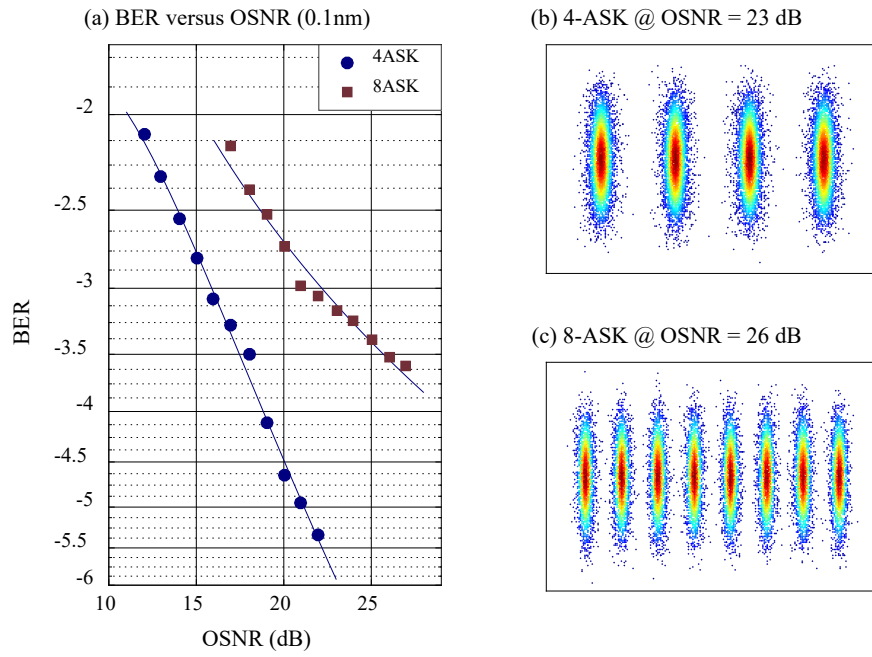


Figure 5–14. (a) BER performance versus OSNR of the proposed Fast-OFDM in B2B transmission; (b) the measured constellation diagram of (b) 4-ASK at OSNR = 23 dB and (c) 8-ASK at OSNR = 26 dB.

the bandwidth is about 9 GHz with an oversampling rate of  $4/3$  while for the (b) 8-ASK the bandwidth is about 6 GHz. It is obvious that the channel is not symmetric nor flat. Consequently, the symmetric convolution cannot be easily applied for the DSB modulated Fast-OFDM, nor for the conventional SSB modulated Fast-OFDM as the transform kernel is not even orthogonal.

Figure 5–14 provides the measured (a) BER performance and the recovered constellation diagrams of (b) 4-ASK and (c) 8-ASK, respectively. In the 4-ASK case, the BER curve goes straightly while in the 8-ASK case, there is slight degradation in the high OSNR region, which is limited by the achievable performance of the system. Nonetheless, the proposed Fast-OFDM scheme with 8-ASK still gets BER performance below the FEC limits at a BER =  $10^{-3}$ .

One thing should be noted in Figure 5–14 (b) and (c). We can observe that though the interference is completely projected to imaginary axis, if there is any residual frequency offset and residual comment phase rotation due to laser phase noise, the interference will interfere with the signal in the real axis, and

may introduce performance degradation. On the other hand, better performance can be expected for the conventional OFDM system than the SSB-FOFDM as there is not interference existed.

## §5.6 Summary

In this chapter, the ICI in the conventional SSB Fast-OFDM is analytically studied. The degradation caused by the ICI and the BER performance are derived in closed-form expressions as the functions of SNR and the number of subcarriers. Simulations are provided to confirm the analysis. To avoid the degradation due to the ICI, we propose a new SSB modulated Fast-OFDM system by using frequency-domain oversampling. Compared to previous schemes, single-tap equalizer can be directly applied for symbol extraction without any limitation. Experiments were successfully carried out to implement the proposed SSB modulated Fast-OFDM signal at 36 Gbps with a spectral efficiency of 6 bit/s/Hz.



# Part II



## Chapter 6

# Orthogonal Chirp-Division Multiplexing

In the orthogonal frequency-division multiplexing (OFDM) based systems, a large bunch of orthogonal narrowband waveforms, or in the name of harmonics from the view of Fourier analysis, are multiplexed to achieve high-speed communications. For example, in the conventional OFDM systems, the orthogonal waveforms are complex exponentials. In the double sideband (DSB) modulated Fast-OFDM, the orthogonal waveforms are replaced by cosines. In the OFDM systems, each waveforms are narrowband and occupies a small portion of the whole bandwidth. Their spectra partially overlap with each other, and all the narrowband waveforms together make up of a wideband signal for high-speed communications, with the spectral efficiency, by means of orthogonality, hitting the maximum from the view of Nyquist and Shannon.

In this chapter, we will be introducing an orthogonal concept for waveform design, which we named orthogonal chirp-division multiplexing (OCDM), for high-speed communications. Literally, the OCDM is a multiplexing scheme that utilizes a large bunch of orthogonal linearly-chirped waveforms for information modulation and transmission.

Before the introduction of OCDM, in communication systems, especially in the wireless communication systems, chirped waveforms are employed for reliable and secure communications because they achieve the purpose of spread

spectrum and thus are robust against the detrimental effects from the hostile channel. The philosophy of using chirped waveforms, or chirp spread spectrum (CSS) in jargon, is to spread the spectrum of a signal over a much wider bandwidth than it should be, gaining remarkable resilience against the impairments from the harsh channel. In the wide spectrum, whose bandwidth is much larger than it should be for a given data rate, only a single chirped waveform is transmitted for communications. If there are more than two modulated chirp waveforms within the same bandwidth and period, interference exists between them. Therefore, CSS is suitable for low data-rate applications by trading the spectral efficiency for reliability and security.

Technically, OCDM is the principle orthogonally synthesizing a large bunch of modulated linear-chirped waveforms for high-speed communication, just as OFDM is the principle that orthogonally synthesizes the modulated harmonics. OFDM is the frequency-division multiplexing (FDM) system that satisfies the orthogonal condition achieving the maximum spectral efficiency, and OCDM achieves the maximum spectral efficiency for CSS. The fundamental behind the OCDM is the Fresnel transform, just as the Fourier transform in the OFDM. In this thesis, moreover, we also derive the discrete Fresnel transform (DFnT) which formulates the digital implementation of the OCDM systems.

This chapter is dedicated to the OCDM, which is organized as follows.

In Section §6.1, we briefly introduce the background of OCDM, and its precursor, chirp spread spectrum. It includes the basic concept of CSS, and its application. Especially, according to the Fresnel transform, we will show how the CSS is evolving into the OCDM, bringing the spectral efficiency of CSS to the maximum.

In Section §6.2, we will focus on the fundamental of the OCDM, the Fresnel integral transformation, which is a versatile formula in mathematics, classic optics, and physics. Except to a brief for the Fresnel transform, we derive the discrete Fresnel transform (DFnT) from the Fresnel transform in the infinitely extended periodic grating, namely the Talbot effect. Based on different conditions, there are various derivations for the DFnT. Moreover, we will show the differences of the DFnT derived in the thesis to other derivations of DFnT. We

will also present the special properties of the DF<sub>n</sub>T derived in this thesis. Of the properties, we pay much attention on the derivation of, probably, the most crucial property that the circular convolution property of the DF<sub>n</sub>T. Based on the derivation, we show that there is a convolution theorem in terms of the DF<sub>n</sub>T which states that the DF<sub>n</sub>T of a circular convolution of two sequences is equal to the convolution of their DF<sub>n</sub>Ts.

In Section §6.3, based on the Fresnel transform and DF<sub>n</sub>T, we present the principle of the OCDM, as a special case of CSS. Compared to OFDM in which Fourier transform is the transformation kernel, in OCDM, it is shown that Fresnel transform serves as the transformation kernel that multiplexes a bunch of modulated linearly-chirped waveforms. Based on the DF<sub>n</sub>T derived in Section §6.2, we present the digital implementation of OCDM. The system model of OCDM under LTI channels is formulated for analysis. Based on the analysis and by utilizing the properties of DF<sub>n</sub>T, we propose an efficient single-tap equalization algorithm for the OCDM to compensate the channel dispersions. Discussions, including the system implementation of OCDM, its compatibility to the OFDM system, and the computational complexity of OCDM system are also provided.

In Section §6.5, numerical simulations are provided for the OCDM systems, under both wireless mobile channel and optical fiber channel. From the simulation results, it is shown that, in virtue of its chirp spread spectrum, the OCDM system is more robust than the OFDM system against the detrimental effects in both wireless and optical fiber channels, and thus it achieves better performance than the OFDM system in various application scenarios.

In Section §6.6, the OCDM system was experimentally implemented in the coherent optical fiber system to validate its feasibility and advantages over the OFDM system. The experimental results coincide with the analysis and simulation results, and it is shown that OCDM system achieves better performance than the OFDM system.

Finally, in Section §6.7, conclusions are provided.

## §6.1 Overview

Chirp relates to a signal whose phase evolves along with time in a certain manner, and it can be found almost everywhere. For example, the spatial frequency of the near-field Fresnel diffraction pattern increases linearly with the distance to the origin of the screen, in Figure 6–1 (a) and (b) [93-96]. In radar systems, the chirp signal is frequency modulated and swept over a wide spectrum with a constant amplitude. By correlating the echoes bouncing from target, pulse compression is achieved as if ‘short’ pulses are emitted and received. The position of the target can be resolved from the temporally delayed pulses [97-99]. In spread-spectrum systems, digital binary information is encoded by modulating the frequency of a carrier, sweeping the frequency linearly from low to high as ‘up-chirp’ for bit ‘1’ or from high to low as ‘down-chirp’ for bit ‘0’, as shown in Figure 6–1 (c) and (d) [100-105]. The chirp signal uses a wideband spectrum for transmission and is resistant to detrimental effects, such as channel noise, multipath fading and Doppler effects within the mobile radio channel.

For the purpose of communication, the chirp signal is of spread-spectrum approach which guarantees secure and robust communication for applications including military, underwater and aerospace communications [106-108]. In the recent ultra-wideband (UWB) standard by the IEEE 802.15.4a group [109], the chirp signal is adopted to satisfy the requirement of FCC on the radiation power spectral mask for the unlicensed UWB systems. Meanwhile, the chirp signal achieves what a UWB system is supposed to do, i.e., ranging, measuring and communicating [110-112].

Conventionally, the chirp signal is usually generated by analog devices in filtering approach by surface acoustic wave (SAW) devices [113-117] or in frequency-modulation approach by voltage controlled oscillator taking the advantages of the mature CMOS technology [118-120]. In the chirp spread-spectrum (CSS) or frequency-modulated systems, a broad spectrum is occupied for modulating information. Spectral efficiency is sacrificed for higher processing gain, the capability of multipath resolution, and other merits of the chirp signal as well. In a given period  $T$  and bandwidth  $B$ , a single chirp is modulated for

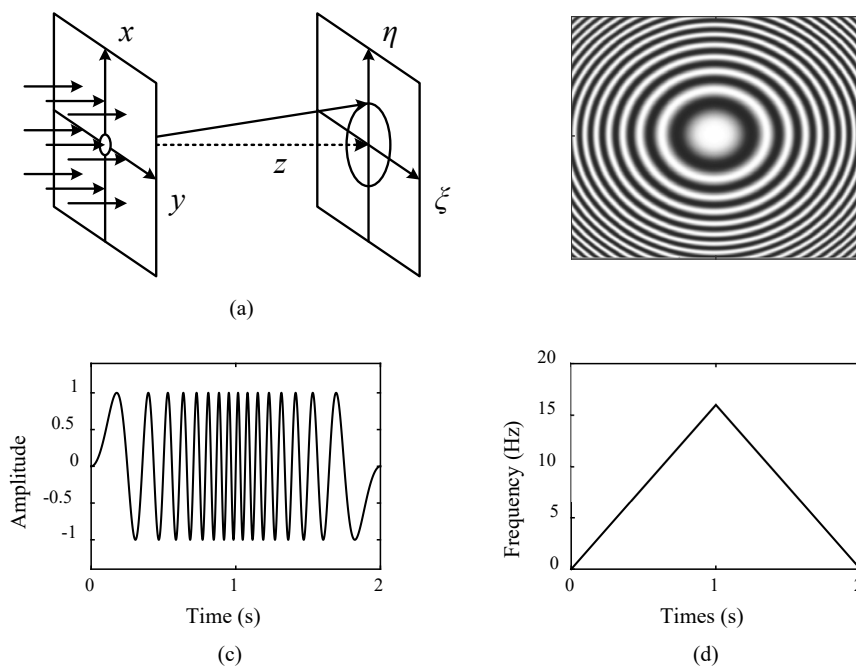


Figure 6–1. Illustration of chirps: (a) Near-field Kirchhoff-Fresnel diffraction of a circular aperture, and (b) its diffraction pattern on the second plate; (c) linear chirp waveform which is ‘up-chirp’ from 0 to 1 second and is ‘down-chirp’ from 1 to 2 second, and (d) its spectrogram.

transmission as shown in Figure 6–2 (a). If there exists more than one chirp within the same period and bandwidth, inter-chirp interference occurs. As a result, the chirp or frequency-modulated signal is attractive for low-rate applications in which reliable communication is in priority.

To increase the data rate of the UWB system, multi-code UWB is proposed by dividing the entire spectrum into a bank of spectrally separated chirps [110], referring to Figure 6–2 (a). Each chirp is modulated by binary codes, such as, the Walsh-Hadamard code. At the receiver, the transmitted information is recovered by retrieving the orthogonal codes from the modulated chirps over the entire bandwidth.

Heuristically, in this thesis we came to think about if there is a way of synthesizing a bank of chirps in the same period and bandwidth without any interference, and both of the amplitude and phase of the chirp can be used for modulation. If yes, can we implement such system by using the advanced digital

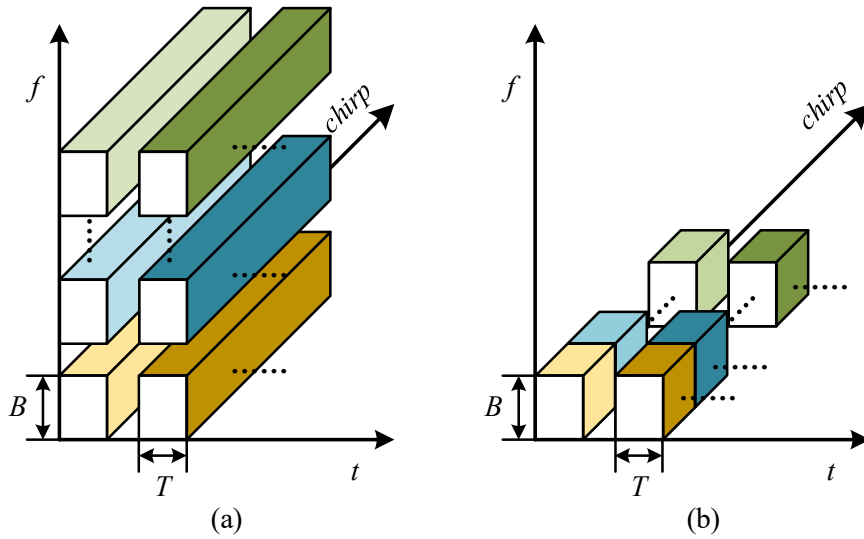


Figure 6–2. Illustration of (a) the multi-code chirp waveform and (b) the orthogonal chirp-division multiplexing in the temporal-frequency-chirp dimension.

signal processing (DSP) technology in the digital domain rather than in the analog domain?

In the chapter, we introduce the principle of OCDM that is to orthogonally multiplex a large number of linearly-chirped waveforms within the same bandwidth, for communication at the maximum of spectral efficiency. As shown in Figure 6–2 (b), a bunch of chirp waveforms overlap temporally and spectrally in the OCDM. The phase and/or amplitude of each chirp signal are modulated, for example, by phase shift keying (PSK) or quadrature amplitude modulation (QAM). The modulated chirps are orthogonal along the chirp dimension, without interference to each other for transmission.

We show that the fundamental mechanism behind the OCDM is the Fresnel transform, just as the Fourier transform in orthogonal frequency division multiplexing (OFDM). In this section, digital implementation of the OCDM system using discrete Fresnel transform (DFnT) is presented. Specifically, the inverse DFnT (IDFnT) generates the OCDM signal at the transmitter, and the DFnT recovers the OCDM signal at the receiver.

We then analyze the transmission of the OCDM signal under linear time-

invariant (LTI) or quasi-static channels which can generalize most of the practical linear communication channels, like coaxial cables, optical fibers and mobile radio channels etc. According to the convolution property of the Fresnel transform, it is shown that the channel distortion can be compensated by using either time-domain or frequency-domain equalizer.

Moreover, according to the eigen-decomposition of DF<sub>n</sub>T, a more efficient single-tap equalization algorithm is proposed for the OCDM system. The algorithm is based on single-tap frequency domain equalization (FDE), and it is more efficient than the aforementioned two equalization schemes.

## §6.2 Fresnel Integral Transformation

Fresnel transform is an integral transformation originating from classical optics [93-96]. It is the formula that mathematically describes the behavior of the near-field optical diffraction. As the single slit is repeated periodically, the diffraction pattern is repeated, and as a result a Talbot image is formed. Various DF<sub>n</sub>Ts are derived to describe the coefficients of the Talbot effects of different conditions.

In this section, we present the continuous Fresnel transform in Subsection §6.2.1. Based on the Talbot effect of infinitely and periodically repeated slits, DF<sub>n</sub>T is derived in Subsection §6.2.2. For the special formulation, the DF<sub>n</sub>T in this paper possesses a convolution-preservation property that states that the DF<sub>n</sub>T of the circularly convolved sequences equals the circular convolution of their DF<sub>n</sub>Ts. In addition, some useful properties of the DF<sub>n</sub>T are also studied in Subsection §6.2.3.

### §6.2.1 Fresnel Integral

As shown in Figure 6–1 (a), when a monochromatic plain wave with wavelength  $\lambda$  encounters a slit (grating) which is comparable in size to  $\lambda$ , the resulting near-field diffraction pattern observed on a plate at distance  $z$  is given by

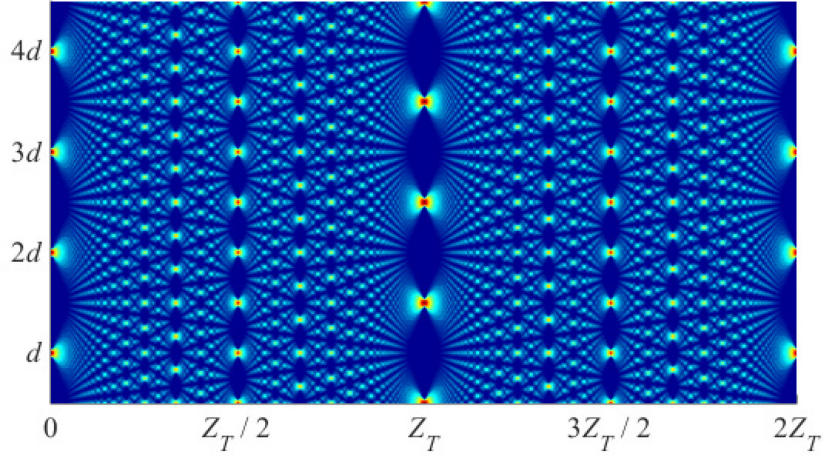


Figure 6–3. Illustration of (a) the multi-code chirp waveform and (b) the orthogonal chirp-division multiplexing in the temporal-frequency-chirp dimension.

$$\hat{s}(\tau) = \mathcal{F}_a \{s(t)\}(\tau) = \frac{e^{-j\frac{\pi}{4}}}{\sqrt{a}} \int s(t) e^{j\frac{\pi}{a}(\tau-t)^2} dt, \quad (6.1)$$

where  $\mathcal{F}_a \{\cdot\}(\cdot)$  denotes the Fresnel transform, and  $a = \lambda z$  is the normalized Talbot distance,  $s(t)$  is the complex transmittance of the grating. In Eq. (6.1),  $\hat{s}(t)$  is called the Fresnel transform of  $s(t)$ . Equivalently, the Fresnel transform can be expressed in the form of convolution [121] as

$$\hat{s}(\tau) = s(\tau) * \varphi_a(\tau), \quad (6.2)$$

where

$$\varphi_a(t) = e^{-j\frac{\pi}{4}} e^{j\frac{\pi}{a}t^2}. \quad (6.3)$$

Fresnel transform, as well as the Fourier transform and fractional Fourier transform, is the special case of linear canonical transform (LCT) [122-125]. Fresnel diffraction is a fundamental phenomenon in optics and quantum physics [126-128], while it is studied almost exclusively by using Fourier analysis. In 1994, Gori revisited the Fresnel transform in his chapter “Why Fresnel is so little known?” from the perspective of the Fresnel transform itself rather than from the Fourier analysis approach [129]. And the important but almost ‘neglected’

property [Theory (1), 129], the Fresnel transform of a linear convolution is

$$\begin{aligned}\hat{r}(\tau) &= \mathcal{F}_a \{h(t) * s(t)\}(\tau) \\ &= \hat{h}(\tau) * s(\tau) = h(\tau) * \hat{s}(\tau).\end{aligned}\tag{6.4}$$

In Eq. (6.4), it states that the Fresnel transform of a convolution equals either one convolving with the Fresnel transform of the other. This is different from the convolution theorem of the Fourier transform which says that the Fourier transform of a convolution equals the product of the Fourier transforms.

### §6.2.2 Derivation of Discrete Fresnel Transform

The discrete form of the Fresnel transform, discrete Fresnel transform (DFnT) describes the coefficients of the optical field of the Talbot image. It is critically important for the numerical evaluation of Fresnel diffraction, and has useful applications in optical imaging and holographic system.

Various formulations for DFnT were proposed depending on the conditions. For example, in the studies of the Talbot array illuminators, the optical derivations of DFnT was proposed by Szwaykowski, Arrizón, and Castañeda *et al.* in [130-135].

In [130], the Talbot coefficients of infinitely periodic gratings at the fractional Talbot distance  $2Z_T/N$  is derived, where  $Z_T$  is the Talbot length, which is defined as

$$\begin{aligned}\hat{r}(\tau) &= \mathcal{F}_a \{h(t) * s(t)\}(\tau) \\ &= \hat{h}(\tau) * s(\tau) = h(\tau) * \hat{s}(\tau).\end{aligned}\tag{6.5}$$

and  $2Z_T$  is called the primary Talbot length. The closed-form of the coefficients is given in [131]. Depending on  $N \equiv 0, 1, 2$  and  $3 \pmod{4}$ , there are four closed-form expressions for the  $N$  coefficients, refer to Eq. (14)-(17) in [131]. In the cases of  $N \equiv 0$  and  $2 \pmod{4}$ , there exists degeneracy in the coefficients which is caused by the destructive interference of the diffraction. Half of the  $N$  coefficients, as a result, become zeros, as indicated by the cross markers in Figure 6–4.

In [132, 133], the coefficients of the Talbot image are given in matrix form.

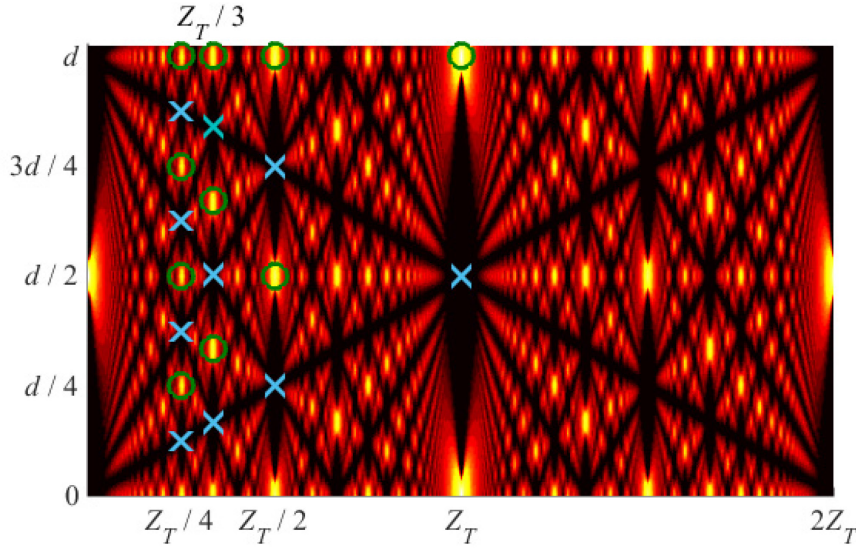


Figure 6–4. Example of the optical field of Talbot image at the fractional Talbot distance; the fields at the crosses ( $\times$ ) are zero due to destructive interference and at the circles ( $\circ$ ) are nonzero.

Accordingly, there are four closed-form DFNT matrices. The DFNT matrices have a size of  $N$  if  $N \equiv 1$  or  $3 \pmod{4}$ , and due to the degeneracy, the size of the matrices reduces to  $N/2$  if  $N \equiv 0$  or  $2 \pmod{4}$ . Mathematically, such degeneracy hinders the applications of DFNT as a linear transformation, because the size of the DFNT matrices is  $N$  if  $N$  is odd, and its size shrinks to  $N/2$ , if  $N$  is even.

There are other formulations for DFNT matrix depending on different assumptions [134-138]. In [134, 135], the DFNT is derived from finite periodic grating. In [136-138] and references therein, algebraic approach to the DFNT, also called chirp Z-transform (CZT) in the signal processing community, is formulated by completing the square of the phase in the DFT. The DFNT matrix in [134-138] has almost the same formulation, see Eq. (17) in [134] and Eq. (12) in [136], and only a single formulation of the DFNT matrix exists without degeneracy. In this thesis, we will name the DFNT in [134-138] as chirp Z-transform.

Although there were various forms of DFNT in the literature, the convolution property of the DFNT has not been discussed yet. In this subsection, we

will derive the DFNT from Talbot image without the degeneracy, and it possesses, as mentioned above, a circular convolution property, which does not always hold for the DFNT in the previous formulations.

### ✚ DERIVATION OF DISCRETE FRESNEL TRANSFORM FROM THE TALBOT EFFECTS

Suppose that the one-dimension grating is repeated infinitely and periodically with a distance  $d$ . Consider the periodic diffraction field within the period from 0 to  $d$  at the fractional of the Talbot distance,  $z = Z_T / N$  with  $Z_T = d^2 / \lambda$ , as shown in Figure 6–4. The one dimensional optical field is

$$\begin{aligned}\hat{s}_T(\eta) &= \frac{1}{\sqrt{\alpha}} e^{-j\frac{\pi}{4}} \int_0^d s(\eta-t) \sum_k e^{j\frac{\pi}{\alpha}(t-kd)^2} dt \\ &= \frac{1}{\sqrt{\frac{d^2}{N}}} e^{-j\frac{\pi}{4}} \int_0^d s(\eta-t) e^{j\frac{\pi}{d^2/N}t^2} \sum_k e^{-j\frac{2\pi}{d/N}kt} e^{j\pi Nk^2} dt.\end{aligned}\quad (6.6)$$

Depending on whether  $N$  is even or odd, the summation in Eq. (6.6) can be further given by

$$\sum_k e^{-j\frac{2\pi}{d/N}kt} e^{j\pi Nk^2} = \begin{cases} \text{III}_{d/N}(t) & N \equiv 0(\text{mod } 2) \\ \text{III}_{d/N}\left(t - \frac{1}{2} \frac{d}{N}\right) & N \equiv 1(\text{mod } 2) \end{cases} \quad (6.7)$$

where  $\text{III}_{d/N}(t)$  is the Dirac comb function, defined as

$$\text{III}_{d/N}(t) = \frac{d}{N} \sum_k \delta\left(t - k \frac{d}{N}\right). \quad (6.8)$$

In Eq. (6.6), the integral interval is within the period from 0 to  $d$ , and thus the summation is count for  $k = 0, 1, \dots, N-1$ . It can be further deduced as

$$\begin{aligned}\hat{s}_T(\eta) &= \frac{1}{\sqrt{N}} e^{-j\frac{\pi}{4}} \\ &\times \begin{cases} \sum_{k=0}^{N-1} s\left(\eta - k \frac{d}{N}\right) e^{j\frac{\pi}{N}k^2} & N \equiv 0(\text{mod } 2) \\ \sum_{k=0}^{N-1} s\left(\eta - \left(k + \frac{1}{2}\right) \frac{d}{N}\right) e^{j\frac{\pi}{N}\left(k + \frac{1}{2}\right)^2} & N \equiv 1(\text{mod } 2) \end{cases}.\end{aligned}\quad (6.9)$$

As a result, the discrete Talbot coefficients at  $\eta = md/N$  if  $N \equiv 0 \pmod{2}$  or  $\eta = (m + 0.5)d/N$  if  $N \equiv 1 \pmod{2}$  are given by

$$\hat{s}_T(m) = \frac{1}{\sqrt{N}} e^{-j\frac{\pi}{4} \sum_{n=0}^{N-1} s\left(n \frac{d}{N}\right)} \times \begin{cases} e^{j\frac{\pi}{N}(m-n)^2} & N \equiv 0 \pmod{2} \\ e^{j\frac{\pi}{N}\left(m-n+\frac{1}{2}\right)^2} & N \equiv 1 \pmod{2} \end{cases} \quad (6.10)$$

From Eq. (6.9) to Eq. (6.10), due to the circulant property of the Talbot effect, we used the substitution  $n = m - k$  to replace the summation index  $k$ . Eq. (6.10) is defined as the discrete Fresnel transform of  $s(n)$ . Accordingly, we formulate the DFNT here by an  $N \times N$  matrix  $\Psi$  as,

$$\Psi(m, n) = \frac{1}{\sqrt{N}} e^{-j\frac{\pi}{4}} \begin{cases} e^{j\frac{\pi}{N}(m-n)^2} & N \equiv 0 \pmod{2} \\ e^{j\frac{\pi}{N}\left(m-n+\frac{1}{2}\right)^2} & N \equiv 1 \pmod{2} \end{cases} \quad (6.11)$$

where  $\Psi(m, n)$  is the  $(m, n)$ -th entry of  $\Psi$ .

The DFNT matrix in Eq. (6.11) also gives the field coefficients of the Talbot image, as indicated by the circular markers in Figure 6–4. As mentioned before, the DFNT in [130-133] is considered at the fraction of the primary Talbot distance  $2Z_T/N$ . There exists degeneracy if  $N$  is even due to the destructive interference, see the cross markers in Figure 6–4. Although the self-images is exactly reproduced at the primary Talbot distance, it is also produced at the Talbot distance  $Z_T$  with only a half period shift  $d/2$ . Hence, the field coefficient at the fraction of Talbot length  $Z_T/N$  could be sufficient to represent the coefficients.

In this subsection, the DFNT gives the close-form coefficients in Eq. (6.11) depending on even or odd  $N$  because the summation in Eq. (6.8) gives two closed-form expressions in Dirac comb for even and odd  $N$ . The degeneracy of the coefficients is avoided, which means that all the coefficients, as indicated at the circles in Figure 6–4, are nontrivial, no matter what  $N$  is. Therefore, the size of the DFNT matrices are always  $N$  no matter what  $N$  is.

### §6.2.3 Properties of the Discrete Fresnel Transform

The DFNT possesses, taking both the even and odd  $N$  in Eq. (6.11), the following properties.

#### UNITARY

That is,  $\Psi^H \Psi = \mathbf{I}$ , where  $\mathbf{I}$  is the  $N$  by  $N$  identity matrix.

#### CIRCULANT

The DFNT matrix is circulant for both even and odd  $N$ . The entries of the DFNT are also periodic, i.e.,  $\Psi(m, n) = \Psi((m + aN)_N, (n + bN)_N) = \Psi(m + aN, n + bN)$ , where  $a, b \in \mathbb{Z}$ , and  $(\cdot)_N$  denotes modulo- $N$ . In addition, if  $N$  is even, the DFNT matrix  $\Psi$  is symmetrical  $\Psi(m, n) = \Psi(n, m)$ , while for odd  $N$ ,  $\Psi$  is not symmetrical, and  $\Psi(m, n) = \Psi(n - 1, m)$ .

The circulant and period properties of the DFNT are crucial for determining the circular convolution property of DFNT. For example, the DFNT defined in [134-138] is not circulant matrix if  $N$  is odd. Thus, we can easily prove that the DFNT in [134-138] does not have the circular convolution property for odd  $N$ .

#### EIGENVALUES AND EIGENVECTORS

The DFNT can be diagonalized (eigen-decomposed) by the DFT matrix. Suppose that the DFT matrix is normalized, the eigenvalues with respect to the  $k$ -th column vector of the DFT matrix are

$$\eta_k = \begin{cases} e^{-j\frac{\pi}{N}k^2} & N \equiv 0 \pmod{2} \\ e^{-j\frac{\pi}{N}k(k+1)} & N \equiv 1 \pmod{2} \end{cases} \quad (6.12)$$

The eigenvalues and eigenvectors can be easily derived using the property that the DFNT in Eq. (6.12) are circulant matrices.

## ✚ DETERMINANT

The determinants of the DFNT matrices are

$$|\Psi| = \prod_{k=0}^{N-1} \eta_k = \begin{cases} e^{-j\frac{\pi}{3}(N-1)\left(N-\frac{1}{2}\right)} & N \equiv 0 \pmod{2} \\ e^{-j\frac{\pi}{3}(N^2-1)} & N \equiv 1 \pmod{2} \end{cases}. \quad (6.13)$$

## ✚ SIMILARITY TRANSFORMATION OF A CIRCULANT MATRIX

The similarity transformation of a circulant matrix  $\mathbf{Z}$  with respect to the DFNT is itself, i.e.,

$$\hat{\mathbf{Z}} = \Psi \mathbf{Z} \Psi^H = \mathbf{Z}, \quad (6.14)$$

where the superscript  $H$  is the Hermitian transpose.

**Proof:**

The first column vector of the circulant matrix  $\mathbf{Z}$  is  $\mathbf{z} = [z(0), z(1), \dots, z(N-1)]^T$ , with the superscript  $T$  denoting matrix transpose. By polynomial decomposition of a circulant matrix,

$$\mathbf{Z} = \sum_{k=0}^{N-1} z(k) \mathbf{L}^k, \quad (6.15)$$

where  $\mathbf{L}$  is an  $N$  by  $N$  down-shift matrix with its first column to be  $[0, 1, 0, \dots, 0]^T$ , Eq. (6.14) can be given by

$$\hat{\mathbf{Z}} = \Psi \mathbf{Z} \Psi^H = \sum_{k=0}^{N-1} z(k) \Psi \mathbf{L}^k \Psi^H. \quad (6.16)$$

First consider that  $N$  is even. If  $k = 0$ , we have  $\Psi \mathbf{L}^0 \Psi^H = \mathbf{L}^0$ . Then, if  $k \neq 0$ , based on the circular property of  $\Psi$ , the  $(m, n)$ -th entry of  $\Psi \mathbf{L}^k \Psi^H$  is

$$\begin{aligned} & \sum_{l=0}^{N-1} \Psi(m, l) \Psi^*((l-k)_N, n) \\ &= \frac{1}{N} \sum_{l=0}^{N-1} e^{j\frac{\pi}{N}(m-l)^2} e^{-j\frac{\pi}{N}(l-k-n)^2} = \delta(m-k-n), \end{aligned} \quad (6.17)$$

where  $\delta(k)$  is the Kronecker delta here. From Eq. (6.17), one can readily deduce

that  $\Psi \mathbf{L}^k \Psi^H = \mathbf{L}^k$ , and Eq. (6.14) becomes

$$\hat{\mathbf{Z}} = \sum_{k=0}^{N-1} z(k) \Psi \mathbf{L}^k \Psi^H = \sum_{k=0}^{N-1} z(k) \mathbf{L}^k = \mathbf{Z}. \quad (6.18)$$

On the other hand, if  $N$  is odd, substituting Eq. (6.11) into (6.17), and similarly one can readily obtain

$$\begin{aligned} & \sum_{l=0}^{N-1} \Psi(m, l) \Psi^*(l - k, n) \\ &= \frac{1}{N} \sum_{l=0}^{N-1} e^{j\frac{\pi}{N}\left(m-l+\frac{1}{2}\right)^2} e^{-j\frac{\pi}{N}\left(l-k-n+\frac{1}{2}\right)^2} = \delta(m - k - n). \end{aligned} \quad (6.19)$$

Consequently, Eq. (6.14) holds for both even and odd  $N$ .

### §6.2.4 The Convolution Theorem of Discrete Fresnel Transform

Here we will investigate the DFNT of a circular convolution. Given two length- $N$  sequences,  $h(n)$  and  $s(n)$ , the DFNT of their circular convolution  $r(n) = h(n) \circledast s(n)$  is

$$\hat{r}(n) = h(n) \circledast \hat{s}(n) = \hat{h}(n) \circledast s(n), \quad (6.20)$$

where  $\circledast$  denotes circular convolution, and  $n = 0, 1, \dots, N-1$ .

**Proof:**

Here we give the circular convolution in matrix form. Define  $\mathbf{H}$  as the  $N$  by  $N$  circulant matrix with its first column to be  $\mathbf{h} = [h(0), h(1), \dots, h(N-1)]^T$ . Similarly,  $\mathbf{S}$  is the circulant matrix with its first column to be  $\mathbf{s} = [s(0), s(1), \dots, s(N-1)]^T$ . The circular convolution in the matrix form is thus

$$\mathbf{r} = \mathbf{H}\mathbf{s} = \mathbf{S}\mathbf{h}. \quad (6.21)$$

Using the property 1 and 5 in Subsection §6.2.3, the DFNT of  $\mathbf{r}$  is

$$\begin{aligned} \hat{\mathbf{r}} &= \Psi \mathbf{r} = \Psi \mathbf{H} \Psi^H \Psi \mathbf{s} = \Psi \mathbf{S} \Psi^H \Psi \mathbf{h} \\ &= \mathbf{H} \Psi \mathbf{s} = \mathbf{H} \hat{\mathbf{s}} \\ &= \mathbf{S} \Psi \mathbf{h} = \mathbf{S} \hat{\mathbf{h}}, \end{aligned} \quad (6.22)$$

for both even and odd  $N$ , where  $\hat{\mathbf{s}} = \Psi \mathbf{s}$  and  $\hat{\mathbf{h}} = \Psi \mathbf{h}$  are the DFNT of  $\mathbf{s}$  and  $\mathbf{h}$ ,

respectively.

It can be observed that the DF<sub>n</sub>T of a circular convolution in Eq. (6.21) is the discrete analogue of the continuous Fresnel transform of a linear convolution in Eq. (6.4). This convolution property is similar to the DFT of a circular convolution and the Fourier transform of a linear convolution. However, in terms of the Fourier transform and DFT, they convert the convolution in one domain to the multiplication in the other domain, and vice versa. On the other hand, both the Fresnel transform and the DF<sub>n</sub>T in this thesis preserve the convolution from one domain to the other domain.

It should be noted that irrespective of whether  $N$  is even or odd, the formulation of DF<sub>n</sub>T in [134-138], refer to [Eq. 17, 134], is the same as the DF<sub>n</sub>T of the even case in Eq. (6.14). Therefore, the DF<sub>n</sub>T in [134-138] has the circular convolution property in Eq. (6.21) if  $N$  is even. However, if  $N$  is odd, the DF<sub>n</sub>T in [134-138] does not possess circulant property and Eq. (6.14), nor the circular convolution property in Eq. (6.21).

### §6.3 Principle of Orthogonal Chirp-Division Multiplexing

As can be induced in Section §6.2, Fresnel transform and the corresponding DF<sub>n</sub>T have quadratic phase, or linear chirp. In this section, according to Fresnel transform, we present the basic principle of OCDM, as a very special case of CSS to achieve the maximum spectral efficiency. The digital implementation of OCDM is based on DF<sub>n</sub>T.

In subsection §6.3.1, we briefly present the CSS and its mathematical model. In subsection §6.3.2, the condition for CSS to achieve OCDM without any interference is derived based on the Fresnel transform, and the digital implementation is present. In subsection §6.3.3, the transmission model of OCDM under LTI channel is presented and analyzed. Based on the analysis and the property of DF<sub>n</sub>T, an efficient single-tap equalization algorithm is proposed based on the properties of DF<sub>n</sub>T. Subsection §6.4 provides the discussions including the relation between the Fourier transform and the Fresnel transform,

DFT and DFnT, the compatibility of the OCDM system to the OFDM system, and, the complexity analysis of the OCDM system.

### §6.3.1 Chirp Spread Spectrum

Most applications of CSS consider the frequency modulated signal, namely chirp, whose frequency evolves linearly or equivalently whose phase quadratically over time,

$$\psi(t) = e^{j(\pi\alpha t^2 + \varphi_0)}, \quad (6.23)$$

where  $\alpha$  is the chirp rate and  $\varphi_0$  is an initial phase. Its instantaneous frequency is

$$f(t) = \frac{1}{2\pi} \frac{d}{dt} [\pi\alpha t^2 + \varphi_0] = \alpha t. \quad (6.24)$$

If the chirp signal is temporally limited within some period  $T$ , the bandwidth of the chirp signal  $B$  is determined by the chirp rate  $\alpha$  and the period  $T$ , i.e.,

$$B \propto (\alpha / T). \quad (6.25)$$

The time-bandwidth product  $\alpha \propto B \times T$  indicates the processing gain of a chirp signal.

In the CSS system, the time-bandwidth product  $BT \gg 1$ , and thus  $B \gg R_s$ , where  $R_s = 1/T$  is the symbol rate. It means that the larger the processing gain is, the less the spectral efficiency becomes. Moreover, in the conventional CSS system, the chirp signal is modulated by analog devices. The advanced modulation formats like QAM cannot be implemented to enhance the spectral efficiency. In the following subsection, we will present the principle of OCDM to maximize the spectral efficiency of the CSS systems.

### §6.3.2 Principle of Orthogonal Chirp-Division Multiplexing

To introduce the Fresnel transform for OCDM, some constraints should be raised. Firstly, the chirp waveforms used for information transmission should

be time-limited. Secondly, we need to adapt the spatial Talbot effect from the optics into the temporal counterpart for OCDM. Based on Eq. (6.5), we define the temporal Talbot distance  $Z_T$  as

$$Z_T = \frac{T^2}{\lambda} \quad (6.26)$$

where  $T$  is the period of a chirp waveform. It can be observed that the temporal parameter  $T$  replaces the periodic distance  $d$  in Eq. (6.5). Supposing that there are  $N$  chirp waveforms, one can obtain the chirp waveform by substituting the fraction of the Talbot distance  $z = Z_T/N$  into Eq. (6.3), and thus  $a = T^2/N$ . The ‘root’ chirp waveform is defined as

$$\begin{aligned} \psi_0(t) &= \Pi_T(t) \varphi_a^*(t) \Big|_{a=\frac{T^2}{N}} \\ &= e^{j\frac{\pi}{4}} e^{-j\pi\frac{N}{T^2}t^2}, \quad 0 \leq t < T \end{aligned} \quad (6.27)$$

where

$$\Pi_T(t) = \begin{cases} 1 & 0 \leq t < T \\ 0 & \text{otherwise} \end{cases}, \quad (6.28)$$

is the rectangular function.

It can be deduced from Eq. (6.27) that the *chirp rate*  $\alpha$  is equivalent to the reciprocal of the *temporal Talbot period*  $a$ ,

$$\alpha = \frac{1}{a} = \frac{N}{T^2}. \quad (6.29)$$

One can get a set of  $N$  chirp waveforms by using the root chirp in Eq. (6.27), and the  $k$ -th,  $k = 0, 1, \dots, N-1$ , chirp waveform is

$$\begin{aligned} \psi_k(t) &= \Pi_T(t) \varphi_{T^2/N}^* \left( t - k \frac{T}{N} \right) \\ &= e^{j\frac{\pi}{4}} e^{-j\pi\frac{N}{T^2} \left( t - k \frac{T}{N} \right)^2}, \quad 0 \leq t < T. \end{aligned} \quad (6.30)$$

It can be readily proved that the chirp waveforms  $\psi_k(t)$  in Eq. (6.30) are mutually orthogonal,

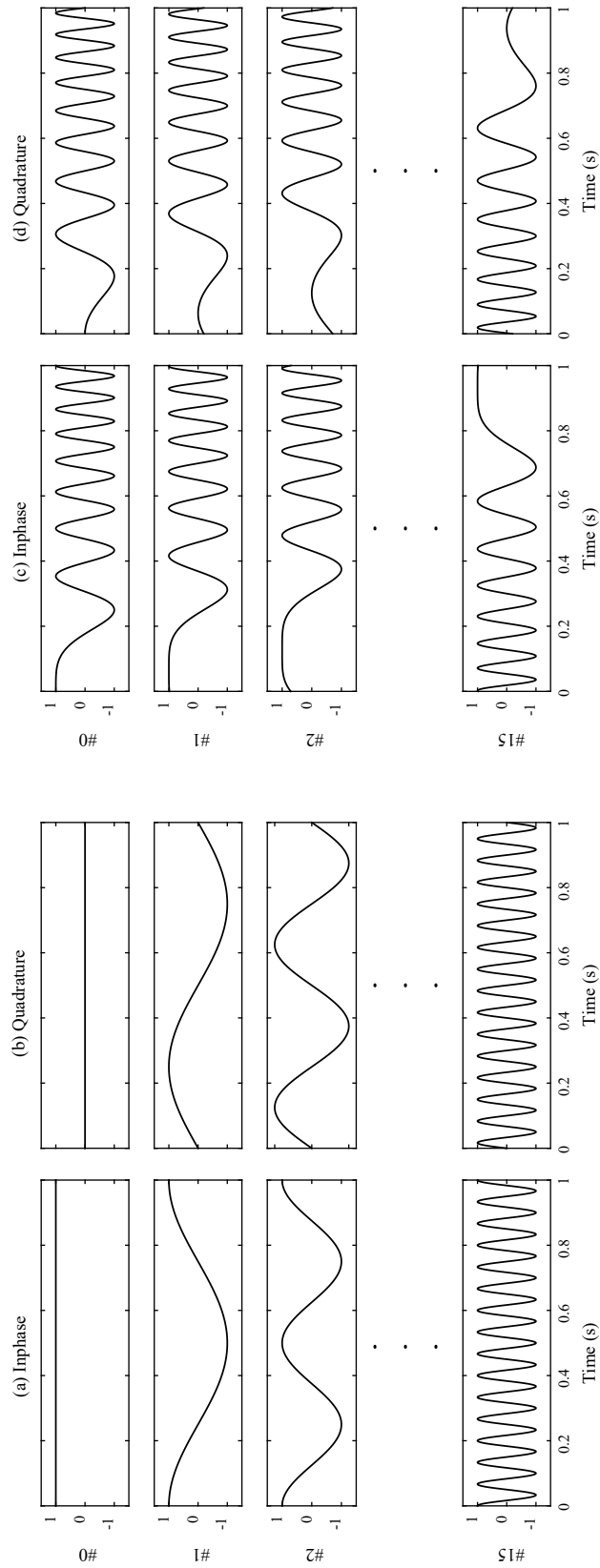


Figure 6–5. Illustration of the families of 16 orthogonal waveforms in OFDM and OCDM. (a) The inphase and (b) the quadrature components of the orthogonal linear exponential waveforms in OFDM, and (c) the inphase and (d) the quadrature components of the orthogonal chirp waveforms in OCDM.

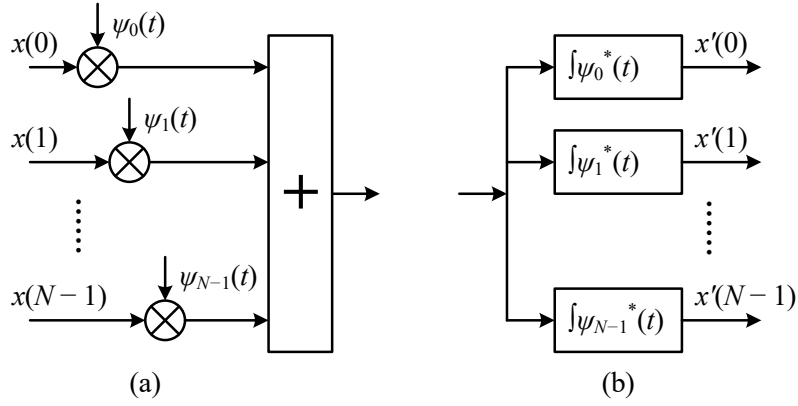


Figure 6–6. Schematic diagram of the OCDM transceiver (a) multiplexing and (b) demultiplexing a bank of  $N$  modulated orthogonal chirp waveforms.

$$\begin{aligned}
 & \int \psi_m^*(t) \psi_n(t) dt \\
 &= \int_0^T e^{j\pi \frac{N}{T^2} \left(t - \frac{mT}{N}\right)^2} e^{-j\pi \frac{N}{T^2} \left(t - \frac{nT}{N}\right)^2} dt = \delta(m-n).
 \end{aligned} \tag{6.31}$$

Eq. (6.30) formulates a set of  $N$  orthogonal chirp waveforms in a given bandwidth and period. Thus, the spectral efficiency of the OCDM increases by  $N$  over the CSS system. To give an illustrative comparison between the OFDM and the OCDM, Figure 6–5 illustrates the linear exponential waveforms in OFDM that are mutually orthogonal in frequency [139-142], and the quadratic exponential waveforms in OCDM that are mutually orthogonal in the dimension of chirp.

### §6.3.2.1 Analog Implementation of OCDM System

In the OCDM system, the amplitude and phase of each chirp can be used for modulation. Thus, pulse amplitude modulation (PAM), PSK, and QAM can be employed. Depending on the modulation formats, symbols are chosen from a codebook  $\chi$  to encode the information bits. Similar to the OFDM symbol that consists of a bank of subcarriers transmitted block by block, the modulated chirps are transmitted in block as well. In an OCDM block, the  $k$ -th symbol modulating the  $k$ -th chirp is  $x(k) \in \chi$ . A bank of synthesized and modulated

chirp signal, see Figure 6–6 (a), is thus

$$s(t) = \sum_{k=0}^{N-1} x(k) \psi_k(t) \quad 0 \leq t < T. \quad (6.32)$$

According to Eq. (6.31),  $x(m)$  can be extracted by the matched filter to the  $m$ -th chirp as shown in Figure 6–6 (b), as

$$\begin{aligned} x'(m) &= \int_0^T s(t) \psi_m^*(t) dt \\ &= \sum_{k=0}^{N-1} x(k) \delta(m-k) = x(m). \end{aligned} \quad (6.33)$$

### §6.3.2.2 Digital Implementation of OCDM System

The OCDM system can be implemented digitally, as shown in Figure 6–7. The discrete time-domain OCDM signal is obtained by sampling the continuous time-domain signal in Eq. (6.32). Since there are two forms of DFNT matrix in Eq. (6.13) depending on  $N$  being even or odd, the discrete OCDM signal is, if  $N$  is even,

$$\begin{aligned} s(n) &= s(t) \Big|_{t=n\frac{T}{N}} = \sum_{k=0}^{N-1} x(k) \psi_k \left( n \frac{T}{N} \right) \\ &= e^{j\frac{\pi}{4} \sum_{k=0}^{N-1} x(k)} e^{-j\frac{\pi}{N} (n-k)^2}, \end{aligned} \quad (6.34)$$

and, if  $N$  is odd,

$$\begin{aligned} s(n) &= s(t) \Big|_{t=\left(n+\frac{1}{2}\right)\frac{T}{N}} = \sum_{k=0}^{N-1} x(k) \psi_k \left( \left(n+\frac{1}{2}\right) \frac{T}{N} \right) \\ &= e^{j\frac{\pi}{4} \sum_{k=0}^{N-1} x(k)} e^{-j\frac{\pi}{N} \left(n-k+\frac{1}{2}\right)^2}. \end{aligned} \quad (6.35)$$

Inspecting Eq. (6.34) and (6.35), one can compare them with the definition of DFNT in Eq. (6.11), and find that they are exactly the IDFNT. Thus, the synthesis of a bank of discretized modulated chirp waveforms can be realized by the IDFNT. To express Eq. (6.34) and (6.35) in a concise matrix form, we stack the symbols in the vector form as  $\mathbf{x} = [x(0), x(1), \dots, x(N-1)]^T$ , and thus the discrete time-domain OCDM signal is

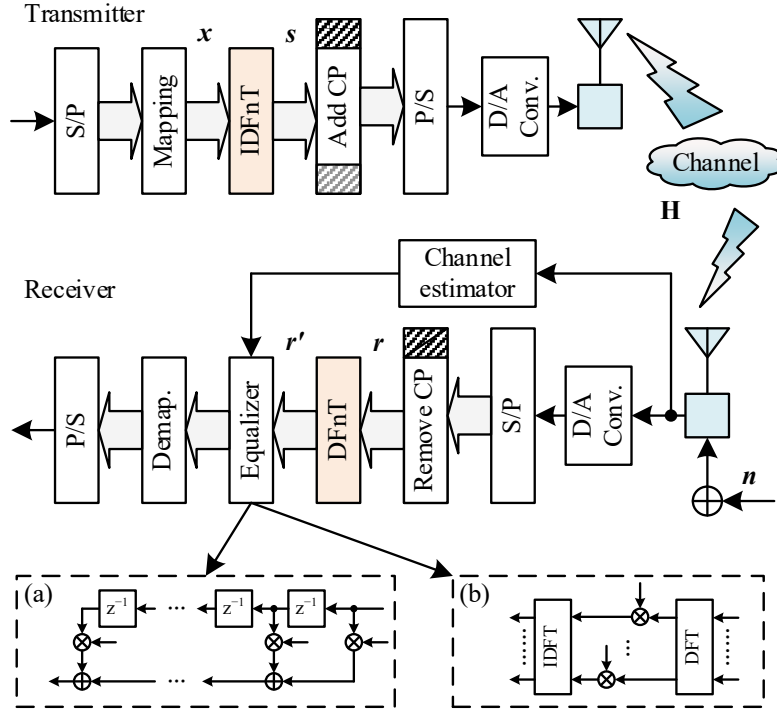


Figure 6–7. Schematic diagram of the proposed digital implementation of OCDM. Insets: Illustrations of (a) time-domain and (b) frequency domain equalizer.

$$\mathbf{s} = \Phi^H \mathbf{x}. \quad (6.36)$$

Since the DFNT matrix is unitary, at the receiver the transmitted information symbols can be recovered by performing the inverse operation, i.e., DFNT. The recovered symbols are thus

$$\mathbf{x}' = \Phi \mathbf{s} = \mathbf{x}. \quad (6.37)$$

### §6.3.3 System Model of OCDM under LTI Channel

In this section, we will formulate the mathematical model of the OCDM signal under the LTI channel with additive white Gaussian noise (AWGN) in the matrix form. The channel is static or quasi-static, which means that the channel response remains constant within one OCDM block, and might change in the next block. It is assumed that the channel information is available at the receiver via some channel estimation method with perfect timing and frequency

synchronization. To avoid inter-symbol interference (ISI), guard interval is inserted between adjacent blocks, just as the OFDM system does. Based on the analysis, we will show that the guard interval can be filled with either zeros, i.e., zero-padded prefix (ZP), or the replica of a portion of the end of the signal, i.e., cyclic prefix (CP).

### §6.3.3.1 OCDM System under LTI Channel with AWGN

In Figure 6–7, the signal transmission is illustrated. Suppose that the maximum channel delay is smaller than the length of guard interval. If the CP is used for guard interval, the signal experienced the channel  $\mathbf{H}$  with AWGN is

$$\mathbf{r} = \mathbf{H}\mathbf{s} + \mathbf{n} = \mathbf{H}\Phi^H \mathbf{x} + \mathbf{n} \quad (6.38)$$

where  $\mathbf{H}$  is the channel impulse response (CIR) matrix and  $\mathbf{n}$  is the AWGN vector. The CIR matrix  $\mathbf{H}$  is circulant, and its first column is  $\mathbf{h} = [h(0), h(1), \dots, h(L-1), 0, \dots, 0]^T$ , where  $h(l)$ ,  $l = 0, \dots, L-1$ , are the CIR taps and  $L$  is the maximum delay spread.

On the other hand, if ZP is used, one can also arrive at Eq. (6.38) by overlap-and-add operation, [Chapter 12, 143]. Therefore, Eq. (6.38) can be a general model for the OCDM signal transmitting under LTI channels based on both CP and ZP.

Before we recover the symbols, we could first compensate the channel  $\mathbf{H}$  in Eq. (6.38), and then perform DFNT to recover the transmitted symbols in  $\mathbf{x}$ . Alternatively, we first perform DFNT on the received signal as

$$\mathbf{r}' = \Phi \mathbf{r} = \Phi \mathbf{H} \mathbf{s} + \Phi \mathbf{n}. \quad (6.39)$$

Based on the convolution property of DFNT in Eq. (6.20), Eq. (6.39) is further described by

$$\begin{aligned} \mathbf{r}' &= \Phi \mathbf{H} \Phi^H \mathbf{x} + \Phi \mathbf{n} \\ &= \mathbf{H} \mathbf{x} + \Phi \mathbf{n}. \end{aligned} \quad (6.40)$$

Therefore, the chirp waveforms  $\Phi^H$  vanish and are transparent to the channel  $\mathbf{H}$  as if symbols are transmitted directly without modulating the chirps after the DFNT at the receiver. In addition, since  $\Phi$  is unitary, the noise  $\Phi \mathbf{n}$  is still

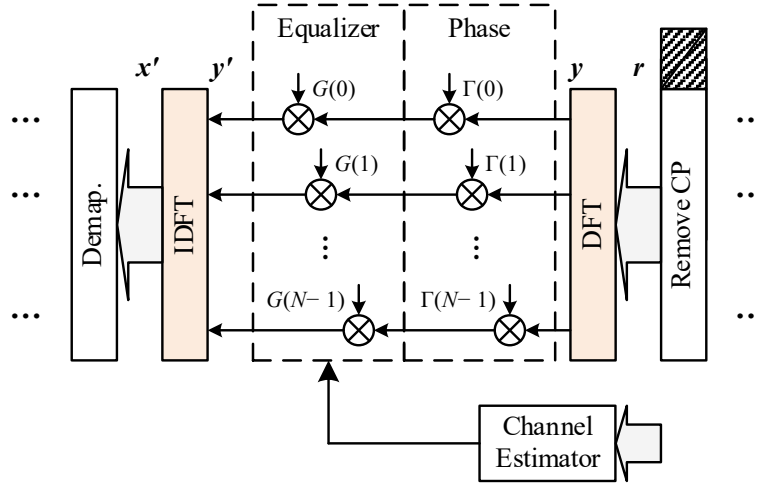


Figure 6–8. Proposed single-tap FDE for the OCDM system.

AWGN.

From Eq. (6.40), the CIR  $\mathbf{H}$  can be compensated by using the multi-tap time-domain equalization (TDE) in Figure 6–7 (a) or by using the more efficient single-tap FDE in Figure 6–7 (b) to recover the symbols  $\mathbf{x}$ . More sophisticated nonlinear equalizers or decoding algorithms, e.g., decision feedback equalizer (DFE) and maximal likelihood (ML) detection, are more powerful for the improvement of performance [82, 144]. However, they complicate the computational and hardware complexity, and we only consider the linear equalizers in this section.

### §6.3.3.2 Proposed Single-Tap Equalization Algorithm for OCDM System

In this subsection, we propose an efficient algorithm based on the FDE for compensating the channel dispersion imposed on the OCDM signal. The diagram of the proposed algorithm is illustrated in Figure 6–8. In the proposed scheme, single-tap equalization is employed, and the IDFnT at the receiver is avoided based on its eigen-decomposition property.

At the receiver, the sampled signal is given in Eq. (6.38). Instead of DFnT in Eq. (6.39), it is firstly transformed into the frequency domain by DFT as

$$\mathbf{y} = \mathbf{F}\mathbf{r} = \mathbf{F}\mathbf{H}\mathbf{\Phi}^H \mathbf{x} + \mathbf{F}\mathbf{n}, \quad (6.41)$$

where  $\mathbf{F}$  is the normalized DFT matrix. Using the identity  $\mathbf{I} = \mathbf{F}^H \mathbf{F}$ , Eq. (6.41) can be further given by

$$\begin{aligned} \mathbf{y} &= \mathbf{F} \mathbf{H} \mathbf{F}^H \mathbf{F} \mathbf{\Phi}^H \mathbf{F}^H \mathbf{F} \mathbf{x} + \mathbf{w} \\ &= \mathbf{\Lambda} \mathbf{\Gamma}^H \mathbf{F} \mathbf{x} + \mathbf{w}, \end{aligned} \quad (6.42)$$

where  $\mathbf{\Lambda} = \mathbf{F} \mathbf{H} \mathbf{F}^H$  is the channel frequency response (CFR) matrix and  $\mathbf{\Gamma}^H = \mathbf{F} \mathbf{\Phi}^H \mathbf{F}^H$  is a coefficient matrix.

According to the eigen-decomposition property of a circulant matrix with respect to DFT, the CFR matrix  $\mathbf{\Lambda}$  is diagonal. The  $k$ -th diagonal entry of  $\mathbf{\Lambda}$  is the CFR at the  $k$ -th frequency bin, or equivalently is the  $k$ -th eigenvalue to the  $k$ -th column vector of  $\mathbf{F}^H$ .

Recalling Eq. (6.11), the DFNT matrix is also circulant. Thus, the matrix  $\mathbf{\Gamma}$  is also a diagonal matrix whose diagonal entries are the eigenvalues of  $\mathbf{\Phi}$  with respect to  $\mathbf{F}^H$ . The eigenvalue of  $\mathbf{\Phi}$  is given in [145], as

$$\Gamma(k) = \begin{cases} e^{-j\frac{\pi}{N}k^2} & N \equiv 0(\text{mod } 2) \\ e^{-j\frac{\pi}{N}k(k-1)} & N \equiv 1(\text{mod } 2) \end{cases}. \quad (6.43)$$

Based on the commutative law of the product of two diagonal matrices, Eq. (6.42) can be further given by

$$\mathbf{y} = \mathbf{\Gamma}^H \mathbf{\Lambda} \mathbf{F} \mathbf{x} + \mathbf{w}. \quad (6.44)$$

Before compensating the CFR  $\mathbf{\Lambda}$ , we first cancel out the phase induced by  $\mathbf{\Gamma}$ . The equalized signal is given by

$$\mathbf{y}' = \mathbf{G} \mathbf{\Gamma} \mathbf{y} = \mathbf{G} \mathbf{\Lambda} \mathbf{F} \mathbf{x} + \mathbf{G} \mathbf{\Gamma} \mathbf{w}, \quad (6.45)$$

where  $\mathbf{G}$  is a diagonal matrix with its  $k$ -th diagonal entry  $G(k)$  to be the coefficients of the single-tap equalizer. For example, if zero-forcing (ZF) criterion is adopted,  $G(k)$  is

$$G_{ZF}(k) = \Lambda^{-1}(k), \quad (6.46)$$

and if minimum mean square error (MMSE) is adopted,  $G(k)$  is

$$G_{MMSE}(k) = \frac{\Lambda^*(k)}{|\Lambda(k)|^2 + \rho^{-1}}, \quad (6.47)$$

where  $\rho$  is the signal-to-noise ratio (SNR). Finally, the signal is transformed by IDFT to recover the transmitted information. If the ZF equalizer is employed, the recovered signal is

$$\mathbf{x}'_{\text{ZF}} = \mathbf{x} + \mathbf{F}^H \mathbf{\Lambda}^{-1} \mathbf{\Gamma} \mathbf{w}, \quad (6.48)$$

and on the other hand if MMSE is used, the signal is

$$\begin{aligned} \mathbf{x}'_{\text{MMSE}} = & \left( \mathbf{F}^H \frac{\mathbf{\Lambda}^H \mathbf{\Lambda}}{\mathbf{\Lambda}^H \mathbf{\Lambda} + \rho^{-1} \mathbf{I}} \mathbf{F} \right) \mathbf{x} \\ & + \mathbf{F}^H \frac{\mathbf{\Lambda}^H}{\mathbf{\Lambda}^H \mathbf{\Lambda} + \rho^{-1} \mathbf{I}} \mathbf{\Gamma} \mathbf{w}. \end{aligned} \quad (6.49)$$

It should be noted that although the ZF equalizer is able to completely remove the channel distortion, it is notorious for noise enhancement. In practice, the MMSE equalizer can efficiently balance the noise enhancement and channel compensation.

## §6.4 Discussions

From previous sections, we can see that Fresnel transform mathematically formulates the OCDM, just as the Fourier transform in OFDM. Inspecting Eq. (6.1) and (6.10), the Fresnel transform and DFNT are trigonometric transforms with quadratic phases. Both the Fresnel transform and Fourier transform are LCT, and they are intimate to each other [122-125].

In this section, we will study the algebraic properties of the Fresnel transform and the Fourier transform. According to the properties, the implementation differences and compatibility of the OCDM and the OFDM are discussed. It is shown that the DFNT can be realized by the DFT using fast Fourier transform algorithms, and thus the OCDM system can be realized by the existing OFDM system without complicating the complexity.

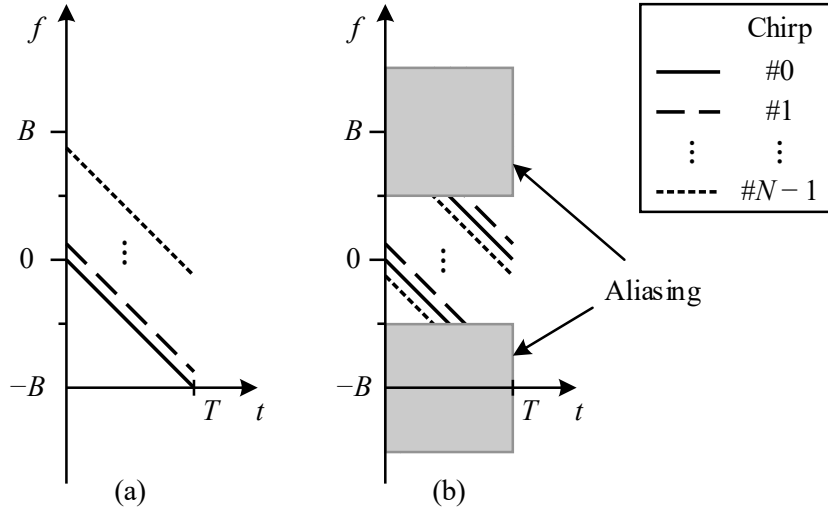


Figure 6–9. Illustrations of the spectra of (a) analog and (b) digital implementations for OCDM. The lines denote the instantaneous frequency of each chirp.

### §6.4.1 Spectra of the Analog and Digital OCDM Signals

There are differences between the continuous- and discrete- time OCDM signals. Firstly, although the sampled chirp in Eqs. (6.34) or (6.35) is from  $\psi_k(t)$  in Eq. (6.30) by uniform sampling, the interpolated continuous-time chirp from Eq. (6.34) or (6.35) is the periodic extension of  $\psi_k(t)$ . Specifically, we have the root chirp

$$\psi'_0(t) = \begin{cases} \phi_{T^2/N}^*(t) & t \in \left(-\frac{T}{2}, \frac{T}{2}\right] \\ \phi_{T^2/N}^*(t - cT) & t \in \left(-\frac{T}{2} + cT, \frac{T}{2} + cT\right] \end{cases} \quad (6.50)$$

as the periodic extension of  $\psi_0(t)$  in Eq. (6.27). The interpolated chirped waveform becomes

$$\psi'_k(t) = \Pi_T(t) \psi'_0\left(t - k \frac{T}{N}\right), \quad (6.51)$$

Moreover, using the periodic property, we can easily prove that the following relation in Eq. (6.34) holds

$$s(n) = \sum_{k=0}^{N-1} x(k) \psi_k \left( n \frac{T}{N} \right) = \sum_{k=0}^{N-1} x(k) \psi'_k \left( n \frac{T}{N} \right), \quad (6.52)$$

for even  $N$ , or with a sampling offset  $2T/N$  for odd  $N$ .

Secondly, the spectrum of the discrete-time OCDM signal is the periodic extension of the continuous-time one. To illustrate the difference, Figure 6–9 provides the spectrograms of the (a) continuous-time and the (b) discrete-time OCDM signals. It can be observed that in Figure 6–9 (a), although each chip signal  $\psi_k(t)$  has a bandwidth of  $B$ , the continuous-time OCDM signal in Eq. (6.32) occupies a bandwidth from  $-B$  to  $B$ . It seems that one cannot meet the Nyquist rate, unless a sampling rate no less than  $2N/T$  is chosen to generate the OCDM signal in Eq. (6.32).

Fortunately, as shown in Figure 6–9 (a), each chirp signal  $\psi_k(t)$  still has a spectral bandwidth of  $B$ . In principle, the spectrum of a discrete-time signal produces its continuous-time counterpart with cyclically extended spectrum. In the OCDM system, if the sampling rate is exactly at  $B = N/T$  Hz, referring to Eq. (6.34), the spectrum of the discrete-time OCDM signal has a period of  $B$ , as shown in Figure 6–9 (b). All the spectra of  $\psi_k(t)$  are folded into the base-band from  $-B/2$  and  $B/2$ . As a result, the discrete-time OCDM signal generates the OCDM signal of folded spectrum, completely preserving the information.

### §6.4.2 Relation between the Fourier Transform and the Fresnel Transform

In the continuous case, the kernel of the most ‘well-known’ Fourier transform is

$$\omega(f, t) = e^{-j2\pi ft}, \quad (6.53)$$

and the expanded kernel of Fresnel transform in Eq. (6.1) is

$$\varphi_a(f, t) = e^{-j\frac{\pi}{4}} e^{j\frac{\pi}{a}(f^2 - 2ft + t^2)}. \quad (6.54)$$

In the discrete case, they are

$$W(m, n) = \frac{1}{\sqrt{N}} e^{j \frac{2\pi}{N} mn}, \quad (6.55)$$

and

$$\Phi(m, n) = \frac{1}{\sqrt{N}} e^{-j \frac{\pi}{4}} \times \begin{cases} e^{j \frac{\pi}{N} (m^2 - 2mn + n^2)} & N \equiv 0 \pmod{2} \\ e^{j \frac{\pi}{4N}} e^{j \frac{\pi}{N} (m^2 + m - 2mn + n^2 - n)} & N \equiv 1 \pmod{2} \end{cases}, \quad (6.56)$$

respectively. The Fresnel transform in Eq. (6.54) or DFNT in Eq. (6.56) consists of the Fourier transform or DFT with additional quadratic phases. In the discrete form, the additional quadratic phases are

$$\Theta_1(m) = e^{-j \frac{\pi}{4}} \times \begin{cases} e^{j \frac{\pi}{N} m^2} & N \equiv 0 \pmod{2} \\ e^{j \frac{\pi}{4N}} e^{j \frac{\pi}{N} (m^2 + m)} & N \equiv 1 \pmod{2} \end{cases}, \quad (6.57)$$

and

$$\Theta_2(n) = \begin{cases} e^{j \frac{\pi}{N} n^2} & N \equiv 0 \pmod{2} \\ e^{j \frac{\pi}{N} (n^2 - n)} & N \equiv 1 \pmod{2} \end{cases}, \quad (6.58)$$

Consequently, the DFNT can be implemented by FFT in three steps:

- 1) multiplying the chirp phase  $\Theta_1$ ,
- 2) performing the DFT by FFT algorithm, and finally
- 3) multiplying the other chirp phase  $\Theta_2$ ,

where  $\Theta_1$  and  $\Theta_2$  are diagonal matrices whose  $m$ -th diagonal entries are  $\Theta_1(m)$  and  $\Theta_2(m)$ , respectively.

### §6.4.3 Compatibility to the OFDM Systems

In the previous subsection, Fresnel transform mathematically formulates the OCDM, just as the Fourier transform in OFDM. Inspecting Eq. (6.1) and (6.11), the Fresnel transform and DFNT are trigonometric transforms of quadratic phases. Both the Fresnel and Fourier transforms are linear canonical transform

[122-125]. The DFnT can be divided into three-step process by using DFT. One would expect that the OCDM can be integrated into the existing OFDM system easily without significant modification.

Figure 6–10 provides the block diagram of the conventional OFDM system (excluding the components in the dashed-line boxes). At the transmitter, the IDFT multiplexes symbols onto parallel subcarriers, and at the receiver DFT performs inverse operation to recover the symbols. After the DFT at the receiver side, single-tap equalizer compensates each subcarriers.

According to the relation between the DFT and the DFnT in Eq. (6.53)-(6.58), the OCDM can be integrated into the OFDM system with the additional operations in the dashed-line boxes. At the transmitter, the three-step operation involving IDFT acts as the IDFnT. At the receiver end, there are two architectures. One is based on the receiver in Figure 6–7, and the other is based on the proposed equalization algorithm in Section IV, refer to Figure 6–8. In receiver #1, it should be noted that, as discussed in Section III-C, the equalizer could be either multi-tap TDE in Figure 6–7 (a) or FDE in Figure 6–7 (b). If FDE is adopted, in addition to single-tap equalizer, there is a DFT and an IDFT operation. The receiver #2 is the same as that in Figure 6–8, which is the conventional FDE structure in the OFDM and SC-FDE systems. It means that the channel estimation and equalization etc., schemes designed for OFDM can be easily adapted into the OCDM system.

In terms of the signal structure, both the OFDM and OCDM systems transmit the modulated waveforms in blocks. Between the blocks, GI is used to avoid ISI. As shown in Subsection §6.3.3, in the OCDM system both CP and ZP can be used for filling the GI. The structure of OCDM signal is the same as that of OFDM signal. As a result, the OCDM signal is also compatible to the OFDM signal. The design of OCDM system can be well integrated into the OFDM system. As a result, the generation and recovery of OCDM signal can be realized using the existing OFDM system with additional operations involving only phase rotation and one more IDFT at the receiver.

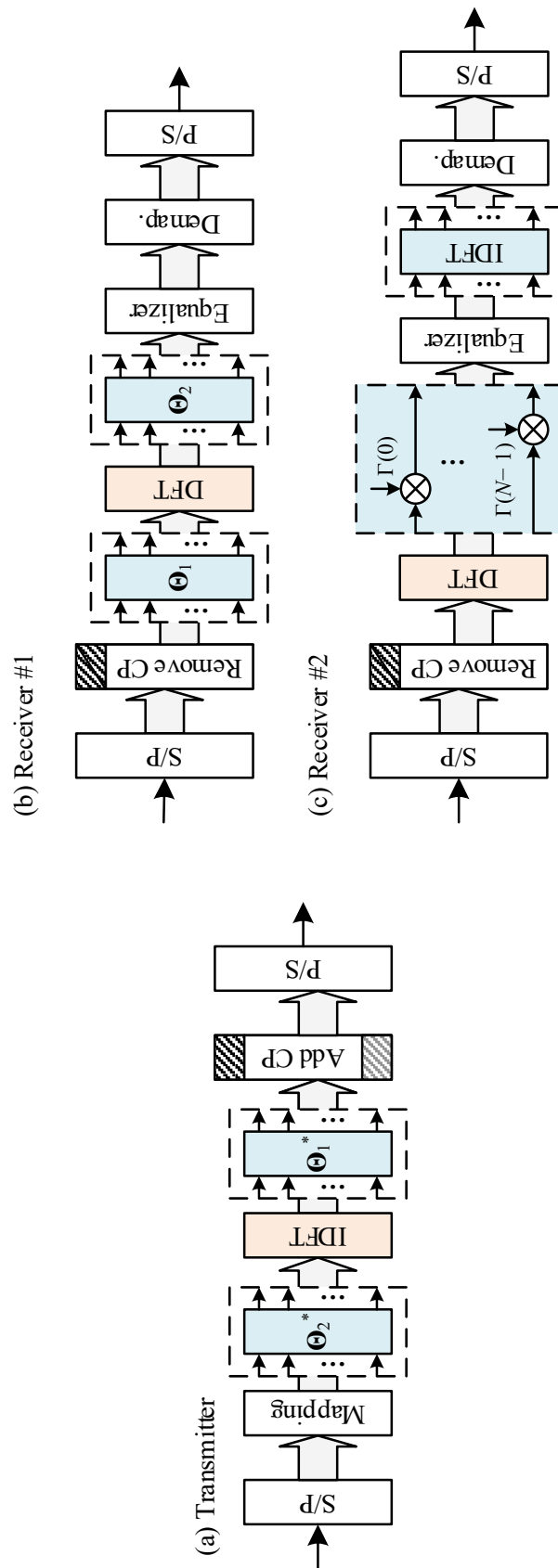


Figure 6–10. Schematic diagram of OFDM system (excluding the dash components) and the diagram of OCSDM system based on the OFDM system (including the dash components).

However, there is difference between the spectra of OFDM and OCDM systems. In the OFDM system, the aliasing signal can be separated by setting subcarriers at the edge of the spectrum to be nulls, and filters are then applied to reject the aliasing signal. In the OCDM system, as discussed in Subsection §6.4.1, the spectrum of the OCDM signal is directly generated by DF<sub>n</sub>T, ranging from  $-B/2$  to  $B/2$ . Thus, before filtering the aliasing signal, up-sampling is applied by a pulse-shaping filter to fit the OCDM spectrum into the OFDM spectrum.

#### §6.4.4 Implementation Complexity of OCDM System

In Figure 6–10, the similarities and differences between the OFDM and OCDM systems are illustrated. In the OCDM system, there are two receiver schemes. For both schemes, the transmitter is the same, and thus the complexity of OCDM system depends on which receiver scheme is adopted.

In this subsection, we compare the arithmetic complexity of the OCDM system to the OFDM system in terms of complex multiplication operations. In addition, the DFT-P-OFDM that is used in the 3GPP LTE standard and SC-FDE is also discussed. It should be noted that there are other compulsory modules in a communication system, such as synchronizations and channel estimation. Additional consideration is required because their complexities vary depending on the algorithms adopted. In this paper, we will not provide these details for brevity.

At the transmitter, there are two additional phase rotations, which require 2 additional complex multiplications per symbol compared to the transmitter of the OFDM system.

If the receiver #1 is adopted, there are also two phase rotation operations. In Figure 6–7, either (a) TDE or (b) FDE can be adopted. The complexity of TDE depends on the number of taps of the transverse filter. If the number of taps is  $L$ , which is larger than the CIR taps, the complexity of the TDE is  $L$  per symbol. On the other hand, in the FDE, besides the single-tap equalizer, it needs two more DFT operations, see Figure 6–7 (b). Therefore, the FDE

TABLE 6-1  
ADDITIONAL ARITHMETIC COMPLEXITY OF THE OCDM SYSTEM COM-  
PARED TO THE OFDM SYSTEM

	Transmitter	Receiver	
SC-FDE	$M - \frac{1}{2} \log_2 N$	$\frac{1}{2} \log_2 N$	
DFT Precoded OFDM	$\frac{1}{2} \log_2 N$	$\frac{1}{2} \log_2 N$	
OCDM	2	Rx #1	TDE $L + 2$
			FDE $\log_2 N + 2$
		Rx #2	$\frac{1}{2} \log_2 N$

scheme requires additional  $\log_2 N$  complex multiplications per symbol. In the applications such as mobile communication whose channel delay spread is relatively large, FDE is more preferable than TDE in terms of computation complexity.

In the receiver scheme #2, besides the phase cancellation and the single-tap equalizer, an additional IDFT is required. Thus, compared to OFDM, the additional complexity is  $0.5 \log N$ .

The additional arithmetical complexity of the OCDM system compared to the OFDM system is provided in Table 6-1. It can be seen that, if the receiver #2 is adopted, the complexity of the OCDM system is slightly increased compared to that of the OFDM with  $(2 + 0.5 \log_2 N)$  multiplications per symbol.

In Table 6-1, the additional complexity of the DFT-P-OFDM compared to the conventional OFDM is provided. The scheme requires a length- $N$  DFT precoder at the transmitter and another length- $N$  IDFT reversing the operation at the receiver. The total additional complexity to that of the OFDM is  $\log_2 N$ .

In SC-FDE system, instead of DFT operation, pulse-shaping filter is used at

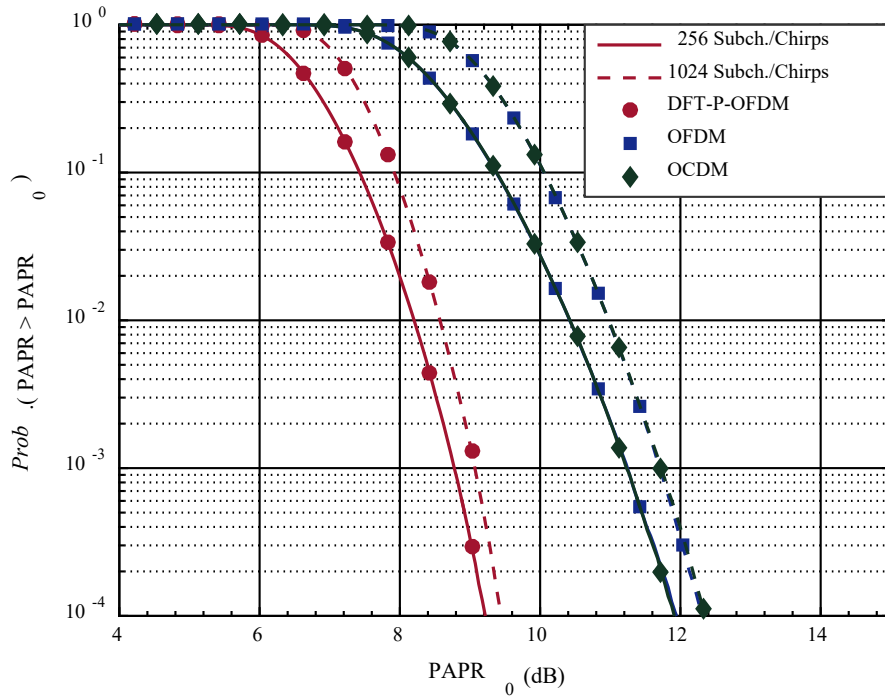


Figure 6–11. The PAPR characteristics of the OFDM, DFT-P-OFDM, and OCDM signals with 256 and 1024 subcarriers/chirps modulated in 16-QAM.

the transmitter. Though the pulse-shaping filter can be implemented by FFT, we assume that the time-domain convolution operation is adopted with an oversampling ratio of 1. If so, the complexity is  $M$  per symbol, where  $M$  is the length of the pulse shaping filter. The filter length  $M$  is usually large enough to control the spectral shape, and it is typically in the order of several tens in practical implementation.

#### §6.4.5 Peak-to-Average Power Ratio of OCDM Signals

In this subsection, simulations are carried out to investigate the PAPR characteristics of the proposed OCDM system. For comparison, we also consider the conventional OFDM, as well as the DFT-P-OFDM for its low PAPR.

In the OCDM system, the number of chirps are 256 and 1024 and the chirps are modulated in 16-QAM. Similarly, there are 256 and 1024 subcarriers in the

conventional OFDM and DFT- OFDM systems. For all three systems, the base-band signal is up-sampled by a factor of 4 to emulate their actual PAPR. The PAPR is evaluated by complementary cumulative distribution function (CCDF), which is defined as the probability of the PAPR of a signal exceeding a threshold  $\text{PAPR}_0$ .

In Figure 6–11, the CCDF of the PAPR in the three systems are provided. It is shown that the DFT-P-OFDM has the best PAPR performance. For example, the probability of PAPR exceeding 8.5 dB is less than  $10^{-2}$ . The OFDM and OCDM systems have the same PAPR performance. The  $\text{PAPR}_0$  for the probabilities of  $10^{-2}$  increases to 11 dB. Higher PAPR may impose more stringent requirements on the device linearity. Note that various PAPR reduction methods in the literature and can be readily applied to the OCDM systems.

## §6.5 Numerical Simulation

In this section, numerical simulations are provided to investigate the proposed OCDM system in both wireless communication systems in §6.5.1 and fiber-optic communication systems in §6.5.2.

### §6.5.1 Wireless Communication Systems

To study the performance of the proposed OCDM system, simulations are performed in wireless channels. The bandwidth is 10 MHz and 1024 chirps are modulated in  $M$ -ary QAM with  $M$  from 4 to 16, and 64. The guard interval is filled with CP, whose length, unless otherwise stated, is chosen larger than the maximum excess delay of the channel to avoid ISI.

For comparison, both the conventional OFDM and the DFT-P-OFDM are also simulated. Their bandwidth is also 10-MHz which is divided into 1024 subcarriers modulated in QAM. CP is also used to fill the guard interval. In the OFDM system, only ZF equalizer is employed in the OFDM system for simplicity, as both the ZF and MMSE equalizers achieve the same bit-error rate (BER) performance in the OFDM system.

The multipath Rayleigh fading channel with 10 rays of equal gain is considered. The maximum excess delay of the channel is 5.4  $\mu\text{s}$ . It is assumed that the channel is quasi-static, i.e. the channel remains static in one OCDM/OFDM block and may vary for the next. Thermal noise, modeled as AWGN, is added at the receiver. The BER is evaluated by signal-to-noise ratio (SNR) which is given in  $E_b / N_0$ , the ratio of bit energy  $E_b$  to the noise power density  $N_0$ . In addition for the receiver with MMSE equalizer, we assume that the receiver has the knowledge of received SNR.

In the simulation for wireless multipath fading channel, we will study these three systems with linear equalizers and also the nonlinear equalizer based on iterative-block decision feedback equalization (IB-DFE) to show the performance differences under different scenarios. Channel coding is also applied to investigate the performance of the three system under multipath fading channel. The low-density parity check (LDPC) code is adopted based on the one standardized in the DVB standard. For the LDPC code, soft decision with a maximum 50 iterations is adopted.

### §6.5.1.1 Performance with Linear Equalizers

In Figure 6–12, the BER performances of the OFDM and OCDM systems are provided. For the OCDM system of ZF equalizer, it requires higher SNR to achieve the same BER compared to the OFDM, especially in low SNR region. The corresponding BER curves approach those of the OFDM as the SNR increases. This degradation is from the noise enhancement of the ZF equalizer, which becomes smaller as the SNR increases.

The OCDM with MMSE equalizer outperforms that with the ZF equalizer as MMSE equalizer is able to balance the channel compensation and noise enhancement. The multipath diversity contributes to its superior performance over that of the OFDM. Although MMSE equalizer is able to effectively suppress noise, it should be noted that, the performance of the OCDM system with MMSE is slightly degraded in the low SNR region. The degradation is more pronounced as the modulation level increases from 4 and 16 to 64-QAM because high level modulation formats are sensitive to noise. For example, in the

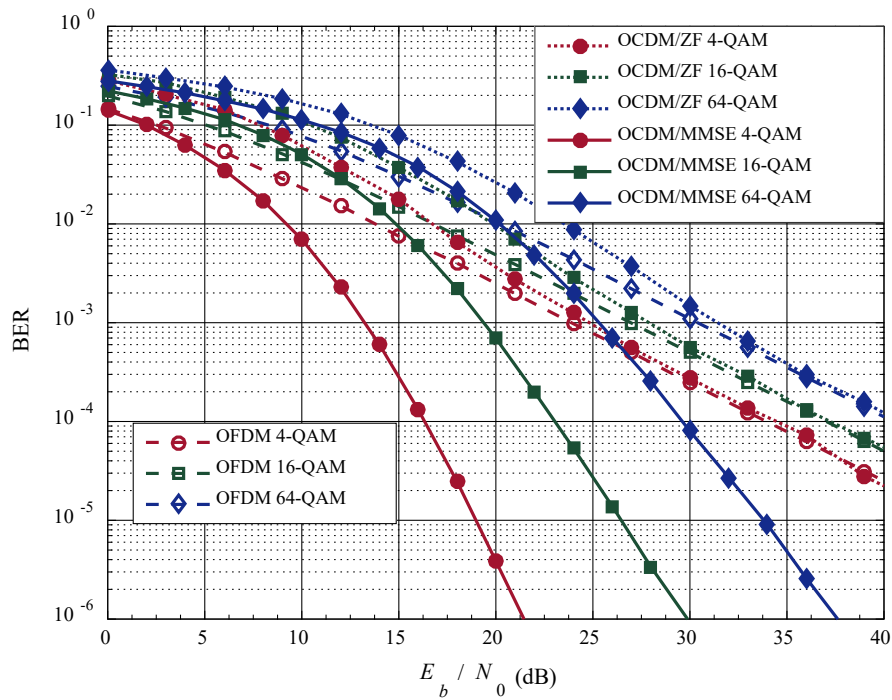


Figure 6–12. BER performances of the OCDM systems with both ZF and MMSE equalizers and the OFDM system under the 10-ray multipath Rayleigh fading channel.

64-QAM case, the OCDM system with MMSE equalizer starts to outperform OFDM system from  $\text{SNR} = 20$  dB. Nonetheless, the OCDM system of MMSE equalizer still gets much better performance than OFDM for  $\text{SNR} > 20$  dB.

In Figure 6–13, the BER performances of the DFT-P-OFDM and OCDM systems are compared when the length of GI is sufficiently large (greater than the maximal delay of the channel). As the DFT-P-OFDM system is also able to spread the symbol over the entire bandwidth, the DFT-P-OFDM gets the same performance as OCDM does.

The BER performance under the EVA channel is provided in Figure 6–14. The power delay profile is provided in Table 6-2. In addition, receive diversity with two antennas based on maximum ratio combining (MRC) is adopted, and the received power is normalized rather than doubled by two antennas. By doing so, the SNR of the received signal after MRC remains unchanged for both single and two receive antennas to show the effect of spatial diversity in the OCDM system. If the receive power is not normalized, 3-dB SNR improvement

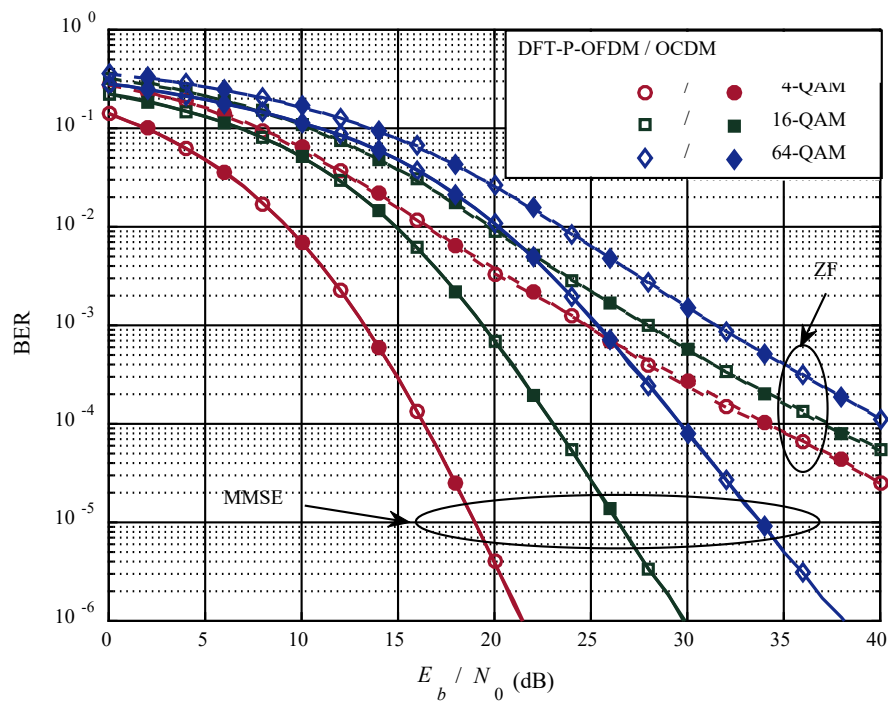


Figure 6–13. BER performances of the OCDM systems and the DFT precoded OFDM system under the 10-ray multipath Rayleigh fading channel.

will be observed over the normalized case.

Without receive diversity, results similar to the equal gain 10-path multipath channel can be observed in the EVA channel in Figure 6–14. However, if receive diversity applies, there is significant performance improvement for both OCDM and OFDM systems. The improvement is more notable for the OCDM system of ZF equalizer. With 2 Rx, the performance of OCDM with ZF is much better than that of the OFDM system, and it even approaches the MMSE case. For the OCDM systems of ZF and MMSE, the effect of noise enhancement is

TABLE 6-2  
POWER DELAY PROFILE OF THE EVA MODEL

Excess tap delay (ns)	0	30	150	310	370	710	1090	1730	2510
Relative Power (dB)	0	-1.5	-1.4	-3.6	-0.6	-9.1	-7.0	-12.0	-16.9

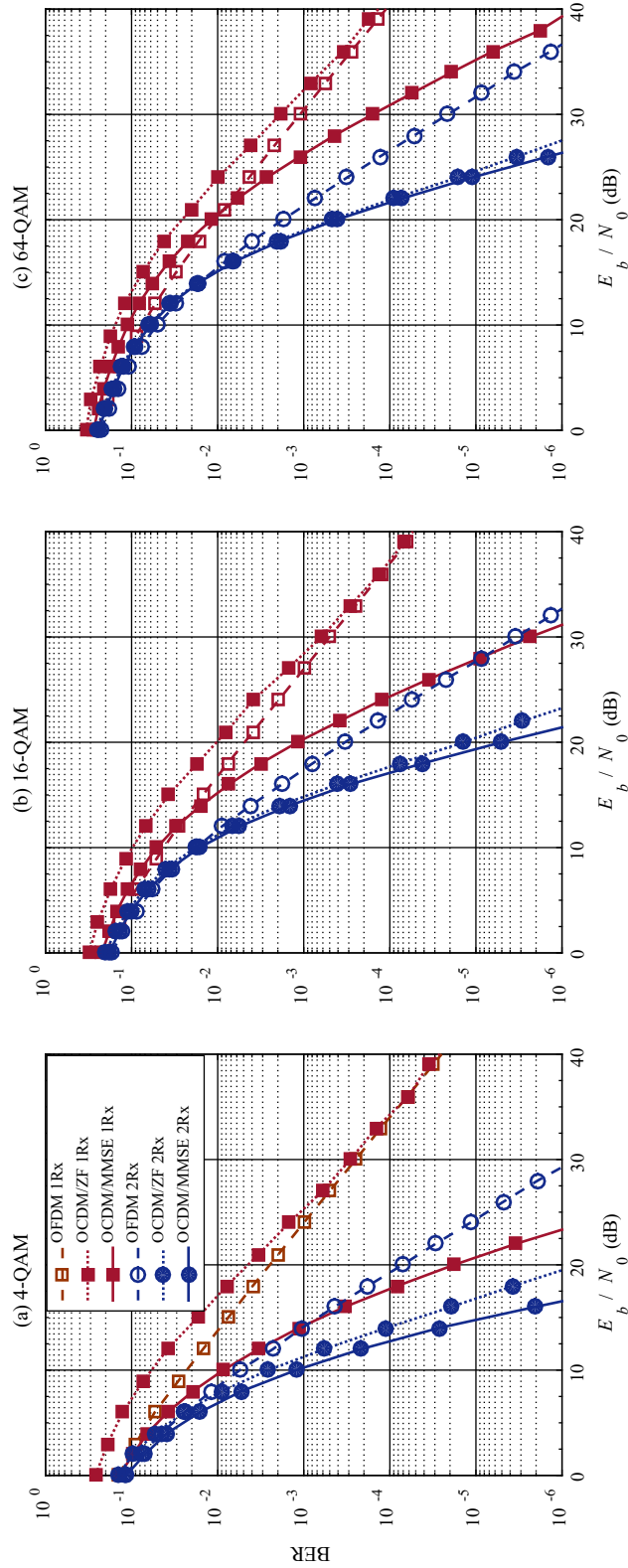


Figure 6-14. BER performance of the OCDM systems with both ZF and MMSE equalizers and the OFDM system under the LTE extended vehicle A channel model with receiver diversity; (a) 4-QAM, (b) 16-QAM, and (c) 64-QAM.

efficiently suppressed by spatial diversity, because spatial diversity can efficiently avoid deep frequency fading by combining the received signals from different antennas constructively. It is more effective for larger number of antennas. Thus with spatial diversity, the noise enlargement problem of the linear equalizers can be efficiently suppressed. The performance in the low SNR region is also improved compared to the single antenna case. For example, in the low SNR region, the performance of the OCDM system is inferior to that of OFDM system without spatial diversity, while with spatial diversity the performance of OCDM is similar to that of OFDM.

### §6.5.1.2 Performance with Insufficient Guard Interval

OCDM exhibits more resilience against the interference due to insufficient GI than the DFT-precoded OFDM. In Figure 6–15, we investigate the performance of the three systems in terms of various cyclic prefix lengths under the EVA channel model. The power delay profile is provided in Table 6-2. The lengths of CP are chosen to be 0.8, 1.6, and 3.2  $\mu\text{s}$  to accommodate the maximum delay of  $\sim 2.5 \mu\text{s}$ . In the case of 4-QAM, the OCDM gets negligible performance degradation for different lengths of CP, while the DFT-P-OFDM has an error floor at the BER of  $10^{-4}$  as the GI reduces to 0.8  $\mu\text{s}$ . For higher modulation level, all the systems get certain degradations. Nonetheless, the OCDM shows higher tolerance to the interference and outperforms the other two systems. For example, in the case of 16-QAM, if the GI is fixed at 1.6  $\mu\text{s}$ , OCDM and the DFT-P-OFDM have the error floor at  $\text{BER} = 2 \times 10^{-5}$  and  $1 \times 10^{-4}$ , respectively.

The benefit of OCDM compared to DFT-P-OFDM can be explained as follows. The DFT-P-OFDM in essence is a block transmitted single-carrier system, where symbols at the edge of a block are susceptible to the interference from adjacent blocks if the GI is not sufficient. The corrupted edge symbols impose irreducible BER. In contrast, OCDM can eliminate this effect by spreading the ISI over the entire OCDM symbol period more evenly. This effect contributes to the improved performance over the DFT-P-OFDM system.

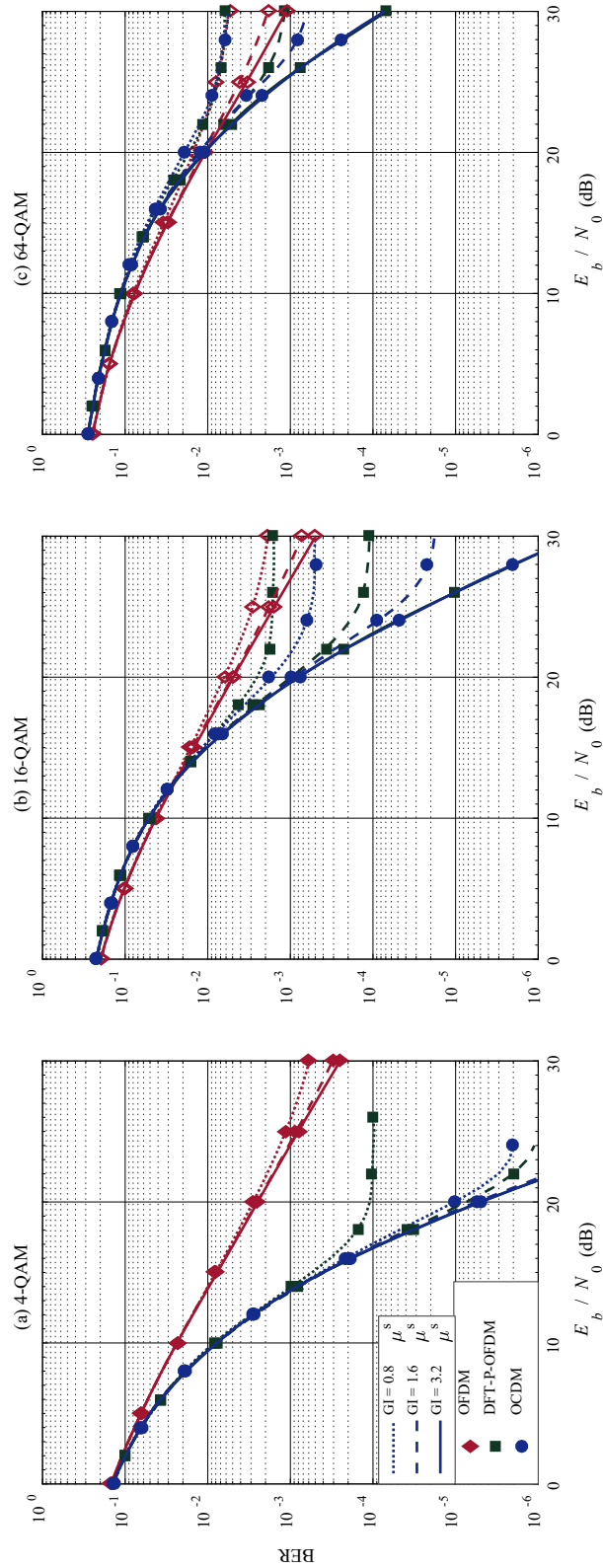


Figure 6–15. BER performance of the OFDM, DFT-precoded OFDM, and OCDM systems under the LTE extended vehicle A channel model with various guard interval length. (a) 4-QAM, (b) 16-QAM, and (c) 64-QAM.

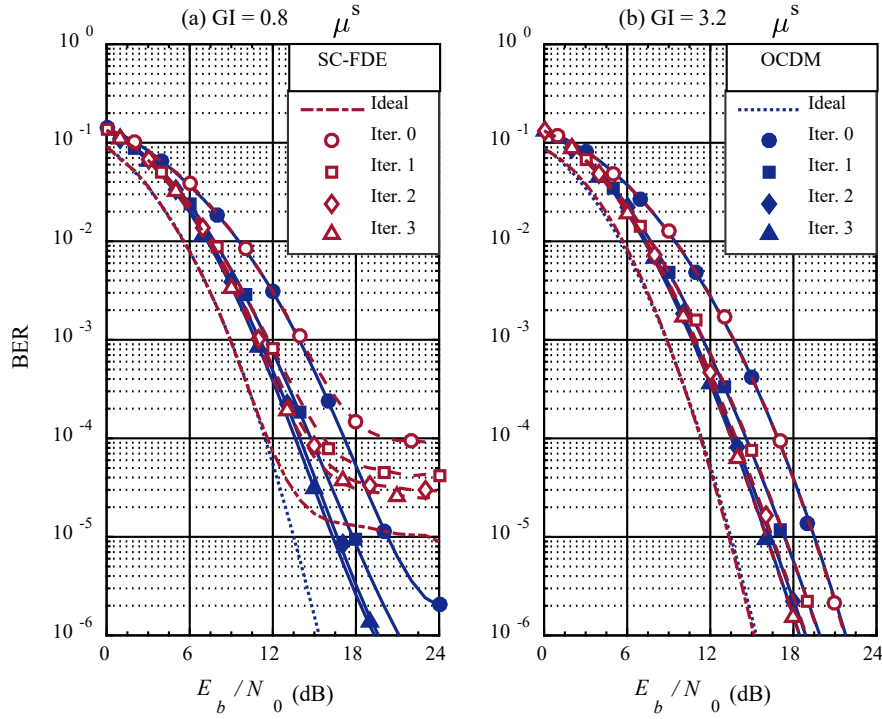


Figure 6–16. The BER performance of SC-FDE and OCDM systems with iterative block decision feedback equalization with (a) 0.8- $\mu$ s and (b) 3.2- $\mu$ s GI.

### §6.5.1.3 Performance with Decision Feedback Equalizers

Nonlinear equalization is able to improve the performance of the DFT-P-OFDM and SC-FDE significantly, approaching the matched-filter bound. In this subsection, we investigate the performance of the iterative block DFE (IB-DFE) [82, 146-148] for the proposed OCDM system without channel coding. In the IB-DFE algorithm, soft-decoding is adopted for each iteration [146]. In addition, we focus on the comparison of the SC-FDE with the proposed OCDM system, and the EVA channel is still adopted. In both systems, 4-QAM is adopted for modulation.

In Figure 6–16, the BER performances of the SC-FDE system and the OCDM system are provided with (a) 8- $\mu$ s and (b) 32- $\mu$ s GI. As the DFT-P-OFDM in essence is a single-carrier system, it can be observed in Figure 6–16 (a) that, if the GI is insufficient, the SC-FDE gets similar performance as the DFT-P-OFDM, and it gets worse performance than the OCDM system.

By applying the IB-DFE technique, we can observe that the BER performance of both the OCDM and SC-FDE improves as the number of iterations increases. The improvement becomes negligible as the number of iterations is greater than 2. For the SC-FDE system in Figure 6–16 (a), the error floor increases from  $1 \times 10^{-4}$  to  $1 \times 10^{-5}$  by applying IB-FDE with 3 iterations. On the other hand, for the OCDM system, by applying IB-FDE with 3 iterations, the performance degradation caused by insufficient GI becomes negligible. In Figure 6–16 (b), as the GI is large enough, both the SC-FDE and OCDM systems achieve the same performance. One can also expect that, the DFT-P-OFDM system performs the same as the SC-FDE, under the same conditions.

In Figure 6–16, the OFDM is not considered since its performance is very poor without channel code. In the following subsection, we will investigate the performance of OFDM, SC-FDE, and OCDM systems with forward error coding (FEC).

#### §6.5.1.4 Channel Coding Performance

In this subsection, low-density parity-check (LDPC) code is employed to investigate the performance of OFDM, SC-FDE, and OCDM systems. Block bit-interleaver is adopted, and the encoded bits are mapped into 4-QAM. EVA channel is adopted, and the GI is chosen to be  $3.2 \mu\text{s}$  to completely avoid the inter-symbol interference (ISI).

Figure 6–17 presents the BER performances of the three systems with code rates = (a)  $2/3$  and (b)  $3/4$ . In both cases, OCDM and SC-FDE have the same performance because the GI is long enough to avoid ISI. Compared to the uncoded case, the coded OFDM gets significant improvement. In Figure 6–17 (a), with a code rate  $2/3$ , the coded OFDM system has similar performance to the OCDM system without IB-DFE. If IB-DFE of 3 iterations is adopted, both the coded SC-FDE and OCDM systems get about 0.6 dB improvement than the coded OFDM system at  $\text{BER} = 1 \times 10^{-5}$ . In Figure 6–17 (b), if the code rate increases to  $3/4$ , with IB-DFE, both the coded SC-FDE and OCDM systems get 1.5 dB improvement than the coded OFDM. In addition, the coded OFDM gets slight degradation to the other two systems without IB-DFE.

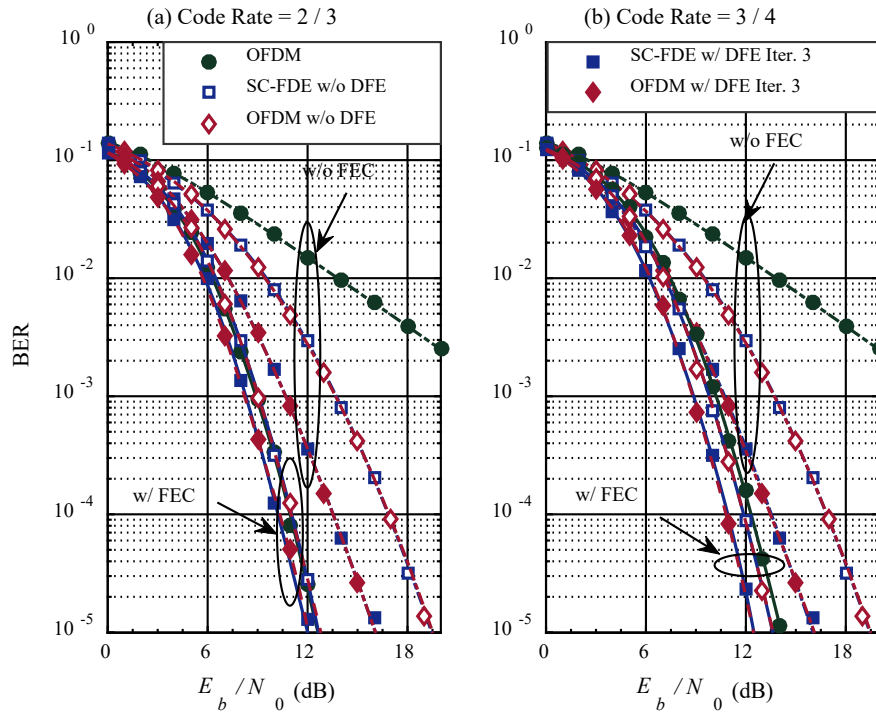


Figure 6–17. The BER performance of the OFDM, SC-FDE and OFDM using forward error coding with 3.2- $\mu$ s GI and code rates of (a) 2 / 3 and (b) 3 / 4.

### §6.5.1.5 Summary

In this chapter, we have proposed the OFDM system for wireless communication systems. Simulations under wireless multipath channel are carried out to validate the feasibility of the proposed OFDM system. The results show that the OFDM outperforms the conventional OFDM system, and that it also exhibits more resilience against the interference due to insufficient GI compared to DFT-P-OFDM and SC-FDE. Consequently, the proposed OFDM system can be an attractive alternative solution for high-speed communication systems.

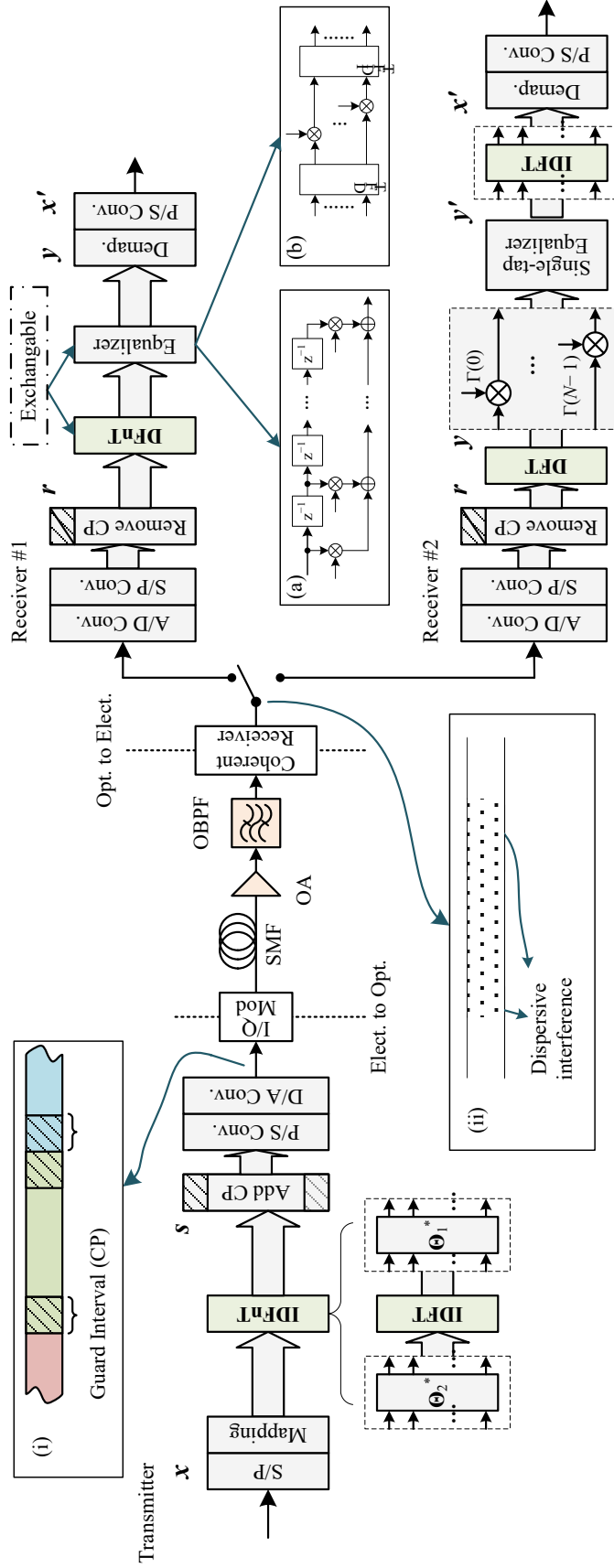


Figure 6–18. Schematic diagram of the CO-OCDM system. Excluding the components in the dashed boxes, the transmitter and receiver #2 form the diagram of a conventional CO-OFDM system. Insets: illustrations of the (i) transmitted OOCDM signal and the (ii) received OOCDM signal distorted by dispersion and noise; (a) time-domain and (b) frequency-domain equalizers in the receiver #1.

### §6.5.2 Fiber-Optic Communication Systems

In this section, numerical simulations are carried out to validate the feasibility of the proposed CO-OCDM system and to investigate its transmission performance over SMF channel. In the simulations, CO-OFDM is also considered for comparison. In both the OFDM and OCDM systems, there are 1024 subcarriers/chirps, which are modulated in quadrature amplitude modulation (QAM). In the CO-OCDM system, receiver #2 is adopted for its efficiency. Channel estimation is achieved by the frequency-domain pilot designed for the CO-OFDM system [149], and it is also adopted for the proposed CO-OCDM system.

The system setup is shown in Figure 6–18. The sampling rate of the D/A and A/D convertors is 10 GS/s, with data rate 20 Gbit/s for 4-QAM or 40 Gbit/s for 16-QAM. In the simulation, from the digital-to-analog process, raised cosine filter of a roll off factor 0.05 is employed to emulate the bandlimited signal with an oversampling ratio of 8.

The wavelength is at 1550 nm; the IQ modulator is operated within linear region. At the receiver, the responsivity of PDs is 1 A/W. The coherent receiver converts the optical signal into the electrical baseband signal. The optical link consists of 80-km SMF loops, and each loop is followed by an optical amplifier. The SMF has a dispersion  $D = 16 \text{ ps}/(\text{km}\cdot\text{nm})$  and loss 0.2 dB/km. The nonlinear Kerr effect in the fiber is considered with a nonlinear coefficient  $2.6 \times 10^{-20} \text{ m}^2/\text{W}$ . It is simulated by split-step Fourier method. After every 80-km transmission, an optical amplifier with a gain of 16 dB compensates the power loss of the signal.

#### §6.5.2.1 Chromatic Dispersion

Chromatic dispersion is the major dispersion effect in SMF, causing pulse broadening. If the bandwidth of the optical signal is  $B$ , the pulse broadening after SMF transmission is

$$\Delta T = \beta_2 LB, \quad (6.59)$$

where  $\beta_2$  is the group velocity dispersion (GVD) parameter,  $L$  is defined as the

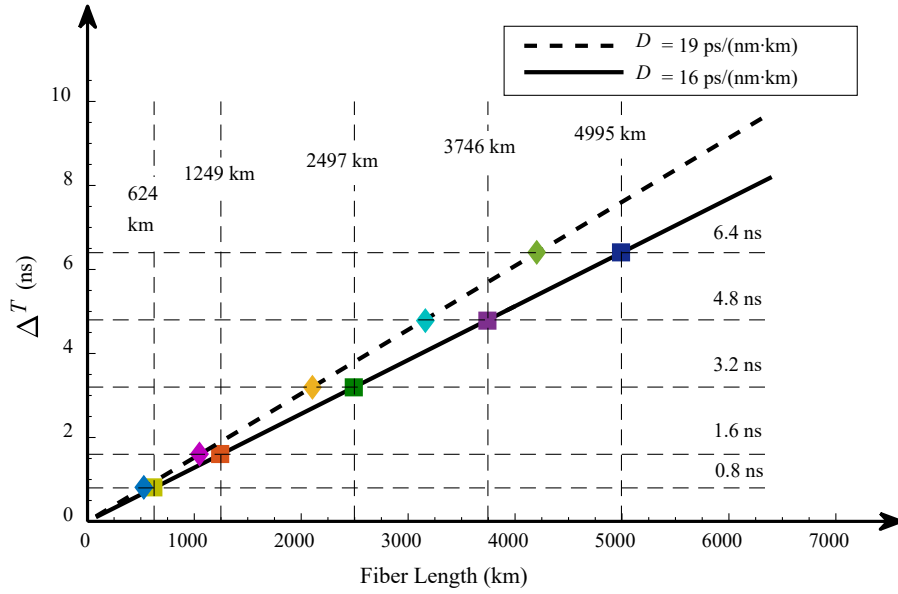


Figure 6–19. Pulse broadening  $\Delta T$  along with the transmission distance of SMF with different dispersion parameters.

length of the fiber. Usually, the dispersion is measured by the dispersion parameter  $D$ , which has units of ps/(km·nm). It is defined as

$$D = -\frac{2\pi}{\lambda^2} c \beta_2, \quad (6.60)$$

where  $c$  is the speed of light and  $\lambda$  is the operating wavelength. In practice, the dispersion parameter  $D$  of the standard SMF is usually from 16 to 23 ps/(km·nm).

Figure 6–19 illustrates the pulse broadening against transmission distance. It can be observed that the pulse broadening increases linearly along with the transmission distance  $L$  and the dispersion parameter  $D$ . For example, for a dispersion parameter  $D = 16$  ps/(km·nm), a 4995-km SMF transmission will cause a  $\Delta T = 6.4$ -ns pulse broadening. If  $D$  increases to 19 ps/(km·nm), the distance decreases to 4400 km.

In Figure 6–20, the performance of CO-OCDM with various GI lengths is evaluated at different transmission distance in terms of average Q factor. In the simulation, to manifest the impact of chromatic dispersion, both the non-

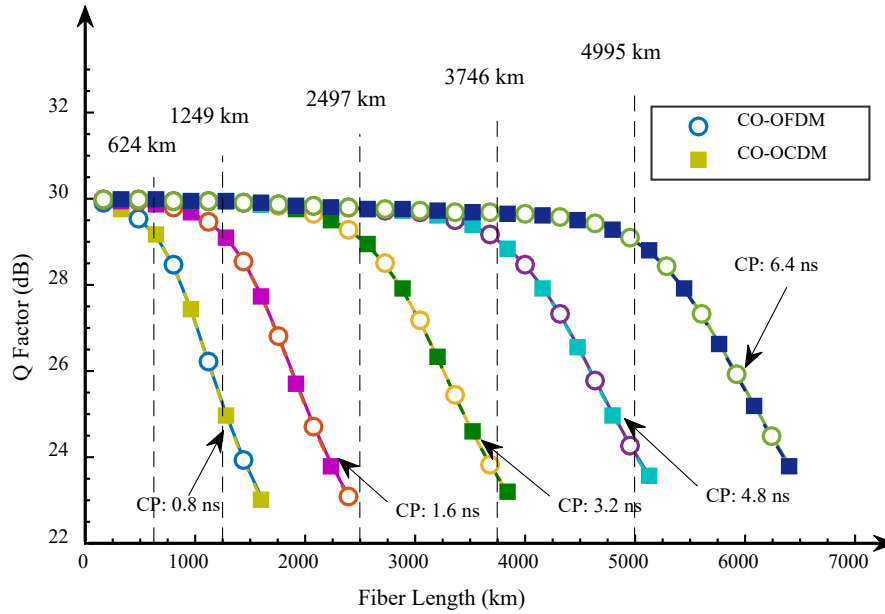


Figure 6–20. Average Q factor versus transmission distance of the CO-OFDM and CO-OCDFM systems with different guard interval (GI) length.

linear effect and inline ASE noise are not included. Noise is added at the receiver at a fixed SNR = 30 dB. It can be observed that both systems do not get obvious degradation as long as the GI length is longer than the pulse broadening. For example, if the GI length = 0.8, 1.6, 3.2, 4.8, or 6.4 ns, the performance starts to degrade if the distance exceeds 624, 1249, 2497, 3746, or 4995 km.

In Figure 6–20, both the CO-OFDM and CO-OCDFM have the same averaged Q factors for the same condition. We will show later that though the averaged Q factors of both systems are the same, the CO-OCDFM system is more resilient to channel impairments due to the spectral fading and noise effects of a communication system. As a result, the CO-OCDFM system exhibits better BER performance than the CO-OFDM.

### §6.5.2.2 Nonlinear Effects

Fiber nonlinearity imposes limitation on the reach of optical systems. In Figure 6–21, we investigate the effect of fiber nonlinearity on the performance of CO-OCDFM. The length of GI is 6.4 ns to support a transmission up to 5000-km. In

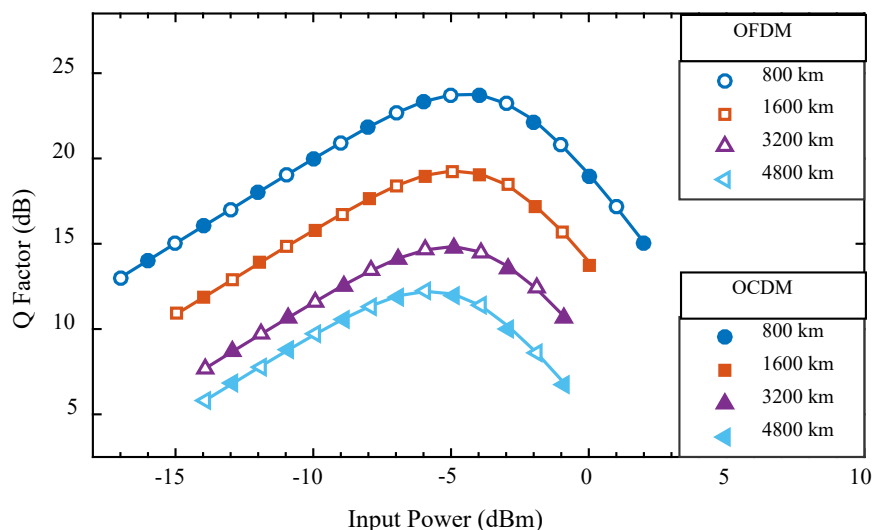


Figure 6–21. Average Q factors versus input powers of CO-OFDM and CO-OCDM systems at various SMF transmission with 6.4-ns GI.

the simulation, in-line ASE noise is introduced by the EDFA with a noise figure of 4.6 after every 80-km SMF transmission. The performance is also evaluated by the average Q factor with various input power.

In Figure 6–21, as the transmission distance increases from 800 km to 5600 km, the optimal input power varies from  $-4.5$  to  $-6$  dBm. The similar nonlinear tolerances of both the OCDM and OFDM systems can be inferred from that they have the same PAPR characteristics, as shown in Figure 6–11.

### §6.5.2.3 OSNR Penalty versus Transmission Distance

In Figure 6–22, we evaluate the OSNR penalties to achieve a  $\text{BER} = 10^{-4}$  at different transmission distances. The input power is fixed at  $-5$  dBm, and no inline noise is considered. The OSNR with 0.1-nm resolution (12.5 GHz at 1550 nm) is measured at the receiver in single polarization. The GI varies from 0.8 to 3.2 ns.

The CO-OCDM system outperforms the CO-OFDM system if the length of GI is the same, though both systems get almost the same average Q-factor as indicated in Figure 6–20 and Figure 6–21. At an OSNR penalty of 6 dB, the CO-OCDM improves transmission distance by 10.1%, 12.4%, 18.9%, and 26.5%

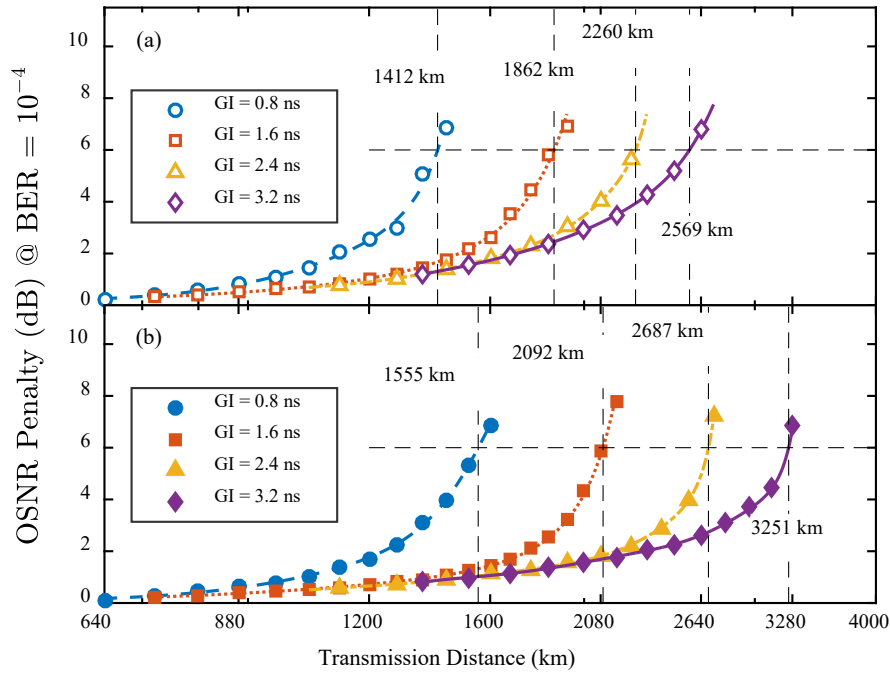


Figure 6–22. OSNR penalties of (a) CO-OFDM and (b) CO-OCDM systems of 16-QAM to achieve a  $\text{BER} = 10^{-4}$  at different transmission distance.

compared to the CO-OFDM for GI = 0.8, 1.6, 2.4, and 3.2 ns, respectively.

The improvement achieved by OCDM is because it is more resilient to channel impairments than OFDM. In the next subsection, we will investigate the reason of this improvement by measuring the channel frequency responses of both systems. Experiments in Section V also confirm the simulation results.

#### §6.5.2.4 BER Performance of Various Modulation Level

In this subsection, we investigate the BER performance of the CO-OCDM systems with various modulation levels. The GI is chosen to be 1.6-ns and 3.2-ns long to support the transmission up to 1200-km and 2400-km, respectively.

In Figure 6–23 (a), the length of GI is 1.6 ns while in Figure 6–23 (b), it is 3.2 ns. In the 4-QAM case, the OSNR penalties at 1200-km are 2 dB for 1.6-ns GI and 1 dB for 3.2-ns GI at a  $\text{BER} = 10^{-6}$ . If 16-QAM is adopted, the penalties become about 3.5 dB and 2 dB, respectively. In both cases, the CO-

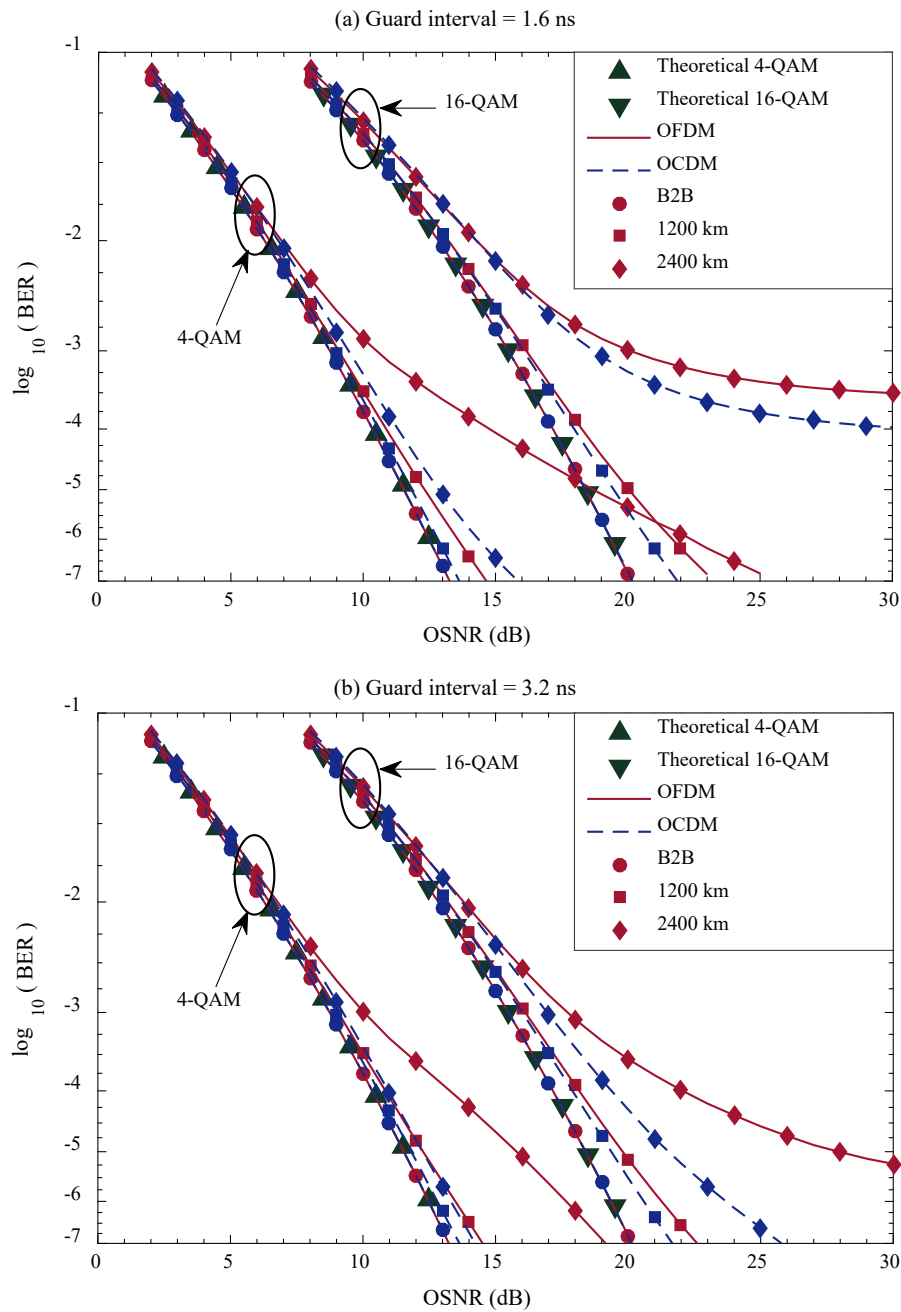


Figure 6–23. BER versus OSNR performance of the CO-OFDM/OCDM systems with (a) 1.6-ns and (b) 3.2-ns GI.

OCDM achieves better BER performance than the CO-OFDM.

As the transmission distance increases to 2400 km, the BER performance penalty, especially for the 16-QAM case, becomes pronounced. In the case of 16-QAM with GI = 1.6 ns, there are even error floors in both systems because

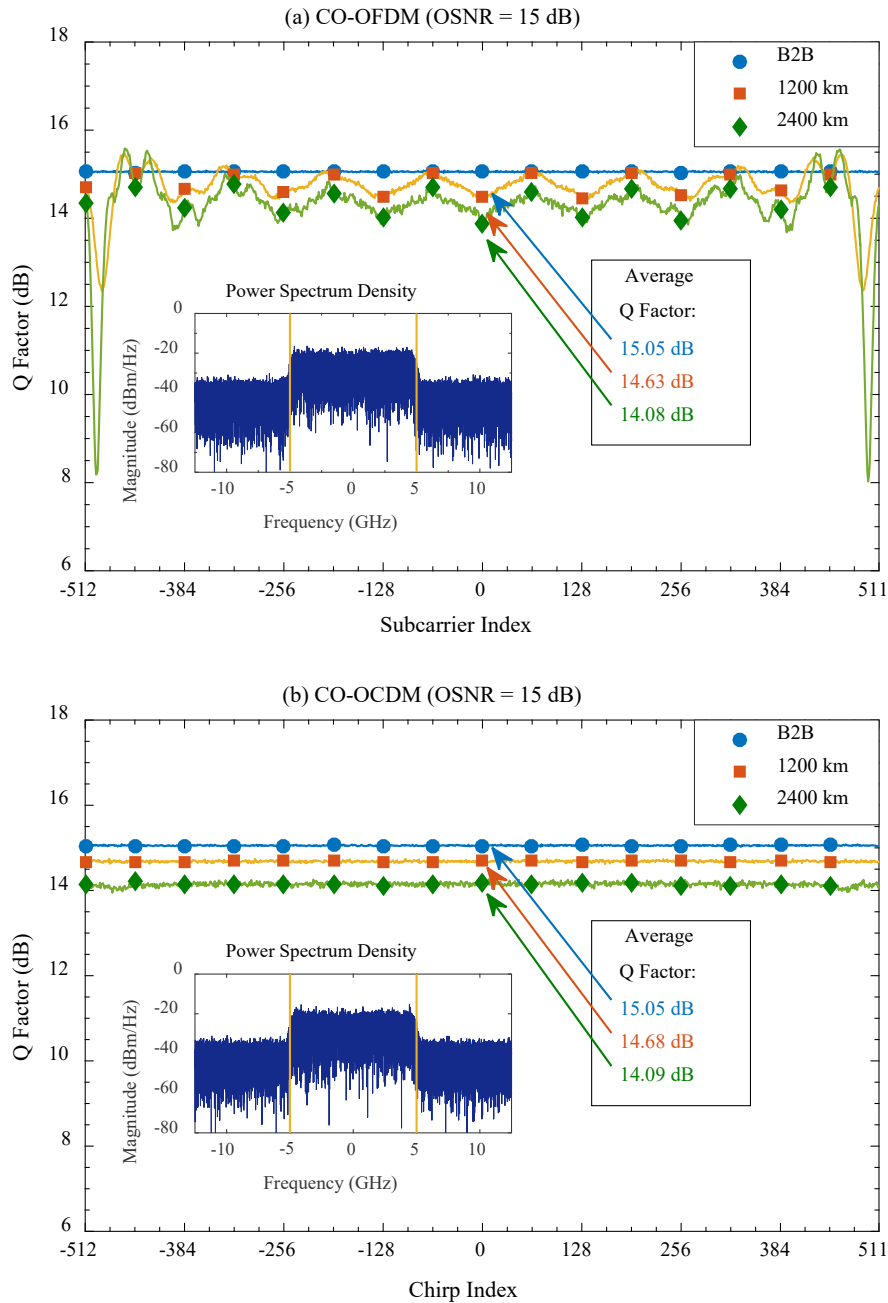


Figure 6–24. Q factor of each (a) subcarrier in the CO-OFDM or each (b) chirp in the CO-OCDFM with 3.2-ns GI at a received OSNR = 15 dB.

high level modulation scheme is more sensitive to the impairments due to insufficient GI. If GI increases to 3.2 ns, the error floor is alleviated. Still, in all cases of 2400-km transmission, the CO-OCDFM system gets better performance than the CO-OFDM. For example, if GI = 3.2 ns, the CO-OFDM system needs additional 2-dB and 3-dB OSNR for 4-QAM and 16-QAM, respectively, to get a  $\text{BER} = 10^{-4}$  compared to the CO-OCDFM.

To investigate the BER performance differences between the CO-OFDM and CO-OCDM, Figure 6–24 provides the measured Q factors of (a) each subcarrier in CO-OFDM and (b) each chirp in CO-OCDM at a OSNR = 15 dB. The Q factor is measured over  $1 \times 10^5$  OFDM symbols by calculating the average signal variance. It can be observed that both systems have the same average Q factors at the same distance. However, the Q factors of the subcarriers in OFDM fluctuates; the higher the frequency is, the lower the Q becomes. The degradation becomes more severe as the distance increases.

In the simulation, the fading impairment is due to the edge effect, and it is explained as follows. In the OFDM, as well as the OCDM system, the aliasing signal at the edge of spectra after resampling (A/D conversion) will be out-of-phase due to the chromatic dispersion. After resampling the OFDM/OCODM signals at Nyquist rate for channel equalization and detection, the out-of-phase aliasing signal in the frequency domain causes the fading effect at the edge of the spectra. Therefore, the BER performance of OFDM system is limited by the noisy subcarriers at high frequency region.

On the other hand, in the CO-OCODM system, despite the uneven spectra, the Q factors of all the chirps are the same as the chirps spread their spectra over the entire bandwidth. As a result, the CO-OCODM system is insensitive to the fading effect.

### §6.5.2.5 Summary

In this subsection, we have proposed the OCOCDM for optical fiber communication. In virtue of chirp spread spectrum, the proposed CO-OCODM is more resilient to channel impairments and gets better BER performance than the CO-OFDM system. It can also be easily integrated into the existing CO-OFDM system with only slight modification. Therefore, based on the widespread CO-OFDM systems, the proposed CO-OCODM can be implemented as an alternative approach, which is more resilient to the channel impairments, to achieve high-speed optical communication.

## §6.6 Experimental Implementation

We implemented experiments to investigate the performance of the CO-OCDM system. In Subsection §6.6.1, the experiment setup of the coherent optical system is introduced, and the experiment results are provided in Subsection §6.6.2, with related discussions.

### §6.6.1 Experimental Setup

The experimental setup is shown in Figure 6–18. At the transmitter, the OCDM signal is fed into an arbitrary waveform generator (AWG) with digital-to-analog (D/A) converters at 12 GS/s. There are 768 chirps which are modulated in 4-QAM and 16-QAM. To separate the aliasing signal, a pulse-shaping filter with up-sampling rate of 4/3 is adopted. Therefore, the bandwidth of the OCDM signal is 9 GHz, and the data rates are 18 Gbit/s for 4-QAM or 36 Gbit/s for 16-QAM. In the OFDM system, 256 out of the 1024 subcarriers are also set to be zeros to achieve an oversampling rate of 4/3. Thus, the data rates of both systems are the same. The length of CP is 32 points. In the experiment, frequency-domain pilot for OFDM [149] is employed for channel estimation, as we used in the simulation. The Schmidl-Cox algorithm proposed for the OFDM system [150] is adopted for symbol synchronization for the CO-OCDM system. The electrical output of the AWG is amplified to drive the optical IQ modulator that is operated in linear region. The operating wavelength of the laser is 1553 nm.

After 80-km SMF transmission, the fiber loss is compensated by an EDFA, following by a 0.8-nm OBPF to remove the out-of-band ASE noise. An optical coherent receiver perceives the optical signal and converts the optical signal back to the electrical baseband signal. A real-time digital phosphor oscilloscope with 50-GS/s analog-to-digital (A/D) converters sample and store the baseband signal for offline processing. In the offline processing, after resampling and synchronization, the information bits are recovered based on Figure 6–18.

In the experiment, CO-OFDM system is provided for comparison. In the

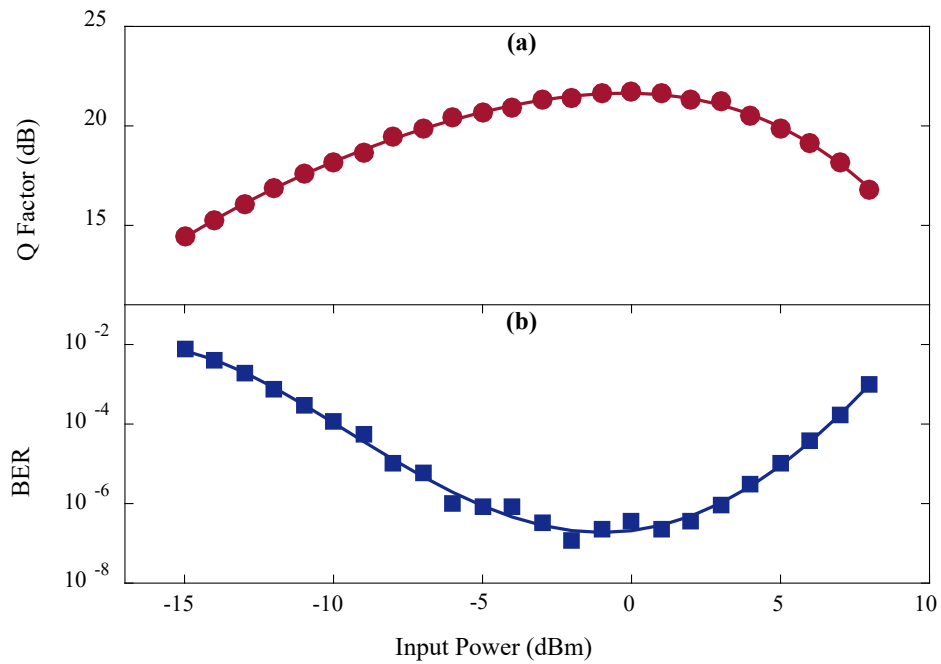


Figure 6–25. (a) Q factor and (b) BER versus Input pPower of the CO-OCDM system over 80-km standard SMF transmission.

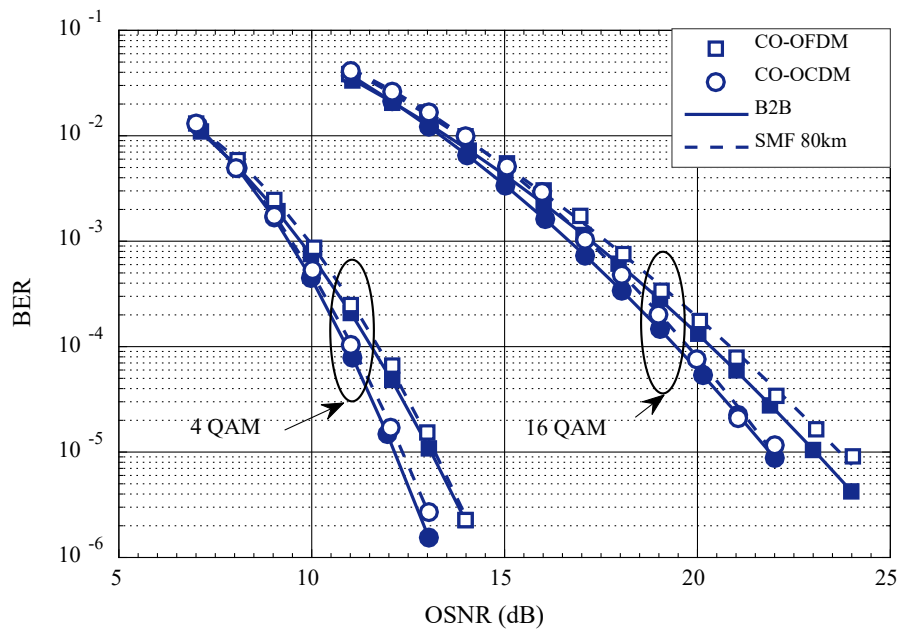


Figure 6–26. Experiments results of the BER versus OSNR of the CO-OFDM and CO-OCDM systems.

CO-OFDM, there are 1024 subcarriers in which 768 subcarriers are used for data modulation. The oversampling rate is thus 4/3. The length of CP is also 32 points. As a result, the data rates of the CO-OFDM and CO-OCDM systems

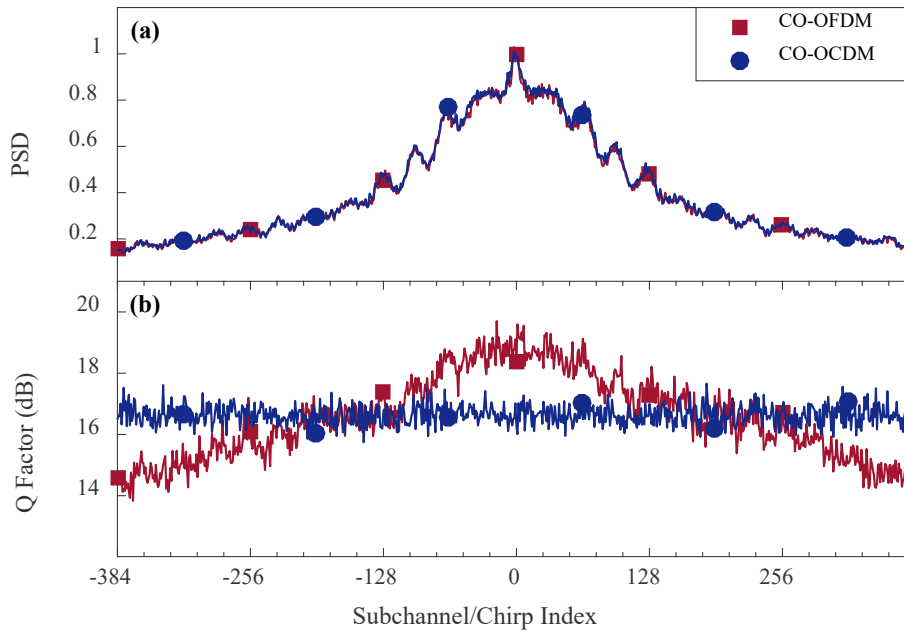


Figure 6–27. The measured (a) power spectral densities (PSDs) and (b) Q-factors of each subchannel/chirp in the CO-OFDM and CO-OCDM systems.

are the same.

### §6.6.2 Experimental Results

To investigate the nonlinear effects of the CO-OCDM system and to determine the optimal input power over fiber transmission, in Figure 6–25, we measured the system performance with various input power over 80-km standard SMF transmission. The performance is evaluated by (a) received Q factor and (b) BER. It can be observed that the optimal input power is approximately 0 dBm. Therefore, in the experiment, we fix the input optical power at 0 dBm for optimal performance.

In Figure 6–26, the measured BER performance of CO-OFDM and CO-OCDM systems are shown. In the low OSNR region, both systems get similar performance. As the OSNR increases, the CO-OCDM requires lower OSNR than the CO-OFDM to achieve the same BER. For example, to reach a  $\text{BER} = 10^{-5}$ , the CO-OCDM system requires about 1 dB OSNR less than the CO-

OFDM system.

To investigate the performance difference between OFDM and OCDM systems, the measured (a) power spectral density (PSD) and (b) Q-factor of the subcarriers in OFDM and that of the chirps in OCDM are provided in Figure 6–27. It can be observed in Figure 6–27 (a) that both systems actually have the same PSD's and the thus same channel frequency responses, and the same average Q-factors. In the experiments, the uneven spectra are mainly caused by the electronic and optical devices, whose frequency responses are not ideally flat. That is, high frequency components experience severe fading effects. As a result, BER performances similar to those in the simulation can be observed in the experiments. In the CO-OFDM, the subcarriers of high frequency are noisier, and its BER performance is limited by the noisy subcarriers in the high frequency region. In contrast, in Figure 6–27 (b), the chirps in the OCDM experience almost the same Q factors and are insensitive to the fading effect.

## §6.7 Conclusion

In this section, we present the principle of orthogonally multiplexing a bank of chirp waveforms whose amplitude and phase are used for modulation. The principle is based on the Fresnel transform, and the convolution theorem of the Fresnel transform gives the analytical approach to model the transmission of OCDM signal in LTI channels. The digital implementation of OCDM system is proposed based on DF<sub>n</sub>T, and it is shown that the chirp waveforms are transparent to the dispersive channel. Both the time-domain and frequency-domain equalizers can be applied for channel compensation. By exploiting the eigen-decomposition of the DF<sub>n</sub>T matrices, a simpler and more efficient single-tap equalization algorithm is proposed for the OCDM system. In terms of the implementation of OCDM system, it is shown that the system is compatible to the OFDM system, and it can be realized using the existing OFDM system without significant modification.

Simulations under wireless multipath channel are carried out to validate the feasibility of the OCDM. The results show that the OCDM is able to exploit

the multipath diversity with linear equalizers and the OCDM with MMSE equalizer outperforms the OFDM system. Furthermore, with the spatial diversity, the noise enhancement of linear equalizers can be efficiently suppressed in the OCDM system. By exploiting the receive diversity, even the OCDM system with ZF equalizer achieves notable performance improvement compared to the OFDM system.

On the other hand, simulations are performed to verify the feasibility of the CO-OCDM system, and the analyses and numerical results show that the CO-OCDM system can efficiently counteract the chromatic dispersion as the CO-OFDM system does. Since the CO-OCDM is insensitive to the fading and noise effect in the fiber-optic system, it achieves better BER performance than the CO-OFDM system. Therefore, the CO-OCDM system could be an attractive scheme for the high-speed optical communication.

Moreover, experiments are implemented for the CO-OFDM system. In the experiments, the results are consistent with the numerical results, and it is shown that the proposed CO-OCDM is more robust against the channel impairment than the CO-OFDM system.

Consequently, for its compatibility to the widespread OFDM system and its capability to counteract the detrimental effects in communication channels, the OCDM system is an attractive alternative solution for the high-speed communication systems.

# Chapter 7

## Conclusions and Future Work

Digital signal processing is the technology underpinning any digital communication system, and especially it becomes critically important in current and future fiber-optic communication systems since the available bandwidth in optical fibers have been squeezed out by the elegant photonic technologies, such as, high-speed optical modulators and receivers, wideband optical amplifiers and wavelength-division multiplexing. The ultimate objective of applying DSP technologies in fiber-optic systems is to devise elegant algorithms to implement highly spectral-efficient modulation schemes which leverage the capacity of the system, and to secure the resilience of the system which guarantees the recovery of information in noisy environments.

In the thesis, several DSP enabled topics, which include both DSB and SSB modulated Fast-OFDM, discrete Fresnel transform, and orthogonal chirp-division multiplexing, are studied. It is mainly divided in two parts. The first part is about the implementation of Fast-OFDM systems, and to tackle the signal recovery and channel compensation problems. The second part is the study of an interesting mathematical tool, discrete Fresnel transform, and the proposal of orthogonal chirp-division multiplexing, based on the DF<sub>n</sub>T and its convolution-preservation property.

Fast-OFDM is a variant of OFDM. Compared to the conventional OFDM, the subcarrier spacing of Fast-OFDM is halved, and Fast-OFDM features unique properties for the halved subcarrier-spacing. However, problems arise as the result of the halved subcarrier-spacing, and the Fast-OFDM systems has lagged behind the conventional OFDM for a long time, since its initial proposal in the beginning of 2000s.

In the DSB Fast-OFDM, although the multiplexing kernel, DCT is orthogonal and possesses a symmetric convolution property, the condition to satisfy the symmetric convolution is however physically impossible. Consequently, in the communication systems whose impulse response is not strictly symmetric, single-tap equalization cannot be applied, with interference causing significant performance degradation. On the other hand, the multiplexing kernel in SSB modulated Fast-OFDM system is a truncated discrete Fourier transform (DFT), which neither possesses a convolution property nor is orthogonal. It means that not only the single-tap equalizers cannot be applied for channel compensation but there exists severe interference between the halved-spacing subcarriers due to the loss of orthogonality even without channel transmission.

To resolve the problems, system designs are proposed for both Fast-OFDM systems in Chapter 4 and Chapter 5, respectively. Technically, frequency-domain oversampling is utilized to de-multiplex the subcarriers of halved-spacing. With properly designed algorithms, single-tap equalization can be applied efficiently for both DSB and SSB based Fast-OFDM systems for channel compensation, and the interference problems therein are completely avoided.

Analyses and numerical simulations are provided to validate the advantages of the proposed schemes, and moreover, experimental implementations were carried out for both of them. Specifically, the DSB modulated Fast-OFDM was successfully demonstrated in both the conventional silica fibers at 1.55  $\mu\text{m}$  and the newly fabricated hollow-core photonic bandgap fiber at 2  $\mu\text{m}$  using intensity-modulation and direct detection. The SSB modulated Fast-OFDM system was implemented in coherent optical systems at 36 Gbit/s at a spectral efficiency of 6 bit/s/Hz, for the first time, thanks to the proposed scheme.

With the proposed Fast-OFDM systems for both DSB and SSB modulation,

the performance gap to the conventional OFDM has been eliminated, and they achieves similar performance with similar system complexity. Therefore, Fast-OFDM is a variant to realize the OFDM system for fiber-optic communications. Especially, the DSB modulated Fast-OFDM in Chapter 4 can serve as an alternative of the discrete multi-tone modulated OFDM system, suitable for base-band transmission systems, such as ADSL, and for optical intensity modulated systems, such as visible light communication using LED, and short-reach fiber-optic systems with intensity-modulation and direct-detection. The SSB modulated Fast-OFDM with no doubt can be a candidate to implement the conventional OFDM system using coherent detection.

## DISCRETE FRESNEL TRANSFORM

Fresnel integral transform is a fundamental and useful mathematical operation that describes the wave-like phenomena in optics and physics. As a mathematical tool, however, it is not as powerful as the Fourier transform, partially because a) a closed-form of Fresnel transform cannot be derived easily, b) there is no decent discrete Fresnel transform that inherits the attractive properties of the Fresnel integral transform, and thus the digital implementation of Fresnel transform is hard, and c) Fourier transform is so powerful and possesses a convolution-multiplication property, and most importantly, there is a corresponding discrete Fourier transform.

In Section §6.2, a discrete Fresnel transform is derived from the Talbot effect of infinitely extended periodic Fresnel diffraction, and it is show that the DF<sub>n</sub>T in this dissertation inherits all the attractive properties of the Fresnel transform. For example, the unitary of the DF<sub>n</sub>T corresponds to the orthogonality of the Fresnel transform. Most importantly, that the DF<sub>n</sub>T of a circular convolution of two functions is equal to the DF<sub>n</sub>T of either one convolving with the other corresponds to that the Fresnel transform of a linear convolution of two functions is equal to the Fresnel transform of either one convolving with the other. As convolution is the basic process in real physical world and systems, the DF<sub>n</sub>T could be a useful mathematical tool for evaluating the systems for the purpose of digital signal processing.

## ORTHOGONAL CHIRP-DIVISION MULTIPLEXING

In Section §6.3, the principle of orthogonal chirp-division multiplexing is proposed as a direct application of the DF<sub>n</sub>T. Compared to the single-carrier modulation with Nyquist signaling and OFDM, OCDM provides a third basic modulation scheme using the orthogonal chirped waveforms for information modulation. OCDM achieves the maximum spectral efficiency of the conventional chirp spread spectrum systems, which are notorious for its poor spectral efficiency. Meanwhile, OCDM inherits the advantages of chirped waveforms, and is more resilient against the noise and interference from the hostile environments than both single-carrier and OFDM systems.

In Section §6.4, the system implementation of OCDM are discussed in detail, and it is shown that the OCDM system can be easily integrated into the wide-spread OFDM systems with slight changes. It means that the OCDM systems can be readily deployed using the legacy OFDM systems to improve the performance. In Section §6.5, numerical simulations are provided to validate the superior advantages promised by OCDM in both wireless and fiber-optic systems, and in Section §6.6, a proof-of-concept experiment was successfully carried out in coherent optical system to confirm the analysis.

Consequently, OCDM system provides another solution to implement high-speed communication systems, for example, including both wireless and fiber-optic systems, and the compatibility of OCDM to the OFDM systems makes the OCDM a comfortable choice to upgrade the existing OFDM systems from a practical view. Nonetheless, in the dissertation, the study of OCDM is mainly focused on physical layer, and the co-existence of OCDM and OFDM in a single system from a high-level perspective would be a challenge work. For example, in our future work, to investigate the OCDM system in a scenario taking the medium access into account for multiuser and multipoint communication networks is a fascinating research topic.

# List of Publications



## JOURNALS

- [1] X. Ouyang, Octavia A. Dobre, and J. Zhao, “Unbiased channel estimation based on the discrete Fresnel transform for CO-OFDM systems,” *IEEE Photon. Technol. Lett.*, 2017, DOI: 10.1109/LPT.2017.2678838.
- [2] X. Ouyang and J. Zhao, “Single sideband modulated coherent optical Fast-OFDM with frequency oversampling,” *IEEE J. Lightw. Technol.*, 2017, DOI: 10.1109/JLT.2017.2675358.
- [3] X. Ouyang and J. Zhao, “Orthogonal chirp division multiplexing for coherent optical fiber communications,” *IEEE J. Lightw. Technol.*, vol. 34, pp. 4376-4386, 2016.
- [4] X. Ouyang and J. Zhao, “Orthogonal chirp division multiplexing,” *IEEE Trans. Commun.*, vol. 64, no. 9, pp. 3946-3957, 2016.
- [5] L. Zhang, X. Ouyang, X. Shao et al., “Experimental demonstration of a real-time high-throughput digital DC blocker for compensating ADC imperfections in optical Fast-OFDM receivers,” *Opt. Express*, vol. 24, no. 13, pp. 14215-14226, 2016/06/27, 2016.
- [6] Xing Ouyang, Cleitus Antony, F. C. G. Gunning et al., “Discrete Fresnel transform and its circular convolution property,” *arXiv:1510.00574*, 2015.
- [7] X. Ouyang, W. Jia, P. Gunning, P. Townsend, and J. Zhao, “Experimental demonstration and field-trial of an improved optical fast OFDM scheme using intensity-modulation and full-field detection,” *IEEE J. Lightw. Technol.*, vol. 33, no. 20, pp. 4353-4359, Aug. 2015.

- [8] X. Ouyang, H. Zhang, Y. Chen, S. Alam, M. Petrovich, F. Poletti, D. Richardson, F. Gunning, and J. Zhao, “Experimental demonstration of improved equalization algorithm for IM/DD fast OFDM,” *IEEE Photon. Technol. Lett.*, vol. 27, no. 16, pp. 1780-1783, June 2015.
- [9] H. Zhang, M. Gleeson, N. Ye, N. Pavarelli, X. Ouyang, et al., “Dense WDM transmission at 2  $\mu\text{m}$  enabled by an Arrayed Waveguide Grating,” *Opt. Lett.*, vol. 40, no. 14, pp. 3308-3311, 2015.
- [10] X. Ouyang and J. Zhao, “Single-tap equalization of fast OFDM signals under a generic linear channel,” *IEEE Commun. Lett.*, vol. 18, no. 8, pp. 1319–1322, Aug. 2014.

#### CONFERENCES

- [11] X. Ouyang and J. Zhao, “Channel equalization for the discrete cosine transform based OFDM,” in 2015 Photonics of Ireland, Cork, Ireland, 2-4 Sep., 2015.
- [12] W. Jia, H. Zhang, X. Ouyang, and J. Zhao, “Generation and transmission of 21.5-Gb/s DPSK signal using a directly modulated laser,” in 2015 Photonics of Ireland, Cork, Ireland, 2-4 Sep., 2015.
- [13] X. Ouyang and J. Zhao, “Performance characterization of optical offset-QAM OFDM for fiber transmission,” in the 9th International Symposium on Communication Systems, Networks and Digital Signal Processing, (CSNDSP), Manchester, United Kingdom, 23-25 July, 2014, pp. 758-762.

# Reference

- [1] C. E. Shannon, "A Mathematical Theory of Communication," *Bell System Technical Journal*, vol. 27, pp. 379-423, 1948.
- [2] C. E. Shannon, "A Mathematical Theory of Communication," *Bell System Technical Journal*, vol. 27, pp. 623-656, 1948.
- [3] T. H. Maiman, "Stimulated Optical Radiation in Ruby," *Nature*, vol. 187, pp. 493-494, 08/06/print 1960.
- [4] A. L. Schawlow and C. H. Townes, "Infrared and Optical Masers," *Physical Review*, vol. 112, pp. 1940-1949, 12/15/ 1958.
- [5] (1960, Oct. 21) Scientists demonstrate optical maser. *Electronics*. 38.
- [6] W. R. Bennett Jr., Ali, Javan, "Gas optical maser," United States Patent, 1964.
- [7] R. N. Hall, G. E. Fenner, J. D. Kingsley *et al.*, "Coherent Light Emission From GaAs Junctions," *Physical Review Letters*, vol. 9, pp. 366-368, 11/01/ 1962.
- [8] Z. I. Alferov, V. Andreev, D. Garbuzov *et al.*, "Investigation of the influence of the AlAs-GaAs heterostructure parameters on the laser threshold current and the realization of continuous emission at room temperature," *Sov. Phys. Semicond*, vol. 4, pp. 1573-1575, 1971.
- [9] I. Hayashi, M. B. Panish, P. W. Foy *et al.*, "Junction Lasers Which Operate Continuously at Room Temperature," *Applied Physics Letters*, vol. 17, pp. 109-111, 1970.
- [10] R. L. Hartman and R. W. Dixon, "Reliability of DH GaAs lasers at elevated temperatures," *Applied Physics Letters*, vol. 26, pp. 239-242, 1975.
- [11] R. L. Hartman, J. C. Dymant, C. J. Hwang *et al.*, "Continuous operation of GaAs-Ga<sub>1-x</sub>Al<sub>x</sub>As double-heterostructure lasers with 30 °C half-lives exceeding 1000 h," *Applied Physics Letters*, vol. 23, pp. 181-183, 1973.
- [12] W. B. Joyce, R. W. Dixon, and R. L. Hartman, "Statistical characterization of the lifetimes of continuously operated (Al,Ga)As double-heterostructure lasers," *Applied Physics Letters*, vol. 28, pp. 684-686, 1976.

- [13] R. L. Hartman, N. E. Schumaker, and R. W. Dixon, "Continuously operated (Al,Ga)As double-heterostructure lasers with 70 °C lifetimes as long as two years," *Applied Physics Letters*, vol. 31, pp. 756-759, 1977.
- [14] A. C. S. Van Heel, "A New Method of transporting Optical Images without Aberrations," *Nature*, vol. 173, pp. 39-39, 01/02/print 1954.
- [15] B. O'Brien, "Optical image forming devices," United States Patent, 1958.
- [16] H. H. Hopkins and N. S. Kapany, "A Flexible Fibrescope, using Static Scanning," *Nature*, vol. 173, pp. 39-41, 01/02/print 1954.
- [17] K. C. Kao and G. A. Hockham, "Dielectric-fibre surface waveguides for optical frequencies," *Proceedings of the Institution of Electrical Engineers-London*, vol. 113, pp. 1151-1158, 1966.
- [18] F. P. Kapron, D. B. Keck, R. D. Maurer *et al.*, "Radiation Losses in Glass Optical Waveguides," *Applied Physics Letters*, vol. 17, pp. 423-425, 1970.
- [19] D. B. Keck, R. D. Maurer, and P. C. Schultz, "On the ultimate lower limit of attenuation in glass optical waveguides," *Applied Physics Letters*, vol. 22, pp. 307-309, 1973.
- [20] M. Kawachi, A. Kawana, and T. Miyashita, "Low-Loss single-mode fibre at the material-dispersion-free wavelength of 1.27  $\mu\text{m}$ ," *Electron. Lett.*, vol. 13, pp. 442-443, 1977.
- [21] T. Miya, Y. Terunuma, T. Hosaka *et al.*, "Ultimate low-loss single-mode fibre at 1.55  $\mu\text{m}$ ," *Electron. Lett.*, vol. 15, pp. 106-108, 1979.
- [22] R. J. Sanferrare, "Terrestrial lightwave systems," *AT&T Technical Journal*, vol. 66, pp. 95-107, Jan-Feb 1987.
- [23] J. Hecht, *City of light: the story of fiber optics*. Oxford; New York: Oxford University Press, 2004.
- [24] G. P. Agrawal, *Fiber-Optic Communication Systems*. 4th Edition ed., Chichester: John Wiley & Sons, 2010.
- [25] J. Senior, *Optical Fiber Communications: Principles and Practice*. 3rd Edition ed. Pearson, 2008.
- [26] K. Fukuchi, T. Kasamatsu, M. Morie *et al.*, "10.92-Tb/s ( $273 \times 40\text{-Gb/s}$ ) triple-band/ultra-dense WDM optical-repeatered transmission experiment," in *Proc. Optical Fiber Communication Conference and International Conference on Quantum Information*, Anaheim, California, 2001, p. PD24.
- [27] J. I. Yamada, S. Machida, and T. Kimura, "2 Gbit/s optical transmission experiments at 1.3  $\mu\text{m}$  with 44 km single-mode fibre," *Electron. Lett.*, vol. 17, pp. 479-480, 1981.
- [28] R. J. Mears, L. Reekie, I. M. Jauncey *et al.*, "Low-noise erbium-doped fibre amplifier operating at 1.54 $\mu\text{m}$ ," *Electron. Lett.*, vol. 23, p. 1026, Sep 10 1987.

- [29] C. A. Brackett, "Dense Wavelength Division Multiplexing Networks - Principles and Applications," *IEEE J. Sel. Areas Commun.*, vol. 8, pp. 948-964, Aug 1990.
- [30] H. Zhang, N. Kavanagh, Z. Li *et al.*, "100 Gbit/s WDM transmission at 2  $\mu\text{m}$ : transmission studies in both low-loss hollow core photonic bandgap fiber and solid core fiber," *Opt. Express*, vol. 23, pp. 4946-51, Feb 23 2015.
- [31] H. Zhang, M. Gleeson, N. Ye *et al.*, "Dense WDM transmission at 2  $\mu\text{m}$  enabled by an arrayed waveguide grating," *Opt. Lett.*, vol. 40, pp. 3308-3311, 2015/07/15 2015.
- [32] H. Zhang, Z. Li, N. Kavanagh *et al.*, "81 Gb/s WDM transmission at 2  $\mu\text{m}$  over 1.15 km of low-loss hollow core photonic bandgap fiber," in *Proc. 2014 European Conference on Optical Communication (ECOC), 21-25 Sept. 2014*, Piscataway, NJ, USA, 2014, p. 3 pp.
- [33] K. Feher, "1024-QAM and 256-QAM coded modems for microwave and cable system applications," *IEEE J. Sel. Areas Commun.*, vol. 5, pp. 357-368, Apr 1987.
- [34] L. K. Tan, J. S. Putnam, F. Lu *et al.*, "A 70-Mb/s variable-rate 1024-QAM cable receiver IC with integrated 10-b ADC and FEC decoder," *IEEE Journal of Solid-State Circuits*, vol. 33, pp. 2205-2218, Dec 1998.
- [35] Y. Koizumi, K. Toyoda, M. Yoshida *et al.*, "1024 QAM (60 Gbit/s) single-carrier coherent optical transmission over 150 km," *Opt. Express*, vol. 20, pp. 12508-12514, May 2012.
- [36] S. Beppu, K. Kasai, M. Yoshida *et al.*, "2048 QAM (66 Gbit/s) single-carrier coherent optical transmission over 150 km with a potential SE of 15.3 bit/s/Hz," *Opt. Express*, vol. 23, pp. 4960-4969, Feb 2015.
- [37] S. Beppu, M. Yoshida, K. Kasai *et al.*, "2048 QAM (66 Gbit/s) single-carrier coherent optical transmission over 150 km with a potential SE of 15.3 bit/s/Hz," in *Proc. Optical Fiber Communication Conference*, San Francisco, California, 2014, p. W1A.6.
- [38] N. K. Fontaine, R. Ryf, H. Chen *et al.*, "30 $\times$ 30 MIMO transmission over 15 spatial modes," in *Proc. Optical Fiber Communication Conference Post Deadline Papers*, Los Angeles, California, 2015, p. Th5C.1.
- [39] B. Jopson and A. Gnauck, "Dispersion compensation for optical-fiber systems," *IEEE Commun. Mag.*, vol. 33, pp. 96-102, Jun 1995.
- [40] T. Yamamoto, "High-Speed Directly Modulated Lasers," in *Proc. Optical Fiber Communication Conference*, Los Angeles, California, 2012, p. OTh3F.5.
- [41] K. Szczerba, T. Lengyel, M. Karlsson *et al.*, "94-Gb/s 4-PAM Using an 850-nm VCSEL, Pre-Emphasis, and Receiver Equalization," *IEEE Photon. Technol. Lett.*, vol. 28, pp. 2519-2521, 2016.

- [42] D. Mahgerefteh, Y. Matsui, X. Zheng *et al.*, “Chirp Managed Laser and Applications,” *IEEE J. Sel. Top. Quantum Electron.*, vol. 16, pp. 1126-1139, 2010.
- [43] Y. Matsui, D. Mahgerefteh, Z. Xueyan *et al.*, “Chirp-managed directly modulated laser (CML),” *IEEE Photon. Technol. Lett.*, vol. 18, pp. 385-387, 2006.
- [44] D. Mahgerefteh, C. Liao, X. Zheng *et al.*, “Error-free 250 km transmission in standard fibre using compact 10 Gbit/s chirp-managed directly modulated lasers (CML) at 1550 nm,” *Electron. Lett.*, vol. 41, pp. 543-544, 2005.
- [45] D. Walker, S. Han, C. Laperle *et al.*, “960-km transmission over G.652 fiber at 10 Gb/s with a laser/electroabsorption Modulator and no optical dispersion compensation,” *IEEE Photon. Technol. Lett.*, vol. 17, pp. 2751-2753, 2005.
- [46] E. L. Wooten, K. M. Kiss, A. Yi-Yan *et al.*, “A review of lithium niobate modulators for fiber-optic communications systems,” *IEEE J. Sel. Top. Quantum Electron.*, vol. 6, pp. 69-82, 2000.
- [47] R. A. Griffin, R. G. Walker, and R. I. Johnstone, “Integrated devices for advanced modulation formats,” in *Proc. IEEE/LEOS Workshop on Advanced Modulation Formats, 2004*, 2004, pp. 39-40.
- [48] M. Erman, P. Jarry, R. Gamonal *et al.*, “Mach-Zehnder modulators and optical switches on III-V semiconductors,” *J. Lightw. Technol.*, vol. 6, pp. 837-846, 1988.
- [49] L. A. Coldren, S. C. Nicholes, L. Johansson *et al.*, “High Performance InP-Based Photonic ICs — A Tutorial,” *J. Lightw. Technol.*, vol. 29, pp. 554-570, 2011.
- [50] P. J. Winzer and R. J. Essiambre, “Advanced modulation formats for high-capacity optical transport networks,” *J. Lightw. Technol.*, vol. 24, pp. 4711-4728, Dec 2006.
- [51] P. J. Winzer and R. J. Essiambre, “Advanced optical modulation formats,” *Proc. IEEE*, vol. 94, pp. 952-985, May 2006.
- [52] G. Agrawal, *Nonlinear Fiber Optics (Fifth Edition)*. Boston: Academic Press, 2012.
- [53] G. P. Agrawal, “Nonlinear fiber optics: its history and recent progress Invited,” *J. Opt. Soc. Am. B-Opt. Phys.*, vol. 28, pp. A1-A10, Dec 2011.
- [54] R. A. Linke and A. H. Gnauck, “High-capacity coherent lightwave systems,” *J. Lightw. Technol.*, vol. 6, pp. 1750-1769, Nov 1988.
- [55] A. H. Gnauck, G. Raybon, S. Chandrasekhar *et al.*, “2.5 Tb/s (64x42.7 Gb/s) transmission over 40x100 km NZDSF using RZ-DPSK format and all-Raman-amplified Spans,” in *Proc. Optical Fiber Communications Conference*, Anaheim, California, 2002, p. FC2.

- [56] M. G. Taylor, "Coherent detection method using DSP for demodulation of signal and subsequent equalization of propagation impairments," *IEEE Photon. Technol. Lett.*, vol. 16, pp. 674-676, Feb 2004.
- [57] I. Dedic, "56 GS/s ADC: Enabling 100GbE," in *Proc. Optical Fiber Communication Conference*, San Diego, California, 2010, p. OThT6.
- [58] K. Kikuchi, "Coherent detection of phase-shift keying signals using digital carrier-phase estimation," in *Proc. Optical Fiber Communication Conference and Exposition and The National Fiber Optic Engineers Conference*, Anaheim, California, 2006, p. OTuI4.
- [59] A. Sano, H. Masuda, T. Kobayashi *et al.*, "69.1-Tb/s (432 x 171-Gb/s) C- and extended L-band transmission over 240 km using PDM-16-QAM modulation and digital coherent detection," in *Proc. Optical Fiber Communication Conference*, San Diego, California, 2010, p. PDPB7.
- [60] M. R. D. Rodrigues and I. Darwazeh, "Fast OFDM: a proposal for doubling the data rate of OFDM schemes," in *Proc. ICT 2002 - International Conference on Telecommunications, 23-26 June 2002*, Beijing, China, 2002, pp. 484-7.
- [61] F. Q. Xiong, "*M*-ary amplitude shift keying OFDM system," *IEEE Trans. Commun.*, vol. 51, pp. 1638-1642, Oct 2003.
- [62] G. D. Mandyam, "On the discrete cosine transform and OFDM systems," in *Proc. Acoustics, Speech, and Signal Processing, 2003. Proceedings. (ICASSP '03). 2003 IEEE International Conference on*, 2003, pp. IV-544-7 vol.4.
- [63] G. D. Mandyam, "Sinusoidal transforms in OFDM systems," *IEEE Transactions on Broadcasting*, vol. 50, pp. 172-184, Jun 2004.
- [64] S. Satish, N. Al-Dhahir, and H. Minn, "A DCT-Based Broadband Multicarrier Transceiver," in *Proc. Proceedings of the IEEE SoutheastCon 2006*, 2006, pp. 175-180.
- [65] N. Al-Dhahir, H. Minn, and S. Satish, "Optimum DCT-based multicarrier transceivers for frequency-selective channels," *IEEE Trans. Commun.*, vol. 54, pp. 911-921, May 2006.
- [66] P. Tan and N. C. Beaulieu, "A Comparison of DCT-Based OFDM and DFT-Based OFDM in Frequency Offset and Fading Channels," *IEEE Trans. Commun.*, vol. 54, pp. 2113-2125, 2006.
- [67] P. Tan and N. C. Beaulieu, "An improved DCT-based OFDM data transmission scheme," in *Proc. 2005 IEEE 16th International Symposium on Personal, Indoor and Mobile Radio Communications*, 2005, pp. 745-749 Vol. 2.
- [68] S. A. Martucci, "Symmetric Convolution and the Discrete Sine and Cosine Transforms," *IEEE Trans. Signal Process.*, vol. 42, pp. 1038-1051, May 1994.

- [69] S. K. Ibrahim, J. Zhao, D. Rafique *et al.*, "Demonstration of world-first experimental optical Fast OFDM system at 7.174 Gbit/s and 14.348 Gbit/s," in *Proc. 36th European Conference and Exhibition on Optical Communication*, 2010, pp. 1-3.
- [70] J. Zhao and A. D. Ellis, "A Novel Optical Fast OFDM with Reduced Channel Spacing Equal to Half of the Symbol Rate per Carrier," in *Proc. Optical Fiber Communication Conference*, San Diego, California, 2010, p. OMR1.
- [71] E. Giacomidis, A. Tsokanos, C. Mouchos *et al.*, "Extensive Comparisons of Optical Fast-OFDM and Conventional Optical OFDM for Local and Access Networks," *Journal of Optical Communications and Networking*, vol. 4, pp. 724-733, 2012/10/01 2012.
- [72] E. Giacomidis, S. Ibrahim, J. Zhao *et al.*, "Experimental Demonstration of Cost-Effective Intensity-Modulation and Direct-Detection Optical Fast-OFDM over 40km SMF Transmission," in *Proc. National Fiber Optic Engineers Conference*, Los Angeles, California, 2012, p. JW2A.65.
- [73] E. Giacomidis, S. K. Ibrahim, J. Zhao *et al.*, "Experimental and theoretical investigations of intensity-modulation and direct-detection optical Fast-OFDM over MMF-links," *IEEE Photon. Technol. Lett.*, vol. 24, pp. 52-54, 2012.
- [74] J. Zhao, "Intensity-Modulation Full-Field Detection Optical Fast OFDM," *Journal of Optical Communications and Networking*, vol. 5, pp. 465-474, 2013/05/01 2013.
- [75] J. Zhao, S. K. Ibrahim, P. Gunning *et al.*, "Chromatic dispersion compensation using symmetric extension based guard interval in optical fast-OFDM," in *Proc. 2011 37th European Conference and Exhibition on Optical Communication*, 2011, pp. 1-3.
- [76] J. Zhao and A. Ellis, "Transmission of 4-ASK Optical Fast OFDM With Chromatic Dispersion Compensation," *IEEE Photon. Technol. Lett.*, vol. 24, pp. 34-36, 2012.
- [77] J. Zhao, S. K. Ibrahim, D. Rafique *et al.*, "Symbol Synchronization Exploiting the Symmetric Property in Optical Fast OFDM," *IEEE Photon. Technol. Lett.*, vol. 23, pp. 594-596, 2011.
- [78] N. Ahmed, T. Nataraja, and K. R. Rao, "Discrete Cosine Transform," *IEEE Trans. Comput.*, vol. C 23, pp. 90-93, 1974.
- [79] S. A. Martucci and R. M. Mersereau, "The symmetric convolution approach to the nonexpansive implementations of FIR filter banks for images," in *Proc. 1993 IEEE International Conference on Acoustics, Speech, and Signal Processing*, 1993, pp. 65-68 vol.5.
- [80] M. Webster, L. Raddatz, I. H. White *et al.*, "A statistical analysis of conditioned launch for gigabit ethernet links using multimode fiber," *J. Lightw. Technol.*, vol. 17, pp. 1532-1541, 1999.

- [81] D. Falconer, S. L. Ariyavisitakul, A. Benyamin-Seeyar *et al.*, "Frequency domain equalization for single-carrier broadband wireless systems," *IEEE Commun. Mag.*, vol. 40, pp. 58-66, Apr 2002.
- [82] N. Benvenuto, R. Dinis, D. Falconer *et al.*, "Single carrier modulation with nonlinear frequency domain equalization: An idea whose time has come — Again," *Proc. IEEE*, vol. 98, pp. 69-96, Jan. 2010.
- [83] R. Kudo, T. Kobayashi, K. Ishihara *et al.*, "Coherent Optical Single Carrier Transmission Using Overlap Frequency Domain Equalization for Long-Haul Optical Systems," *J. Lightw. Technol.*, vol. 27, pp. 3721-3728, 2009/08/15 2009.
- [84] M. Sung, J. Lee, and J. Jeong, "DCT-precoding technique in optical Fast OFDM for mitigating fiber nonlinearity," *IEEE Photon. Technol. Lett.*, vol. 25, pp. 2209-2212, 2013.
- [85] J. Wooler, S. R. Sandoghchi, D. Gray *et al.*, "Overcoming the Challenges of Splicing Dissimilar Diameter Solid-Core and Hollow-Core Photonic Band Gap Fibers," in *Proc. Workshop on Specialty Optical Fibers and their Applications*, Sigtuna, 2013, p. W3.26.
- [86] S. Coleri, M. Ergen, A. Puri *et al.*, "Channel estimation techniques based on pilot arrangement in OFDM systems," *IEEE Transactions on Broadcasting*, vol. 48, pp. 223-229, Sep 2002.
- [87] B. Muquet, Z. D. Wang, G. B. Giannakis *et al.*, "Cyclic prefixing or zero padding for wireless multicarrier transmissions?," *IEEE Trans. Commun.*, vol. 50, pp. 2136-2148, Dec 2002.
- [88] J. Zhao and A. D. Ellis, "Discrete-Fourier transform based implementation for optical fast OFDM," in *Proc. 36th European Conference and Exhibition on Optical Communication*, 2010, pp. 1-3.
- [89] C. Lei, H. Chen, M. Chen *et al.*, "A high spectral efficiency optical OFDM scheme based on interleaved multiplexing," *Opt. Express*, vol. 18, pp. 26149-26154, Dec. 6 2010.
- [90] W. Long, J. Zhang, D. B. Wang *et al.*, "Mitigation of the interference between odd and even terms in optical fast OFDM scheme based on interleaved multiplexing," *IEEE Photon. Technol. Lett.*, vol. 24, pp. 1160-1162, Jul 1 2012.
- [91] X. Ouyang, J. Y. Jin, G. Y. Jin *et al.*, "Interleaved multiplexing optical Fast OFDM without the interference between subchannels," *IEEE Photon. Technol. Lett.*, vol. 25, pp. 378-381, Feb 15 2013.
- [92] J. Proakis and M. Salehi, *Digital Communications*. 5th ed., New York, NY, USA: McGraw-Hill Education, 2007.
- [93] H. F. Talbot, "Facts relating to optical science. No. IV," *Philosophical Magazine Series 3*, vol. 9, pp. 401-407, Dec 1836.

- [94] L. Rayleigh, "On copying diffraction-gratings, and on some phenomena connected therewith," *Philosophical Magazine Series 5*, vol. 11, pp. 196-205, Mar. 1881.
- [95] J. T. Winthrop and C. R. Worthing, "Theory of Fresnel images .I. plane periodic objects in monochromatic light," *Journal of the Optical Society of America*, vol. 55, pp. 373-381, Apr. 1965.
- [96] J. M. Wen, Y. Zhang, and M. Xiao, "The Talbot effect: recent advances in classical optics, nonlinear optics, and quantum optics," *Advances in Optics and Photonics*, vol. 5, pp. 83-130, Mar 2013.
- [97] K. B. Cooper, R. J. Dengler, N. Llombart *et al.*, "THz imaging radar for standoff personnel screening," *IEEE Transactions on Terahertz Science and Technology*, vol. 1, pp. 169-182, Sep 2011.
- [98] R. J. Dengler, K. B. Cooper, G. Chattopadhyay *et al.*, "600 GHz imaging radar with 2 cm range resolution," in *Proc. 2007 IEEE MTT-S International Microwave Symposium, IMS 2007*, Honolulu, HI, United states, 2007, pp. 1371-1374.
- [99] J. R. Klauder, A. C. Price, S. Darlington *et al.*, "The theory and design of chirp radars," *Bell System Technical Journal*, vol. 39, pp. 745-808, 1960.
- [100] S. Darlington, "Demodulation of wideband low-power FM signals," *Bell System Technical Journal*, vol. 43, pp. 339-374, 1964.
- [101] W. Hirt and S. Pasupathy, "Continuous Phase Chirp (CPC) Signals for Binary Data Communication—Part I: Coherent Detection," *IEEE Trans. Commun.*, vol. 29, pp. 836-847, 1981.
- [102] W. Hirt and S. Pasupathy, "Continuous Phase Chirp (CPC) Signals for Binary Data Communication—Part II: Noncoherent Detection," *IEEE Trans. Commun.*, vol. 29, pp. 848-858, 1981.
- [103] F. Russo, "Demodulator structures for pulse-frequency-modulated signals," *IEEE Trans. Aerosp. Electron. Syst.*, vol. 12, pp. 127-130, 1976.
- [104] R. L. Brewster and W. W. S. Jibrail, "Detection of FSK and DPSK data signals by pulse-compression," *IEE Proc. F Radar and Signal Process.*, vol. 129, pp. 273-280, 1982.
- [105] J. Pinkney, R. Behin, A. Sesay *et al.*, "High-speed DQPSK chirp spread spectrum system for indoor wireless applications," *Electron. Lett.*, vol. 34, pp. 1910-1911, Oct 1998.
- [106] A. Kadri, R. K. Rao, and J. Jiang, "Low-power chirp spread spectrum signals for wireless communication within nuclear power plants," *Nuclear Technology*, vol. 166, pp. 156-169, May 2009.
- [107] C. He, M. Ran, Q. Meng *et al.*, "Underwater acoustic communications using *M*-ary chirp-DPSK modulation," in *Proc. 2010 IEEE 10th International Conference on Signal Processing, ICSP2010, October 24, 2010 - October 28, 2010*, Beijing, China, 2010, pp. 1544-1547.

- [108] M. Palmese, G. Bertolotto, A. Pescetto *et al.*, “Experimental validation of a chirp-based underwater acoustic communication method,” in *Proc. 7th European Conference on Noise Control 2008, EURONOISE 2008, June 29, 2008 - July 4, 2008*, Paris, France, 2008, pp. 147-152.
- [109] “Wireless Medium Access Control (MAC) and Physical Layer (PHY) Specifications for Low-Rate Wireless Personal Area Networks (WPANs),” in *IEEE Standard 802.15.4a-2007*, ed, 2007, pp. 1-203.
- [110] H. P. Liu, “Multicode ultra-wideband scheme using chirp waveforms,” *IEEE J. Sel. Areas Commun.*, vol. 24, pp. 885-891, Apr. 2006.
- [111] I. Dotlic and R. Kohno, “Low complexity chirp pulsed ultra-wideband system with near-optimum multipath performance,” *IEEE Trans. Wireless Commun.*, vol. 10, pp. 208-218, Jan 2011.
- [112] L. Yang and G. B. Giannakis, “Ultra-wideband communications — An idea whose time has come,” *IEEE Signal Process. Mag.*, vol. 21, pp. 26-54, 2004.
- [113] A. Springer, M. Huemer, L. Reindl *et al.*, “A robust ultra-broad-band wireless communication system using SAW chirped delay lines,” *IEEE Transactions on Microwave Theory and Techniques*, vol. 46, pp. 2213-2219, Dec 1998.
- [114] D. P. Morgan, “A history of surface acoustic wave devices,” *International Journal of High Speed Electronics and Systems*, vol. 10, pp. 553-602, 2000.
- [115] D. R. Arsenault and P. Das, “SAW Fresnel transform devices and their applications,” in *Proc. 1977 Ultrasonics Symposium*, New York, NY, USA, 1977, pp. 969-973.
- [116] V. P. Plessky and L. M. Reindl, “Review on SAW RFID tags,” *IEEE Trans. Ultrason., Ferroelect., Freq. Control*, vol. 57, pp. 654-68, Mar 2010.
- [117] R. Brocato, J. Skinner, G. Wouters *et al.*, “Ultra-wideband SAW correlator,” *IEEE Trans. Ultrason., Ferroelect., Freq. Control*, vol. 53, pp. 1554-6, Sep 2006.
- [118] A. Georgiadis and M. Detratti, “A linear, low-power, wideband CMOS VCO for FM-UWB applications,” *Microwave and Optical Technology Letters*, vol. 50, pp. 1955-1958, Jul 2008.
- [119] J. Ryckaert, G. Van der Plas, V. De Heyn *et al.*, “A 0.65-to-1.4 nJ/burst 3-to-10 GHz UWB all-digital TX in 90 nm CMOS for IEEE 802.15.4a,” *IEEE Journal of Solid-State Circuits*, vol. 42, pp. 2860-2869, Dec 2007.
- [120] S. Solda, M. Caruso, A. Bevilacqua *et al.*, “A 5 Mb/s UWB-IR transceiver front-end for wireless sensor networks in 0.13  $\mu\text{m}$  CMOS,” *IEEE Journal of Solid-State Circuits*, vol. 46, pp. 1636-1647, Jul 2011.
- [121] J. T. Winthrop and C. R. Worthing, “Convolution formulation of Fresnel diffraction,” *Journal of the Optical Society of America*, vol. 56, pp. 588-591, 1966.

- [122] M. Moshinsk and C. Quesne, "Linear canonical transformations and their unitary representations," *Journal of Mathematical Physics*, vol. 12, pp. 1772-1780, 1971.
- [123] S. C. Pei and J. J. Ding, "Eigenfunctions of linear canonical transform," *IEEE Trans. Signal Process.*, vol. 50, pp. 11-26, Jan 2002.
- [124] L. M. Bernardo, "ABCD matrix formalism of fractional Fourier optics," *Optical Engineering*, vol. 35, pp. 732-740, Mar 1996.
- [125] E. Sejdic, I. Djurovic, and L. Stankovic, "Fractional Fourier transform as a signal processing tool: An overview of recent developments," *Signal Processing*, vol. 91, pp. 1351-1369, Jun 2011.
- [126] H. G. de Chatellus, E. Lacot, W. Glastre *et al.*, "Theory of Talbot lasers," *Physical Review A*, vol. 88, p. 12, Sep 2013.
- [127] Y. Park, G. Popescu, K. Badizadegan *et al.*, "Fresnel particle tracing in three dimensions using diffraction phase microscopy," *Opt. Lett.*, vol. 32, pp. 811-813, Apr 1 2007.
- [128] R. Iwanow, D. A. May-Arrioja, D. N. Christodoulides *et al.*, "Discrete Talbot effect in waveguide arrays," *Phys Rev Lett*, vol. 95, p. 053902, Jul 29 2005.
- [129] F. Gori, "Why is the Fresnel transform so little known?," in *Current Trends in Optics*, J. C. Dainty, Ed., ed: Academic Press, 1994, pp. 139-148.
- [130] P. Szwaykowski and V. Arrizon, "Talbot array illuminator with multilevel phase gratings," *Appl. Optics*, vol. 32, pp. 1109-14, Mar 1 1993.
- [131] C. H. Zhou and L. R. Liu, "Simple equations for the calculation of a multilevel phase grating for Talbot array illumination," *Opt. Commun.*, vol. 115, pp. 40-44, Mar 1 1995.
- [132] V. Arrizon and J. Ojeda-Castaneda, "Fresnel diffraction of substructured gratings: matrix description," *Opt. Lett.*, vol. 20, pp. 118-20, Jan 15 1995.
- [133] V. Arrizon, J. G. Ibarra, and J. OjedaCastaneda, "Matrix formulation of the Fresnel transform of complex transmittance gratings," *J. Opt. Soc. Am. A*, vol. 13, pp. 2414-2422, Dec 1996.
- [134] S. B. Tucker, J. Ojeda-Castaneda, and W. T. Cathey, "Matrix description of near-field diffraction and the fractional Fourier transform," *J. Opt. Soc. Am. A*, vol. 16, pp. 316-322, Feb 1999.
- [135] K. B. Wolf and G. Krotzsch, "Geometry and dynamics in the Fresnel transforms of discrete systems," *J. Opt. Soc. Am. A*, vol. 24, pp. 2568-2577, Sep 2007.
- [136] L. Rabiner, R. Schafer, and C. Rader, "The chirp z-transform algorithm," *IEEE Trans. Audio Electroacoust.*, vol. 17, pp. 86-92, 1969.
- [137] L. Rabiner, "The chirp z-transform algorithm - A lesson in serendipity," *IEEE Signal Process. Mag.*, vol. 21, pp. 118-119, Mar 2004.

- [138] I. Aizenberg and J. T. Astola, "Discrete generalized Fresnel functions and transforms in an arbitrary discrete basis," *IEEE Trans. Signal Process.*, vol. 54, pp. 4261-4270, Nov 2006.
- [139] R. W. Chang, "Synthesis of band-limited orthogonal signals for multichannel data transmission," *Bell System Technical Journal*, vol. 45, pp. 1775-1796, 1966.
- [140] S. B. Weinstein and P. M. Ebert, "Data transmission by frequency-division multiplexing using discrete Fourier transform," *IEEE Trans. Commun. Technol.*, vol. Co19, pp. 628-634, 1971.
- [141] J. Armstrong, "OFDM for optical communications," *J. Lightw. Technol.*, vol. 27, pp. 189-204, Jan-Feb 2009.
- [142] A. J. Lowery and L. B. Du, "Optical orthogonal division multiplexing for long haul optical communications: A review of the first five years," *Opt. Fiber Technol.*, vol. 17, pp. 421-438, Oct 2011.
- [143] A. Goldsmith, *Wireless Communications*. 1st ed. Cambridge University Press, 2005.
- [144] B. Ng, C. T. Lam, and D. Falconer, "Turbo frequency domain equalization for single-carrier broadband wireless systems," *IEEE Trans. Wireless Commun.*, vol. 6, pp. 759-767, Feb 2007.
- [145] Xing Ouyang, Cleitus Antony, F. C. G. Gunning *et al.*, "Discrete Fresnel transform and its circular convolution property," *arXiv.org*, vol. arXiv:1510.00574, 2015.
- [146] N. Benvenuto and S. Tomasin, "Iterative design and detection of a DFE in the frequency domain," *IEEE Trans. Commun.*, vol. 53, pp. 1867-1875, Nov 2005.
- [147] F. Silva, R. Dinis, N. Souto *et al.*, "Approaching the matched filter bound with block transmission techniques," *Transactions on Emerging Telecommunications Technologies*, vol. 23, pp. 76-85, Jan 2012.
- [148] A. Silva, J. Assunção, R. Dinis *et al.*, "Performance evaluation of IB-DFE-based strategies for SC-FDMA systems," *EURASIP Journal on Wireless Communications and Networking*, vol. 2013, pp. 1-10, 2013.
- [149] Y. S. Liu, Z. H. Tan, H. J. Hu *et al.*, "Channel Estimation for OFDM," *IEEE Communications Surveys and Tutorials*, vol. 16, pp. 1891-1908, 2014.
- [150] T. M. Schmidl and D. C. Cox, "Robust frequency and timing synchronization for OFDM," *IEEE Trans. Commun.*, vol. 45, pp. 1613-1621, 1997.